Computational analysis of the impact of façade geometrical details on wind flow and pollutant dispersion

Computational analysis of the impact of façade geometrical details on wind flow and pollutant dispersion

PROEFSCHRIFT

ter verkrijging van de graad van doctor aan de Technische Universiteit Eindhoven, op gezag van de rector magnificus prof.dr.ir. F.P.T. Baaijens, voor een commissie aangewezen door het College voor Promoties, in het openbaar te verdedigen op vrijdag 24 September 2021 om 13:30 uur

door

Xing Zheng

geboren te Chongqing, P.R. China

Dit proefschrift is goedgekeurd door de promotoren en de samenstelling van de promotiecommissie is als volgt:

voorzitter:	prof.dr.ir. M.C.J. Hornikx
1e promotor:	prof.dr.ir. B. Blocken
copromotor:	dr. H. Montazeri
leden:	prof.dr.ir. J.L.M. Hensen
	prof.dr. T. Stathopoulos
	prof.dr. T. Auer *(Technical University of Munich)*
	prof.dr. Y. Tominaga *(Niigata Institute of Technology)*
	prof.dr. X. Zhou *(Tongji University)*
adviseurs:	dr.ing. C. Gromke *(Karlsruhe Institute of Technology)*

Het onderzoek of ontwerp dat in dit proefschrift wordt beschreven is uitgevoerd in overeenstemming met de TU/e Gedragscode Wetenschapsbeoefening.

Computational analysis of the impact of façade geometrical details on wind flow and pollutant dispersion

A catalogue record is available from the Eindhoven University of Technology Library
ISBN: 978-90-386-5373-0
NUR code 955 – Bouwkunde
Published as issue 323 in de Bouwstenen series of the Department of the Built Environment of the Eindhoven University of Technology

Printed by ADC Dereumaux
Cover design: Xing Zheng

Summary

Detailed knowledge of wind-flow patterns around buildings is essential for a complete understanding of wind-induced ventilation, infiltration, pollutant dispersion, wind loads and wind comfort and safety. Many traditional and contemporary building façades are characterized by geometrical protrusions and recessions, such as balconies. Earlier studies have demonstrated that the near-façade wind flow is strongly influenced by the façade geometrical details, however, a systematic investigation of the impact of façade geometrical details on wind flow and pollutant dispersion around buildings has not yet been performed. This PhD project aims to obtain fundamental knowledge about the impact of façade geometrical details on the wind flow and pollutant dispersion around buildings using high-fidelity computational fluid dynamics (CFD). The thesis consists of the following 7 chapters:

In Chapter 1 the relevance, the problem statement, research objectives and the methodology of the current research are introduced.

Chapter 2 presents a comparative assessment of the performance of two turbulence modeling approaches, Reynolds-averaged Navier-Stokes (RANS) and large-eddy simulation (LES), in predicting near-façade airflow patterns and mean surface pressure distributions for buildings with balconies. The evaluation is based on a detailed validation with wind-tunnel measurements of wind-induced mean surface pressure for a high-rise building with balconies. The results show that RANS and LES can accurately predict the mean pressure coefficients (C_p) on the windward façade with balconies when the approaching wind is perpendicular to the façade ($\theta = 0°$). However, LES performs better than RANS for wind directions 90° and 180° since RANS systematically underestimates the absolute C_p. Large differences however are found in the computed flow fields on the balcony spaces. Because RANS systematically underestimates the absolute values of both C_p and the mean wind speed on the balconies, it is suggested that building design based on RANS might result in excessive ventilation and in too high wind nuisance levels.

Chapter 3 presents a detailed LES analysis of the impact of different geometrical characteristics of building balconies on the mean surface pressure across building façades and the mean wind speed on balcony spaces. The focus is on (i) the presence of balconies on different façades, (ii) balcony depth, (iii) balcony parapet walls, (iv) balcony partition walls and (v) density of balconies. The results indicate that deeper balconies lead to higher mean wind speed on windward balcony spaces. Adding partition walls can substantially increase the absolute C_p on the windward façade, reduce the absolute C_p on the leeward façade and reduce the mean wind speed on the balcony spaces.

In Chapter 4, guidelines for minimum domain size for LES simulations of wind flow and pollutant dispersion in long street canyons are developed. The LES simulations are conducted based on a detailed validation with wind-tunnel measurements of pollutant dispersion in a long street canyon. It is shown that LES can accurately predict the mean wind speed and mean pollutant concentration within long street canyons. However, the domain size has a significant impact on the results. The minimum requirement for domain width is 2.5H and for domain height 7.5H is recommended, where H is the height of the street canyon.

Chapter 5 presents a detailed LES analysis of the impact of building balconies on wind flow and pollutant dispersion in long street canyons. Four cases are evaluated: (i) a street canyon without façade balconies, (ii) a street canyon with balconies at both windward and leeward façades, (iii) a street canyon with balconies only at the windward façade and (iv) a street canyon with balconies only at the leeward façade. The results show that the presence of balconies can considerably reduce the mean wind speed and hence increase the mean pollutant concentration within street canyons. The highest area-averaged mean pollutant concentrations within the canyon in the vertical center plane are indeed observed for the case with balconies on both façades.

Chapter 6 provides the limitations and recommendations for future work and a general discussion. Finally, Chapter 7 summarizes the results of the previous chapters and provides the conclusions.

Acknowledgments

The research presented in this dissertation was a long journey and could only become fruitful with the help and support extended by many people. I would like to express my gratitude to lots of people who have helped me through the years of my PhD studies.

I would like to express my sincere gratitude and appreciation to my supervisor, prof. dr. ir. Bert Blocken, for providing me with the opportunity to work on this exciting topic in the unit Building Physics and Services and for his open mind regarding my research interest. His dedication, integrity, passion for science and commitment to work have aided my professional and personal growth. This thesis could not have been completed at this time without his concern. I would like to thank my daily supervisor dr. Hamid Montazeri who has played a vital role in motivating me to expand my knowledge. His professional feedback, tough questions and critical comments have definitely sharpened my mind and enhanced my learning skills.

I would like to thank the members of the thesis committee: prof. dr. Ted Stathopoulos, prof. dr. Jan Hensen, prof. dr. Yoshihide Tominaga, prof. dr. Thomas Auer, prof. dr. Xuanyi Zhou and dr. Christof Gromke for accepting to be a part of this committee and for their valuable time. It was an honor for me to obtain their valuable feedback on the thesis.

In particular, I would like to acknowledge dr. Christof Gromke for offering scientific advice and insights during this project. I am very grateful to him for his speedy feedback and his willingness to share knowledge. My sincere thanks also go to dr. ir. Twan van Hooff for his knowledge and the excellent advice he provided to me. I would like to extend special thanks to dr. Alessio Ricci for his encouragement during this project and for answering my questions patiently. My thanks also go to Samy Iousef, dr. Luyang Kang, dr. Qiang Zhou, dr. Baifeng Ji and Nestoras Antoniou for their inputs when I was struggling with my research during the first year. I thank prof. dr. Tong Zhang for his friendly advice on my research. I would like to thank Jan Diepens and Harrie Smulders for offering administrative and hardware support. Thanks to the secretaries at Building Physics and Services: Moniek

Sanders, Léontine Harmsen and Nathaly Rombley, for providing administrative support and for all of the great and meaningful chats we have had over the years.

Over the past couple of years, I have had the opportunity to work closely with very talented researchers, I would like to thank my former and present colleagues in the group of Urban Physics: dr. Yasin Toparlar, dr. Ivo Kalkman, dr. Paul Mannion, dr. Adelya Khayrullina, dr. Fabio Malizia, dr. Zhijun Wang, dr. Rahim Rezaeiha, dr. Stefanie Gillmeier, dr. Xuelin Zhang, dr. Wei Yin, Katarina Kosutova, Raffaele Vasaturo, Feiyu Geng, Argyrios Papadopoulos, Olga Palusci, Anto Moediartianto, Thijs van Druenen, Marlies Verbruggen, Rob Vervoort, Claudio Alanis Ruiz, Lili Xia, Yu-Hsuan Juan, Mutmainnah Sudirman, Peng Qin, Anjali Krishnan, Muxi Lei, Josip Zuzul, Sadra Sahebzadeh, Evgenya Mamulova, Bart van Gael, dr. Rubina Ramponi, dr. Jorge Isaac Peren Montero and dr. Xinrong Wang.

I would like to thank the company of researchers and friends whom I have had the good fortune of meeting in the past years: dr. Ji Li, Bin Meng, Jinglun Du, Anna Kaja, dr. Walker Shalika, Youfang Peng, dr. Yaxing Du, Yu Zhang, Shaojuan Zhang, Basar Bozkaya, dr. Luyi Xv, dr. Chang Liu, dr. Gang Liu, dr. Zhengying Liu, Yuxuan Chen, Xiaoxiao Zhang, Tao Liu, Winnie Franco Santos, Xuan Ling, Hoss Karimi, dr. Karin Kompatscher, dr. Peipeng Li, dr. Gengzhe Wang, dr. Qingliang Yu, Qingfeng Xv, dr. Wen Jiang, dr. Xin Chen, dr. Hung-Chu Chen, Deniz Tuzcuoglu, Mohammad Mukit, Douwe Smits, Ellen Driehuizen, Nore Smits, Yixiao Ma, Huiqing Wang, Hailin Zheng, Shengchen Yin, Li Lv, dr. Chi Feng, dr. Shanshan Shi, dr. Jiachuan Yang, Xuan Chen, Liutao Chen, Ge Yu and dr. Mei Liu. Thanks to the E.S.D.A. Chronos (Debate association in Eindhoven) for spending time organizing all the debates and allowing me to enjoy these extracurricular events. Special thanks to Alessandro Sona, Wenbin Shao and Leon Kersten, for exchanges of our opinions all these years and the nice talks we spent together.

I would like to acknowledge the Chinese Ministry of Education for financially supporting a part of this research. Without its contribution, this work would not have been possible.

Finally, I am ever grateful to my family, siblings, friends and acquaintances who have extended plenty of moral support and encouragement at all times, even in the most unexpected circumstances. I would particularly like to express deep gratitude to my wife Tianchen Dai, who has stood by me in all the difficult moments. I am indebted to my two lifelines, my parents. Their unconditional support allows me to concentrate on my studies and pursue my personal goals. This dissertation will be my best gift for them.

Table of contents

Table of contents

Chapter 1
Introduction

1.1 Background

"Ventus autem est aeris fluens unda cum incerta motus redundantia."[1]

(De Architectura, Book 1, by Vitruvius)

Vitruvius, the Roman architect during Caesar Augustus' reign, knew the phenomenon of morning breezes as well as the irregular winds which blow only during certain seasons of the year (Nova, 2006). In his book, *De Architectura*, he pointed out the importance of the relationship between wind and architecture, and how they might relate in good proportion to each other (Morgan, 1914). He believed that wind plays an important role in creating comfortable and healthy dwellings. At that time, in the 1st century BC, the entire population of the great city of Rome was slightly over one million.

Two thousand years later, urbanization is presenting major challenges to our living environment. It has resulted in the unintended side-effects of air pollution (Chan and Yao, 2008), wind discomfort and danger (Kaseb et al., 2020), the urban heat island effect and heat waves (Zhou et al., 2004) and huge growth in energy consumption (Al-Mulali et al., 2012; Cai et al., 2009). For example, the global building sector accounts for over 30% of the world's final energy consumption (International Energy Agency, 2018a) and nearly 30% of the global carbon dioxide emissions (International Energy Agency, 2018b). Additionally,

[1] English: Wind is a flowing wave of air, moving hither and thither indefinitely.

poor air quality is a considerable threat to human health. Exposure to high levels of pollution significantly increases the risk of respiratory, lung and cardiovascular diseases, cancer and can cause chronic health effects (Brunekreef and Holgate, 2002). In 2016, over 80% of the people living in urban areas that monitor air pollution were exposed to air quality levels exceeding the limits specified by World Health Organization (World Health Organization, 2016). The rapid pace of urbanization “created” built environments with heterogeneous physical characteristics. The construction of buildings inevitably changes the microclimate. Wind speed, wind direction, air pollution, wind-driven rain, temperature and relative humidity are all examples of physical aspects that make up the outdoor climate and are changed by the presence of buildings (Blocken and Carmeliet, 2004). Changes of these quantities depend on the density, arrangement, shape, size and orientation of buildings. Today, science and engineering are strongly intertwined in urban physics, which can provide quantitative guidelines regarding the developments taking place in a built environment, from a large scale, i.e., urban planning to a small scale, i.e., architectural design (Blocken, 2015).

In architectural design, the façade is a very important aspect, as it sets the tone for the rest of the building both from the aesthetical and the building physics point of view. Façades of historical as well as contemporary buildings can be characterized by protrusions and recessions for functionality or aesthetics (Figs. 1). In the modern era, advanced construction technologies offer architects a high degree of flexibility and a wide range of options in façade design. For many contemporary buildings, the façades are constituted with geometrical details such as balconies, louvers, window sills, mullions and arcades (Fig. 2). These façade geometrical details are important due to their impact on environmental quality and energy efficiency.

Fig. 1 Palazzo Ducale (building on the left, constructed in 14th century AD) and Biblioteca Nazionale Marciana (building on the right, constructed in 16th century AD), in Venice, photo by the author.

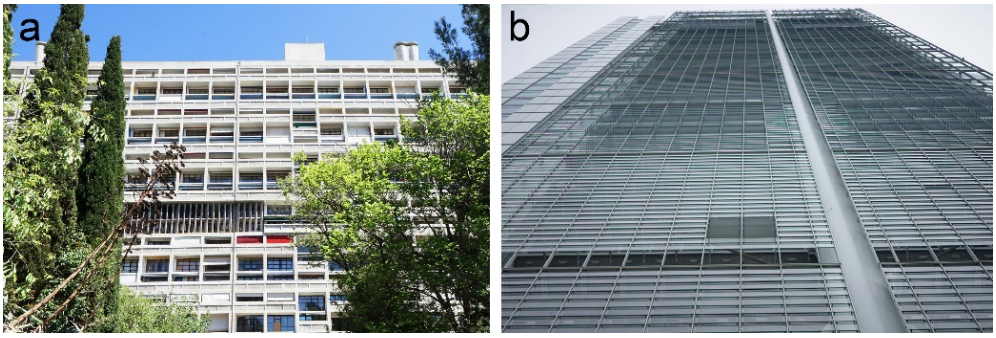

Fig. 2 (a) Unité d'habitation, in Marseille, and (b) Grattacielo Intesa Sanpaolo, in Turin, photos by the author.

To enhance the environmental quality and the building energy efficiency, the ability to accurately predict the microclimate and the building energy performance is important. Building façade geometrical details can adversely affect the urban wind flow, modify the urban microclimate and change the pollutant removal efficiency (Llaguno-Munitxa et al., 2017). Building energy simulation (BES) programs are widely used for building design and operation (Crawley et al., 2008). These programs combine many first-principle and empirical models to describe the relevant energy flow processes in and around buildings (Clarke, 2001). For example, the exterior surface pressure coefficients are used as input parameters for analyzing natural ventilation and infiltration flow rates (Ramponi et al., 2014). The

accurate prediction of natural ventilation, therefore, depends on the uncertainty involved in the pressure coefficient (C_p) data used in BES tools (Cóstola et al., 2009; Ramponi et al., 2014). Existing studies have suggested that the presence of building façade geometrical details like balconies can strongly modify the surface C_p distribution (Montazeri and Blocken, 2013).

From this perspective, gaining a better understanding of the impact of façade geometrical details on the wind flow pattern around buildings is crucial for the accurate evaluation of wind-induced natural ventilation (Cóstola et al., 2009; Ramponi et al., 2014), infiltration airflow, pollutant dispersion (Cui et al., 2020), surface convective heat transfer (Kahsay et al., 2019; Montazeri et al., 2015), wind comfort (Blocken and Carmeliet, 2008; Montazeri et al., 2013; Murakami, 1990a) and wind loads on building façades and building components (Stathopoulos, 1984).

1.2 Problem statement

To the best knowledge of the author, the first studies on wind flow around buildings with façade geometrical details have been conducted since the 1980s. Experimental studies for a building with balconies and a building with mullions were published in 1988 (Stathopoulos and Zhu, 1988) and 1990 (Stathopoulos and Zhu, 1990), respectively. In these two pioneering studies, the influence of balconies or mullions on building surface pressures was measured in the atmospheric boundary layer open-circuit wind tunnel at the Concordia University. In 1990, a pioneering numerical study was published (Murakami, 1990b). A very remarkable part of that study was a detailed CFD simulation of the near-façade wind flow field for a high-rise building with balconies (Blocken, 2014).

In subsequent years, the impact of the presence of façade details and their geometrical characteristics on buildings were studied by several authors (Ai et al., 2013, 2011; Hui et al., 2019; Maruta et al., 1998; Montazeri et al., 2013; Yuan et al., 2018). It was revealed that the geometrical characteristics of the façade details can have a strong impact on the near-façade wind flow patterns (Fig. 3a), surface mean/peak pressure, air change rate, surface convective heat transfer coefficient and building aerodynamic force.

The majority of previous studies on façade geometrical details were performed for isolated buildings. In recent years, urban street canyons with façade geometrical details have gained attention. Studies on street canyons indicate that the façade geometrical

details could modify the wind flow pattern (Fig. 3b) and pollutant concentration inside street canyons (Cui et al., 2020; Karkoulias et al., 2019; Murena and Mele, 2016).

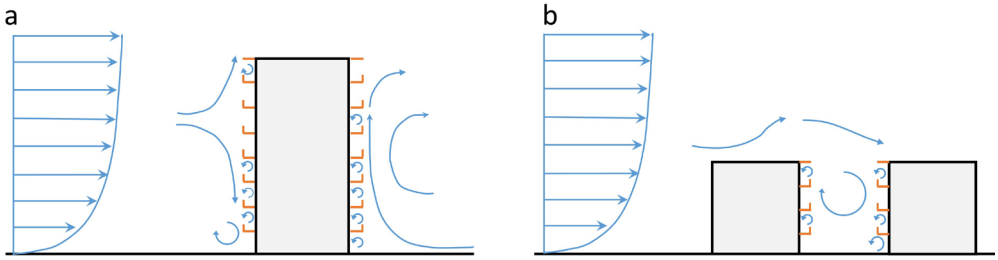

Fig. 3 Schematic representation of (a) wind flow around an isolated building with balconies and (b) wind flow around a street canyon with balconies.

Investigations of the influence of façade geometrical details on buildings can be conducted by full-scale on-site measurements, wind-tunnel measurements and computational fluid dynamics (CFD) simulations. Each of these methods has specific advantages and disadvantages.

Accurate and reliable on-site (field) measurements are highly valuable as they represent the real conditions, although they are usually only performed at a limited number of points in space and time. It is possible to conduct on-site measurements for a given real building with façade geometrical details. However, to investigate the impact of the geometrical characteristics of the façade details, on-site measurements of real buildings with different façade details are required and meanwhile, ideally the other parameters such as the main building dimensions and the meteorological conditions should be similar to allow a good comparison, which is very challenging and can even be impossible to achieve. As a result, on-site measurements have only been performed for some case studies, where a single specific geometrical configuration of façade details has been evaluated (Omrani et al., 2017).

Wind tunnel experiments allow detailed control over the experimental conditions. Detailed analysis of the flow features can be performed using state-of-the-art flow measurement techniques, such as Particle Image Velocimetry (PIV) and Laser Doppler Anemometry (LDA). However, due to the shielding effect of the façade geometrical details, it is challenging to capture the near-façade flow field through PIV or LDA in the small spaces in-between the façade geometrical details. Moreover, due to the limited size of the test section in the wind tunnel, the building scale is usually smaller than 1/20. Scaling renders

the façade surface elements very small, which can lead to incompatible similarity requirements.

CFD is relatively cheaper than on-site measurements and wind tunnel experiments and it does not suffer from potentially incompatible similarity constraints. CFD allows full control over the boundary conditions and easily and efficiently allows parametric studies to be performed (Ramponi and Blocken, 2012). Moreover, it is capable of providing all relevant variables in the entire computational domain (Blocken, 2015). However, accuracy and reliability are major concerns in CFD simulations and therefore, verification and validation are imperative.

Among the aforementioned methods, CFD simulation is the preferred one for carrying out extensive in-depth flow analyses for buildings with façade geometrical details. This is because CFD simulations can be performed in full scale and high-resolution data of the wind flow can be obtained. As the presence of façade geometrical details can generate local flow separation, recirculation and reattachment near building surfaces, the high-resolution results obtained from CFD can provide physical insights into these complex flow features in-between or in the vicinity of these façade geometrical details (Montazeri and Blocken, 2013). Relevant variables such as static pressure, pollutant concentration and wind velocity components can be obtained by CFD, which provides the possibility of conducting an in-depth analysis of the mechanism of wind flow and pollutant transport. Additionally, to explore the impact of geometrical characteristics of façade details, cases with different configurations and geometrical parameters should be tested. CFD is a suitable tool that easily allows such parametric studies.

Therefore, this thesis adopts the CFD approach to investigate the impact of façade geometrical details in general, and building balconies in specific, on the wind flow and pollutant dispersion processes. In spite of some numerical studies on buildings with façade geometrical details been performed in the past, the identified research gaps are as follows:

Research gap 1: Lack of information on the performance of RANS versus LES for buildings with façade geometrical details.

Recent reviews of the literature indicate that the two most popular CFD approaches in wind engineering and urban physics, by far, are Large-eddy simulation (LES) and steady Reynolds-Averaged Navier-Stokes (RANS) (Blocken, 2018). CFD validation studies on buildings with balconies show that the good performance of the RANS approach in

predicting surface wind pressure is only observed on the windward side for perpendicular (θ = 0°) and oblique (θ = 45°) wind directions (Montazeri and Blocken, 2013). This is mainly attributed to deficiencies of RANS in accurately reproducing flow separation, recirculation and reattachment (Murakami, 1993) and its inability to capture vortex shedding in the wake. The façade geometrical details introduce a multitude of areas with flow separation, recirculation and reattachment which can amplify the detrimental impact of the steady RANS deficiencies on the simulation results. Previous studies have compared the performance of RANS and LES for the simulation of the mean and instantaneous flow field around buildings without façade geometrical details and have consistently shown the superior performance of LES (Blocken, 2018; Murakami et al., 1992, 1990; Rodi, 1997; Stathopoulos, 1997). Therefore, validation studies with more advanced scale-resolving turbulence modeling approaches, i.e. LES, are needed.

Research gap 2: Lack of knowledge of the impact of balcony geometrical characteristics on near-façade wind flow and surface pressure.

The geometrical characteristics of building balconies can strongly affect not only the mean and peak surface pressures (Maruta et al., 1998) but also the wind speed on balcony spaces (Montazeri et al., 2013). For instance, modifying balcony geometrical characteristics on high-rise buildings can improve wind conditions on balcony spaces (Blocken and Carmeliet, 2008; Montazeri et al., 2013; Murakami, 1990a). Previous CFD studies on buildings with balconies have generally adopted the 3D steady RANS approach, while the use of LES was limited. Moreover, the impact of the geometrical characteristics of balconies has been investigated in a few studies with a focus on the balcony depth (Ai et al., 2011; Izadyar et al., 2020; Omrani et al., 2017), the height of the parapet walls (Ai et al., 2011) and the presence and the shape of partition walls (Mozaffari Ghadikolaei et al., 2020; Omrani et al., 2017). However, in these studies, different boundary conditions and building dimensions were considered and, therefore, the conclusions were not always consistent. From this perspective, it is imperative to conduct a systematic parametric study on geometrical characteristics for the optimal aerodynamic design of building balconies.

Research gap 3: Lack of guidelines for domain size for large-eddy simulation of pollutant dispersion in generic urban street canyons.

Certain urban morphologies such as street canyons can lead to airflow complexity such as additional recirculation and reattachment. Urban street canyons where long narrow

streets are bordered by building walls on both sides are known to be susceptible to high air pollution concentrations, certainly when the wind direction is perpendicular to the canyon axis. Wind flow and dispersion fields inside and in the vicinity of urban street canyons are important aspects of urban air quality studies. In the past, many studies have investigated the pollutant dispersion in generic street canyons through CFD simulations with the RANS approach (O'Neill et al., 2016; Zhong et al., 2015). Recently, there has been a growing interest to employ LES to address the shortcomings of the RANS approach (Blocken, 2018; Lateb et al., 2016). The results obtained through LES have been found to match closer to experimental results (Antoniou et al., 2017; Salim et al., 2011; Tominaga and Stathopoulos, 2011). Even though LES is intrinsically superior over RANS, LES results tend to be more sensitive to the many computational settings and parameters that have to be set by the user, including the computational grid topology, computational domain size, and boundary conditions. Previous LES simulations for generic street canyons adopted a wide range of different domain sizes. Accurate LES simulations require a sufficient domain size to minimize the effects of artificial boundary conditions on the results. However, the vast majority of these guidelines on domain sizes are directed to RANS simulations. For saving numerical resources without compromising accuracy, a systematic investigation is needed to provide guidelines for the domain size of LES simulations on generic street canyons.

Research gap 4: Lack of investigation of pollutant dispersion in street canyons with façade geometrical details using large-eddy simulations.

Many buildings in street canyons are characterized by façade geometrical details such as balconies. The residents on balcony spaces and pedestrians on streets might be exposed to high levels of pollutants (Karkoulias et al., 2019; Murena and Mele, 2016). Past studies on pollutant dispersion in street canyons with façade geometrical details have been conducted with the RANS approach (Cui et al., 2020; Karkoulias et al., 2019). However, previous studies have shown that CFD simulations using the RANS approach are deficient in capturing the complexities of near-field pollutant dispersion. These deficiencies do not only result in inaccuracies in the wind flow prediction, as stated earlier, but also in inaccuracies in modeling turbulent mass transport. The turbulence-induced transport of pollutants in RANS is almost exclusively computed based on the gradient diffusion hypothesis (Tominaga and Stathopoulos, 2007). This hypothesis is not always valid and the turbulent transport can perform differently, i.e., through the so-called counter-gradient (CG) turbulent diffusion

shown in the past (Gousseau et al., 2011; Rossi et al., 2010; van Hooff et al., 2014), whereby the turbulent mass flux is directed from a low-concentration area to a high-concentration area. On the other hand, LES has superior performance in pollutant dispersion around buildings, which can reproduce the CG turbulent diffusion (Gousseau et al., 2015). As turbulence can act as the main mechanism controlling pollutant removal from urban canopies (Antoniou et al., 2017; Kubilay et al., 2017; Liu and Wong, 2014), it is desirable to use LES to investigate the pollutant dispersion process in street canyons.

1.3 Research objectives

The main objective of this research is to obtain fundamental knowledge about the impact of façade geometrical details on the wind flow and pollutant dispersion around buildings. This leads to the following sub-objectives:

- Compare and validate CFD models for buildings with façade geometrical details.
- Investigate the impact of balcony geometrical characteristics on wind speed on balcony spaces and surface pressure for isolated buildings.
- Develop guidelines for LES simulations for wind flow and pollutant dispersion in generic street canyons.
- Explore the impact of building balconies on wind flow and pollutant dispersion in generic street canyons.

1.4 Methodology

Geometries of high-rise buildings and generic street canyons, and the types and dimensions of balconies are selected for investigation. For the high-rise buildings, different geometrical characteristics of building balconies are considered. In total, 12 cases are examined. For all cases, a 12-story building with dimensions width × depth × height = 24 × 24 × 48 m^3 (w:d:h = 1:1:2) is used. Based on the position and the geometrical characteristics of the balconies, the cases are classified into five groups (Fig. 4a) to investigate (i) balconies present or not, (ii) balcony depth, (iii) balcony parapet walls, (iv) balcony partition walls and (v) density of balconies. The generic street canyons are composed of two 4-story buildings. The height and depth of the buildings is 12 m. The distance between the two buildings or canyon width is 12 m (aspect ratio H/W = 1). Four street canyon cases are considered (Fig. 4b): (i) a street canyon case without balcony, (ii) a street canyon case with balconies

positioned at both windward and leeward façades, (iii) a street canyon case with balconies positioned only at the windward façade and (iv) a street canyon case with balconies positioned only at the leeward façade.

CFD validation studies for a generic high-rise building and a generic street canyon using data from wind tunnel measurements are conducted. The wind tunnel measurement of mean surface pressures is conducted for a façade of a high-rise building model with façade geometrical details under different approach-flow wind directions (Stathopoulos and Zhu, 1988). The dimensions of the reduced-scale building model is: width × depth × height = 0.152 × 0.152 × 0.3 m^3 (1:400 scale, w:d:h ≈ 1:1:2, 60.8 m × 60.8 m × 120 m in full scale). The validation study is performed for the building with balconies of 0.01 m depth (4 m in full scale) and 0.0025 m high (1 m in full scale) parapet walls using LES and 3D steady RANS. The performances on the prediction of mean surface pressure coefficient and mean wind speed on balcony spaces between the two approaches are compared. In the validation study for generic street canyons, the wind-tunnel measurement of the mean velocity field and the mean concentration of tracer gas in long street canyons by Gromke and Ruck (2009) is used. The street canyon model consisted of two parallel buildings with width × depth × height = 1.2 × 0.12 × 0.12 m^3 (1:150 scale, 180 m × 18 m × 18 m in full scale). The width of the street between the two parallel buildings was 0.12 m (18 m in full scale), yielding an aspect ratio equal to 1. Large-eddy simulations (LES) approach is employed in the CFD validation.

The validated CFD models are adopted to evaluate the aforementioned cases (shown in Fig. 4) and to explore the impact of façade geometrical details on (i) wind flow and surface static pressure for high-rise buildings and (ii) wind flow and pollutant dispersion for generic street canyons.

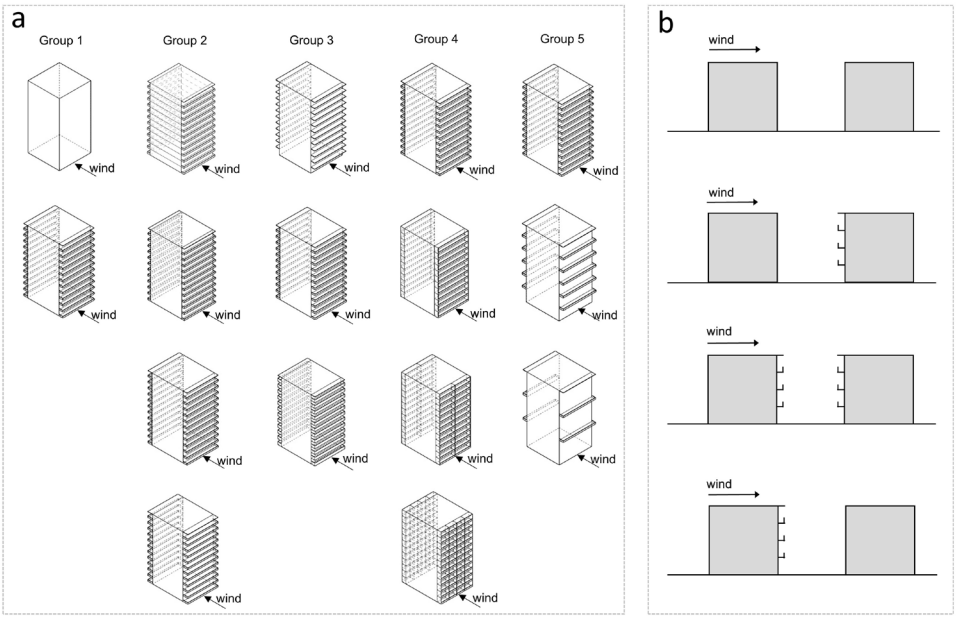

Fig. 4 Schematic representation of the CFD simulations to investigate: (a) the geometrical characteristics of buildings balconies for isolated buildings and (b) street canyons without and with balconies.

1.5 Thesis outline

This thesis is structured as follows:

Chapter 2: Comparative assessment of two turbulence modeling approaches, RANS and LES in predicting the near-façade airflow patterns and mean surface pressure for buildings with balconies. The evaluation is based on a detailed validation with wind-tunnel measurements of wind-induced mean surface pressure on the façade of a reduced-scale high-rise building;

Chapter 3: LES analysis of the impact of different geometrical characteristics of building balconies on mean surface pressure on the building façades and mean wind speed on balcony spaces. The focus is on (i) balconies present or not, (ii) balcony depth, (iii) balcony parapet walls, (iv) balcony partition walls and (v) density of balconies;

Chapter 4: Development of guidelines for minimum requirements of the domain size for 2.5D LES simulations of wind flow and pollutant dispersion in generic street canyons. The

LES simulations are conducted based on a detailed validation with wind-tunnel measurements of pollutant dispersion in a long street canyon;

Chapter 5: LES analysis of the impact of building balconies on wind flow and pollutant dispersion in generic street canyons. Four cases are evaluated: (i) a street canyon without balcony, (ii) a street canyon with balconies on both windward and leeward façades, (iii) a street canyon with balconies only on the windward façade and (iv) a street canyon with balconies only on the leeward façade.

The contents and the results of these chapters are further discussed in Chapter 6 (Limitations, future work and discussion) and the conclusions are outlined in Chapter 7 (Conclusions).

References

Ai, Z., Mak, C., Niu, J., 2013. Numerical investigation of wind-induced airflow and interunit dispersion characteristics in multistory residential buildings. Indoor Air 23, 417–429. https://doi.org/10.1111/ina.12041

Ai, Z., Mak, C., Niu, J., Li, Z., 2011. The assessment of the performance of balconies using computational fluid dynamics. Build. Serv. Eng. Res. Technol. 32, 229–243. https://doi.org/10.1177/0143624411404646

Al-Mulali, U., Binti, C.N., Sab, C., Fereidouni, H.G., 2012. Exploring the bi-directional long run relationship between urbanization, energy consumption, and carbon dioxide emission. Energy 46, 156–167. https://doi.org/10.1016/j.energy.2012.08.043

Antoniou, N., Montazeri, H., Wigo, H., Neophytou, M.K.-A., Blocken, B., Sandberg, M., 2017. CFD and wind-tunnel analysis of outdoor ventilation in a real compact heterogeneous urban area: Evaluation using “air delay.” Build. Environ. 126, 355–372. https://doi.org/10.1016/j.buildenv.2017.10.013

Blocken, B., 2018. LES over RANS in building simulation for outdoor and indoor applications: A foregone conclusion? Build. Simul. https://doi.org/10.1007/s12273-018-0459-3

Blocken, B., 2015. Computational Fluid Dynamics for urban physics: Importance, scales, possibilities, limitations and ten tips and tricks towards accurate and reliable simulations. Build. Environ. 91, 219–245. https://doi.org/10.1016/j.buildenv.2015.02.015

Blocken, B., 2014. 50 years of Computational Wind Engineering: Past, present and future. J. Wind Eng. Ind. Aerodyn. 129, 69–102.

https://doi.org/https://doi.org/10.1016/j.jweia.2014.03.008

Blocken, B., Carmeliet, J., 2008. Pedestrian wind conditions at outdoor platforms in a high-rise apartment building: generic sub-configuration validation, wind comfort assessment and uncertainty issues. Wind Struct. 11, 51–70. https://doi.org/10.12989/was.2008.11.1.051

Blocken, B., Carmeliet, J., 2004. Pedestrian Wind Environment around Buildings: Literature Review and Practical Examples. J. Therm. Envel. Build. Sci. 28, 107–159. https://doi.org/10.1177/1097196304044396

Brunekreef, B., Holgate, S.T., 2002. Air pollution and health. Lancet 360, 1233–1242. https://doi.org/10.1016/S0140-6736(02)11274-8

Cai, W.G., Wu, Y., Zhong, Y., Ren, H., 2009. China building energy consumption: Situation, challenges and corresponding measures. Energy Policy 37, 2054–2059. https://doi.org/10.1016/j.enpol.2008.11.037

Chan, C.K., Yao, X., 2008. Air pollution in mega cities in China. Atmos. Environ. 42, 1–42. https://doi.org/10.1016/j.atmosenv.2007.09.003

Clarke, J., 2001. Energy simulation in building design. Butterworth-Heinemann,Oxford.

Cóstola, D., Blocken, B., Hensen, J.L.M., 2009. Overview of pressure coefficient data in building energy simulation and airflow network programs. Build. Environ. 44, 2027–2036. https://doi.org/10.1016/j.buildenv.2009.02.006

Crawley, D.B., Hand, J.W., Kummert, M., Griffith, B.T., 2008. Contrasting the capabilities of building energy performance simulation programs. Build. Environ. 43, 661–673. https://doi.org/10.1016/j.buildenv.2006.10.027

Cui, D., Li, X., Du, Y., Mak, C.M., Kwok, K., 2020. Effects of envelope features on wind flow and pollutant exposure in street canyons. Build. Environ. 106862. https://doi.org/10.1016/j.buildenv.2020.106862

Gousseau, P., Blocken, B., Stathopoulos, T., van Heijst, G.J.F., 2015. Near-field pollutant dispersion in an actual urban area: Analysis of the mass transport mechanism by high-resolution Large Eddy Simulations. Comput. Fluids 114, 151–162. https://doi.org/10.1016/j.compfluid.2015.02.018

Gousseau, P., Blocken, B., van Heijst, G.J.F., 2011. CFD simulation of pollutant dispersion around isolated buildings: On the role of convective and turbulent mass fluxes in the prediction accuracy. J. Hazard. Mater. 194, 422–434. https://doi.org/10.1016/j.jhazmat.2011.08.008

Gromke, C., Ruck, B., 2009. On the impact of trees on dispersion processes of traffic

emissions in street canyons. Boundary-Layer Meteorol. 131, 19–34. https://doi.org/10.1007/s10546-008-9301-2

Hui, Y., Yuan, K., Chen, Z., Yang, Q., 2019. Characteristics of aerodynamic forces on high-rise buildings with various façade appurtenances. J. Wind Eng. Ind. Aerodyn. 191, 76–90. https://doi.org/10.1016/j.jweia.2019.06.002

International Energy Agency, 2018a. World Energy Balances: Overview (2018 Edition)). Paris.

International Energy Agency, 2018b. CO2 Emissions From Fuel Combustion Highlights. Paris.

Izadyar, N., Miller, W., Rismanchi, B., Garcia-Hansen, V., 2020. A numerical investigation of balcony geometry impact on single-sided natural ventilation and thermal comfort. Build. Environ. 106847. https://doi.org/10.1016/j.buildenv.2020.106847

Kahsay, M.T., Bitsuamlak, G.T., Tariku, F., 2019. CFD simulation of external CHTC on a high-rise building with and without façade appurtenances. Build. Environ. 165, 106350. https://doi.org/10.1016/j.buildenv.2019.106350

Karkoulias, V.A., Marazioti, P.E., Georgiou, D.P., Maraziotis, E.A., 2019. Computational Fluid Dynamics modeling of the trace elements dispersion and comparison with measurements in a street canyon with balconies in the city of Patras, Greece. Atmos. Environ. 117210. https://doi.org/10.1016/j.atmosenv.2019.117210

Kaseb, Z., Hafezi, M., Tahbaz, M., Delfani, S., 2020. A framework for pedestrian-level wind conditions improvement in urban areas: CFD simulation and optimization. Build. Environ. 184, 107191. https://doi.org/10.1016/j.buildenv.2020.107191

Kubilay, A., Neophytou, M.K.-A., Matsentides, S., Loizou, M., Carmeliet, J., 2017. The pollutant removal capacity of urban street canyons as quantified by the pollutant exchange velocity. Urban Clim. 21, 136–153. https://doi.org/https://doi.org/10.1016/j.uclim.2017.06.003

Lateb, M., Meroney, R.N., Yataghene, M., Fellouah, H., Saleh, F., Boufadel, M.C., 2016. On the use of numerical modelling for near-field pollutant dispersion in urban environments − A review. Environ. Pollut. 208, 271–283. https://doi.org/10.1016/j.envpol.2015.07.039

Liu, C.-H., Wong, C.C.C., 2014. On the pollutant removal, dispersion, and entrainment over two-dimensional idealized street canyons. Atmos. Res. 135-136, 128–142. https://doi.org/10.1016/j.atmosres.2013.08.006

Llaguno-Munitxa, M., Bou-Zeid, E., Hultmark, M., 2017. The influence of building geometry on street canyon air flow: Validation of large eddy simulations against wind tunnel experiments. J. Wind Eng. Ind. Aerodyn. 165, 115–130.

https://doi.org/10.1016/j.jweia.2017.03.007

Maruta, E., Kanda, M., Sato, J., 1998. Effects on surface roughness for wind pressure on glass and cladding of buildings. J. Wind Eng. Ind. Aerodyn. 74, 651–663. https://doi.org/10.1016/S0167-6105(98)00059-2

Montazeri, H., Blocken, B., 2013. CFD simulation of wind-induced pressure coefficients on buildings with and without balconies: Validation and sensitivity analysis. Build. Environ. 60, 137–149. https://doi.org/10.1016/j.buildenv.2012.11.012

Montazeri, H., Blocken, B., Derome, D., Carmeliet, J., Hensen, J.L.M., 2015. CFD analysis of forced convective heat transfer coefficients at windward building facades: Influence of building geometry. J. Wind Eng. Ind. Aerodyn. 146, 102–116. https://doi.org/10.1016/j.jweia.2015.07.007

Montazeri, H., Blocken, B., Janssen, W.D., van Hooff, T., 2013. CFD evaluation of new second-skin facade concept for wind comfort on building balconies: Case study for the Park Tower in Antwerp. Build. Environ. 68, 179–192. https://doi.org/10.1016/j.buildenv.2013.07.004

Morgan, M.H., 1914. De architectura libri decem, English Translation.

Mozaffari Ghadikolaei, F., Ossen, D.R., Mohamed, M.F., 2020. Effects of wing wall at the balcony on the natural ventilation performance in medium-rise residential buildings. J. Build. Eng. 31, 101316. https://doi.org/10.1016/j.jobe.2020.101316

Murakami, S., 1993. Comparison of various turbulence models applied to a bluff body. J. Wind Eng. Ind. Aerodyn. 46-47, 21–36. https://doi.org/10.1016/0167-6105(93)90112-2

Murakami, S., 1990a. Computational wind engineering. J. Wind Eng. Ind. Aerodyn. 36, 517–538. https://doi.org/10.1016/0167-6105(90)90335-A

Murakami, S., 1990b. Computational wind engineering. J. Wind Eng. Ind. Aerodyn. 36, 517–538. https://doi.org/10.1016/0167-6105(90)90335-A

Murakami, S., Mochida, A., Hayashi, Y., 1990. Examining the κ-ϵ model by means of a wind tunnel test and large-eddy simulation of the turbulence structure around a cube. J. Wind Eng. Ind. Aerodyn. 35, 87–100. https://doi.org/10.1016/0167-6105(90)90211-T

Murakami, S., Mochida, A., Hayashi, Y., Sakamoto, S., 1992. Numerical study on velocity-pressure field and wind forces for bluff bodies by κ-ϵ, ASM and LES. J. Wind Eng. Ind. Aerodyn. 44, 2841–2852. https://doi.org/10.1016/0167-6105(92)90079-P

Murena, F., Mele, B., 2016. Effect of balconies on air quality in deep street canyons. Atmos. Pollut. Res. 7, 1004–1012. https://doi.org/10.1016/j.apr.2016.06.005

Nova, A., 2006. The role of the winds in architectural theory from Vitruvius to Scamozzi, Aeolian Winds and the Spirit in Renaissance Architecture: Academia Eolia Revisited. Routledge.

O'Neill, J.J., Cai, X.-M., Kinnersley, R., 2016. Stochastic backscatter modelling for the prediction of pollutant removal from an urban street canyon: A large-eddy simulation. Atmos. Environ. 142, 9–18. https://doi.org/10.1016/j.atmosenv.2016.07.024

Omrani, S., Garcia-Hansen, V., Capra, B.R., Drogemuller, R., 2017. On the effect of provision of balconies on natural ventilation and thermal comfort in high-rise residential buildings. Build. Environ. 123, 504–516. https://doi.org/10.1016/j.buildenv.2017.07.016

Ramponi, R., Angelotti, A., Blocken, B., 2014. Energy saving potential of night ventilation: Sensitivity to pressure coefficients for different European climates. Appl. Energy 123, 185–195. https://doi.org/10.1016/j.apenergy.2014.02.041

Ramponi, R., Blocken, B., 2012. CFD simulation of cross-ventilation for a generic isolated building: Impact of computational parameters. Build. Environ. 53, 34–48. https://doi.org/10.1016/j.buildenv.2012.01.004

Rodi, W., 1997. Comparison of LES and RANS calculations of the flow around bluff bodies. J. Wind Eng. Ind. Aerodyn. 69-71, 55–75. https://doi.org/10.1016/S0167-6105(97)00147-5

Rossi, R., Philips, D.A., Iaccarino, G., 2010. A numerical study of scalar dispersion downstream of a wall-mounted cube using direct simulations and algebraic flux models. Int. J. Heat Fluid Flow 31, 805–819. https://doi.org/10.1016/j.ijheatfluidflow.2010.05.006

Salim, S.M., Buccolieri, R., Chan, A., Sabatino, S. Di, 2011. Numerical simulation of atmospheric pollutant dispersion in an urban street canyon: Comparison between RANS and LES. Jnl. Wind Eng. Ind. Aerodyn. 99, 103–113. https://doi.org/10.1016/j.jweia.2010.12.002

Stathopoulos, T., 1997. Computational wind engineering: Past achievements and future challenges. J. Wind Eng. Ind. Aerodyn. 67-68, 509–532. https://doi.org/10.1016/S0167-6105(97)00097-4

Stathopoulos, T., 1984. Wind loads on low-rise buildings: a review of the state of the art. Eng. Struct. 6, 119–135. https://doi.org/10.1016/0141-0296(84)90005-1

Stathopoulos, T., Zhu, X., 1990. Wind pressures on buildings with mullions. J. Struct. Eng. 116, 2272–2291.

Stathopoulos, T., Zhu, X., 1988. Wind pressures on building with appurtenances. J. Wind Eng. Ind. Aerodyn. 31, 265–281. https://doi.org/10.1016/0167-6105(88)90008-6

Tominaga, Y., Stathopoulos, T., 2011. CFD modeling of pollution dispersion in a street canyon: Comparison between LES and RANS. J. Wind Eng. Ind. Aerodyn. 99, 340–348. https://doi.org/10.1016/j.jweia.2010.12.005

Tominaga, Y., Stathopoulos, T., 2007. Turbulent Schmidt numbers for CFD analysis with various types of flowfield. Atmos. Environ. 41, 8091–8099. https://doi.org/10.1016/j.atmosenv.2007.06.054

van Hooff, T., Blocken, B., Gousseau, P., van Heijst, G.J.F., 2014. Counter-gradient diffusion in a slot-ventilated enclosure assessed by LES and RANS. Comput. Fluids 96, 63–75. https://doi.org/10.1016/j.compfluid.2014.02.020

World Health Organization, 2016. WHO Global Urban Ambient Air Pollution Database (update 2016). Geneva, Switzerland.

Yuan, K., Hui, Y., Chen, Z., 2018. Effects of facade appurtenances on the local pressure of high-rise building. J. Wind Eng. Ind. Aerodyn. 178, 26–37. https://doi.org/10.1016/j.jweia.2018.05.004

Zhong, J., Cai, X.-M., Bloss, W.J., 2015. Modelling the dispersion and transport of reactive pollutants in a deep urban street canyon: Using large-eddy simulation. Environ. Pollut. 200, 42–52. https://doi.org/10.1016/j.envpol.2015.02.009

Zhou, L., Dickinson, R.E., Tian, Y., Fang, J., Li, Q., Kaufmann, R.K., Tucker, C.J., Myneni, R.B., 2004. Evidence for a significant urbanization effect on climate in China. Proc. Natl. Acad. Sci. U. S. A. 101, 9540–4. https://doi.org/10.1073/pnas.0400357101

Chapter 2

CFD simulations of wind flow and mean surface pressure for buildings with balconies: Comparison of RANS and LES

This chapter has been published as a peer-reviewed journal paper:

CFD simulations of wind flow and mean surface pressure for buildings with balconies: Comparison of RANS and LES

X. Zheng, H. Montazeri, B. Blocken

Building and Environment 173, 106747

Abstract: Façade geometrical details can substantially influence the near-façade airflow patterns and pressures. This is especially the case for building balconies as their presence can lead to multiple separation and recirculation areas near the façades and hence large changes in surface pressure distribution. Computational fluid dynamics (CFD) has been widely used to investigate the impact of building balconies, mainly based on the steady Reynolds-averaged Navier-Stokes (RANS) approach. The objective of the present study is to evaluate the performance of steady RANS versus large-eddy simulations (LES) in predicting the near-façade airflow patterns and mean surface pressure coefficients (C_p) for a building with balconies for three wind directions θ = 0°, 90°, 180°, where 0° is perpendicular to the façade under study. The evaluation is based on validation with wind-tunnel measurements of C_p. The results show that both RANS and LES can accurately predict C_p on the windward façade for θ = 0° with average absolute deviations of 0.113 and 0.091 from the measured data, respectively. For the other two wind directions, LES is clearly superior. For θ = 90°, the average absolute deviations for RANS and LES are 0.302 and 0.096, while these are 0.161 and 0.038 for θ = 180°. Large differences are found in the computed flow fields on the balcony spaces. Because RANS systematically underestimates the absolute values of both C_p and mean wind speed on the balconies, it is suggested that building design based on RANS might result in excessive ventilation and in too high wind nuisance level.

2.1 Introduction

Building façade geometrical details such as balconies can significantly affect the near-façade airflow patterns and the surface pressure distributions on building façades [1–5]. For example, the presence of balconies can change the local mean pressure coefficient (C_p) on the windward façade of a high-rise building by about 0.7 [2]. Similarly, it can lead to a reduction of about 30% in the surface-averaged C_p on the windward façade of a low-rise building [4]. Therefore, a better understanding of the impact of façade geometrical details in general, and building balconies in particular on the near-façade airflow patterns and the pressure distributions on the façade is essential for the accurate evaluation of wind-induced natural ventilation [6,7], wind comfort on balcony spaces [8], pollutant dispersion [9], wind loads on building walls and building components [10] and convective heat transfer at building surfaces [11–13].

Apart from wind-tunnel testing [1–3,5,14,15], computational fluid dynamics (CFD) has been used to investigate the impact of building façade geometrical details on the near-façade airflow and the local and surface-averaged wind-induced pressure on the façades. An overview of CFD studies on buildings with façade geometrical details is given in Table 1. It can be seen that the vast majority of these studies focused on buildings with balconies. In addition, steady Reynolds-averaged Navier-Stokes (RANS) simulations have been widely used in these studies, while the use of more advanced scale-resolving turbulence modeling approaches is scarce, and limited to the studies by Ai and Mak [16], Llaguno-Munitxa et al. [17] and Murena & Mele [18] in which large-eddy simulation (LES) and scale-adaptive simulation (SAS) have been used. The good performance of RANS approach in predicting the C_p on the windward façade of a building with balconies for both perpendicular ($\theta = 0^\circ$) and oblique ($\theta = 45^\circ$) wind directions was shown in Ref. [5]. However, such good performance could not be shown for the leeward façade, where steady RANS systematically underestimated the absolute value of C_p for the two wind directions [4]. This is mainly attributed to the well-known deficiencies of steady RANS in accurately reproducing flow separation, recirculation and reattachment, and its inability to capture vortex shedding in the wake [19]. The additional façade geometrical features introduce a multitude of areas with flow separation, recirculation and reattachment which can amplify the impact of the steady RANS deficiencies on the calculated C_p. LES, on the other hand, can provide accurate

descriptions of the mean and instantaneous flow field around isolated buildings [20–23] and in complex urban areas [24–27], and the wind induced aerodynamic loads on building surfaces [28–32]. For example, LES has been widely employed to obtain the mean and fluctuating pressure on surfaces of low-rise buildings [33], buildings with wall openings [34], super-tall buildings [35], building-like square cylinders [36–39], high-rise buildings with elliptical shape [40], and standard tall buildings [41–47]. Several earlier studies have compared the performance of RANS and LES and showed the superior performance of LES [48–55], though it is usually achieved at the expense of rather large requirements in terms of computational resources [26,48,56,57]. However, almost all these studies were performed for buildings with smooth façades. To the best knowledge of the authors, the performance of RANS and LES for buildings with façade geometrical details has not yet been systematically investigated. Therefore, the objective of the present paper is to investigate the ability of steady RANS and LES to reproduce wind flow and mean surface pressure coefficients for buildings with balconies in order to gain insights into their performance for CFD simulations for buildings with various types of façade geometrical details. The study is performed for different approach-flow wind directions and based on validation with wind-tunnel measurements of mean surface pressure coefficients by Stathopoulos and Zhu [2].

Table 1. Overview of CFD studies on airflow around buildings with façade geometrical details.

Reference	Building configuration (building height)	Façade geometrical details	Turbulence modeling approach	Wind direction	Validation	Investigated parameter
(Murakami, 1990) [27]	19-story (-)[1]	Balconies	Steady RANS	0°[2]	No	V
(Prianto & Depecker, 2002) [58]	2-story (8.5 m)	Balconies	Steady RANS	0°	No	V
(Ai et al., 2011) [59]	5-story (15 m)	Balconies	Steady RANS	0°	Yes [1]	V, C_p
(Ai et al., 2011) [60]	5-, 10- and 15-story (15 m, 30 m and 45 m)	Balconies	Steady RANS	0°, 22.5°, 45°, 67.5°, 90°	Yes [1]	C_p
(Ai et al., 2013) [61]	5-story (15 m)	Balconies	Steady RANS	0°	Yes [1]	V, ACH
(Montazeri et al., 2013) [8]	22-story (78 m)	Double skin/balconies	Steady RANS	0°-360° (30° intervals)	Yes [1]	V
(Montazeri & Blocken, 2013) [4]	5-story (15 m)	Balconies	Steady RANS	0°, 45°	Yes [1]	C_p
(Ai & Mak, 2016) [16]	5-story (13.5 m)	Balconies	LES	0°, 45°, 90°	Yes [62]	ACH, PC
(Murena & Mele, 2016) [18]	4-strory (18 m)[3]	Balconies	SAS	0°[4]	No	PC
(Llaguno-Munitxa et al., 2017) [17]	5-strory (-)[1,3]	Balconies	LES	0°[4]	Yes [17]	V
(Omrani et al., 2017) [63]	36-story (-)[1]	Balconies	Steady RANS	0°, 45°, 90°, 180°	Yes [63]	V
(Kahsay et al., 2019) [12]	30-story (100 m)	Horizontal/vertical shadings	Steady RANS	0°, 22.5°, 45°, 67.5°, 90°	Yes [64]	CHTC
(Karkoulias et al. 2019) [9]	7-story (28 m)[3]	Balconies	RANS	0°[4]	Yes	PC

V = Mean velocity, C_p = Mean pressure coefficient, ACH = Air change rate per hour, PC = Pollutant concentration, CHTC = Convective heat transfer coefficient, SAS = Scale-adaptive simulation

[1] Building height was not reported.

[2] Approximately 0°.

[3] Cases were considered as street canyons.

[4] Perpendicular to the long street canyon axis.

In Section 2, the wind-tunnel experiments are briefly described. Section 3 presents the computational settings and parameters. The validation of the CFD results is provided in Section 4. Section 5 compares the results obtained by RANS and LES. A discussion on limitations of this study and the main conclusions are presented in Sections 6 and 7, respectively.

2.2 Description of the wind-tunnel experiment

Stathopoulos and Zhu [2] measured mean surface pressures on the façade of a reduced-scale model of a high-rise building with different types of balconies and for different approach-flow wind directions at a scale 1:400. The measurements were performed in the atmospheric boundary layer open-circuit wind-tunnel of the Centre for Building Studies at Concordia University. The wind-tunnel test section was 12.2 m long and had a cross-section of 1.8 × 1.8 m^2. The approach-flow mean velocity and longitudinal turbulence intensity profiles were measured at the center of the turntable in the empty tunnel (i.e. without building model present) [2], and hence represent the so-called incident profiles [65]. The profiles (shown in Fig. 1) reproduced an open country terrain exposure with aerodynamic roughness length of 0.0001 m (model scale, corresponding to 0.04 m at full scale), and the reference wind speed (U_{ref}) of approximate 14 m/s at gradient height (H_g = 0.625 m, corresponding to 250 m at full scale). The incident longitudinal turbulence intensity ranged from 20% near ground level to about 7% at gradient height [2].

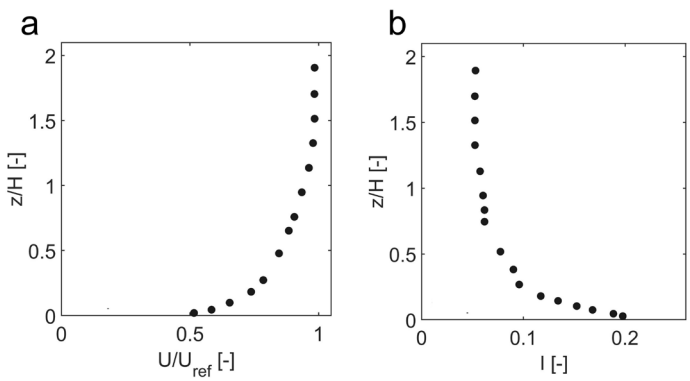

Fig. 1. Measured profiles of (a) normalized mean wind speed U/U_{ref} and (b) turbulence intensity I, modified from [2].

The 30-story isolated building model had dimensions W × D × H = 0.152 × 0.152 × 0.3 m^3 (60.8 × 60.8 × 120 m^3 at full scale). Balconies were provided only on one façade (Fig. 2).

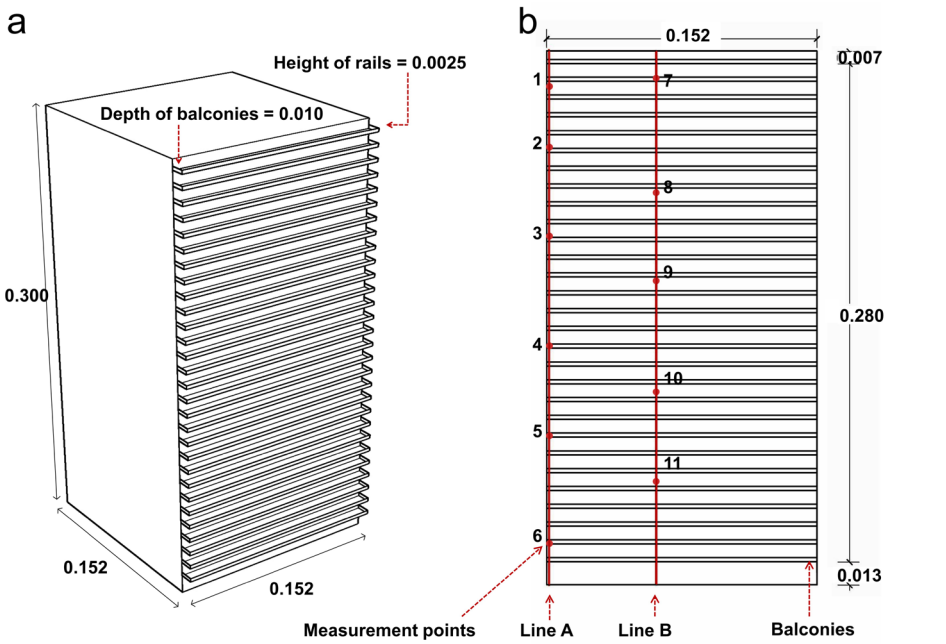

Fig. 2 (a) Geometry of building model and balconies; (b) Measurement points and lines used for CFD validation. All dimensions are in meter at model scale.

Four types of balcony were tested: (i) balconies with 0.005 m depth (2 m at full scale) without a parapet wall, (ii) balconies with 0.01 m depth (4 m at full scale) without a parapet wall, (iii) balconies with 0.01 m depth and 0.0025 m (1 m at full scale) parapet walls, and (iv) balconies with 0.01 m depth (4 m at full scale) and 0.005 m parapet walls (2 m at full scale). The measurements were performed for 3 approach-flow wind directions relative to the façade with the balconies: 0°, 90°, and 180°. In the present study, the focus will be on the case with balconies of 0.01 m depth and with 0.0025 m parapet walls (Fig. 2). The pressure measurements were performed along 7 vertical lines located on the façade with balconies. In the present study, the measured data along two of these lines will be used. Note that the measured data along the other five lines were not reported in Ref. [2]. In the remainder of this paper, we will refer to the two lines as line A (located 0.0015 m (0.6 m in full scale) from

the left edge of the façade with balconies) and line B (located 0.061 m (24.4 m in full scale) from the left edge of the façade with balconies). The measurements were performed using a SETRA-237 pressure transducer. The overall uncertainty of the C_p measurements was estimated to be less than 5% [66].

2.3 CFD simulations: Computational settings and parameters

2.3.1 Computational domain and grid

The CFD simulations are performed at the reduced scale (wind-tunnel scale). For the RANS simulations, the dimensions of the computational domain are based on the best practice guidelines by Franke et al. [67] and Tominaga et al. [68]. The upstream and downstream domain lengths are 5H and 15H, respectively, where H is the height of the building model (= 0.3 m). The height of the domain is 5H. The computational grids are generated using the surface-grid extrusion technique developed by van Hooff and Blocken [69]. The RANS domain for $\theta = 0°$ and 90° is shown in Fig. 3a, and the grid on the building and ground surfaces is shown in Figs. 3b-d. The grid consists of 5,230,396 hexahedral cells. 31, 8, and 4 cells are used along the width and depth of the balconies and along the height of parapet walls, respectively (Fig. 3c). The maximum stretching ratio of 1.2 controls the cells in the whole computational domain, which is in line with the best practice guidelines [67,68]. The grid resolution is based on a grid-sensitivity analysis using three different grids generated by coarsening and refining the basic grid. The details of the grid-sensitivity analysis will be provided in Section 3.4. Note that the grid shown in Figs. 3a-d is also used for $\theta = 90°$, while another grid with the same topology and resolution is made for $\theta = 180°$.

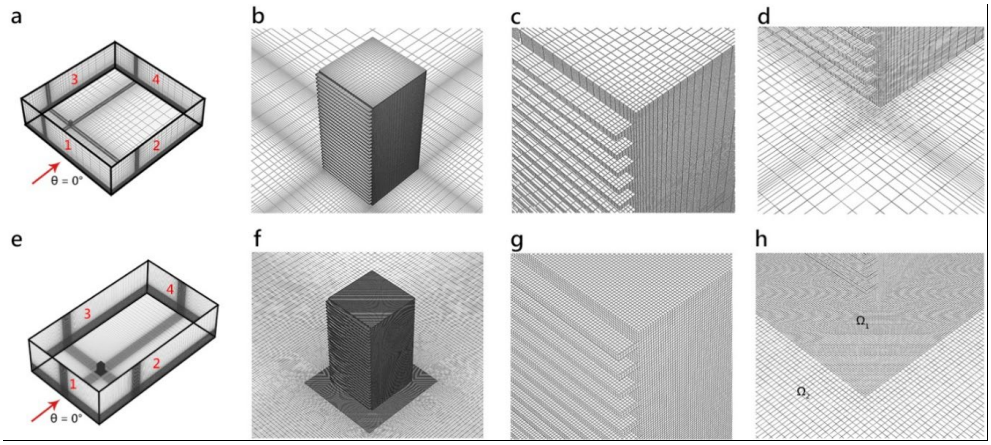

Fig. 3. (a-d) Computational grid for RANS simulation ($\theta = 0°$): (a) Grid at the bottom and side faces of the domain; (b) Grid at the building surfaces and part of ground surface; (c) Grid at the surfaces of balconies near the roof and (d) near the ground. (e-h) Same for the computational grid for LES ($\theta = 0°$).

Figs. 3e-h display the domain and the grid for the LES simulation for $\theta = 0°$. The upstream domain length is limited to 4H to reduce the extent of unintended streamwise gradients in the approach-flow profiles [70–72]. The downstream domain length is 10H [67,68]. The height of the domain is 4H, which is smaller than the one recommended by Franke et al. [67] and Tominaga et al. [68], in order to reduce the total number of cells and the computational time. The resulting blockage ratio is 1.4%, which is well below the maximum value of 3.0% recommended by the aforementioned guidelines [67,68]. A non-conformal grid is employed, where the whole domain is discretized into two subdomains: Ω_1 (the inner grid) and Ω_2, where subdomain Ω_1 is extended up to a distance of approximately H/6 away from the building surfaces (Fig. 3h). The grid refinement ratio between the adjacent subdomains is 1:2, which is in line with recommendations by Iousef et al. [70]. Cubic cells (cells with the same x, y, z lengths) are applied in subdomain Ω_1, with 120, 8, and 2 cells along the width and depth of the balconies and along the height of parapet walls, respectively (Fig. 3g). In subdomain Ω_2 hexahedral cells with a stretching ratio of 1.05 are used. In this case, the total number of cells is 19,267,200. The quality of the LES grid is evaluated using LES index of quality (LES_{IQ}), which will be presented in Section 3.5. Note that additional grids with the same topology and the same grid resolution are made for $\theta = 90°$ and $\theta = 180°$.

2.3.2 Boundary conditions

For θ = 0°, in both Figs. 3a and e, plane 1 is the inlet plane, plane 4 is the outlet plane, and planes 2 and 3 are the side planes. For the RANS simulation, for θ = 90° (Fig. 3a), planes 3 and 2 are the inlet and the outlet planes, respectively, and planes 1 and 4 are the side planes.

The inlet boundary conditions are based on the measured data (Fig. 1). Eq. (1) is employed to fit the measured vertical profile of the mean wind speed U, where κ is the von Karman constant (= 0.41). Note that u^*_{ABL} is estimated to be 0.7 m/s based on the measured mean wind speed, while the aerodynamic roughness length z_0 = 0.0001 m has been reported in Ref. [2]. The turbulent kinetic energy k is calculated according to Eq. (2), based on the mean wind velocity U from Eq. (1) and the measured longitudinal turbulence intensity I_u [2]. In Eq. (2), a = 1 is chosen according to Tominaga et al. [68]. The turbulence dissipation rate ε is calculated using Eq. (3). For LES, the vortex method [73,74] is adopted to impose a time-dependent velocity profile at the inlet of the domain. It was shown that this method could accurately reproduce the mean velocity field [75] and mean pressure coefficients on building surfaces [47]. The number of vortices N_V is 8500, which is based on $N_V = N/4$ where N is the number of grid cells at the inlet plane [76].

$$U(z) = \frac{u^*_{ABL}}{k} \ln\left(\frac{z + z_0}{z_0}\right) \tag{1}$$

$$k(z) = a\left(I_u(z)U(z)\right)^2 \tag{2}$$

$$\varepsilon(z) = \frac{u^{*3}_{ABL}}{k(z + z_0)} \tag{3}$$

For the RANS simulations, the standard wall functions by Launder and Spalding [77] with roughness modification by Cebeci and Bradshaw [78] are applied at the ground surface. The sand grain roughness height k_s and the roughness constant C_s are determined according to their consistent relationship with the aerodynamic roughness length z_0 (Eq. 4) derived by Blocken et al. [79].

$$k_s = \frac{9.793 z_0}{C_s} \tag{4}$$

For the LES, the Werner-Wengle wall functions are applied [80], which assumes either a linear or 1/7 power law distribution of instantaneous velocity in the first cell [81]. Zero static gauge pressure is applied at the outlet plane and symmetry boundary conditions (zero normal gradients of all variables) are imposed at the top and lateral sides of the domains in both RANS and LES simulations.

2.3.3 Solver settings

The commercial CFD code ANSYS Fluent 18.0 is employed to perform the simulations. The RANS simulations are performed on the HPC cluster of the Unit Building Physics & Services at the Department of the Built Environment of Eindhoven University of Technology. The cluster has a 16-core node (Intel(R) Xeon(R) CPU - X5650 @ 2.7 GHz). The LES simulations are performed on the Dutch national supercomputer SURFSARA, Cartesius (www.surfsara.nl) with a 24-core node (Intel(R) Xeon(R) CPU - E5-2690 v3 @ 2.6 GHz).

For the RANS simulations, the realizable k-ε turbulence model is used for closure [82]. This turbulence model has been successfully used on many occasions in the past for CFD simulations of wind flow around buildings and in urban areas [4,83–87]. Second-order discretization schemes are utilized for both the convection and the viscous terms of the governing equations. The SIMPLE algorithm is used for the pressure-velocity coupling. Convergence is assumed to be obtained when the scaled normalized residuals stabilize at a minimum of 10^{-4} for continuity, 10^{-7} for x, y and z momentum and 10^{-6} for k and ε. In addition, values of the mean surface static pressures at all measurement points along lines A and B (shown in Fig. 2b) are monitored to ensure that they remain constant throughout the iterations near the end of the iterative process.

For the LES simulations, the wall-adapting local eddy viscosity subgrid-scale model (WALE) is employed with the constant $C_{wale} = 0.325$. Pressure-velocity coupling is performed using the fractional step method in combination with the non-iterative time advancement scheme [81]. For pressure interpolation and time discretization, second-order schemes are applied. The time step is $\Delta t = 4\times10^{-5}$ s. The resulting maximum and volume-averaged Courant-Friedrichs-Lewy number (CFL) are 1.287 and 0.046, respectively. Note that the CFL number larger than 1 occurs only in a few cells close to the leading edge of the building roof. The LES simulations are initialized with the solution of steady RANS simulations. Then the LES initializations run for $T_{init} = 1.52$ s, corresponding to approximately 5 flow-through times

($T_{flow\text{-}through} = L_x/U_{ref}$, where L_x is the length of the computational domain, U_{ref} is the reference wind speed that is taken at the gradient height). After the initialization, the statistical sampling is conducted for T_{avg} = 6.67 s, which is approximately 21 flow-through times.

2.3.4 Grid-sensitivity study for the RANS grid

The grid-sensitivity analysis for the RANS grid is performed for θ = 0°. Two additional grids are generated: a fine gird and a coarse grid, where the coarsening and refining is performed with an overall linear factor of approximately 1.3. The fine and coarse grids have 8,421,600 and 2,310,016 cells, where 10 and 6 cells are used along the depth of each balcony, respectively. Fig. 4 presents C_p along line A (Figs. 4a and b) and line B (Fig. 4c) obtained from the three grids. The average absolute difference between the $C_{p\text{-}coarse}$ and the $C_{p\text{-}basic}$ is 0.036, while this is 0.016 between the $C_{p\text{-}basic}$ grid and $C_{p\text{-}fine}$. The grid-convergence index (GCI) proposed by Roache [88], given by Eq. (5), is also used to estimate the error in the $C_{p\text{-}basic}$ and $C_{p\text{-}coarse}$:

$$GCI_2(\%) = \frac{F_s|(C_{p\text{-}2} - C_{p\text{-}1})|r^p}{1 - r^p} \times 100\% \quad (5)$$

where r is the linear grid refinement factor, p is the formal order of accuracy, which in this analysis is considered to be 2 since second-order discretization schemes are used for the simulations. The safety factor F_s = 1.25 is taken, which is the recommended value when three or more grids are considered [88]. $C_{p\text{-}2}$ is the mean pressure coefficient from a relatively coarse grid and $C_{p\text{-}1}$ is the mean pressure coefficient from a relatively fine grid. For the windward façade, the surface-averaged GCI_{basic} grid and GCI_{coarse} are 2.35% and 3.42%, respectively. It indicates that the basic grid provides nearly grid-independent results and it is therefore used in the remainder of the study for the RANS simulations.

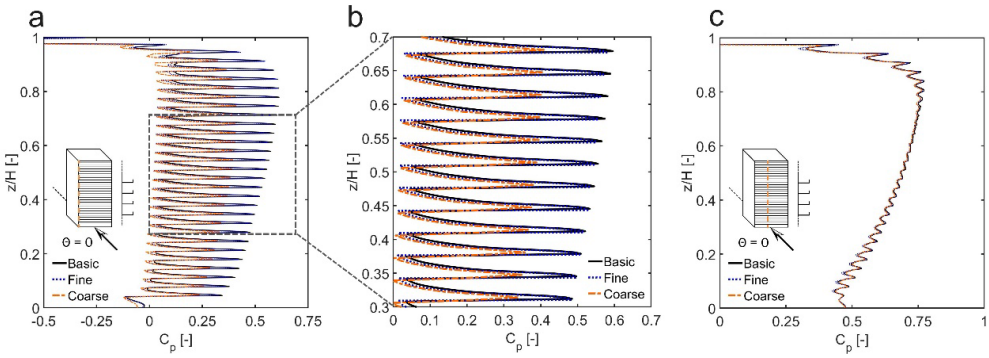

Fig. 4. Results for RANS grid-sensitivity analysis: C_p (a) along line A (b) detail view along line A and (c) along line B for the three grids.

2.3.5 Index of quality for the LES grid

The LES index of quality (LES_{IQ}) is used to measure the quality of the LES grid. This index is defined as the ratio of the resolved turbulent kinetic energy to the total turbulent kinetic energy, which will be examined with the equation by Celik et al. [89] involving the molecular viscosity ν and turbulent viscosity ν_{sgs}.

$$LES_{IQ} = \frac{k_{resolved}}{k_{total}} = \frac{1}{1 + 0.05\left(\frac{\nu + \nu_{sgs}}{\nu}\right)^{0.53}} \tag{6}$$

According to Pope [90], in a well-resolved computation, at least 80% of the turbulent kinetic energy is resolved. Fig. 5 shows profiles of LES_{IQ} along 5 vertical lines in the vertical centerplane for θ = 0°. The results indicate that the computation clearly resolves a large portion of the total turbulent kinetic energy along the 5 lines, with the overall average and minimum LES_{IQ} of 92.6% and 79.4%, respectively. For the whole domain, the volume-averaged amount of total kinetic energy resolved is 92.9%. As a result, if the threshold of 80% is used, it may conclude that the LES computations resolve a sufficient amount of turbulent kinetic energy.

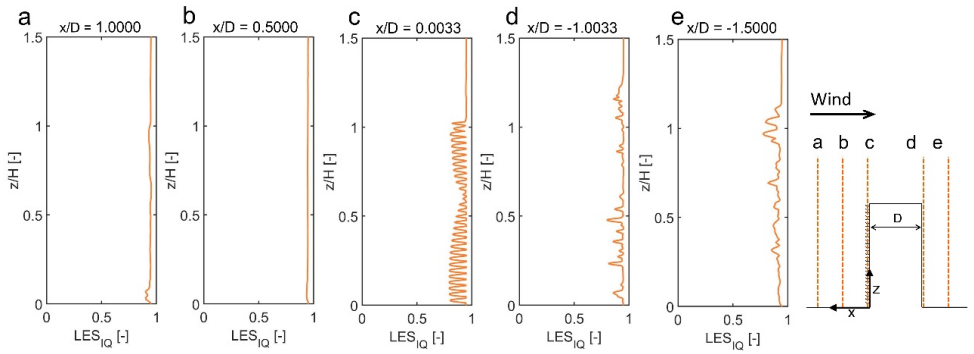

Fig. 5. Profiles of LES_{IQ} in vertical centerplane for ϑ = 0°: (a) x/D = 1, (b) x/D = 0.5, (c) x/D = 0.0033, (d) x/D = -1.0033 and (e) x/D = -1.5.

2.4 CFD simulations: validation

The C_p predicted by RANS and LES are compared with the measured data [2] for the three wind directions. Note that for θ = 0° and θ = 90°, the measured data at point 8 (the second point on line B as shown in Fig. 2) was not reported in Ref. [2]. The C_p is computed as:

$$C_p = \frac{P - P_0}{0.5\rho U_{ref}^2} \tag{7}$$

where P is the mean static pressure on the building surface, P_0 is the reference static pressure, ρ is the air density (1.225 kg/m^3), and U_{ref} is the reference wind speed that is taken at the gradient height. Note that, according to the information provided in Ref. [66], the Pitot-static tube was mounted at the gradient height above the test-section floor, while its exact distance relative to the building model was not reported. This is because the wind-tunnel at Concordia University has a test section roof that can be adjusted to enable a zero longitudinal static pressure gradient, therefore the actual measurement location for the reference pressure was not that important in the measurements. However, in the CFD simulations, the top of the computational domain is a horizontal surface, which causes streamwise gradients along the domain length. In the present study, the static pressure obtained by the CFD simulations at the point 0.6 m upstream of the building and at the same height of the Pitot-static tube in the measurements is taken as the reference pressure (P_0). Note that at this point, small streamwise static pressure gradients are observed in both

RANS and LES results. The resulting P_0 values are 4.1 Pa and 3.5 Pa for RANS and LES, respectively.

In order to quantify the agreement between the CFD (RANS and LES) results and the wind-tunnel results, absolute deviations and two other validation metrics are used: fractional bias (FB) and normalized mean square error (NMSE) [91]. The metrics are calculated using Eqs. (8) and (9):

$$\mathrm{NMSE} = \frac{[(C_{p(WT)} - C_{p(CFD)})^2]}{[C_{p(WT)}][C_{p(CFD)}]} \tag{8}$$

$$\mathrm{FB} = \frac{2([C_{p(WT)}] - [C_{p(CFD)}])}{[C_{p(WT)}] + [C_{p(CFD)}]} \tag{9}$$

where the square brackets indicate averaging over the data points.

Table 2 lists the values of the validation metrics and Fig. 6 compares the simulated and measured C_p along lines A and B for the three approach-flow wind directions.

Table 2. Validation metrics for C_p.

			Line A		Line B		Overall	
		Ideal value	RANS	LES	RANS	LES	RANS	LES
θ = 0°	Absolute deviation	0	0.172	0.133	0.026	0.027	0.113	0.091
θ = 90°	Absolute deviation	0	0.289	0.090	0.307	0.104	0.302	0.096
	NMSE	0	0.313	0.023	0.363	0.028	0.371	0.025
	FB	0	0.537	0.141	0.575	0.164	0.581	0.151
θ = 180°	Absolute deviation	0	0.175	0.036	0.147	0.041	0.161	0.038
	NMSE	0	0.275	0.009	0.224	0.013	0.305	0.010
	FB	0	0.501	0.086	0.455	0.110	0.525	0.096

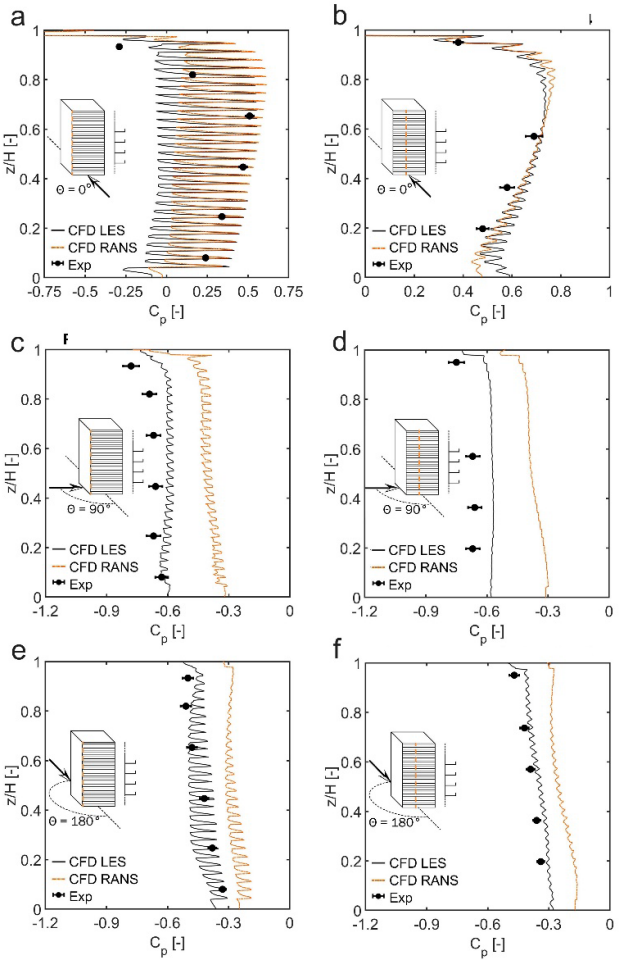

Fig. 6. Comparison between C_p obtained by CFD (RANS and LES) and from wind-tunnel measurements, along (a) line A and (b) line B at ϑ = 0°; (c-d) same for ϑ = 90° and (e-f) ϑ =180°.

For θ = 0°, the overall average absolute deviations (lines A and B combined) for RANS and LES are 0.113 and 0.091, respectively. A fairly good agreement can be seen between CFD and wind-tunnel along line B for both RANS and LES (Fig. 6b), with the average absolute deviations of 0.026 and 0.027. For line A, these deviations increase to 0.172 and 0.133, respectively (Fig. 6a). Note that FB and NMSE cannot be used for variables that have both positive and negative values within the same set [70,91,92], hence, they are not reported for θ = 0° in Table 2. Fig. 6a shows large vertical C_p gradients along line A, which makes the validation difficult. Therefore, in this study, a small sensitivity analysis is performed with as parameter the vertical position of the measurement points along the two lines. Fig. 7 shows

the results of the sensitivity analysis for points 2, 3, 4 and 5 on line A (as shown in Fig. 2). It indicates a significant sensitivity of C_p to the vertical location of the measurement points. For example, if the measured point 5 in the wind-tunnel would shift upward by $\Delta z = 0.001$ m, the absolute deviations between RANS and wind-tunnel would decrease from 0.129 to 0.046. For LES, this reduction would be from 0.132 to 0.004 (Fig. 7d). In the remainder of this paper, all analyses will be performed based on the original reported position in the measurements.

For $\theta = 90°$, both steady RANS and LES tend to overpredict C_p along the vertical lines but this overprediction is much more pronounced for steady RANS with an overall average absolute deviation of 0.302, while this is 0.096 for LES. The overall agreement of LES remains fairly good in terms of NMSE = 0.025 (Table 2), which is about one order of magnitude smaller than RANS.

For $\theta = 180°$, the deficiency of RANS in reproducing C_p can also be clearly observed, where the overall absolute deviation goes up to 0.161, while this is 0.038 for LES. The underprediction of the absolute value of C_p on the leeward façade by RANS is in line with the results of previous studies (e.g. [4,93,94]).

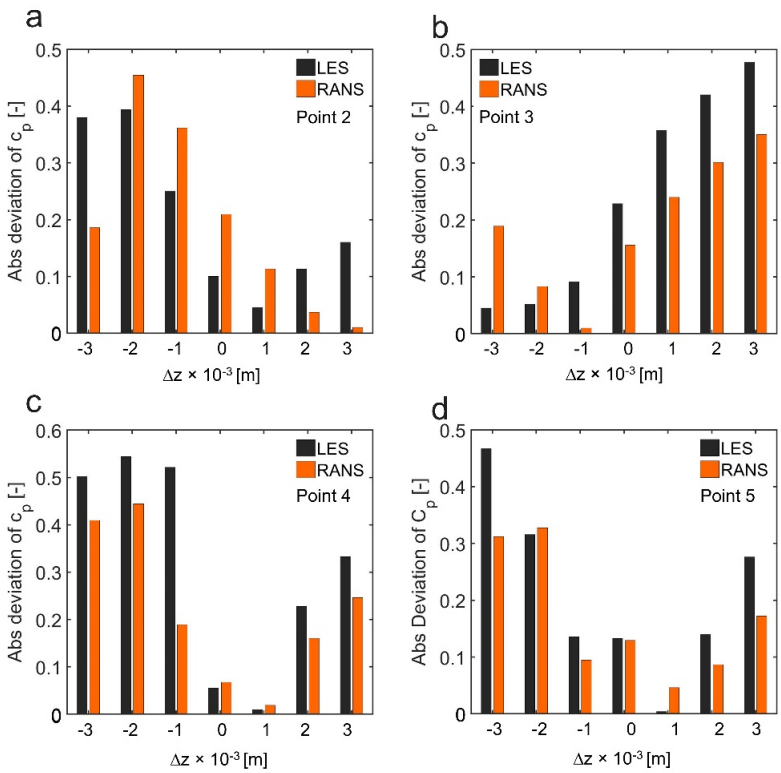

Fig. 7. The sensitivity of absolute deviation of C_p to the vertical position for (a) Point 2; (b) Point 3; (c) Point 4 and (d) Point 5 along line A shown in Fig. 2b.

2.5 CFD simulations: Comparison between RANS and LES

The results provided in Section 4 clearly show the different performance of RANS and LES in predicting the C_p at the measurement points, especially for θ = 90° and 180°. In this section, a detailed analysis of (i) C_p, (ii) mean wind speed ratio (K), and (iii) maximum mean wind speed ratio (K_{max}) is provided to better understand the performance of the two approaches and to provide more insight into the distribution of C_p, K and K_{max} on the balcony areas. The analysis is performed for the three approach-flow wind directions.

2.5.1 RANS versus LES at θ = 0°

Figs. 8a and b present C_p on the windward façade by RANS and LES, respectively. Fig. 8c shows the difference between C_p by the two approaches, i.e. $\Delta C_{p\ (LES\text{-}RANS)} = C_{p\ (LES)} - C_{p\ (RANS)}$. It can be seen that strong suction acts on the top floor for both RANS and LES. The largest

differences occur at this level where the maximum underestimation and overestimation of the LES results by RANS occur in the middle ($\Delta C_{p\ (LES\text{-}RANS)}$ = 0.610) and near the edges ($\Delta C_{p\ (LES\text{-}RANS)}$ = -0.461) of the façade, respectively. For the other parts of the façade, RANS and LES perform fairly similar with local absolute $\Delta C_{p\ (LES\text{-}RANS)}$ lower than 0.150. For the entire windward façade, the surface-averaged C_p values obtained by RANS and LES are 0.507 and 0.511, respectively ($\Delta C_{p\ (LES\text{-}RANS)}$ = 0.004), indicating a very close agreement between the two approaches.

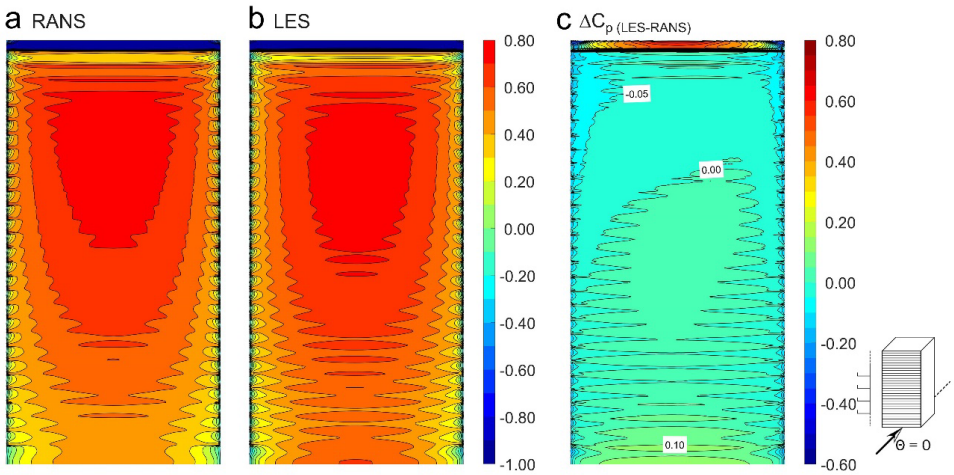

Fig. 8. Distributions of C_p on the façade with balconies at ϑ = 0° obtained by (a) RANS and (b) LES, and (c) $\Delta C_{p\ (LES\text{-}RANS)}$.

Figs. 9a and b display contours of the mean wind speed ratio K in horizontal planes at pedestrian height (1.75 m in full scale above balcony level) for levels 2, 11, 20 and 29 predicted by RANS and LES, respectively. K is defined as the local mean wind speed normalized by $U_{ambient}$ (= 6.347 m/s), which is the "undisturbed" mean wind speed at pedestrian height above ground level. Fig. 9c shows the difference $\Delta K_{(LES\text{-}RANS)} = K_{(LES)} - K_{(RANS)}$. Both RANS and LES predict high wind-speed regions at the edges of the balconies, while low wind-speed regions can be observed in the middle of the planes (Figs. 9a and b). Compared to LES, RANS underestimates the local K for all levels (also those not shown in Fig. 9). The area-weighted average K for levels 2, 11, 20 and 29 by LES are 0.959, 0.815, 0.6667 and 1.038, respectively. They are underestimated by RANS by 34.9%, 33.3%, 17.4% and 38.9%, respectively.

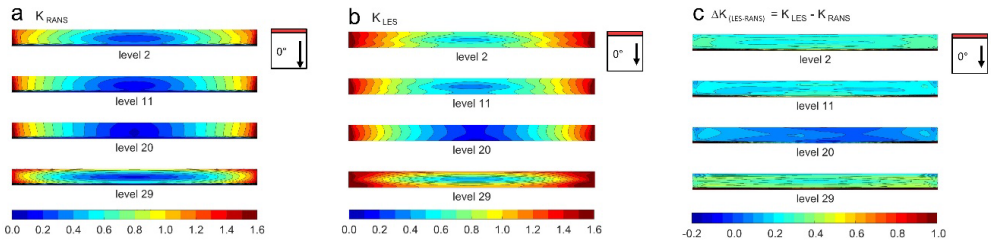

Fig. 9. Contours of mean wind speed ratio K in horizontal planes at pedestrian height (1.75 m at equivalent full scale) on balconies for levels 2, 11, 20 and 29 for $\vartheta = 0°$, obtained by (a) RANS and (b) LES, and (c) $\Delta K_{(LES\text{-}RANS)}$ for the same levels.

Fig. 10 presents the K distribution and 2D velocity vector fields in the vertical centerplane near levels 2, 11, 19 and 29. Both RANS and LES predict the flow separation from the top-edge of the parapet wall of the top floor that leads to a strong suction pressure on the façade (see Figs. 8a and b). The stagnation point occurs at around level 19. For balconies on levels 28 and 29, the interaction between the airflow directed from the stagnation region upward leads to clockwise recirculation areas on the balcony spaces. These recirculation areas can also be found for all balconies above level 21 (not shown in Fig. 10). Compared to LES, RANS underestimates the mean velocity on the balcony spaces. For the stagnation region (near level 19) where the wind speed is relatively low, RANS and LES predict fairly similar results. For the levels between level 17 and level 1, the downwash flow separates at the balcony parapet walls, leading to anticlockwise recirculation areas on each balcony space. Again, compared to LES, steady RANS underestimates the mean velocity on these balcony spaces.

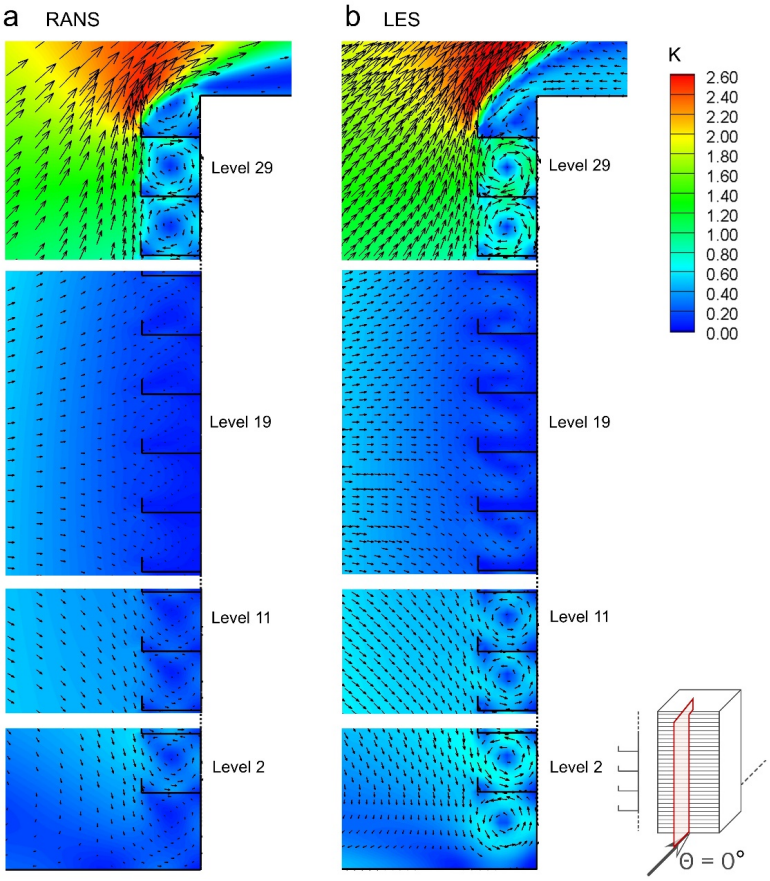

Fig. 10. Distribution of mean wind speed ratio K and 2D velocity vector field in the vertical centerplane near the balconies of levels 2, 11, 20, and 29 for $\vartheta = 0°$ obtained by (a) RANS and (b) LES.

Fig. 11 presents K_{max} taken from the horizontal planes at pedestrian height for all balconies as obtained by RANS and LES. The maximum local mean wind speed ratio (K_{max}) that is sometimes used to evaluate the wind environment [95,96] is defined as $K_{max} = U_{max}/U_{ambient}$, where U_{max} is the maximum local mean wind speed at pedestrian height on each balcony space. Note that, as shown in Fig. 9, balconies on the high-rise building are partly exposed to strong winds, which may cause wind discomfort and wind danger for people on balcony spaces. It can be seen that, compared to LES, RANS predicts substantially lower K_{max} for all levels. In this case, the average absolute difference for all balconies is 0.249, while the maximum absolute difference is 0.457, which occurs on level 28.

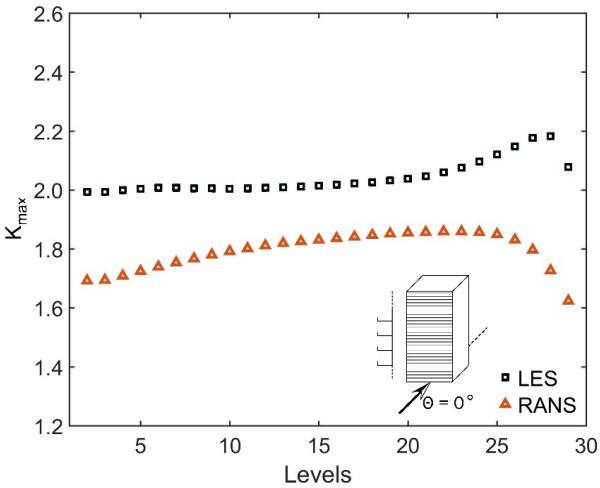

Fig. 11. Maximum mean wind speed ratio K_{max} in horizontal planes at pedestrian height (1.75 m at equivalent full scale) from level 2 to level 29 for ϑ = 0°.

2.5.2 RANS versus LES at θ = 90°

Fig. 12 presents the distribution of C_p across the façade at θ = 90° by RANS and LES, revealing large differences between the simulation results by the two approaches. RANS clearly underestimates the absolute value of local C_p across the entire façade except in a small region close to the leading edge of the top floor (Fig. 12c). The surface-averaged C_p obtained by RANS and LES are -0.369 and -0.578, respectively ($\Delta C_{p\,(LES\text{-}RANS)}$ = -0.209).

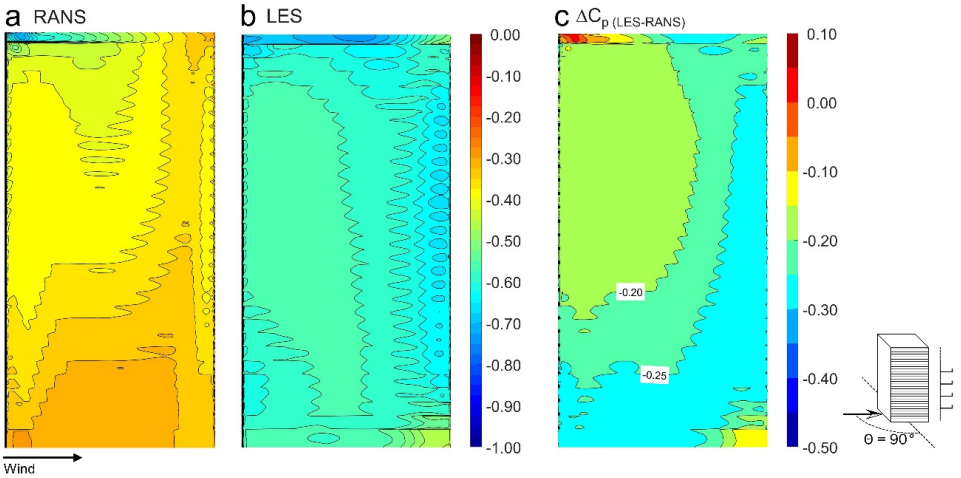

Fig. 12. Distribution of C_p on the façade with balconies for $\vartheta = 90°$ obtained by (a) RANS and (b) LES, and (c) $\Delta C_{p\ (LES\text{-}RANS)}$.

Fig. 13 illustrates the K_{max} in the horizontal planes at pedestrian height for all balconies obtained by RANS and LES. Compared to LES, RANS predicts substantially lower K_{max} for all levels. In this case, the average absolute difference for all balconies is about 0.542, while the maximum absolute difference is 0.647 that occurs on level 6.

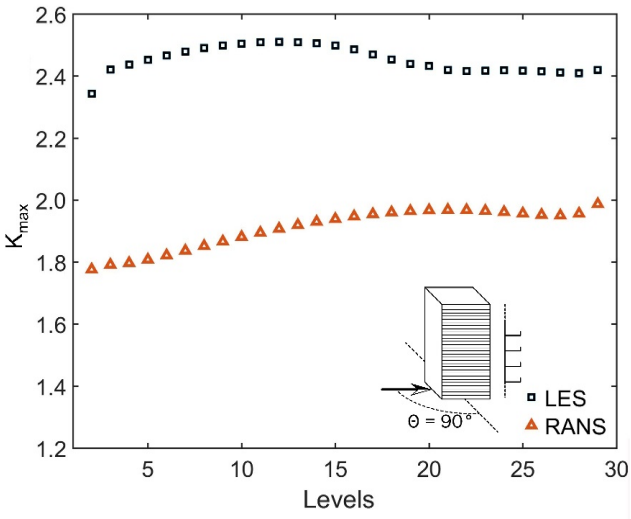

Fig. 13. Maximum mean wind speed ratio K_{max} in horizontal planes at pedestrian height (1.75 m at equivalent full scale) from levels 2 to 29 for $\vartheta = 90°$.

2.5.3 RANS versus LES at θ = 180°

Fig. 14 presents the C_p distribution obtained by RANS and LES for θ = 180°. Compared to LES, RANS underpredicts the absolute value of C_p across the entire façade. The maximum and minimum underprediction occur in areas close to the façade edges and in the central region of the façade, respectively (Fig. 14c). The surface-averaged C_p by RANS and LES are -0.251 and -0.357, respectively ($\Delta C_{p\ (LES\text{-}RANS)}$ = -0.106).

Concerning K in horizontal planes at pedestrian height for levels 2, 11, 20 and 29, compared to LES, RANS mostly predicts lower local K for every level. The area-weighted average K of levels 2, 11, 20 and 29 by LES are 0.313, 0.388, 0.380, and 0.229, which are underestimated by RANS by 34.9%, 32.5%, 46.2% and 67.9%, respectively.

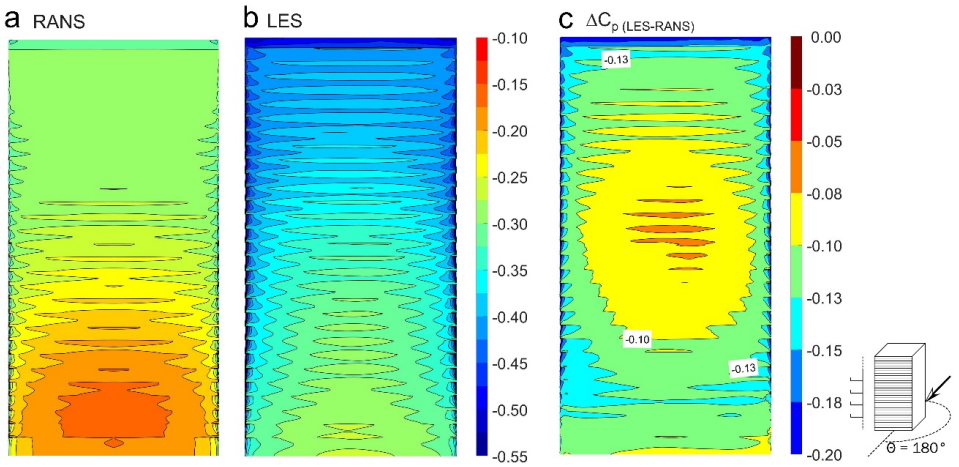

Fig. 14. Distribution of C_p on the façade with balconies for ϑ = 180° obtained by (a) RANS and (b) LES, and (c) $\Delta C_{p\ (LES\text{-}RANS)}$.

Fig. 15 provides the mean wind speed ratio (K) and the 2D velocity vector field in the vertical centerplane. It can be seen that RANS significantly underestimates the wind speed near level 29. This underestimation leads to the overestimation of C_p in this region (see Fig. 14c). A similar underestimation of the wind speed by RANS can be seen for levels 1 and 2, which is in line with previous CFD studies of ground-level wind conditions in the wake of buildings [56,97]. A likely reason for these discrepancies is the performance of RANS in

overestimating the turbulent kinetic energy in separation and recirculation areas, which generally leads to an underestimation of the mean wind speed in these areas [19,20].

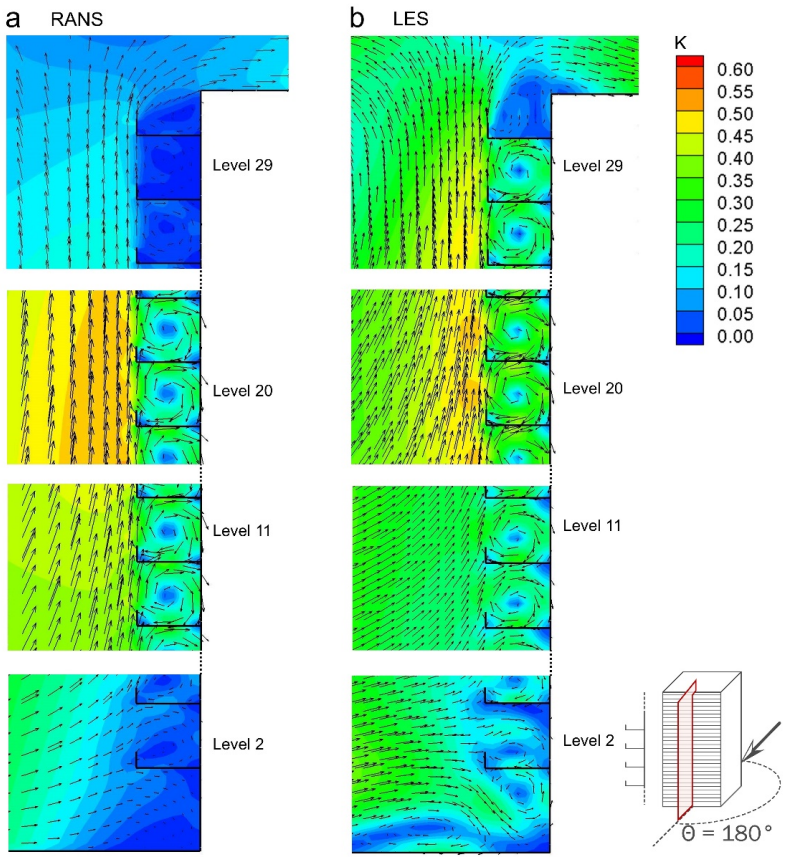

Fig. 15. Distributions of mean wind speed ratio K and 2D velocity vector field in vertical centerplane on the balconies of level 2, 11, 20, and 29 at ϑ = 180° (a) by RANS and (b) by LES.

Fig. 16 shows K_{max} in the horizontal planes at pedestrian height for all balconies obtained by RANS and LES. RANS provides larger K_{max} for levels 2, 3 and 4 than LES, where the maximum absolute difference of 0.122 occurs on the second level. For all other levels, RANS substantially underestimates K_{max}, where the maximum absolute difference is 0.343 that can be observed on level 18.

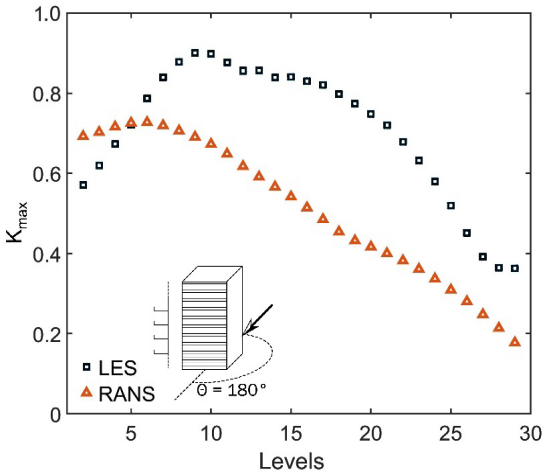

Fig. 16. Maximum mean wind speed ratio K_{max} in horizontal planes at pedestrian height (1.75 m equivalent full scale) from level 2 to level 29 for ϑ = 180°.

2.6 Discussion [2]

It is important to highlight the limitations of this study:

- In this study, the validation is performed based on mean pressure coefficients. This is due to the lack of available high-resolution experimental data of wind velocity for buildings with balconies. Further research is required to (i) perform high-resolution wind-tunnel or on-site measurements of wind speed on balcony spaces, and (ii) conduct additional detailed CFD validation studies where the focus would be on wind speed on building balconies.

[2] Note that the computational cost for the LES simulation is more than two orders of magnitude larger than the steady RANS simulation. Assuming an HPC cluster with a 16-core node (Intel(R) Xeon(R) CPU - X5650 @ 2.7 GHz) is used for both RANS and LES, the computational time for the RANS simulations will be less than 8 hours, while the LES simulation will take more than 8 weeks. It is recommended that the choice of the model (RANS vs. LES) should be made depending on which parameter is the target parameter.

- The simulations are performed for only three approaching wind directions: θ = 0°, 90° and 180°. This is due to the lack of available high-quality experimental data for buildings with balconies under oblique wind directions. Further research should focus on the performance of RANS and LES for oblique wind directions.
- The focus of the present study is on the comparison between RANS and LES. As RANS can only predict the mean pressure coefficients, the validation studies are performed for mean pressure coefficients. Future work should focus on the performance of LES in predicting surface r.m.s. and peak pressure coefficients for buildings with balconies. It should be noted that there is still a lack of high-resolution experimental data of surface r.m.s. and peak pressure coefficients for buildings with balconies. Therefore, high-quality wind-tunnel measurements should also be performed in the future.
- This study only focuses on an isolated high-rise building with balconies. The presence of surrounding buildings may lead to more airflow complexity such as additional recirculation and reattachment [98], and would modify the mean and r.m.s. surface pressure [45,99–101] and wind speed on balcony spaces [102]. Therefore, the conclusions in this paper should be used with caution towards buildings surrounded by other buildings. Further evaluation of the performance of RANS and LES should be performed by considering the impact of building surroundings.

2.7 Conclusions

This paper evaluates the performance of steady RANS and LES in predicting the near-façade airflow patterns and mean surface pressure coefficient (C_p) for a building with balconies. Three wind directions are considered: θ = 0°, 90°, and 180°.

The evaluation is based on validation with wind-tunnel measurements of mean surface pressure on the façade with balconies. The results of the CFD validation show that LES can accurately predict C_p on the building façade with balconies for θ = 0°, 90°, and 180° with average absolute deviations of 0.091, 0.096 and 0.038, respectively. RANS predicts a satisfactory agreement with the experiments only for θ = 0°, with an average absolute deviation of 0.113. For θ = 90° and θ = 180°, however, RANS substantially underestimates

the absolute value of the C_p with average absolute deviations of 0.302 and 0.161, respectively. Further detailed analysis is performed based on the RANS and LES results, and the following conclusions are obtained:

- For θ = 0°, RANS and LES generally predict similar local C_p except at the top floor. The surface-averaged C_p obtained by RANS and LES are 0.507 and 0.511, respectively. Compared to LES, RANS generally underestimates the absolute value of local C_p on the façade at θ = 90° and θ = 180°. The surface-averaged C_p obtained by RANS and LES for θ = 90° are -0.369 and -0.578, respectively, and for θ = 180° they are -0.251 and -0.357, respectively.
- Compared to LES, RANS generally underestimates the mean wind speed ratio K in horizontal planes at pedestrian height on all levels for θ = 0° and θ = 180°. For example, the area-weighted average K at levels 2, 11, 20 and 29 for θ = 0° is underestimated by 34.9%, 33.3%, 17.4% and 38.9%, respectively, and for θ = 180° it is underestimated by 34.9%, 32.5%, 46.2% and 67.9%, respectively. For θ = 90°, compared to LES, RANS overestimates K in some regions, while providing underestimations in others.
- Compared to LES, RANS underestimates K_{max} on all levels for θ = 0° and 90°. For θ = 180°, RANS predicts larger K_{max} for levels 2, 3 and 4, and smaller K_{max} for the other levels.

These results suggest that for studies of natural ventilation of buildings and wind comfort on building balconies, for which distributions of building façade C_p are required, using RANS instead of LES can result in underestimated computed ventilation airflow rates and in underestimated computed wind speed ratios. In other words, building design based on RANS might result in too high actual ventilation flow rates and in too high actual wind speed, resulting in too high wind nuisance level.

Acknowledgments

The authors gratefully acknowledge the partnership with ANSYS CFD. This work has been sponsored by NWO Exacte en Natuurwetenschappen (Physical Sciences) for the use of supercomputer facilities, with financial support from the Nederlandse Organisatie voor Wetenschappelijk Onderzoek (Netherlands Organization for Scientifici Research, NWO).

References

[1] I. Chand, P.K. Bhargava, N.L.V. Krishak, Effect of balconies on ventilation inducing aeromotive force on low-rise buildings, Build. Environ. 33 (1998) 385–396. https://doi.org/10.1016/S0360-1323(97)00054-1.

[2] T. Stathopoulos, X. Zhu, Wind pressures on building with appurtenances, J. Wind Eng. Ind. Aerodyn. 31 (1988) 265–281. https://doi.org/10.1016/0167-6105(88)90008-6.

[3] E. Maruta, M. Kanda, J. Sato, Effects on surface roughness for wind pressure on glass and cladding of buildings, J. Wind Eng. Ind. Aerodyn. 74 (1998) 651–663. https://doi.org/10.1016/S0167-6105(98)00059-2.

[4] H. Montazeri, B. Blocken, CFD simulation of wind-induced pressure coefficients on buildings with and without balconies: Validation and sensitivity analysis, Build. Environ. 60 (2013) 137–149. https://doi.org/10.1016/j.buildenv.2012.11.012.

[5] T. Stathopoulos, X. Zhu, Wind pressures on buildings with mullions, J. Struct. Eng. 116 (1990) 2272–2291.

[6] L. Gullbrekken, S. Uvsløkk, T. Kvande, K. Pettersson, B. Time, Wind pressure coefficients for roof ventilation purposes, J. Wind Eng. Ind. Aerodyn. 175 (2018) 144–152. https://doi.org/10.1016/j.jweia.2018.01.026.

[7] R. Ramponi, A. Angelotti, B. Blocken, Energy saving potential of night ventilation: Sensitivity to pressure coefficients for different European climates, Appl. Energy. 123 (2014) 185–195. https://doi.org/10.1016/j.apenergy.2014.02.041.

[8] H. Montazeri, B. Blocken, W.D. Janssen, T. van Hooff, CFD evaluation of new second-skin facade concept for wind comfort on building balconies: Case study for the Park Tower in Antwerp, Build. Environ. 68 (2013) 179–192. https://doi.org/10.1016/j.buildenv.2013.07.004.

[9] V.A. Karkoulias, P.E. Marazioti, D.P. Georgiou, E.A. Maraziotis, Computational Fluid Dynamics modeling of the trace elements dispersion and comparison with measurements in a street canyon with balconies in the city of Patras, Greece, Atmos. Environ. (2019) 117210. https://doi.org/10.1016/j.atmosenv.2019.117210.

[10] T. Stathopoulos, Wind loads on low-rise buildings: a review of the state of the art, Eng. Struct. 6 (1984) 119–135. https://doi.org/10.1016/0141-0296(84)90005-1.

[11] H. Montazeri, B. Blocken, Extension of generalized forced convective heat transfer coefficient expressions for isolated buildings taking into account oblique wind directions, Build. Environ. 140 (2018) 194–208. https://doi.org/10.1016/j.buildenv.2018.05.027.

[12] M.T. Kahsay, G.T. Bitsuamlak, F. Tariku, CFD simulation of external CHTC on a high-rise building with and without façade appurtenances, Build. Environ. 165 (2019) 106350. https://doi.org/10.1016/j.buildenv.2019.106350.

[13] H. Montazeri, B. Blocken, New generalized expressions for forced convective heat transfer coefficients at building facades and roofs, Build. Environ. 119 (2017) 153–168. https://doi.org/10.1016/J.BUILDENV.2017.04.012.

[14] Y. Hui, K. Yuan, Z. Chen, Q. Yang, Characteristics of aerodynamic forces on high-rise buildings with various façade appurtenances, J. Wind Eng. Ind. Aerodyn. 191 (2019) 76–90. https://doi.org/10.1016/j.jweia.2019.06.002.

[15] K. Yuan, Y. Hui, Z. Chen, Effects of facade appurtenances on the local pressure of high-rise building, J. Wind Eng. Ind. Aerodyn. 178 (2018) 26–37. https://doi.org/10.1016/j.jweia.2018.05.004.

[16] Z.T. Ai, C.M. Mak, Large eddy simulation of wind-induced interunit dispersion around multistory buildings, Indoor Air. 26 (2016) 259–273. https://doi.org/10.1111/ina.12200.

[17] M. Llaguno-Munitxa, E. Bou-Zeid, M. Hultmark, The influence of building geometry on street canyon air flow: Validation of large eddy simulations against wind tunnel experiments, J. Wind Eng. Ind. Aerodyn. 165 (2017) 115–130. https://doi.org/10.1016/j.jweia.2017.03.007.

[18] F. Murena, B. Mele, Effect of balconies on air quality in deep street canyons, Atmos. Pollut. Res. 7 (2016) 1004–1012. https://doi.org/10.1016/J.APR.2016.06.005.

[19] S. Murakami, Comparison of various turbulence models applied to a bluff body, J. Wind Eng. Ind. Aerodyn. 46–47 (1993) 21–36. https://doi.org/10.1016/0167-6105(93)90112-2.

[20] Y. Tominaga, A. Mochida, S. Murakami, S. Sawaki, Comparison of various revised k–ε models and LES applied to flow around a high-rise building model with 1:1:2 shape placed within the surface boundary layer, J. Wind Eng. Ind. Aerodyn. 96 (2008) 389–411. https://doi.org/10.1016/j.jweia.2008.01.004.

[21] Y. Du, B. Blocken, S. Pirker, A novel approach to simulate pollutant dispersion in the built environment: transport-based recurrence CFD, Build. Environ. (2019) 106604. https://doi.org/10.1016/j.buildenv.2019.106604.

[22] S. Murakami, A. Mochida, K. Hibi, Three-dimensional numerical simulation of air flow around a cubic model by means of large eddy simulation, J. Wind Eng. Ind. Aerodyn. 25 (1987) 291–305. https://doi.org/10.1016/0167-6105(87)90023-7.

[23] Y. Tominaga, S. Murakami, A. Mochida, CFD prediction of gaseous diffusion around a cubic model using a dynamic mixed SGS model based on composite grid technique, J. Wind Eng. Ind. Aerodyn. 67–68 (1997) 827–841. https://doi.org/10.1016/S0167-6105(97)00122-0.

[24] N. Antoniou, H. Montazeri, H. Wigo, M.K.-A. Neophytou, B. Blocken, M. Sandberg, CFD and wind-tunnel analysis of outdoor ventilation in a real compact heterogeneous urban area: Evaluation using “air delay,” Build. Environ. 126 (2017) 355–372. https://doi.org/10.1016/j.buildenv.2017.10.013.

[25] P. Gousseau, B. Blocken, T. Stathopoulos, G.J.F. van Heijst, CFD simulation of near-field pollutant dispersion on a high-resolution grid: A case study by LES and RANS for a building group in downtown Montreal, Atmos. Environ. 45 (2011) 428–438. https://doi.org/10.1016/j.atmosenv.2010.09.065.

[26] Y. Tominaga, T. Stathopoulos, CFD simulation of near-field pollutant dispersion in the urban environment: A review of current modeling techniques, Atmos. Environ. 79 (2013) 716–730. https://doi.org/10.1016/j.atmosenv.2013.07.028.

[27] S. Murakami, Computational wind engineering, J. Wind Eng. Ind. Aerodyn. 36 (1990) 517–538. https://doi.org/10.1016/0167-6105(90)90335-A.

[28] Y. Luo, H. Liu, H. Xue, K. Lin, Large-eddy simulation evaluation of wind loads on a high-rise building based on the multiscale synthetic eddy method, Adv. Struct. Eng. 22 (2019) 997–1006. https://doi.org/10.1177/1369433218794258.

[29] M.. Leschziner, Computational modelling of complex turbulent flow - expectations, reality and prospects, J. Wind Eng. Ind. Aerodyn. 46–47 (1993) 37–51. https://doi.org/10.1016/0167-6105(93)90113-3.

[30] T. Tamura, K. Nozawa, K. Kondo, AIJ guide for numerical prediction of wind loads on buildings, J. Wind Eng. Ind. Aerodyn. 96 (2008) 1974–1984. https://doi.org/10.1016/j.jweia.2008.02.020.

[31] A.K. Dagnew, G.T. Bitsuamlak, Computational evaluation of wind loads on buildings: A review, Wind Struct. An Int. J. 16 (2013) 629–660. https://doi.org/10.12989/was.2013.16.6.629.

[32] M. Ricci, L. Patruno, I. Kalkman, S. de Miranda, B. Blocken, Towards LES as a design tool: Wind loads assessment on a high-rise building, J. Wind Eng. Ind. Aerodyn. 180 (2018) 1–18. https://doi.org/10.1016/j.jweia.2018.07.009.

[33] K. Nozawa, T. Tamura, Large eddy simulation of the flow around a low-rise building immersed in a rough-wall turbulent boundary layer, J. Wind Eng. Ind. Aerodyn. 90 (2002) 1151–1162. https://doi.org/10.1016/S0167-6105(02)00228-3.

[34] K. Hibi, H. Ueda, T. Wakahara, K. Shimada, Use of large eddy simulation to measure fluctuating pressure fields around buildings with wall openings, J. Wind Eng. Ind. Aerodyn. 46–47 (1993) 239–244. https://doi.org/10.1016/0167-6105(93)90289-Z.

[35] B. Yan, Q. Li, Large-eddy simulation of wind effects on a super-tall building in urban environment conditions, Struct. Infrastruct. Eng. 12 (2016) 765–785. https://doi.org/10.1080/15732479.2015.1051997.

[36] S. Murakami, A. Mochida, S. Sakamoto, CFD analysis of wind-structure interaction for oscillating square cylinders, J. Wind Eng. Ind. Aerodyn. 72 (1997) 33–46. https://doi.org/10.1016/S0167-6105(97)00245-6.

[37] Y. Maruyama, T. Tamura, Y. Okuda, M. Ohashi, LES of fluctuating wind pressure on a 3D square cylinder for PIV-based inflow turbulence, J. Wind Eng. Ind. Aerodyn. 122 (2013) 130–137. https://doi.org/10.1016/j.jweia.2013.07.001.

[38] Y. Cao, T. Tamura, H. Kawai, Investigation of wall pressures and surface flow patterns on a wall-mounted square cylinder using very high-resolution Cartesian mesh, J. Wind Eng. Ind. Aerodyn. 188 (2019) 1–18. https://doi.org/10.1016/j.jweia.2019.02.013.

[39] S. Sakamoto, S. Murakami, A. Mochida, Numerical study on flow past 2D square cylinder by Large Eddy Simulation: Comparison between 2D and 3D computations, J. Wind Eng. Ind. Aerodyn. 50 (1993) 61–68. https://doi.org/10.1016/0167-6105(93)90061-R.

[40] B.W. Yan, Q.S. Li, Detached-eddy and large-eddy simulations of wind effects on a high-rise structure, Comput. Fluids. 150 (2017) 74–83. https://doi.org/10.1016/j.compfluid.2017.02.009.

[41] S.J. Daniels, I.P. Castro, Z.-T. Xie, Peak loading and surface pressure fluctuations of a tall model building, J. Wind Eng. Ind. Aerodyn. 120 (2013) 19–28. https://doi.org/10.1016/j.jweia.2013.06.014.

[42] H. Aboshosha, A. Elshaer, G.T. Bitsuamlak, A. El Damatty, Consistent inflow turbulence generator for LES evaluation of wind-induced responses for tall buildings, J. Wind Eng. Ind. Aerodyn. 142 (2015) 198–216. https://doi.org/10.1016/j.jweia.2015.04.004.

[43] A.K. Dagnew, G.T. Bitsuamlak, Computational evaluation of wind loads on a standard tall building using les, Wind Struct. An Int. J. 18 (2014) 567–598. https://doi.org/10.12989/was.2014.18.5.567.

[44] A.L. Braun, A.M. Awruch, Aerodynamic and aeroelastic analyses on the CAARC standard tall building model using numerical simulation, Comput. Struct. 87 (2009) 564–581. https://doi.org/10.1016/j.compstruc.2009.02.002.

[45] A. Elshaer, H. Aboshosha, G. Bitsuamlak, A. El Damatty, A. Dagnew, LES evaluation of wind-induced responses for an isolated and a surrounded tall building, Eng. Struct. 115 (2016) 179–195. https://doi.org/10.1016/j.engstruct.2016.02.026.

[46] S. Huang, Q.S. Li, S. Xu, Numerical evaluation of wind effects on a tall steel building by CFD, J. Constr. Steel Res. 63 (2007) 612–627. https://doi.org/10.1016/J.JCSR.2006.06.033.

[47] B.W. Yan, Q.S. Li, Inflow turbulence generation methods with large eddy simulation for wind effects on tall buildings, Comput. Fluids. 116 (2015) 158–175. https://doi.org/10.1016/j.compfluid.2015.04.020.

[48] B. Blocken, LES over RANS in building simulation for outdoor and indoor applications: A foregone conclusion?, Build. Simul. 11 (2018) 821–870. https://doi.org/10.1007/s12273-018-0459-3.

[49] W. Rodi, Comparison of LES and RANS calculations of the flow around bluff bodies, J. Wind Eng. Ind. Aerodyn. 69–71 (1997) 55–75. https://doi.org/10.1016/S0167-6105(97)00147-5.

[50] C.J. Baker, Wind engineering—Past, present and future, J. Wind Eng. Ind. Aerodyn. 95 (2007) 843–870. https://doi.org/10.1016/j.jweia.2007.01.011.

[51] T. Stathopoulos, Computational wind engineering: Past achievements and future challenges, J. Wind Eng. Ind. Aerodyn. 67–68 (1997) 509–532.

https://doi.org/10.1016/S0167-6105(97)00097-4.

[52] S. Murakami, A. Mochida, Y. Hayashi, Examining the κ-ϵ model by means of a wind tunnel test and large-eddy simulation of the turbulence structure around a cube, J. Wind Eng. Ind. Aerodyn. 35 (1990) 87–100. https://doi.org/10.1016/0167-6105(90)90211-T.

[53] S. Murakami, A. Mochida, Y. Hayashi, S. Sakamoto, Numerical study on velocity-pressure field and wind forces for bluff bodies by κ-ϵ, ASM and LES, J. Wind Eng. Ind. Aerodyn. 44 (1992) 2841–2852. https://doi.org/10.1016/0167-6105(92)90079-P.

[54] Y. Tominaga, T. Stathopoulos, CFD modeling of pollution dispersion in a street canyon: Comparison between LES and RANS, J. Wind Eng. Ind. Aerodyn. 99 (2011) 340–348. https://doi.org/10.1016/j.jweia.2010.12.005.

[55] Y. Tominaga, T. Stathopoulos, CFD modeling of pollution dispersion in building array: Evaluation of turbulent scalar flux modeling in RANS model using LES results, J. Wind Eng. Ind. Aerodyn. 104–106 (2012) 484–491. https://doi.org/10.1016/j.jweia.2012.02.004.

[56] R. Yoshie, A. Mochida, Y. Tominaga, H. Kataoka, K. Harimoto, T. Nozu, T. Shirasawa, Cooperative project for CFD prediction of pedestrian wind environment in the Architectural Institute of Japan, J. Wind Eng. Ind. Aerodyn. 95 (2007) 1551–1578. https://doi.org/10.1016/j.jweia.2007.02.023.

[57] K. Hanjalic, Will RANS survive LES? A view of perspectives, J. Fluids Eng. 127 (2005) 831. https://doi.org/10.1115/1.2037084.

[58] E. Prianto, P. Depecker, Characteristic of airflow as the effect of balcony, opening design and internal division on indoor velocity, Energy Build. 34 (2002) 401–409. https://doi.org/10.1016/S0378-7788(01)00124-4.

[59] Z. Ai, C. Mak, J. Niu, Z. Li, Q. Zhou, The effect of balconies on ventilation performance of low-rise buildings, Indoor Built Environ. 20 (2011) 649–660. https://doi.org/10.1177/1420326X11409457.

[60] Z. Ai, C. Mak, J. Niu, Z. Li, The assessment of the performance of balconies using computational fluid dynamics, Build. Serv. Eng. Res. Technol. 32 (2011) 229–243. https://doi.org/10.1177/0143624411404646.

[61] Z. Ai, C. Mak, J. Niu, Numerical investigation of wind-induced airflow and interunit dispersion characteristics in multistory residential buildings, Indoor Air. 23 (2013)

417–429. https://doi.org/10.1111/ina.12041.

[62] E. Dascalaki, M. Santamouris, A. Argiriou, C. Helmis, D.N. Asimakopoulos, K. Papadopoulos, A. Soilemes, On the combination of air velocity and flow measurements in single sided natural ventilation configurations, Energy Build. 24 (1996) 155–165. https://doi.org/10.1016/0378-7788(96)00973-5.

[63] S. Omrani, V. Garcia-hansen, B. Capra, R. Drogemuller, On the effect of provision of balconies on natural ventilation and thermal comfort in high-rise residential buildings, Build. Environ. (2017). https://doi.org/10.1016/j.buildenv.2017.07.016.

[64] E.R. Meinders, K. Hanjalic, R.J. Martinuzzi, Experimental Study of the Local Convection Heat Transfer From a Wall-Mounted Cube in Turbulent Channel Flow, J. Heat Transfer. 121 (1999) 564. https://doi.org/10.1115/1.2826017.

[65] B. Blocken, T. Stathopoulos, J. Carmeliet, Wind environmental conditions in passages between two long narrow perpendicular buildings, J. Aerosp. Eng. 21 (2008) 280–287. https://doi.org/10.1061/(ASCE)0893-1321(2008)21:4(280).

[66] X. Zhu, Wind pressures on buildings with appurtenances, MSc thesis, Concordia University, 1987.

[67] J. Franke, A. Hellsten, H. Schlünzen, B. Carissimo, Best practice guideline for the CFD simulation of flows in the urban environment, Meteorological Inst., COST, Hamburg, Germany, 2007.

[68] Y. Tominaga, A. Mochida, R. Yoshie, H. Kataoka, T. Nozu, M. Yoshikawa, T. Shirasawa, AIJ guidelines for practical applications of CFD to pedestrian wind environment around buildings, J. Wind Eng. Ind. Aerodyn. 96 (2008) 1749–1761. https://doi.org/10.1016/j.jweia.2008.02.058.

[69] T. van Hooff, B. Blocken, Coupled urban wind flow and indoor natural ventilation modelling on a high-resolution grid: A case study for the Amsterdam ArenA stadium, Environ. Model. Softw. 25 (2010) 51–65. https://doi.org/10.1016/j.envsoft.2009.07.008.

[70] S. Iousef, H. Montazeri, B. Blocken, P.J.V. van Wesemael, On the use of non-conformal grids for economic LES of wind flow and convective heat transfer for a wall-mounted cube, Build. Environ. 119 (2017) 44–61. https://doi.org/10.1016/j.buildenv.2017.04.004.

[71] B. Blocken, J. Carmeliet, T. Stathopoulos, CFD evaluation of wind speed conditions

in passages between parallel buildings—effect of wall-function roughness modifications for the atmospheric boundary layer flow, J. Wind Eng. Ind. Aerodyn. 95 (2007) 941–962. https://doi.org/10.1016/j.jweia.2007.01.013.

[72] B. Blocken, Computational Fluid Dynamics for urban physics: Importance, scales, possibilities, limitations and ten tips and tricks towards accurate and reliable simulations, Build. Environ. 91 (2015) 219–245. https://doi.org/10.1016/j.buildenv.2015.02.015.

[73] F. Mathey, D. Cokljat, J.P. Bertoglio, E. Sergent, Assessment of the vortex method for Large Eddy Simulation inlet conditions, Prog. Comput. Fluid Dyn. An Int. J. 6 (2006) 58. https://doi.org/10.1504/PCFD.2006.009483.

[74] E. Sergent, Vers une méthodologie de couplage entre la simulation des grandes échelles et les modèles statistiques, Ecully, Ecole centrale de Lyon, 2002.

[75] Z.T. Ai, C.M. Mak, Large-eddy Simulation of flow and dispersion around an isolated building: Analysis of influencing factors, Comput. Fluids. 118 (2015) 89–100. https://doi.org/10.1016/j.compfluid.2015.06.006.

[76] A. Gerasimov, Quick guide to setting up LES-type simulations, version 1.4., European Technology Group, ANSYS Sweden AB, 2016.

[77] B.E. Launder, D.B. Spalding, The numerical computation of turbulent flows, Comput. Methods Appl. Mech. Eng. 3 (1974) 269–289. https://doi.org/10.1016/0045-7825(74)90029-2.

[78] T. Cebeci, P. Bradshaw, Momentum transfer in boundary layers, New York, 1977.

[79] B. Blocken, T. Stathopoulos, J. Carmeliet, CFD simulation of the atmospheric boundary layer: wall function problems, Atmos. Environ. 41 (2007) 238–252. https://doi.org/10.1016/j.atmosenv.2006.08.019.

[80] H. Werner, H. Wengle, Large-eddy simulation of turbulent flow over and around a cube in a plate channel, in: Turbul. Shear Flows 8, Springer Berlin Heidelberg, Berlin, Heidelberg, 1993: pp. 155–168. https://doi.org/10.1007/978-3-642-77674-8_12.

[81] ANSYS Inc., Release 18.0, Theory Guide, ANSYS Inc, Canonsburg, PA 15317, USA, 2017.

[82] T.-H. Shih, W.W. Liou, A. Shabbir, Z. Yang, J. Zhu, A new k-ϵ eddy viscosity model for high reynolds number turbulent flows, Comput. Fluids. 24 (1995) 227–238. https://doi.org/10.1016/0045-7930(94)00032-T.

[83] J. Allegrini, A. Kubilay, Wind sheltering effect of a small railway station shelter and its impact on wind comfort for passengers, J. Wind Eng. Ind. Aerodyn. 164 (2017) 82–95. https://doi.org/10.1016/j.jweia.2017.02.013.

[84] T. Defraeye, J. Carmeliet, A methodology to assess the influence of local wind conditions and building orientation on the convective heat transfer at building surfaces, Environ. Model. Softw. 25 (2010) 1813–1824. https://doi.org/10.1016/j.envsoft.2010.06.002.

[85] H. Montazeri, F. Montazeri, CFD simulation of cross-ventilation in buildings using rooftop wind-catchers: Impact of outlet openings, Renew. Energy. 118 (2018) 502–520. https://doi.org/10.1016/j.renene.2017.11.032.

[86] B. Blocken, W.D. Janssen, T. van Hooff, CFD simulation for pedestrian wind comfort and wind safety in urban areas: General decision framework and case study for the Eindhoven University campus, Environ. Model. Softw. 30 (2012) 15–34. https://doi.org/10.1016/j.envsoft.2011.11.009.

[87] Y. Tominaga, T. Stathopoulos, Numerical simulation of dispersion around an isolated cubic building: Comparison of various types of k–ε models, Atmos. Environ. 43 (2009) 3200–3210. https://doi.org/10.1016/J.ATMOSENV.2009.03.038.

[88] P.J. Roache, Quantification of uncertainty in computational fluid dynamics, Annu. Rev. Fluid Mech. 29 (1997) 123–160. https://doi.org/10.1146/annurev.fluid.29.1.123.

[89] I.B. Celik, Z.N. Cehreli, I. Yavuz, Index of Resolution Quality for Large Eddy Simulations, J. Fluids Eng. 127 (2005) 949. https://doi.org/10.1115/1.1990201.

[90] S.B. Pope, Turbulent flows, Cambridge University Press, 2000.

[91] M. Schatzmann, H. Olesen, J. Franke, COST 732 model evaluation case studies: approach and results, Cost Action. (2010).

[92] T. van Hooff, B. Blocken, Y. Tominaga, On the accuracy of CFD simulations of cross-ventilation flows for a generic isolated building: Comparison of RANS, LES and experiments, Build. Environ. 114 (2017) 148–165. https://doi.org/10.1016/j.buildenv.2016.12.019.

[93] K. Nore, B. Blocken, J.V. Thue, On CFD simulation of wind-induced airflow in narrow ventilated facade cavities: Coupled and decoupled simulations and modelling limitations, Build. Environ. 45 (2010) 1834–1846.

https://doi.org/10.1016/j.buildenv.2010.02.014.

[94] F. Xing, D. Mohotti, K. Chauhan, Study on localised wind pressure development in gable roof buildings having different roof pitches with experiments, RANS and LES simulation models, Build. Environ. 143 (2018) 240–257. https://doi.org/10.1016/j.buildenv.2018.07.026.

[95] X. Xu, Q. Yang, A. Yoshida, Y. Tamura, Characteristics of pedestrian-level wind around super-tall buildings with various configurations, J. Wind Eng. Ind. Aerodyn. 166 (2017) 16–73. https://doi.org/10.1016/j.jweia.2017.03.013.

[96] X. Zhang, K.T. Tse, A.U. Weerasuriya, S.W. Li, K.C.S. Kwok, C.M. Mak, J. Niu, Z. Lin, Evaluation of pedestrian wind comfort near 'lift-up' buildings with different aspect ratios and central core modifications, Build. Environ. 124 (2017) 245–257. https://doi.org/10.1016/J.BUILDENV.2017.08.012.

[97] B. Blocken, T. Stathopoulos, J.P.A.J. van Beeck, Pedestrian-level wind conditions around buildings: Review of wind-tunnel and CFD techniques and their accuracy for wind comfort assessment, Build. Environ. 100 (2016) 50–81. https://doi.org/10.1016/j.buildenv.2016.02.004.

[98] Y. Du, C.M. Mak, B. Tang, Effects of building height and porosity on pedestrian level wind comfort in a high-density urban built environment, Build. Simul. 11 (2018) 1215–1228. https://doi.org/10.1007/s12273-018-0451-y.

[99] C.-H. Chang, R.N. Meroney, The effect of surroundings with different separation distances on surface pressures on low-rise buildings, J. Wind Eng. Ind. Aerodyn. 91 (2003) 1039–1050. https://doi.org/10.1016/S0167-6105(03)00051-5.

[100] T. Nozu, T. Tamura, K. Takeshi, K. Akira, Mesh-adaptive LES for wind load estimation of a high-rise building in a city, J. Wind Eng. Ind. Aerodyn. 144 (2015) 62–69. https://doi.org/10.1016/j.jweia.2015.05.007.

[101] A. Elshaer, A. Gairola, K. Adamek, G. Bitsuamlak, Variations in wind load on tall buildings due to urban development, Sustain. Cities Soc. 34 (2017) 264–277. https://doi.org/10.1016/j.scs.2017.06.008.

[102] B. Blocken, J. Carmeliet, Pedestrian wind conditions at outdoor platforms in a high-rise apartment building: generic sub-configuration validation, wind comfort assessment and uncertainty issues, Wind Struct. 11 (2008) 51–70. https://doi.org/10.12989/was.2008.11.1.051.

Chapter 3

CFD analysis of the impact of geometrical characteristics of building balconies on near-façade wind flow and surface pressure

This chapter has been published as a peer-reviewed journal paper:

CFD analysis of the impact of geometrical characteristics of building balconies on near-façade wind flow and surface pressure

X. Zheng, H. Montazeri, B. Blocken

Building and Environment 200, 107904

Abstract: The presence of building balconies can significantly modify the near-façade wind flow pattern and surface pressures. The present study evaluates the impact of building balcony geometry on mean wind speed on balcony spaces and wind-induced mean surface pressure for generic high-rise buildings. The focus is on balconies that extend along the entire width of the building façade. Large-eddy simulations (LES), validated with wind tunnel experiments, are conducted to investigate the impact of (i) balconies present or not, (ii) balcony depth, (iii) balcony parapet walls, (iv) balcony partition walls, and (v) density of balconies. The results indicate that the balcony geometry can greatly affect the mean wind speed on balcony spaces and the local and façade-averaged mean pressure coefficient (C_p). The presence of balconies can increase the façade-averaged C_p over the windward and leeward façades by 5.2% and 8.9%, respectively. These numbers rise to 23.5% and 23.3% when two partition walls are added at the lateral edges of the façades. Adding five partition walls can reduce the overall area-averaged wind speed on balcony spaces by 68.0% compared to the case without partition walls. These findings can be useful in developing, designing and constructing buildings with façade geometrical details that improve building ventilation, air quality and wind comfort.

3.1 Introduction

The presence of large-scale roughness on building façades can significantly influence the near-façade wind flow and surface pressure distributions [1,2]. For example, balconies on the windward façade of a high-rise building can change the local mean surface pressure coefficient (C_p) from -0.36 to 0.34 [3]. In addition, the geometrical characteristics of building balconies can strongly affect not only the wind speed on balcony spaces [4], but also the peak and mean surface pressures [3,5]. This is especially the case for high-rise buildings where the high wind speed around the building can lead to wind discomfort or even wind danger on building balcony space [4,6]. Therefore, knowledge on the impact of the geometrical characteristics of building balconies on the near-façade wind flow is crucial to assess wind comfort and safety on balcony spaces [4,7,8], wind-induced natural ventilation [9] and infiltration in buildings [10], local and façade-averaged convective heat transfer coefficients on building façades [11–13], and wind loads on building surfaces [14].

Several studies have been performed to investigate the impact of the presence of balconies and of their geometrical characteristics. Tables 1 and 2 provide overviews of wind tunnel and computational fluid dynamics (CFD) studies on buildings with balconies, respectively. They list the number of stories, the objective of the study, whether or not different geometrical characteristics have been evaluated and if so, which ones, and the wind directions and performance indicators used. For studies using CFD, additional information about the turbulence modeling approach and building scale is also provided. The following observations are made:

In these wind tunnel studies, the focus has been on either surface pressures (mean, rms and peak) or aerodynamic forces. While the vast majority of CFD studies focused on either the mean surface pressure or mean wind velocity, only a few studies have investigated mean surface pressure and mean wind speed simultaneously.

The majority of CFD studies focused on the presence of balconies, which means that only one specific balcony geometry was evaluated. The impact of the geometrical characteristics of balconies for isolated buildings has been investigated only in a few studies [9,15–17], with the focus on the balcony depth [9,15,16], the height of parapet walls [15] and the presence and shape of partition walls [9,17]. Note that in these studies, different boundary conditions and building dimensions were considered, and the conclusions were not always consistent.

The CFD studies generally adopted the 3D steady Reynolds-Averaged Navier-Stokes (RANS) approach, while the use of large-eddy simulation (LES) was limited to only a few studies [18–20]. An earlier study on a building with balconies found that steady RANS can accurately predict the mean pressure coefficient (C_p) on the windward façade of a building for both perpendicular ($\theta = 0°$) and oblique ($\theta = 45°$) wind directions, while it systematically underestimates the absolute value of C_p on the leeward façade for these two wind directions ($\theta = 0°$ and $\theta = 45°$) [1]. This is mainly because of the deficiencies of steady RANS in capturing the complexities of the near-façade wind flow, which include multiple areas of flow separation, recirculation and reattachment generated by the balconies [21–23]. LES, on the other hand, is capable of predicting the inherently unsteady wind flow [24–27]. The superior performance of LES compared to steady RANS and unsteady RANS has been shown for mean and instantaneous flow fields around isolated buildings (e.g. [21–24,28–30]) and in urban areas (e.g. [23,26,31–35]). LES can provide accurate descriptions of surface C_p of a high-rise building with balconies for both the windward and the leeward façades [18]. Therefore, it is desirable to use LES for highly accurate CFD for buildings with balconies.

Table 1. Overview of wind tunnel studies on wind flow around buildings with balconies.

Reference	Building stories (height (m))	Research objective	Geometrical characteristic	Wind direction (°)	Performance indicator
Stathopoulos & Zhu, 1988 [3]	30 (120)	GB	Dep, PW	0, 90, 180	Mean/ r.m.s./ peak c_p
Maruta et al., 1998 [36]	26 (75)	GB	Dep, Par	0, 5, 10, 13, 15, 20	Mean/ r.m.s/ peak c_p
Chand et al., 1998 [37]	5 (15)	PB	N/A	0, 45	Mean c_p
Ludena et al., 2016 [38]	15 (55)	GB	Par	0-180[1]	Mean/ peak c_p
Chowdhury et al., 2017 [39]	15 (55)	GB	Par	0-180[1]	Mean/ peak c_p
Yuan et al., 2018 [5]	- (150)[2]	GB	Con, Den, Dep	0- 45, (5 intervals)	Mean/ peak c_p
Hui et al., 2019 [40]	- (150)[2]	GB	Con, Den, Dep	0- 45, (5 intervals)	AF

[1] Information about wind direction intervals was not reported.

[2] Information about building stories was not reported.

GB = Geometrical characteristic of balconies, Dep = Depth of balconies, PW = Parapet wall, c_p = Pressure coefficient, Par = Partition wall, PB = Presence of balconies (a specific balcony geometry was considered), N/A = Not applicable, Con = Horizontal continuity of balconies, Den = Density of balconies, AF = Aerodynamic forces.

Table 2. Overview of CFD studies on wind flow around buildings with balconies.

Reference	Building scale	Building stories (height in full scale (m))	Research objective	Geometrical characteristic	Turbulence modeling approach	Wind direction (°)	Performance indicator
Murakami, 1990 [41]	Full	19 (-)[1]	PB	N/A	RANS	0[2]	V
Prianto & Depecker, 2002 [42]	Full	2 (8.5)	PB	N/A	RANS	0	V
Blocken & Carmeliet, 2008 [8]	Full	8 (26)	GB	N/A	RANS	0-360, (30 intervals)	V
Ai et al., 2011 [43]	Reduced	5 (15)	PB	N/A	RANS	0	Mean c_p, V
Ai et al., 2011 [15]	Reduced	5, 10, 15 (15, 30, 45)	GB	Dep, PW	RANS	0-90, (22.5 intervals)	Mean c_p
Ai et al., 2013 [44]	Reduced	5 (15)	PB	N/A	RANS	0	V, ACH
Montazeri et al., 2013 [4]	Full	22 (78)	GB	DS	RANS	0-360, (30 intervals)	V
Montazeri & Blocken, 2013 [1]	Reduced	5 (15)	PB	N/A	RANS	0, 45	Mean c_p
Ai & Mak, 2016 [19]	Reduced	5 (13.5)	PB	N/A	LES	0, 45, 90	ACH, PC
Murena & Mele, 2016 [45]	Full	4 (18)[3]	GB	Con, Dep	SAS	0[4]	PC
Laguno-Munitxa et al., 2017 [20]	Reduced	5 (-)[1,3]	PB	N/A	LES	0[4]	V
Omrani et al., 2017 [9]	Full	36 (-)[1]	GB	Dep, Par	RANS	0, 45, 90, 180	V
Karkoulias et al., 2019 [46]	Full	7 (28)[3]	GB	BF	RANS	0[4]	PC
Cui et al., 2020 [47]	Full	4 (12)[3]	PB	N/A	RANS	0[4]	V, PC

Izadyar et al., 2020 [16]	Full	13 (42)	GB	Dep	RANS	0	V
Ghadikolaei et al., 2020 [17]	Full	6 (20.4)	GB	Par	RANS	0, 45	V, ACH
Zheng et al., 2020 [18]	Reduced	30 (120)	PB	N/A	LES, RANS	0	V, Mean c_p

[1] Information about building height was not reported.

[2] Approximately 0°.

[3] The focus was on street canyons.

[4] Perpendicular to the long street axis.

PB = Presence of balconies (a specific balcony geometry was considered), N/A = Not applicable, V = Mean velocity, GB = Geometrical characteristic of balconies, c_p = Pressure coefficient, Dep = Depth of balconies, ACH = Air exchange rate, DS = Double skin, Con = Horizontal continuity of balconies, SAS = Scale adaptive simulation, PC = Pollutant concentration, Par = Partition wall, BF = Balconies on different façades.

This paper investigates the impact of the geometrical characteristic of building balconies on the near-façade mean wind flow patterns and mean surface pressures. LES simulations are performed to investigate the impact of (i) balconies present or not, (ii) balcony depth, (iii) balcony parapet walls, (iv) balcony partition walls and (v) density of balconies.

This paper contains six sections. In Section 2, the wind tunnel experiments by Stathopoulos and Zhu [3] and the validation study are briefly outlined. Section 3 describes the computational settings and parameters for the CFD simulations. Section 4 presents the CFD results. Finally, limitations and future work (Section 5) and conclusions (Section 6) are provided.

3.2 CFD validation study

In this study, the wind tunnel experiments by Stathopoulos and Zhu [3] are used for the CFD validation. Since this validation study has been published as a separate paper [18], only the outline is briefly mentioned here.

3.2.1 Wind tunnel experiment

In the wind tunnel experiments, the surface pressure on the façades of a reduced-scale model of a high-rise building with balconies was measured in an open-circuit atmospheric boundary layer wind tunnel. Fig. 1 illustrates the building model with dimensions: width × depth × height = 0.152 × 0.152 × 0.3 m^3 (1:400 scale, w:d:h ≈ 1:1:2, 60.8 m × 60.8 m × 120 m in full scale). Balconies with 0.01 m depth (4 m in full scale) and 0.0025 m high (1 m in full scale) parapet walls were installed on one of the building façades where the surface pressures were measured along 7 vertical lines. In the present validation study, the measured data along two of the lines will be used. They will be referred to as line A (located 0.061 m from the left edge of the building model) and line B (located 0.0015 m from the left edge of the building model), as shown in Fig. 1. The overall uncertainty of the mean pressure coefficient (C_p) measurements was estimated to be less than 5% [48].

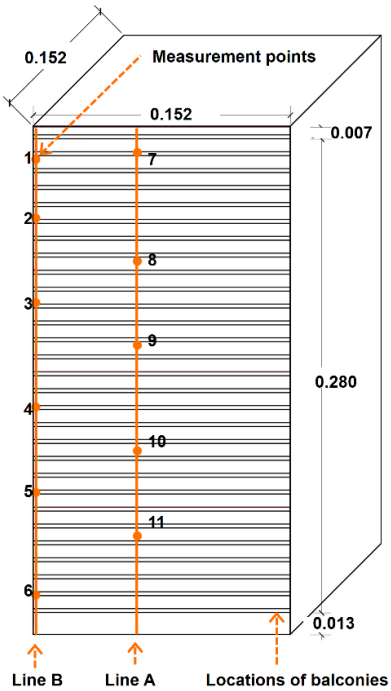

Fig. 1. The geometry of the building model, locations of balconies, and measurement points and lines used for CFD validation. All dimensions are in meter in model scale.

3.2.2 CFD validation: computational settings and parameters

Two computational grids are made of the reduced-scale building model in the wind tunnel measurements for approaching wind directions θ = 0° (wind flow perpendicular to the windward façade with balconies) and θ = 180°. The computational domains and grids are made based on the best practice guidelines [49–52]. The grids are generated with the surface-grid extrusion technique [53]. Cubic cells are applied near the building, with 120 and 8 cells along the width and depth of the balconies, respectively. The total number of cells is 19,267,200. More information about the computational domain and grid can be found in Ref. [18]. The boundary conditions are listed in Table 3.

Table 3. CFD validation: boundary conditions.

Boundary	Boundary conditions

Inlet	Velocity inlet	$U(z)=\frac{u^*_{ABL}}{\kappa}\ln(\frac{z+z_0}{z_0})$ (1)
		$k(z)=a\left(I_u(z)U(z)\right)^2$ (2)
		$\varepsilon(z)=\frac{u^{*3}_{ABL}}{\kappa(z+z_0)}$ (3)
Outlet	Pressure outlet	Static gauge pressure = 0 Pa
Top and lateral sides	Slip conditions	Normal gradients of all variables = 0
Ground and building walls	No-slip conditions	Werner-Wengle wall functions [54]

The inlet boundary conditions are based on the measured incident vertical profiles of mean wind speed U and longitudinal turbulence intensity I_u [3]. The mean wind velocity U is given by Eq. (1), where the atmospheric boundary layer friction velocity, u^*_{ABL} and aerodynamic roughness length, z_0, are 0.7 m/s and 0.0001 m, respectively. κ is the von Karman constant (= 0.41). The turbulent kinetic energy is computed using Eq. (2), where a = 1 is chosen according to Tominaga et al. [50], the longitudinal turbulence intensity I_u takes the measured value. The turbulence dissipation rate ϵ is based on Eq. (3). The vortex method [55] is adopted to impose a time-dependent velocity profile at the inlet of the domain. The number of vortices N_V is 8500, which is based on the recommendation by Ref. [56], i.e., N_V = N/4 where N is the number of grid cells at the inlet plane.

The commercial CFD code ANSYS/Fluent 18.0 is used to perform the simulations. The simulations are isothermal. LES simulates the transient flow by solving the filtered Navier-Stokes equations and modeling the turbulence of the sub-filter scales by a subgrid-scale model. The filtered Navier-Stokes equations are:

$$\frac{\partial \bar{u}_i}{\partial x_i}=0 \tag{4a}$$

$$\frac{\partial \bar{u}_i}{\partial t}+\frac{\partial}{\partial x_j}(\bar{u}_i\bar{u}_j)=-\frac{1}{\rho}\frac{\partial \bar{p}}{\partial x_i}+\frac{\partial}{\partial x_j}(2\nu \bar{s}_{ij})-\frac{\partial \tau_{ij}}{\partial x_j} \tag{4b}$$

where the overbars indicate the filtered variables, and $\bar{s}_{ij}$ is the rate of strain tensor. The subgrid-scale Reynolds stresses (τ_{ij}) appear due to the filter operation:

$$\tau_{ij}=\overline{u_iu_j}-\bar{u}_i\bar{u}_j \tag{5}$$

Subgrid-scale (SGS) models used to provide closure usually adopt the Boussinesq hypothesis:

$$\tau_{ij} - \frac{1}{3}\tau_{kk}\delta_{ij} = -2\mu_{SGS}\bar{s}_{ij} \tag{6}$$

where μ_{SGS} is the SGS turbulent viscosity. The isotropic part of the SGS stresses τ_{kk} is not modeled but added to the filtered static pressure term. In the present study, the wall-adapting local eddy viscosity (WALE) subgrid-scale (SGS) model [57] is used to obtain μ_{SGS} (Eq. (7)):

$$\mu_{SGS} = \rho(C_W\Delta)^2 \frac{\left(S_{ij}^d S_{ij}^d\right)^{3/2}}{\left(\bar{s}_{ij}\bar{s}_{ij}\right)^{5/2} + \left(S_{ij}^d S_{ij}^d\right)^{5/4}} \tag{7}$$

where the WALE constant C_w = 0.325 [58]. Grid filter width $\Delta = V^{1/3}$, where V is the volume of the computational cell. s_{ij}^d is defined as:

$$s_{ij}^d = 1/2\left(\left(\frac{\partial\bar{u}_i}{\partial x_j}\right)^2 + \left(\frac{\partial\bar{u}_j}{\partial x_i}\right)^2\right) - 1/3\,\delta_{ij}\left(\frac{\partial\bar{u}_k}{\partial x_k}\right)^2 \tag{8}$$

Pressure-velocity coupling is performed using the fractional step method in combination with the non-iterative time advancement scheme. Second-order schemes are applied for pressure interpolation and time discretization. The time step Δt is 4×10^{-5} s. The maximum Courant-Friedrichs-Lewy (CFL) number is 1.287 and the volume-averaged CFL number is 0.046. The simulations are initialized with the solution from 3D steady RANS simulations with the realizable k-ε turbulence model [59]. Then the LES initialization runs for T_{init} = 1.52 s, corresponding to approximately 5 flow-through times ($T_{flow\text{-}through} = L_x/U_{max}$, where L_x is the length of the computational domain). After the initialization, the LES simulation and sampling are conducted for T_{avg} = 6.67 s, which is approximately 21 flow-through times. Further information about the other settings and parameters are reported in Ref. [18].

3.2.3 CFD validation: results

Fig. 2 compares the simulated and measured C_p along lines A and B for θ = 0° and θ = 180°. C_p is computed as:

$$C_p = \frac{P - P_0}{0.5\rho U_{ref}^2} \tag{9}$$

where P is the mean pressure on the building surface, P_0 is the reference static pressure, ρ is the air density (1.225 kg/m^3), and U_{ref} is the mean wind speed at the gradient height in the wind tunnel (H_g = 0.625 m). For θ = 0°, a fairly good agreement can be observed between the CFD and wind tunnel results along line A with an average absolute deviation of 0.027. Note that the measured data at point 8 was not reported in Ref. [3]. The average absolute deviation along line B is 0.133. The possible reason for this deviation could be due to the measurement uncertainty associated with the exact location of the pressure taps given the large vertical C_p gradients on the balcony spaces. More detailed information on the sensitivity of the absolute deviation of C_p to the vertical position of the measurement points has been provided in Ref. [18]. For θ = 180°, the agreement is good with the average absolute deviations of 0.041 and 0.036 for lines A and B, respectively.

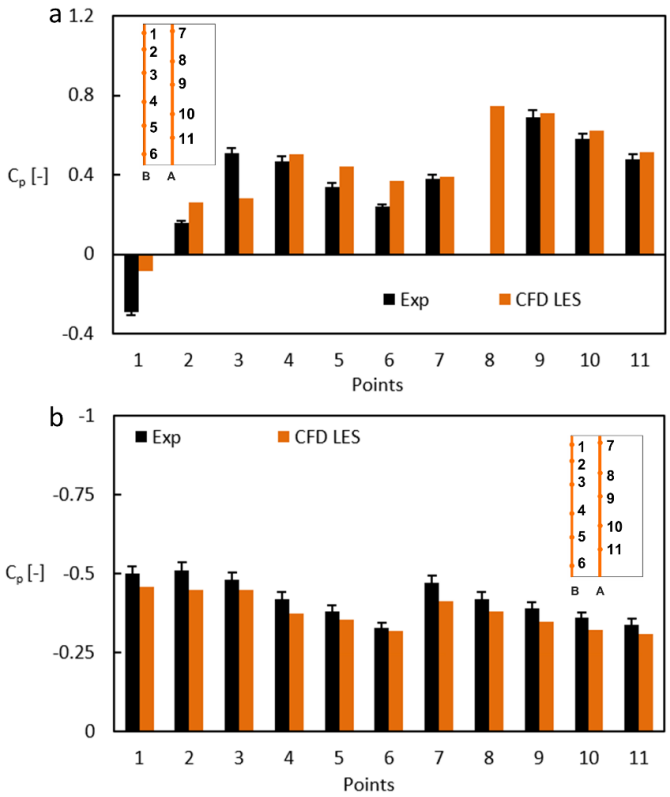

Fig. 2. CFD validation: comparison between C_p obtained by CFD and wind tunnel (a) for ϑ = 0°, note that the measured data at point 8 was not reported in Ref. [3], and (b) ϑ = 180°.

3.3 CFD simulations

3.3.1 List of cases

In this study, twelve cases are considered. For all the cases, a 12-story building with dimensions width × depth × height = 24 × 24 × 48 m^3 (w:d:h = 1:1:2) is used, inspired by the building geometry in the wind tunnel measurements mentioned in subsection 2.1. In all the cases the building is assumed to be perfectly airtight, hence ventilation and infiltration are zero. Based on the position and geometrical characteristics of the balconies, the cases can be classified into five groups (Fig. 3):

- Group 1 (to investigate the impact of the presence of balconies): a reference case without balconies (case Ref.) and case L-1. For case L-1, twelve balconies are located at equidistant points on both windward and leeward façades (Fig. 4a). The balconies are 24 m wide and 3 m deep and have 1 m high parapet walls. Note that the balcony on level 12 is roofed.
- Group 2 (to investigate the impact of balcony depth): case D-1 (building with 1 m deep balconies), case D-2 (2 m deep balconies), case L-1 (3 m deep balconies) and case D-3 (4 m deep balconies). Note that for case D-3, the depth of the balconies is larger than the values commonly used in real buildings. Nevertheless, in the present study, a rather wide range is investigated to gain insight into the impact of balcony depth on the near-façade wind flow and surface pressure, which is in line with previous studies on the impact of balcony depth [3,9,47].
- Group 3 (to investigate the impact of the presence and height of parapet walls): case W-1 (without parapet wall), case L-1 (1 m high parapet walls) and case W-2 (2 m high parapet walls). Note that in real buildings, balcony spaces are mostly equipped with parapet walls with the height of about 1 m. Case W-1 represents the balconies with parapet walls consisting of pipe railing [60], which allows airflow to pass through. Some balconies on high-rise buildings are equipped with glass parapet walls taller than an adult for safety reasons, which is represented by case W-2.

- Group 4 (to investigate the impact of the presence and number of partition walls): case L-1 (without partition walls), case P-1 (two partition walls on lateral edges of the façades), case P-2 (three partition walls, two on the lateral edges and one in the middle of the façades) and case P-3 (five partition walls at equidistant locations). Note that such partition walls in-between are commonly used to divide units for residential buildings.
- Group 5 (to investigate the impact of the density of balconies): case L-1 (balconies on all 12 levels), case I-1 (balconies on levels 3, 5, 7, 9 and 11) and case I-2 (balconies only on levels 5 and 9). Note that cases like I-1 or I-2 can be found on split-level apartments.

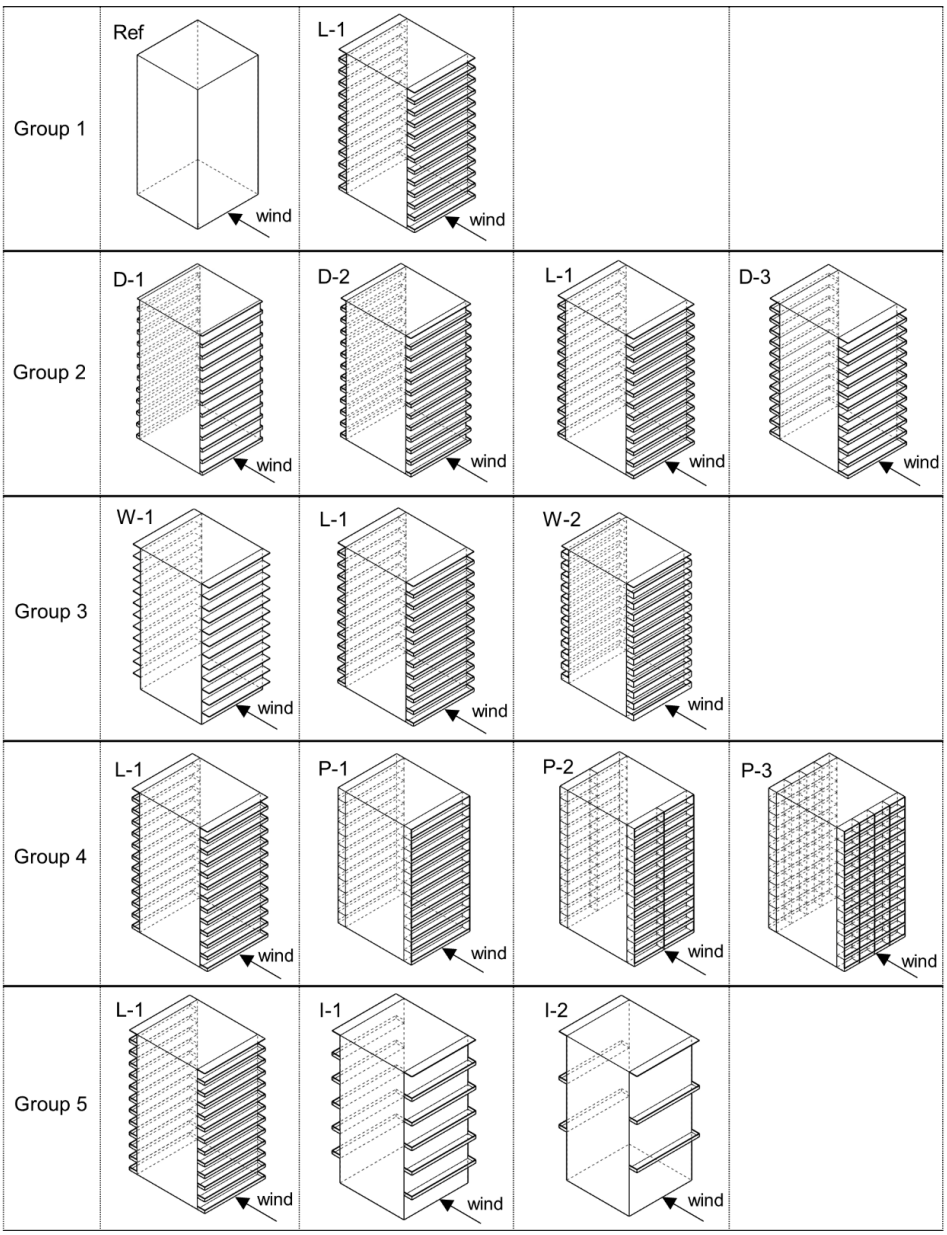

Fig. 3. List of cases presented in the five groups (the arrows indicate the wind direction).

3.3.2 Computational domain and grid

The simulations are performed in full scale. Fig. 4a shows the building geometry of case L-1. Fig. 4b displays the computational domain. The upstream domain length, lateral domain length, downstream domain length, and domain height are 4h, 4h, 10h, and 5h (h, height of the building), respectively (Fig. 4b). Note that the upstream domain length is limited to 4h

to reduce the extent of unintended streamwise gradients in the inlet profiles [51,61]. The domain height (5h) is smaller than the one recommended by Tominaga et al. [50], in order to reduce the total number of cells and the computational time. The resulted blockage ratio is 1.18%, which is well below the maximum value recommended by the above-mentioned guidelines [50], i.e. 3%. A non-conformal grid is employed, where the whole domain is discretized into two subdomains: Ω_1 (the inner subdomain) and Ω_2 with a 1:2 grid refinement ratio between the adjacent subdomains as suggested by Ref. [52]. Subdomain Ω_1 consists of cubic cells and it is extended up to a distance of h/6 away from the building surfaces (see Fig. 4c and d), i.e. from the location where high velocity gradients are expected to occur. The edge length of the cubic cells is h/192 (i.e. 16 cells per floor, and 4 cells along the height of parapet walls for case L-1). In subdomain Ω_2, hexahedral cells with a stretching ratio of about 1.04 are used. The same topology and resolution are used for all the cases. The total number of cells is 16,566,528 for all cases, except for case D-3, where it is 17,543,792. The adequacy of the grid resolution is confirmed by a grid-sensitivity study that will be provided in subsection 3.5.

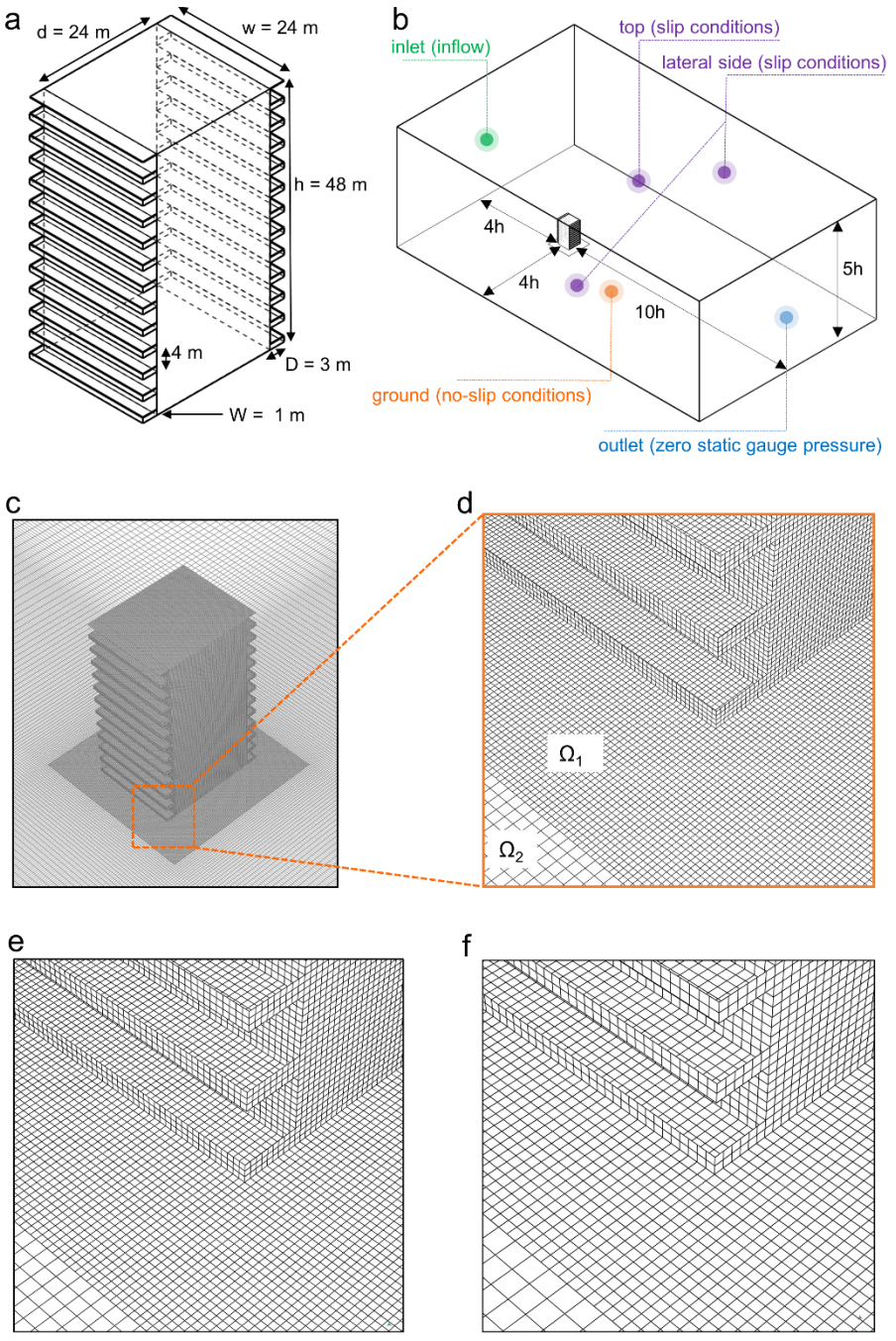

Fig. 4. Case L-1: (a) building geometry, (b) computational domain and boundary conditions, (c) basic computational grid (16.6 million cells) at building surfaces and part of the ground surface, and (d) details of the basic grid near the bottom of the building. Details of grids for grid-sensitivity analysis: (e) coarse grid (7.9 million cells) and (f) coarser grid (3.9 million cells).

3.3.3 Boundary condition

At the inlet of the domain, the neutral atmospheric boundary layer inlet profiles of mean wind speed (Eq. (1) and Fig. 5a), turbulent kinetic energy (Eq. (10) with empirical constant C_μ equal to 0.09 and Fig. 5b) and turbulence dissipation rate (Eq. (3) and Fig. 5c) proposed by Richards and Hoxey [62] are imposed.

$$k(z) = \frac{u^{*2}_{ABL}}{\sqrt{C_\mu}} \tag{10}$$

It is assumed that the building is situated on a large grass-covered terrain with an aerodynamic roughness length z_0 = 0.03 m [63] and an atmospheric boundary layer friction velocity u^*_{ABL} = 0.3 m/s. The corresponding mean wind velocity at 10 m height U_{10} = 4.15 m/s and the reference mean wind velocity at building roof height (48 m) U_{ref} = 5.27 m/s. All simulations are performed for θ = 0° (approach flow perpendicular to the windward façade). The vortex method [55,64] is adopted at the inlet of the domain to generate a time-dependent velocity profile. The number of vortices N_V = 11426, following Ref. [56]. As shown in Fig. 4b, zero static gauge pressure is applied at the outlet plane and slip conditions are applied on the top and lateral sides. The building and ground surfaces are modeled as no-slip conditions. The Werner-Wengle wall functions are applied for modeling flow parameters in the near-wall regions [54].

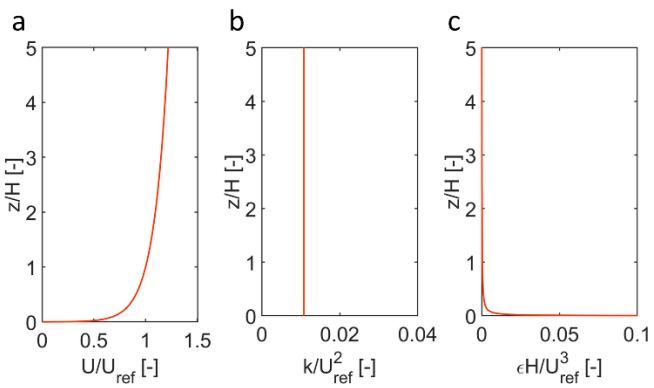

Fig. 5. Inlet profiles of (a) dimensionless mean velocity (U/U_{ref}), (b) dimensionless turbulent kinetic energy (k/U_{ref}^2) and (c) dimensionless turbulence dissipation rate ($\varepsilon H/U_{ref}^3$).

3.3.4 Solver settings

Following the validation study reported in subsection 2.2, LES with the wall-adapting local eddy viscosity (WALE) SGS model is employed for the simulations. The time step (Δt) is 0.02 s for all the cases. The maximum CFL number ranges from 0.957 to 1.255, which mainly occurs close to the leading edge of the building roof. The other solver settings are identical to those in the validation study. All the LES simulations are started from the solution of 3D steady RANS simulations with the realizable k-ϵ turbulence model [59], and the computation is run during 470 s (approximately 5 flow-through times) to remove the influence of the initial condition before data sampling. Then, data are sampled and averaged over a period of 1920 s (approximately 20 flow-through times).

3.3.5 Grid-sensitivity study

A grid-sensitivity analysis is carried out for case L-1. A basic (Fig. 4d), coarse (Fig. 4e) and coarser (Fig. 4f) grid are made based on the same overall grid topology, For the basic, coarse and coarser grid, 4, 3 and 2 cells are used along the height of parapet walls, respectively, and the length of the cubic cells near the building is h/192, h/144 and h/96, respectively. The total number of cells for the basic, coarse and coarser grid is 16.6, 7.9 and 3.9 million, respectively. The corresponding time steps are 0.02, 0.025 and 0.042 s, respectively, resulting in the maximum CFL number of 1.11, 0.99 and 1.00, respectively.

The results of the C_p along vertical lines (x/w = 0.125 and x/w = 0.5) on the windward and leeward façades obtained by the three grids are compared in Fig. 6a-d. Only a limited dependency of C_p on the grid resolution is observed. The overall absolute difference (the two lines combined) between the coarse grid and the basic grid is 0.016. This is 0.027 between the coarser grid and the basic grid. Therefore, the basic grid is adopted for the remainder of this study.

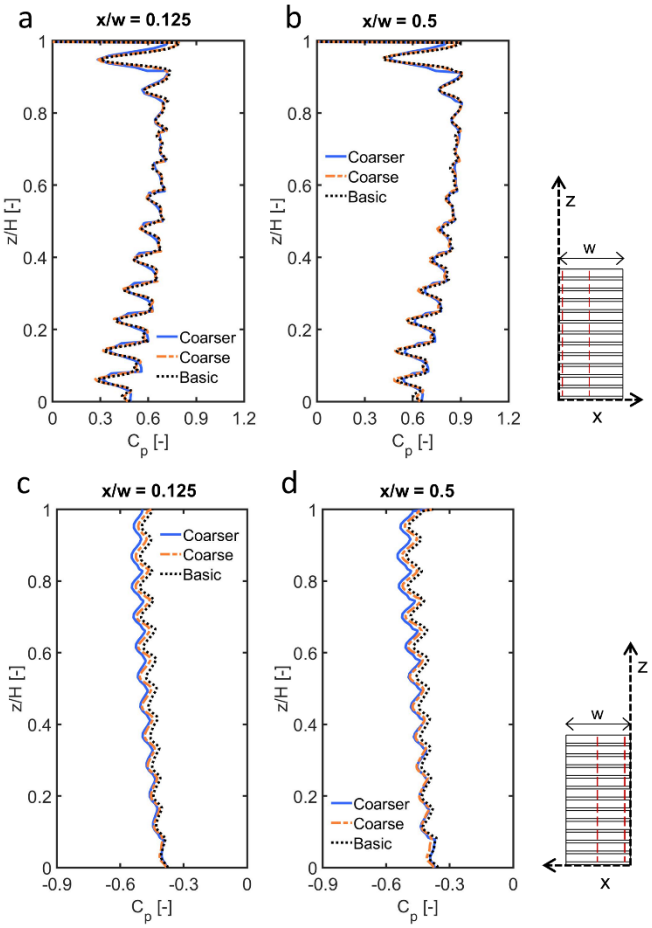

Fig. 6. Comparison of mean surface pressure coefficient (C_p) obtained from the basic, coarse and coarser grid along two vertical lines (a) x/w = 0.125, (b) x/w = 0.5 on the windward façade, (c-d) same on the leeward façade.

3.4 Results

The following target parameters are selected:

- *Mean wind speed ratio (K) in the vertical centerplane.* It is defined as the mean wind speed divided by $U_{ambient}$ (= 2.92 m/s, the "undisturbed" mean wind speed at the inlet plane at 1.75 m above the ground level).
- *Mean wind speed ratio (K) in horizontal planes at the pedestrian height (= 1.75 m) on balcony spaces.* The focus will be on (i) the K distribution and (ii) the maximum and area-averaged K, denoted as K_{max} and K_{avg}, respectively.

- *C_p on the windward and leeward façades.* The C_p is calculated according to Eq. (9), where P is the mean pressure on the building surface, ρ is the air density (1.225 kg/m^3), and P_0 is the reference static pressure = 0.5 Pa, taken 100 m upstream of the building at the roof height where the streamwise static pressure gradients are almost negligible. U_{ref} is 5.27 m/s. The façade-averaged C_p is denoted as $C_{p,avg}$.

3.4.1 Impact of balconies present or not

The impact of the presence of balconies on K and C_p is investigated by comparing the results of the reference case (building without balconies) and case L-1 (with balconies on both façades). The results are presented in Figs. 7, 8 and 9a. The following observations are made:

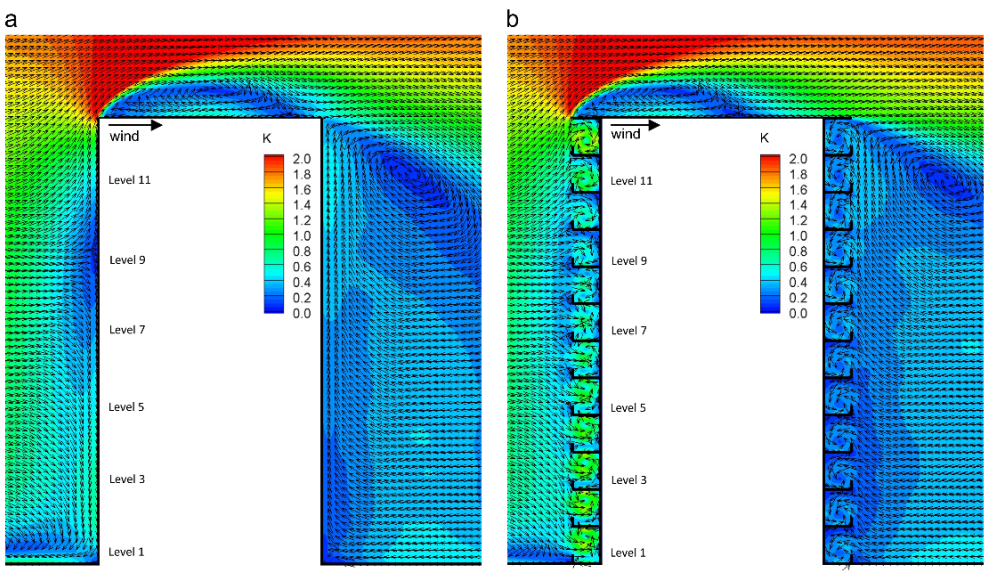

Fig. 7. Distributions of K and 2D velocity vector field in the vertical centerplane for (a) the reference case and (b) case L-1.

- Fig. 7a and b illustrates the distributions of K and the velocity vector field in the vertical centerplane. For the reference case without balconies, the stagnation point on the windward façade is located at about 0.7h (h is the building height). For case L-1, multiple stagnation areas are found near the parapet walls, and at the upper part of

the balcony spaces of levels 8-10 (Fig. 7b). On levels 9-12, the upwash flow separates at the edges of the parapet walls and introduces a clockwise vortex on each balcony space. For levels 6-8, two vortices are visible between the balconies: a counterclockwise vortex in the upper part, and a clockwise vortex in the lower part on each balcony space. For levels 1-5, the downwash flow leads to a primary counterclockwise vortex in the higher part and a secondary clockwise vortex in the lower part. For the balconies on the leeward façade, the interaction with the upward-directed airflow leads to a counterclockwise vortex on all the balcony spaces. Note that the presence of the balcony and its roof at level 12 significantly affects the reattachment point on the roof. For the reference case, the reattachment occurs at around 0.8d (d is the depth of the building) in relation to the leading edge of the building (Fig. 7a), while for case L-1, it occurs at 0.6d (Fig. 7b).

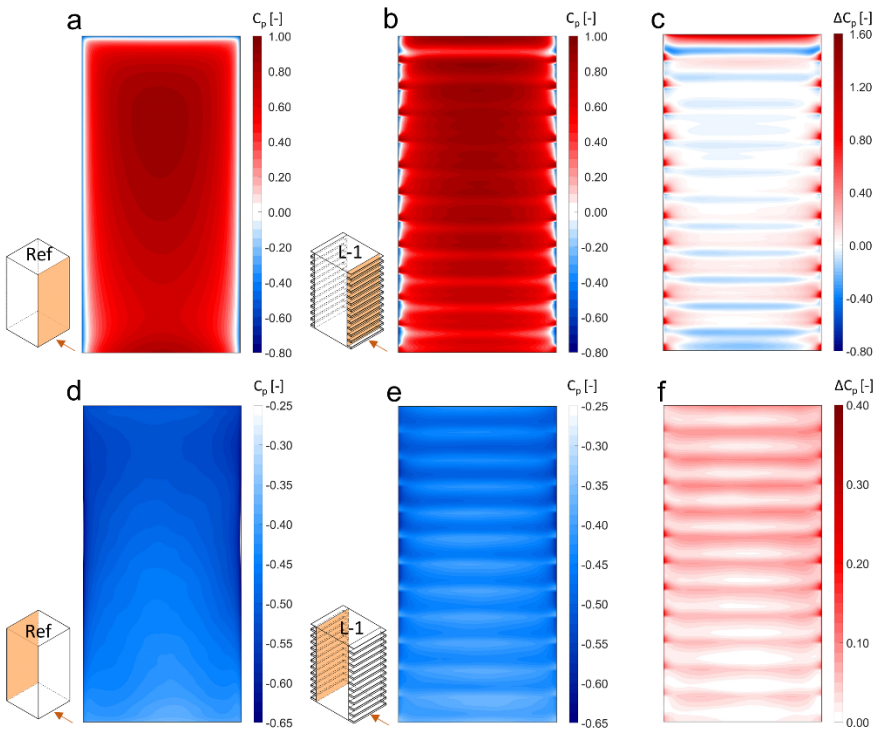

Fig. 8. Distributions of C_p on windward façades of (a) the reference case, (b) case L-1, and (c) $\Delta C_{p\,(L-1)} = C_{p\,(L-1)} - C_{p\,(Ref.)}$. (d-f) Same for leeward façades.

- Fig. 8a and b displays C_p on the windward façade of the reference case and case L-1, respectively. Fig. 8c presents the C_p difference between the two cases, i.e. $\Delta C_{p\,(L-1)} = C_{p\,(L-1)} - C_{p\,(Ref.)}$. Fig. 8a-c shows that the presence of balconies leads to high-pressure areas close to the lateral edges of the façade behind the parapet walls, which is due to the impingement of the accelerated wind flow towards the lateral edges onto the lateral parapet walls yielding stagnation areas. This is in line with the results in Ref. [3]. For level 12, C_p increases at the upper part of the façade where ΔC_p reaches its maximum value ($\Delta C_p = 1.63$). In the lower part of the façade on level 12, however, C_p decreases to the extent that ΔC_p experiences a local minimum of -0.362. For the ground level, the presence of the balconies results in a mild reduction of C_p on a large part of the façade. For the entire windward façade, however, the presence of balconies increases $C_{p,avg}$ from 0.616 to 0.648 (about 5.2%, shown in Fig. 9a).
- Fig. 8d and e displays C_p over the leeward façade of the two cases. $\Delta C_{p\,(L-1)} = C_{p\,(L-1)} - C_{p\,(Ref.)}$ is presented in Fig. 8f. By adding balconies on both façades (case L-1), C_p either increases (i.e. becomes less negative) or remains unchanged across the leeward façade. The increase is more pronounced at the upper part of the façade. The maximum ΔC_p is 0.285, which occurs close to the edges behind the parapet walls on level 7. The presence of balconies increases $C_{p,avg}$ from -0.486 to -0.443 (about 8.9%, shown in Fig. 9a).

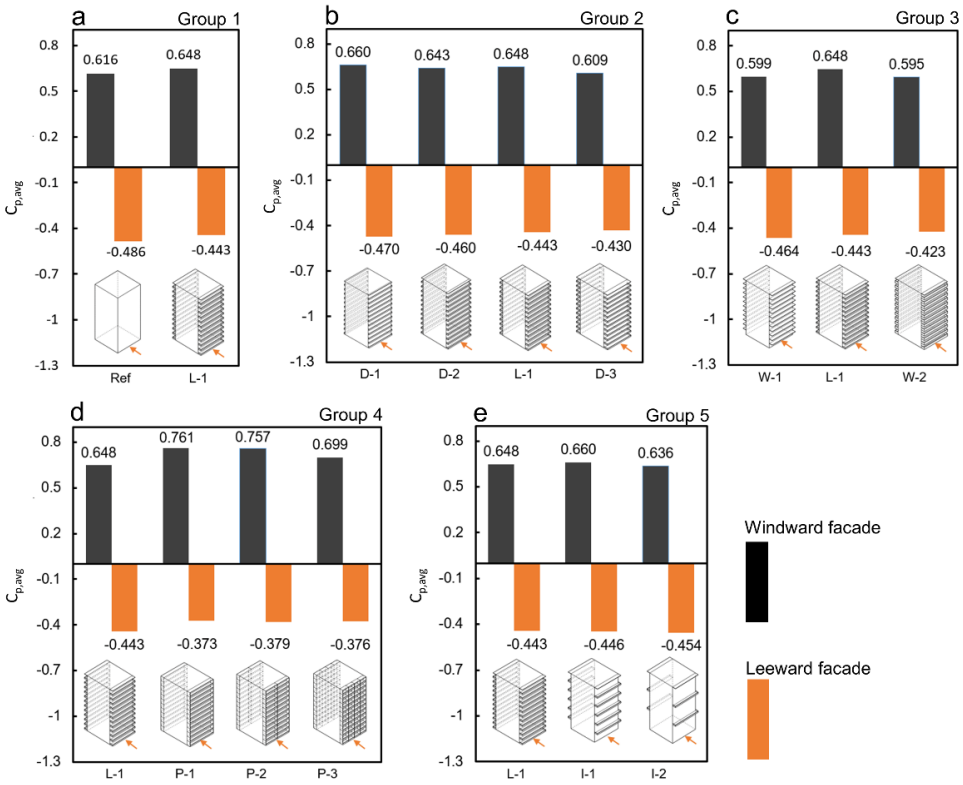

Fig. 9. $C_{p,avg}$ for windward and leeward façades of buildings in groups 1-5 as presented in Fig. 3.

3.4.2 Impact of balconies depth

The impact of the balcony depth on K and C_p is investigated based on the simulations for the cases in group 2. Fig. 10 displays K in the vertical centerplane near the windward façade and in horizontal planes at a height of 1.75 m above each floor level (pedestrian height). Fig. 11a shows the K_{avg} and K_{max} for the same horizontal planes on balcony spaces. The following observations are made:

- Fig. 10a, c, e and g indicates that by increasing the depth of balconies, larger recirculation zones with larger velocity are formed on all balcony spaces. In this case, K_{avg} increases for all levels, except level 12 (Fig. 11a).
- By increasing the depth from 1 m to 2, 3 and 4 m, the overall K_{avg} (all balconies combined) increases from 0.62 to 0.77 (by 23.7%), 0.97 (by 56.0%) and 1.09 (by 75.6%), respectively.

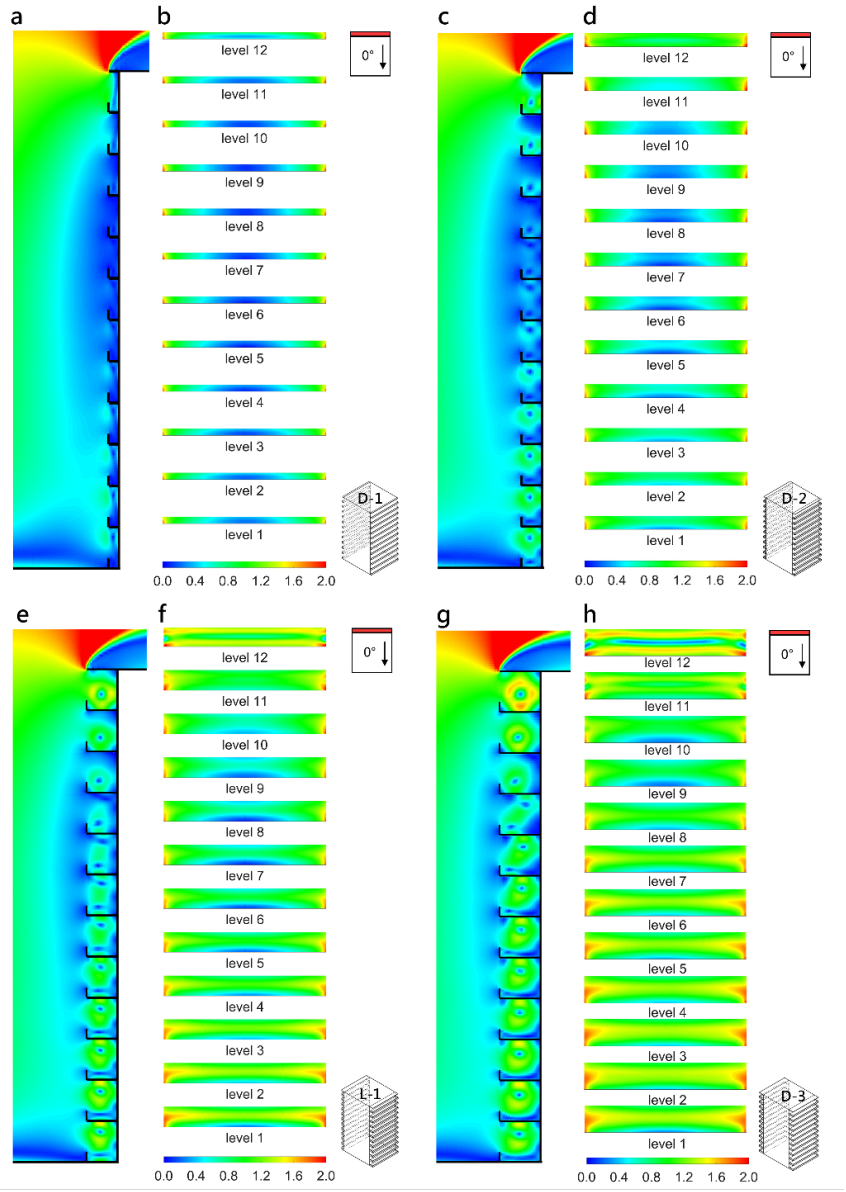

Fig. 10. Impact of balcony depth: K distributions in vertical centerplane near windward façades for (a) D-1 (D = 1 m), (c) case D-2 (D = 2 m), (e) case L-1 (D = 3 m), and (g) case D-3 (D = 4 m). (b, d, f and h) K distributions in horizontal planes at the pedestrian height on windward balconies for the same cases.

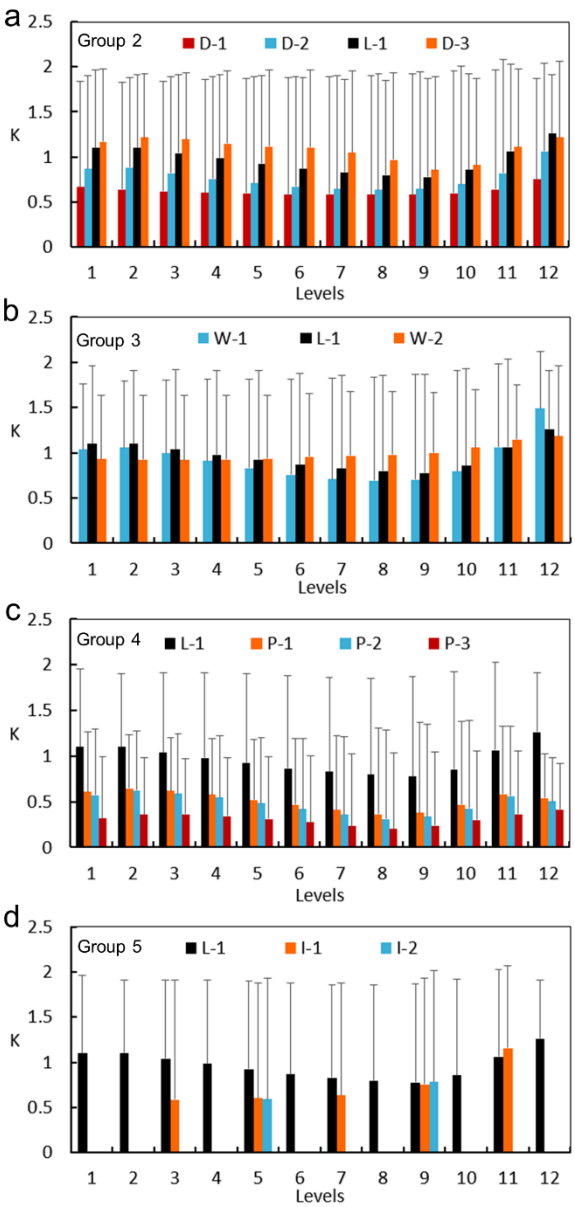

Fig. 11. K_{avg} (shown by color bars) and K_{max} (shown by vertical lines with cap) in horizontal planes at the pedestrian height for buildings in (a) group 2, (b) group 3, (c) group 4 and (d) group 5.

Fig. 12 shows C_p and ΔC_p (relative to the reference case) distributions across the windward and leeward façades of case D-1 (D = 1 m), case D-2 (D = 2 m), case L-1 (D = 3 m) and case D-3 (D = 4 m). Fig. 9b presents $C_{p,avg}$. The following observations are made:

- Fig. 12e-g (windward façade) shows that similar ΔC_p distributions are observed across the windward façades of cases D-1 (D = 1 m), D-2 (D = 2 m) and L-1 (D = 3 m). In this case, $C_{p,avg}$ is 0.660, 0.643 and 0.648, respectively (see Fig. 9b), i.e. 7.1%, 4.4% and 5.2% larger than that for the reference case. For the case with D = 4 m (case D-3), a stronger impact on the C_p occurs in the region between levels 1 and 9, where the pressure decreases (Fig. 12h) because of the relatively larger wind speed on the balcony spaces (see Fig. 10g). In this case, $C_{p,avg}$ is 0.609 (see Fig. 9b), which is only 1.1% smaller than the reference case.
- Fig. 12i-p (leeward façade) shows that by increasing the depth of the balconies, $C_{p,avg}$ increases, i.e. becomes less negative (Fig. 9b). For D = 1, 2, 3 and 4 m, $C_{p,avg}$ is -0.470, -0.460, -0.443, and -0.430, i.e. 3.3%, 5.4%, 8.9%, and 11.5% larger than the reference case, respectively.

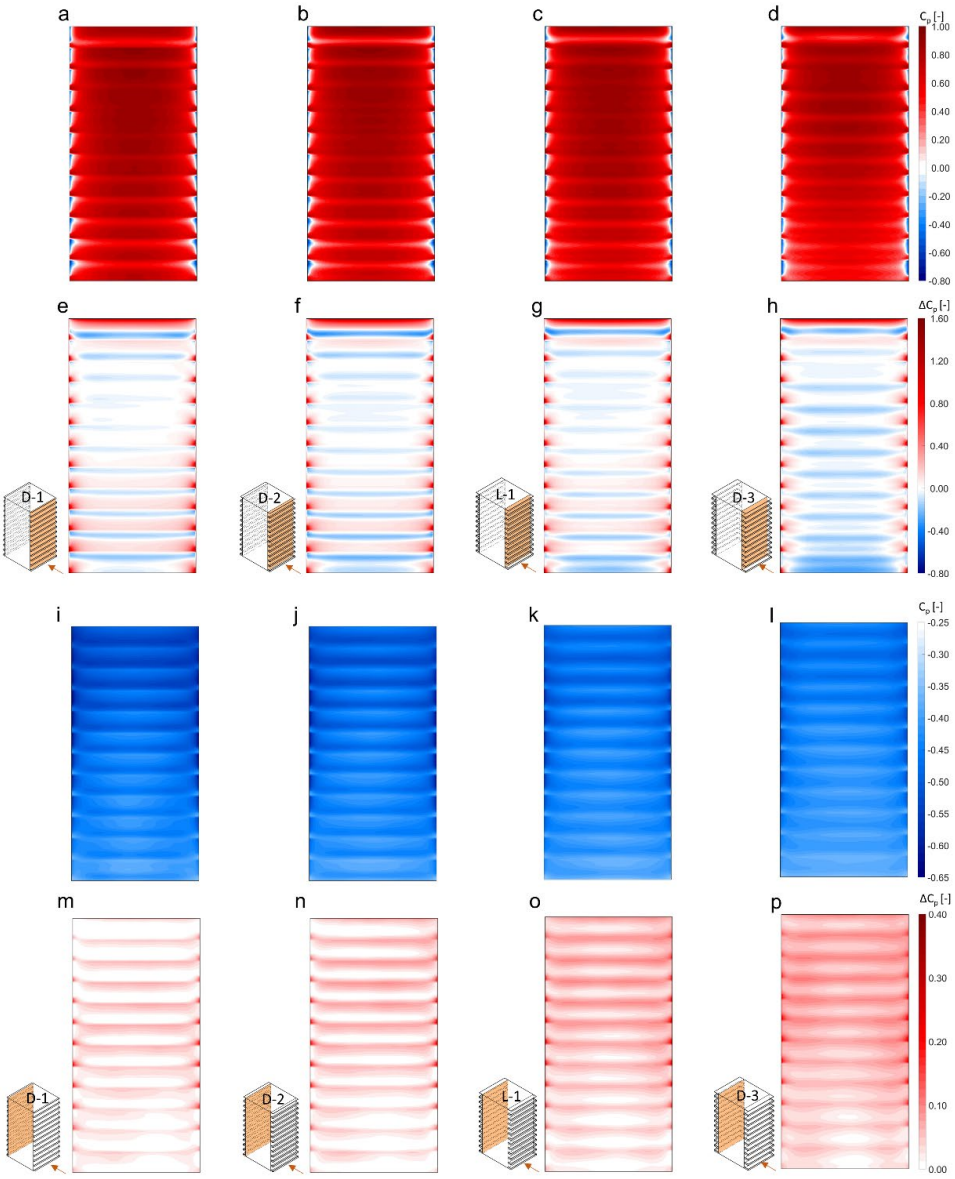

Fig. 12. Impact of balcony depth: C_p distributions on windward façades of (a) case D-1 (D = 1m), (b) case D-2 (D = 2 m), (c) case L-1 (D = 3 m), and (d) case D-3 (D = 4 m), and (e-h) ΔC_p (pressure difference relative to the reference case) for the same cases. (i-p) Same for leeward façades.

3.4.3 Impact of balcony parapet wall

The impact of the presence and the height of parapet walls on K and C_p is investigated for the three cases in group 3: case W-1 (W = 0 m), case L-1 (W = 1 m) and case W-2 (W = 2

m). Fig. 13 displays the K distributions in the vertical centerplane near the windward façade and in the horizontal planes at 1.75 m above each floor level. Fig. 11b provides the K_{max} and K_{avg} in the same horizontal planes. The following observations are made:

- For level 12, the largest K_{avg} is obtained for case W-1 (W = 0 m), followed by case L-1 (W = 1 m) and case W-2 (W = 2 m), with values of 1.49, 1.26 and 1.18, respectively. In this case, K_{max} is 2.12, 1.91 and 1.96, respectively.
- For levels 5-11, compared to the other two cases, case W-2 (W= 2 m) experiences higher local K on balcony spaces in the vertical centerplane (Fig. 13e). This is because of the airflow is forced to enter the balcony spaces through the small openings and is more confined by the parapet walls, which results in a strong flow recirculation on the balcony spaces. For balconies with higher parapet walls on levels 5-11, larger local K in the middle of the horizontal planes (Fig. 13b, d and f) and larger K_{avg} (Fig. 11b) is observed. It should be noted that K_{max} occurs near the lateral edges of the façade for all the cases on levels 5-11, and 2 m parapet walls can significantly reduce the local K close to the lateral edges, resulting in the smallest local K_{max} values (Fig. 11b).

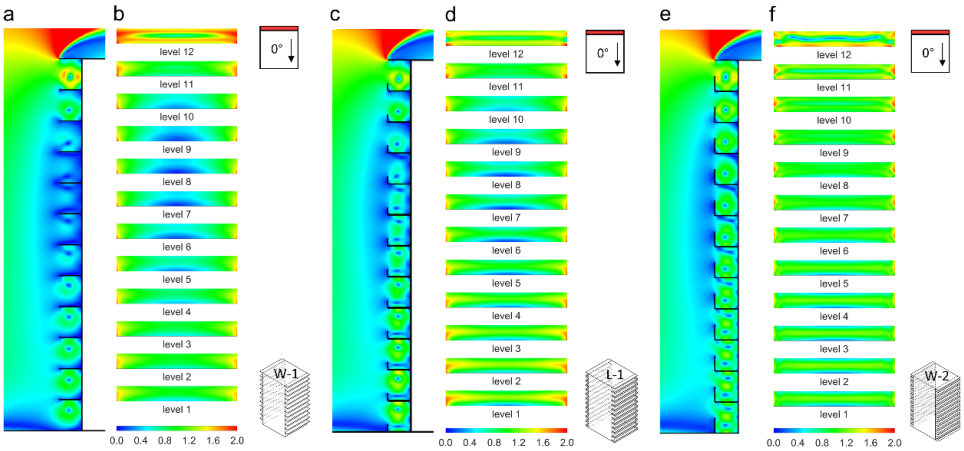

Fig. 13. Impact of balcony parapet walls: K distributions in the vertical centerplane near windward façades for (a) case W-1 (W = 0 m), (c) case L-1 (W = 1 m), and (e) case W-2 (W = 2 m). (b, d and f) K distributions in horizontal planes at the pedestrian height on windward balconies for the same cases.

- For levels 1-4, unlike the other two cases, case W-2 experiences a relatively uniform K distribution. This leads to lower K_{avg} and K_{max} compared to cases W-1 and L-1 (Fig. 11b).

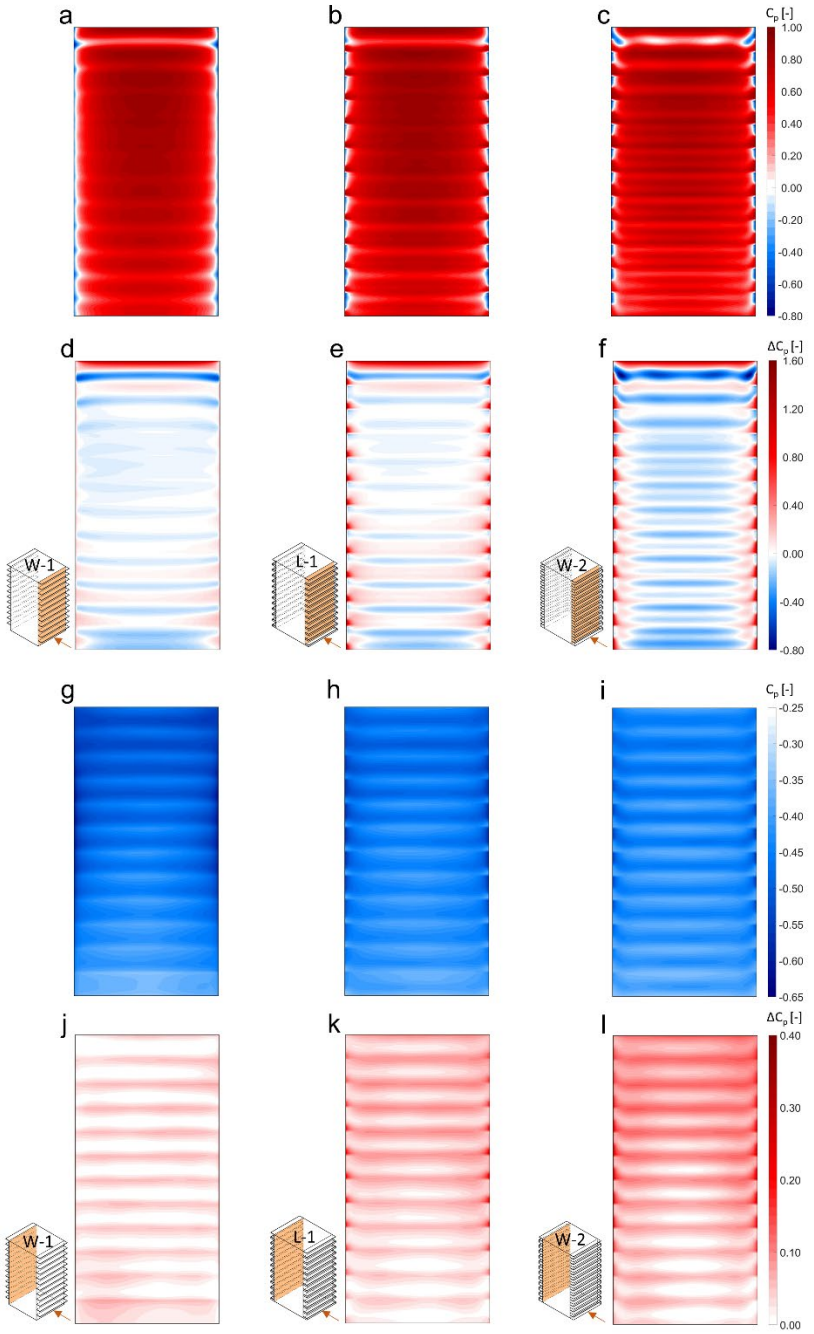

Fig. 14. Impact of balcony parapet wall: C_p distributions on windward façades for buildings with balconies: (a) case W-1 (W = 0 m), (b) case L-1 (W = 1 m), and (c) case W-2 (W = 2 m), and (d-f) ΔC_p (pressure difference relative to the reference case) for the same cases. (g-l) Same for leeward façades.

Fig. 14 shows the C_p and ΔC_p (relative to the reference case) distributions for the three cases. Fig. 9c presents $C_{p,avg}$. The following observations are made:

- Fig. 14a-f (windward façade): compared to the case without parapet wall (case W-1), the presence of 1 m high parapet walls (case L-1) leads to higher-pressure areas near the lateral edges of the windward façade (see Fig. 14d and e), and $C_{p,avg}$ increases from 0.599 to 0.648. By adding the 2 m high parapet walls (case W-2), the local C_p reduces significantly (Fig. 14c and f), and $C_{p,avg}$ reduces to 0.595 (see Fig. 9c).

Fig. 14g-l (leeward façade): by increasing W, C_p increases across the façade. As shown in Fig. 9c, for case W-1 (W = 0 m), case L-1 (W = 1 m) and case W-2 (W = 2 m), $C_{p,avg}$ is −0.464, −0.443, and -0.423, i.e. 4.5%, 8.2% and 13.0% larger than the reference case, respectively.

3.4.4 Impact of partition wall

The impact of partition walls is investigated based on the simulations for group 4. Fig. 15 displays the K distributions in horizontal planes at the 1.75 m above each floor level on the windward balconies for case L-1 (without partition walls), case P-1 (with two partition walls on lateral edges of the façades), case P-2 (with three partition walls, two on the lateral edges and one in the middle of the façades), and case P-3 (with five partition walls at equidistant locations, two of which are located on the lateral edges of the façades). Fig. 11c shows K_{max} and K_{avg} in the same horizontal planes. The following observations are made:

- For case L-1, without partition walls, a rather large stagnation region is formed upstream of the windward façade. The stagnation pressure forces the impinging wind flow to deviate horizontally, towards the lateral edges, which leads to higher wind speed near these edges. However, the presence of partition walls at the lateral edges of the façade (case P-1) impedes this horizontal flow and leads to small lateral pressure gradients on each balcony space (Fig. 16b), in turn yielding a significant reduction in both K_{max} and K_{avg} in the horizontal planes (Fig. 15b).
- By increasing the number of partition walls, K_{max} and K_{avg} decrease monotonically. The overall K_{avg} (all the balconies combined) for cases P-1, P-2 and P-3 is 0.51, 0.47 and 0.31, i.e. 47.4%, 51.6% and 68.0% smaller than case L-1, respectively.

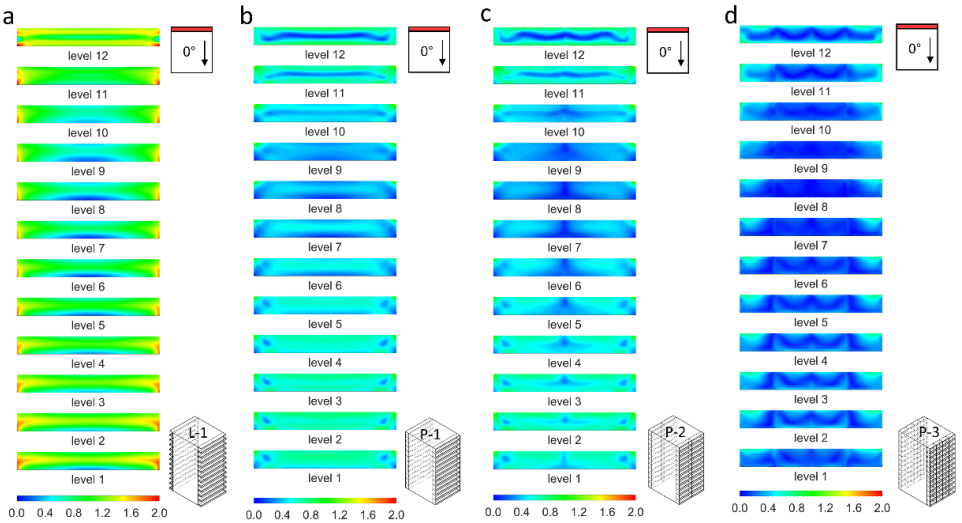

Fig. 15. Impact of balcony partition wall: K distributions in horizontal planes at the pedestrian height of (a) case L-1, (b) case P-1, (c) case P-2 and (d) case P-3.

Fig. 16 shows the C_p and ΔC_p (relative to the reference case) distributions for the four cases. Fig. 9d presents $C_{p,avg}$. The following observations are made:

- Fig. 16a-h displays the impact of partition walls on the C_p distributions across the windward façade. The presence of partition walls on both lateral edges (case P-1) reduces the spanwise pressure gradients across the façade (Fig. 16b). A similar pressure distribution can also be observed for case P-2 (Fig. 16c) when additional partition walls are used in the middle. For case P-3 when three additional partition walls are used, larger spanwise pressure gradients are observed across the middle and side partitions (Fig. 16d).
- Adding only two partition walls (at the lateral edges) strongly increases $C_{p,avg}$ on the windward façade, from 0.648 to 0.761 (an increase by 17.4%, i.e. 23.5% larger than the reference case). However, by further increasing the number of partition walls, $C_{p,avg}$ on the windward façade decreases (Fig. 16g and h). For cases P-2 and P-3, $C_{p,avg}$ is 0.759 and 0.699, i.e. 23.2% and 13.5% larger than the reference case, respectively (Fig. 9d). Still, every case with partition walls has a much higher windward $C_{p,avg}$ than the reference case.

- Fig. 16i-p displays the impact of partition walls on the C_p distributions across the leeward façade. The presence of partition walls on both lateral edges (case P-1) strongly increases the local C_p across the façade (see Fig. 16n). In this case, $C_{p,avg}$ increases from -0.443 to -0.373 (by about 15.8%, i.e. 23.3% larger than the reference case).
- By increasing the number of partition walls, on each balcony space, rather uniform-pressure regions are formed between consecutive partition walls on the leeward façade (Fig. 16k and l). Nevertheless, this has an insignificant impact on $C_{p,avg}$. For cases P-2 and P-3, $C_{p,avg}$ is -0.379 and -0.376, i.e. 22.0% and 22.6% larger than the reference case, respectively (Fig. 9d).

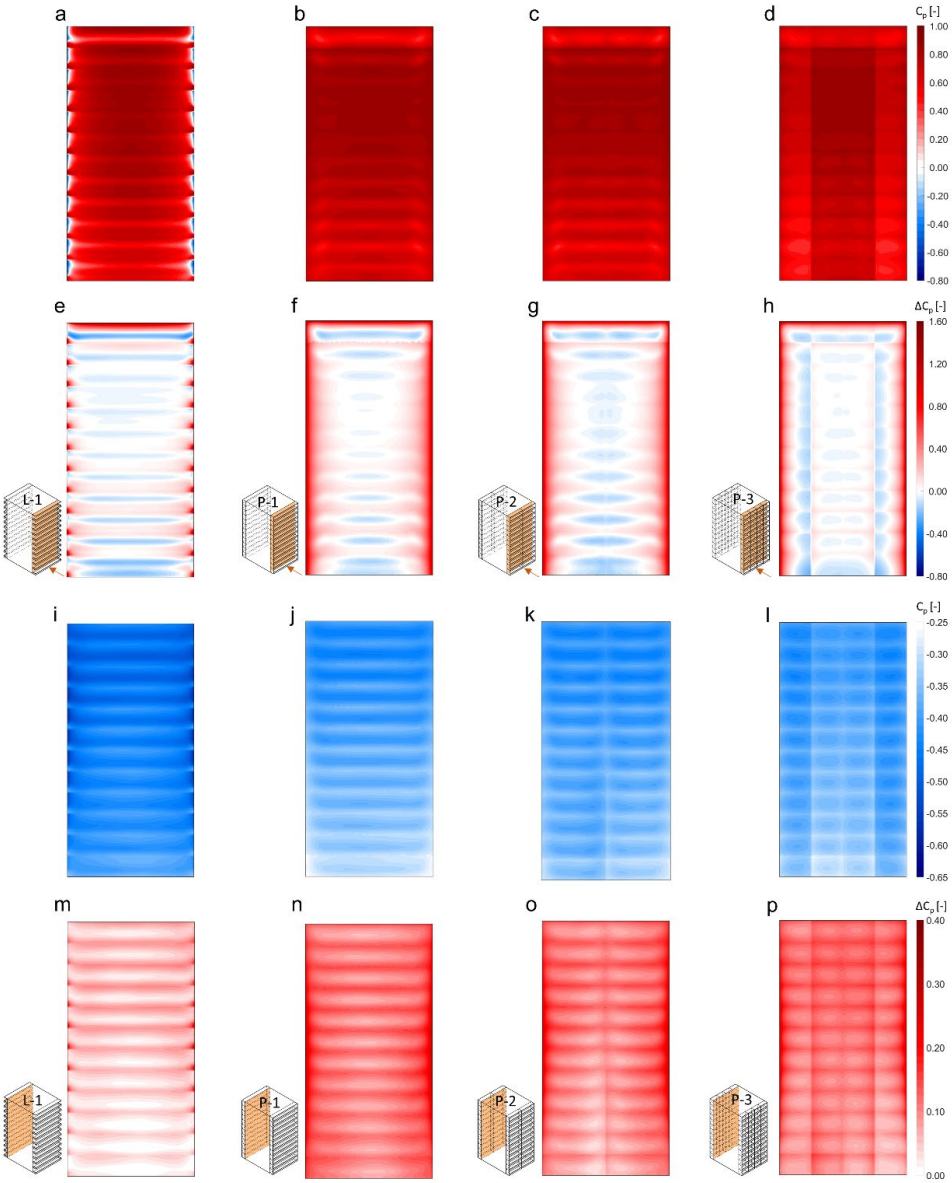

Fig. 16. Impact of balcony partition walls: C_p distributions on windward façades for buildings with balconies: (a) without a partition wall (case L-1), (b) with two partition walls (case P-1), (c) with three partition walls (case P-2) and (d) with five partition walls (case P-3), and (e-h) ΔC_p (pressure difference relative to the reference case) for the same cases. (i-p) Same for leeward façades.

3.4.5 Impact of density of balconies

The impact of the density of balconies is investigated based on the simulations for group 5: case L-1 (balconies on all levels), case I-1 (balconies on levels 3, 5, 7, 9 and 11), and case I-2 (balconies on levels 5 and 9). Fig. 17 displays the distributions of the mean wind speed ratio (K) in the vertical centerplane near the windward façade (Fig. 17a, c and e) and horizontal planes at a height of 1.75 m above each floor level (Fig. 17b, d and f). Fig. 11d shows K_{max} and K_{avg} in the horizontal plane of each level. The density of balconies can significantly affect the flow pattern near the windward façade, and also on the balcony spaces. For the three cases, for balconies below level 8, the downwash flow separates at the edge of the balconies, and a counter-clockwise vortex with relatively high wind speed is formed below each balcony floor (Fig. 17a, c and e). For these balconies, by decreasing the density of balconies, the local K and K_{max} in the horizontal plane at the pedestrian height decreases (Fig. 11d). The overall K_{avg} (all the balconies combined) for cases I-1 and I-2 is 0.75 and 0.68, i.e. 22.7% and 29.9% smaller than that for case L-1, respectively.

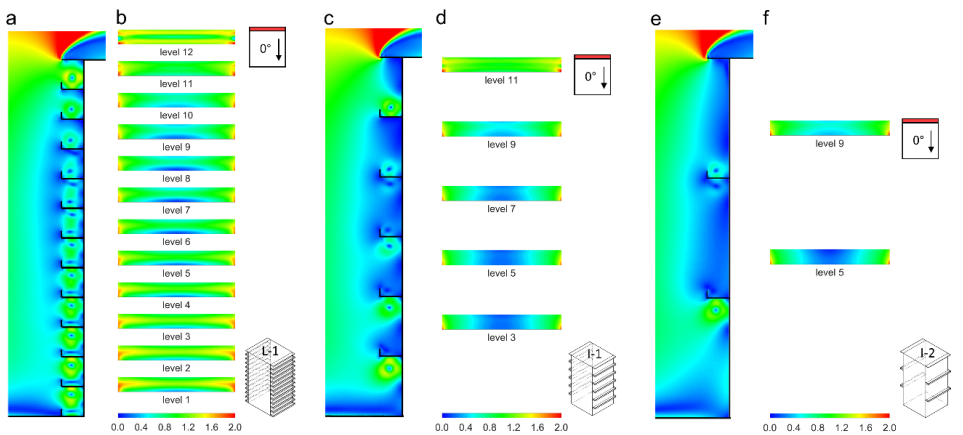

Fig. 17. K distributions in the vertical centerplane near windward façades for (a) case L-1, (c) case I-1 and (e) case I-2. (b, d and f) K distributions in horizontal planes at the pedestrian height on windward balconies for the same cases.

Fig. 18 shows C_p and ΔC_p distributions (relative to the reference case) for the three cases. Fig. 9e presents $C_{p,avg}$. The following observations are made:

- Fig. 18a-f shows that the impact of the density of balconies on C_p on the windward façade on levels 7-10 is rather insignificant. For the balconies located below level 7, however, a clear increase in C_p can be observed close to the lateral edges of the

façade behind the parapet walls while a reduction of C_p can be observed below each balcony. This C_p reduction effect is due to the counter-clockwise vortex with relatively high wind speed below each balcony floor (see Fig. 17a, c and e). $C_{p,avg}$ on the windward façade of cases L-1, I-1, I-2 is 0.648, 0.660 and 0.636 (Fig. 9e), i.e. 5.2%, 7.5% and 3.2% larger than the reference case, respectively.

- Fig. 18g-l shows that for the leeward façades of all the cases, the presence of balconies increases the local C_p close to the lateral edges of the façade behind the parapet wall and below each balcony floor. For cases L-1, I-1 and I-2, $C_{p,avg}$ is -0.443, -0.446, and -0.454, i.e. 8.9%, 8.2% and 6.6% larger than the reference case, respectively.

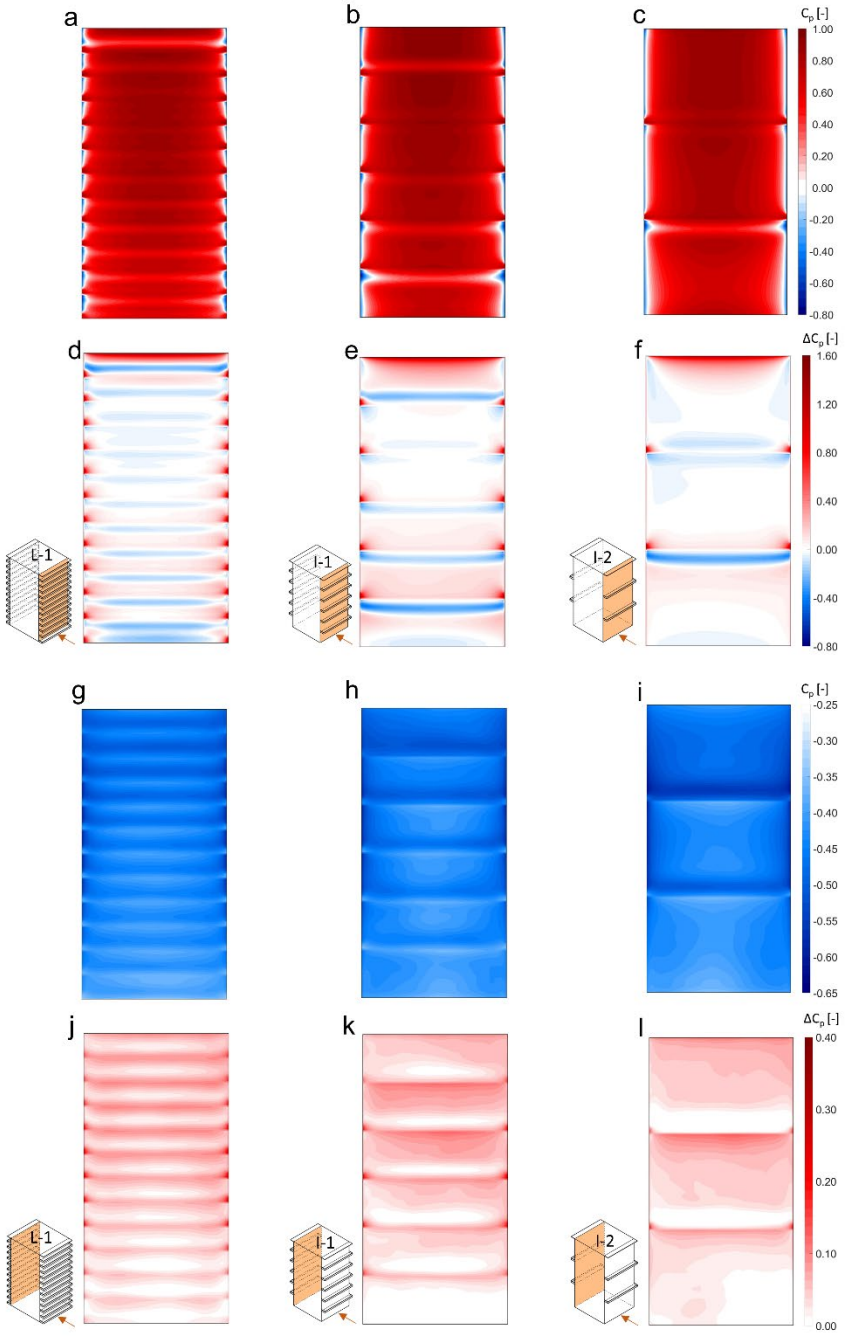

Fig. 18. Impact of density of balconies: C_p distributions on windward façades for buildings with: (a) balconies on every level (case L-1), (b) balconies on levels 3, 5, 7, 9 and 11 (case I-1), and (c) balconies on levels 5 and 9 (case I-2), and (d-f) ΔC_p (pressure difference relative to the reference case) for the same cases. (g-l) Same for leeward façades.

3.5 Limitations and future work

Although this study has performed a systematic sensitivity analysis based on a large number of parameters and CFD simulations, there are still a number of limitations that provide opportunities for future work:

- In the present study, the focus is on the mean surface pressure coefficient and the mean wind speed. It should be noted that research on building ventilation and infiltration is mostly performed based on mean surface pressure coefficients [65–67]. In addition, also studies on pedestrian-level wind comfort and wind safety assessment are generally performed based on the mean wind speed [6,23,28,68–70]. Given the importance of peak pressures for wind loads [71–73], future work should consider the impact of balcony geometry on peak surface pressures.
- In this study, all the cases are assumed to be fully closed, i.e. airtight buildings without any openings. The exterior surface pressure coefficients of enclosed buildings are widely used as input parameters in building energy simulation tools to predict ventilation and infiltration [65–67]. It should be noted however that earlier studies have shown that the presence of open windows (or doors) on building façades can affect the near-façade wind flow and the local and surface-averaged static pressure [74]. Therefore, future studies should consider cases for which building balconies coexist with open windows (or doors).
- This study is only performed for one inflow wind speed and for perpendicular wind directions ($\theta = 0°$ and 180°). For low wind speeds, natural or mixed (combined forced and natural) convection heat transfer may be dominant that can significantly affect the near-façade wind flow. Previous studies have indicated that balconies can also significantly affect the mean surface pressure under oblique wind directions [3,4]. Future work should focus on the impact of wind speed and wind direction.
- This study only focuses on an isolated high-rise building with balconies. The presence of surrounding buildings may lead to complexities of wind flow and would modify the surface pressure and near-façades flow field [75–78].
- This study focuses on balconies that extend along the entire width of the building façade. Future work should focus on other types of building balcony such as discontinuous balconies. Earlier studies have shown that façade and roof

geometrical details can also significantly affect the near-façade airflow patterns [79–83]. The focus of this study is on building balconies, which are generally the most prominent façade elements. This work can be extended to include other types of building surface geometrical details.

3.6 Conclusions

In this study, the impact of geometrical characteristics of building balconies on the near-façade wind flow field, mean wind speed on balcony spaces, and wind-induced mean surface pressure for a high-rise building is investigated. The target parameters are the mean wind speed ratio at the pedestrian height on the balconies (local: K, area-averaged: $K_{avg,}$ maximum: K_{max}) and the mean surface pressure coefficient (local: C_p, façade-averaged: $C_{p,avg}$). LES simulations are performed to investigate the impact of (i) balconies present or not, (ii) balcony depth, (iii) balcony parapet walls, (iv) balcony partition walls, and (v) density of balconies. Within the range of parameters evaluated in the present study, the following conclusions are made:

a. Balconies present or not
   - The presence of balconies increases $C_{p,avg}$ on both windward façade and leeward façade by 5.2% and 8.9%, respectively. Note that for negative C_p values, the term “increase” refers to a less negative value and hence a lower absolute value of C_p.

b. Impact of balcony depth
   - Increasing the depth of balconies leads to larger recirculation zones with higher mean wind speed on windward balcony spaces, resulting in a larger K_{avg}. For example, by increasing the depth of balconies from 1 m to 4 m, the overall K_{avg} (all balconies combined) increases by 75.6%.
   - In general, increasing the depth of balconies from 1 m to 2, 3 and 4 m reduces $C_{p,avg}$ on windward façade. From 1 m to 4 m, $C_{p,avg}$ reduces from 0.660 to 0.609.
   - For the leeward façade, increasing the depth of balconies from 1 m to 4 m can increase $C_{p,avg}$ from -0.470 to -0.430.

c. Impact of balcony parapet walls

- Adding 1 m high parapet walls has an insignificant impact on K_{avg} and K_{max} on the windward balconies.
- By increasing the height of the parapet walls from 1 m to 2 m, K_{max} on the windward balconies decreases substantially.
- For the windward façade, the presence of 1 m high parapet walls increases $C_{p,avg}$ from 0.599 to 0.648. By increasing the height of the parapet walls from 1 m to 2 m, $C_{p,avg}$ reduces from 0.648 to 0.595.
- For the leeward façade, the presence of 1 m high parapet walls increases the $C_{p,avg}$ from -0.464 to -0.443. As the height increases from 1 m to 2 m, $C_{p,avg}$ increases further to -0.423.

d. Impact of balcony partition walls

- Adding partition walls can significantly reduce the K_{avg} and K_{max} on the windward balconies. The maximum reduction in the overall K_{avg} (68.0%) is achieved when five partition walls are used. This is about 51.6% and 47.4% when only three and two partition walls are implemented, respectively.
- Adding partition walls can significantly increase $C_{p,avg}$. For example, by adding two partition walls at the lateral edges of the façades, $C_{p,avg}$ increases from 0.648 to 0.761, and from -0.443 to -0.373 for the windward and leeward façades, respectively.

e. Impact of density of balconies

- For the windward façade, by decreasing the density of balconies, K_{avg} substantially reduces for balconies located below the stagnation area.
- For the three cases tested, no correlation between the density of the balconies and $C_{p,avg}$ is observed for both windward and leeward façades. For the windward façade, the case with 5 balconies (on levels 3, 5, 7, 9 and 11) shows the largest $C_{p,avg}$ (= 0.660). For the leeward façade, the largest $C_{p,avg}$ is obtained for the case with 12 balconies (= -0.443).

The present findings can be useful in developing, designing and constructing buildings with façade details that improve ventilation, air quality and wind comfort.

Acknowledgments

This work has been sponsored by NWO Exacte en Natuurwetenschappen (Physical Sciences) for the use of supercomputer facilities, with financial support from the Nederlandse Organisatie voor Wetenschappelijk Onderzoek (Netherlands Organization for Scientifici Research, NWO). This work was carried out on the Dutch national e-infrastructure with the support of SURF Cooperative. The authors gratefully acknowledge the partnership with ANSYS CFD.

References

[1] H. Montazeri, B. Blocken, CFD simulation of wind-induced pressure coefficients on buildings with and without balconies: Validation and sensitivity analysis, Build. Environ. 60 (2013) 137–149. doi:10.1016/j.buildenv.2012.11.012.

[2] D. Cui, Z. Ai, C. ming Mak, K. Kwok, P. Xue, The influence of envelope features on interunit dispersion around a naturally ventilated multi-story building, Build. Simul. 11 (2018) 1245–1253. doi:10.1007/s12273-018-0460-x.

[3] T. Stathopoulos, X. Zhu, Wind pressures on building with appurtenances, J. Wind Eng. Ind. Aerodyn. 31 (1988) 265–281. doi:10.1016/0167-6105(88)90008-6.

[4] H. Montazeri, B. Blocken, W.D. Janssen, T. van Hooff, CFD evaluation of new second-skin facade concept for wind comfort on building balconies: Case study for the Park Tower in Antwerp, Build. Environ. 68 (2013) 179–192. doi:10.1016/j.buildenv.2013.07.004.

[5] K. Yuan, Y. Hui, Z. Chen, Effects of facade appurtenances on the local pressure of high-rise building, J. Wind Eng. Ind. Aerodyn. 178 (2018) 26–37. doi:10.1016/j.jweia.2018.05.004.

[6] B. Blocken, 50 years of Computational Wind Engineering: Past, present and future, J. Wind Eng. Ind. Aerodyn. 129 (2014) 69–102. doi:https://doi.org/10.1016/j.jweia.2014.03.008.

[7] S. Murakami, Computational wind engineering, J. Wind Eng. Ind. Aerodyn. 36 (1990) 517–538. doi:10.1016/0167-6105(90)90335-A.

[8] B. Blocken, J. Carmeliet, Pedestrian wind conditions at outdoor platforms in a high-rise apartment building: generic sub-configuration validation, wind comfort assessment and uncertainty issues, Wind Struct. 11 (2008) 51–70.

doi:10.12989/was.2008.11.1.051.

[9] S. Omrani, V. Garcia-Hansen, B.R. Capra, R. Drogemuller, On the effect of provision of balconies on natural ventilation and thermal comfort in high-rise residential buildings, Build. Environ. 123 (2017) 504–516. doi:10.1016/J.BUILDENV.2017.07.016.

[10] G. Hong, B.S. Kim, Field measurements of infiltration rate in high rise residential buildings using the constant concentration method, Build. Environ. 97 (2016) 48–54. doi:10.1016/j.buildenv.2015.11.027.

[11] H. Montazeri, B. Blocken, D. Derome, J. Carmeliet, J.L.M. Hensen, CFD analysis of forced convective heat transfer coefficients at windward building facades: Influence of building geometry, J. Wind Eng. Ind. Aerodyn. 146 (2015) 102–116. doi:10.1016/j.jweia.2015.07.007.

[12] H. Montazeri, B. Blocken, Extension of generalized forced convective heat transfer coefficient expressions for isolated buildings taking into account oblique wind directions, Build. Environ. 140 (2018) 194–208. doi:10.1016/j.buildenv.2018.05.027.

[13] M.T. Kahsay, G.T. Bitsuamlak, F. Tariku, CFD simulation of external CHTC on a high-rise building with and without façade appurtenances, Build. Environ. 165 (2019) 106350. doi:10.1016/j.buildenv.2019.106350.

[14] T. Stathopoulos, Wind loads on low-rise buildings: a review of the state of the art, Eng. Struct. 6 (1984) 119–135. doi:10.1016/0141-0296(84)90005-1.

[15] Z. Ai, C. Mak, J. Niu, Z. Li, The assessment of the performance of balconies using computational fluid dynamics, Build. Serv. Eng. Res. Technol. 32 (2011) 229–243. doi:10.1177/0143624411404646.

[16] N. Izadyar, W. Miller, B. Rismanchi, V. Garcia-Hansen, A numerical investigation of balcony geometry impact on single-sided natural ventilation and thermal comfort, Build. Environ. (2020) 106847. doi:10.1016/j.buildenv.2020.106847.

[17] F. Mozaffari Ghadikolaei, D.R. Ossen, M.F. Mohamed, Effects of wing wall at the balcony on the natural ventilation performance in medium-rise residential buildings, J. Build. Eng. 31 (2020) 101316. doi:10.1016/j.jobe.2020.101316.

[18] X. Zheng, H. Montazeri, B. Blocken, CFD simulations of wind flow and mean surface pressure for buildings with balconies: Comparison of RANS and LES, Build. Environ. 173 (2020) 106747. doi:10.1016/j.buildenv.2020.106747.

[19] Z.T. Ai, C.M. Mak, Large eddy simulation of wind-induced interunit dispersion around multistory buildings, Indoor Air. 26 (2016) 259–273. doi:10.1111/ina.12200.

[20] M. Llaguno-Munitxa, E. Bou-Zeid, M. Hultmark, The influence of building geometry on street canyon air flow: Validation of large eddy simulations against wind tunnel experiments, J. Wind Eng. Ind. Aerodyn. 165 (2017) 115–130. doi:10.1016/j.jweia.2017.03.007.

[21] S. Murakami, Comparison of various turbulence models applied to a bluff body, J. Wind Eng. Ind. Aerodyn. 46-47 (1993) 21–36. doi:10.1016/0167-6105(93)90112-2.

[22] Y. Tominaga, A. Mochida, S. Murakami, S. Sawaki, Comparison of various revised k–ε models and LES applied to flow around a high-rise building model with 1:1:2 shape placed within the surface boundary layer, J. Wind Eng. Ind. Aerodyn. 96 (2008) 389–411. doi:10.1016/j.jweia.2008.01.004.

[23] B. Blocken, LES over RANS in building simulation for outdoor and indoor applications: A foregone conclusion?, Build. Simul. 11 (2018) 821–870. doi:10.1007/s12273-018-0459-3.

[24] W. Rodi, Comparison of LES and RANS calculations of the flow around bluff bodies, J. Wind Eng. Ind. Aerodyn. 69-71 (1997) 55–75. doi:10.1016/S0167-6105(97)00147-5.

[25] S. Murakami, A. Mochida, K. Hibi, Three-dimensional numerical simulation of air flow around a cubic model by means of large eddy simulation, J. Wind Eng. Ind. Aerodyn. 25 (1987) 291–305. doi:10.1016/0167-6105(87)90023-7.

[26] N. Antoniou, H. Montazeri, H. Wigo, M.K.-A. Neophytou, B. Blocken, M. Sandberg, CFD and wind-tunnel analysis of outdoor ventilation in a real compact heterogeneous urban area: Evaluation using “air delay,” Build. Environ. 126 (2017) 355–372. doi:10.1016/j.buildenv.2017.10.013.

[27] X. Zhou, A. Ying, B. Cong, H. Kikumoto, R. Ooka, L. Kang, H. Hu, Large eddy simulation of the effect of unstable thermal stratification on airflow and pollutant dispersion around a rectangular building, J. Wind Eng. Ind. Aerodyn. 211 (2021) 104526. doi:10.1016/j.jweia.2021.104526.

[28] T. Stathopoulos, Computational wind engineering: Past achievements and future challenges, J. Wind Eng. Ind. Aerodyn. 67-68 (1997) 509–532. doi:10.1016/S0167-6105(97)00097-4.

[29] S. Murakami, A. Mochida, Y. Hayashi, Examining the κ-ϵ model by means of a wind tunnel test and large-eddy simulation of the turbulence structure around a cube, J. Wind Eng. Ind. Aerodyn. 35 (1990) 87–100. doi:10.1016/0167-6105(90)90211-T.

[30] J. Liu, J. Niu, CFD simulation of the wind environment around an isolated high-rise building: An evaluation of SRANS, LES and DES models, Build. Environ. 96 (2016) 91–106. doi:10.1016/j.buildenv.2015.11.007.

[31] Y. Tominaga, T. Stathopoulos, CFD modeling of pollution dispersion in building array: Evaluation of turbulent scalar flux modeling in RANS model using LES results, J. Wind Eng. Ind. Aerodyn. 104-106 (2012) 484–491. doi:10.1016/j.jweia.2012.02.004.

[32] R. Yoshie, A. Mochida, Y. Tominaga, H. Kataoka, K. Harimoto, T. Nozu, T. Shirasawa, Cooperative project for CFD prediction of pedestrian wind environment in the Architectural Institute of Japan, J. Wind Eng. Ind. Aerodyn. 95 (2007) 1551–1578. doi:10.1016/j.jweia.2007.02.023.

[33] K. Hanjalic, Will RANS survive LES? A view of perspectives, J. Fluids Eng. 127 (2005) 831. doi:10.1115/1.2037084.

[34] Y. Tominaga, T. Stathopoulos, CFD simulation of near-field pollutant dispersion in the urban environment: A review of current modeling techniques, Atmos. Environ. 79 (2013) 716–730. doi:10.1016/j.atmosenv.2013.07.028.

[35] P. Gousseau, B. Blocken, T. Stathopoulos, G.J.F. van Heijst, CFD simulation of near-field pollutant dispersion on a high-resolution grid: A case study by LES and RANS for a building group in downtown Montreal, Atmos. Environ. 45 (2011) 428–438. doi:10.1016/j.atmosenv.2010.09.065.

[36] E. Maruta, M. Kanda, J. Sato, Effects on surface roughness for wind pressure on glass and cladding of buildings, J. Wind Eng. Ind. Aerodyn. 74 (1998) 651–663. doi:10.1016/S0167-6105(98)00059-2.

[37] I. Chand, P.K. Bhargava, N.L.V. Krishak, Effect of balconies on ventilation inducing aeromotive force on low-rise buildings, Build. Environ. 33 (1998) 385–396. doi:10.1016/S0360-1323(97)00054-1.

[38] L. Ludena, A.G. Chowdhuryb, B. Hajrac, M. Moravej, M.A. Mooneghi, P. Irwin, I. Zisis, The effect of balconies on the wind induced loads on a fifteen story building, in: Proc., 4th Am. Assoc. Wind Eng. Work., Miami, 2016.

[39] A.G. Chowdhury, L. Ludena, M. Moravej, M.A. Mooneghi, P. Irwin, Wind Loads on

Buildings with Balcony Glass Handrails, in: Ninth Asia-Pacific Conf. Wind Eng., The University of Auckland, Auckland, 2017.

[40] Y. Hui, K. Yuan, Z. Chen, Q. Yang, Characteristics of aerodynamic forces on high-rise buildings with various façade appurtenances, J. Wind Eng. Ind. Aerodyn. 191 (2019) 76–90. doi:10.1016/j.jweia.2019.06.002.

[41] S. Murakami, Computational wind engineering, J. Wind Eng. Ind. Aerodyn. 36 (1990) 517–538. doi:10.1016/0167-6105(90)90335-A.

[42] E. Prianto, P. Depecker, Characteristic of airflow as the effect of balcony, opening design and internal division on indoor velocity, Energy Build. 34 (2002) 401–409. doi:10.1016/S0378-7788(01)00124-4.

[43] Z. Ai, C. Mak, J. Niu, Z. Li, Q. Zhou, The effect of balconies on ventilation performance of low-rise buildings, Indoor Built Environ. 20 (2011) 649–660. doi:10.1177/1420326X11409457.

[44] Z. Ai, C. Mak, J. Niu, Numerical investigation of wind-induced airflow and interunit dispersion characteristics in multistory residential buildings, Indoor Air. 23 (2013) 417–429. doi:10.1111/ina.12041.

[45] F. Murena, B. Mele, Effect of balconies on air quality in deep street canyons, Atmos. Pollut. Res. 7 (2016) 1004–1012. doi:10.1016/J.APR.2016.06.005.

[46] V.A. Karkoulias, P.E. Marazioti, D.P. Georgiou, E.A. Maraziotis, Computational Fluid Dynamics modeling of the trace elements dispersion and comparison with measurements in a street canyon with balconies in the city of Patras, Greece, Atmos. Environ. (2019) 117210. doi:10.1016/j.atmosenv.2019.117210.

[47] D. Cui, X. Li, Y. Du, C.M. Mak, K. Kwok, Effects of envelope features on wind flow and pollutant exposure in street canyons, Build. Environ. (2020) 106862. doi:10.1016/J.BUILDENV.2020.106862.

[48] X. Zhu, Wind pressures on buildings with appurtenances, MSc thesis, Concordia University, 1987.

[49] J. Franke, A. Hellsten, H. Schlünzen, B. Carissimo, Best practice guideline for the CFD simulation of flows in the urban environment, Meteorological Inst., COST, Hamburg, Germany, 2007.

[50] Y. Tominaga, A. Mochida, R. Yoshie, H. Kataoka, T. Nozu, M. Yoshikawa, T. Shirasawa, AIJ guidelines for practical applications of CFD to pedestrian wind environment

around buildings, J. Wind Eng. Ind. Aerodyn. 96 (2008) 1749–1761. doi:10.1016/j.jweia.2008.02.058.

[51] B. Blocken, Computational Fluid Dynamics for urban physics: Importance, scales, possibilities, limitations and ten tips and tricks towards accurate and reliable simulations, Build. Environ. 91 (2015) 219–245. doi:10.1016/j.buildenv.2015.02.015.

[52] S. Iousef, H. Montazeri, B. Blocken, P.J.V. van Wesemael, On the use of non-conformal grids for economic LES of wind flow and convective heat transfer for a wall-mounted cube, Build. Environ. 119 (2017) 44–61. doi:10.1016/j.buildenv.2017.04.004.

[53] T. van Hooff, B. Blocken, Coupled urban wind flow and indoor natural ventilation modelling on a high-resolution grid: A case study for the Amsterdam ArenA stadium, Environ. Model. Softw. 25 (2010) 51–65. doi:10.1016/j.envsoft.2009.07.008.

[54] H. Werner, H. Wengle, Large-eddy simulation of turbulent flow over and around a cube in a plate channel, in: Turbul. Shear Flows 8, Springer Berlin Heidelberg, Berlin, Heidelberg, 1993: pp. 155–168. doi:10.1007/978-3-642-77674-8_12.

[55] E. Sergent, Vers une méthodologie de couplage entre la simulation des grandes échelles et les modèles statistiques, Ecully, Ecole centrale de Lyon, 2002.

[56] A. Gerasimov, Quick guide to setting up LES-type simulations, version 1.4., European Technology Group, ANSYS Sweden AB, 2016.

[57] F. Nicoud, F. Ducros, Subgrid-scale stress modelling based on the square of the velocity gradient tensor, Flow, Turbul. Combust. 62 (1999) 183–200.

[58] ANSYS Inc., Release 18.0, Theory Guide, ANSYS Inc, Canonsburg, PA 15317, USA, 2017.

[59] T.-H. Shih, W.W. Liou, A. Shabbir, Z. Yang, J. Zhu, A new k-ϵ eddy viscosity model for high reynolds number turbulent flows, Comput. Fluids. 24 (1995) 227–238. doi:10.1016/0045-7930(94)00032-T.

[60] W. Samuel, Typology: European Balconies - issuu, (2016). https://issuu.com/samwill89/docs/typology-balcony_not_faced.

[61] B. Blocken, J. Carmeliet, T. Stathopoulos, CFD evaluation of wind speed conditions in passages between parallel buildings—effect of wall-function roughness modifications for the atmospheric boundary layer flow, J. Wind Eng. Ind. Aerodyn.

95 (2007) 941–962. doi:10.1016/j.jweia.2007.01.013.

[62] P.J. Richards, R.P. Hoxey, Appropriate boundary conditions for computational wind engineering models using the k-ε turbulence model, J. Wind Eng. Ind. Aerodyn. (1993) 145–153. doi:10.1016/B978-0-444-81688-7.50018-8.

[63] J. Wieringa, Updating the Davenport roughness classification, J. Wind Eng. Ind. Aerodyn. 41 (1992) 357–368. doi:10.1016/0167-6105(92)90434-C.

[64] F. Mathey, D. Cokljat, J.P. Bertoglio, E. Sergent, Assessment of the vortex method for Large Eddy Simulation inlet conditions, Prog. Comput. Fluid Dyn. An Int. J. 6 (2006) 58. doi:10.1504/PCFD.2006.009483.

[65] R. Ramponi, A. Angelotti, B. Blocken, Energy saving potential of night ventilation: Sensitivity to pressure coefficients for different European climates, Appl. Energy. 123 (2014) 185–195. doi:10.1016/j.apenergy.2014.02.041.

[66] R. Ramponi, I. Gaetani, A. Angelotti, Influence of the urban environment on the effectiveness of natural night-ventilation of an office building, Energy Build. 78 (2014) 25–34. doi:10.1016/j.enbuild.2014.04.001.

[67] D. Cóstola, B. Blocken, J.L.M. Hensen, Overview of pressure coefficient data in building energy simulation and airflow network programs, Build. Environ. 44 (2009) 2027–2036. doi:10.1016/j.buildenv.2009.02.006.

[68] B. Blocken, T. Stathopoulos, J.P.A.J. van Beeck, Pedestrian-level wind conditions around buildings: Review of wind-tunnel and CFD techniques and their accuracy for wind comfort assessment, Build. Environ. 100 (2016) 50–81. doi:10.1016/j.buildenv.2016.02.004.

[69] C.J. Baker, Wind engineering—Past, present and future, J. Wind Eng. Ind. Aerodyn. 95 (2007) 843–870. doi:10.1016/j.jweia.2007.01.011.

[70] B. Blocken, W.D. Janssen, T. van Hooff, CFD simulation for pedestrian wind comfort and wind safety in urban areas: General decision framework and case study for the Eindhoven University campus, Environ. Model. Softw. 30 (2012) 15–34. doi:10.1016/j.envsoft.2011.11.009.

[71] D.W. Etheridge, Unsteady flow effects due to fluctuating wind pressures in natural ventilation design—instantaneous flow rates, Build. Environ. 35 (2000) 321–337. doi:https://doi.org/10.1016/S0360-1323(99)00021-9.

[72] N. Le Roux, X. Faure, C. Inard, S. Soares, L. Ricciardi, Reduced-scale study of wind

influence on mean airflows inside buildings equipped with ventilation systems, Build. Environ. 58 (2012) 231–244. doi:https://doi.org/10.1016/j.buildenv.2012.07.007.

[73] J. Wang, P. Van Phuc, Q. Yang, Y. Tamura, LES study of wind pressure and flow characteristics of flat-roof-mounted solar arrays, J. Wind Eng. Ind. Aerodyn. 198 (2020) 104096. doi:https://doi.org/10.1016/j.jweia.2020.104096.

[74] F. Xing, D. Mohotti, K. Chauhan, Experimental and numerical study on mean pressure distributions around an isolated gable roof building with and without openings, Build. Environ. 132 (2018) 30–44. doi:10.1016/j.buildenv.2018.01.027.

[75] S. Murakami, K. Uehara, H. Komine, Amplification of wind speed at ground level due to construction of high-rise building in urban area, J. Wind Eng. Ind. Aerodyn. 4 (1979) 343–370. doi:10.1016/0167-6105(79)90012-6.

[76] C.-H. Chang, R.N. Meroney, The effect of surroundings with different separation distances on surface pressures on low-rise buildings, J. Wind Eng. Ind. Aerodyn. 91 (2003) 1039–1050. doi:10.1016/S0167-6105(03)00051-5.

[77] T. Nozu, T. Tamura, K. Takeshi, K. Akira, Mesh-adaptive LES for wind load estimation of a high-rise building in a city, J. Wind Eng. Ind. Aerodyn. 144 (2015) 62–69. doi:10.1016/j.jweia.2015.05.007.

[78] N. Antoniou, H. Montazeri, M. Neophytou, B. Blocken, CFD simulation of urban microclimate: Validation using high-resolution field measurements, Sci. Total Environ. 695 (2019) 133743. doi:https://doi.org/10.1016/j.scitotenv.2019.133743.

[79] J. Wang, Q. Yang, Y. Tamura, Effects of building parameters on wind loads on flat-roof-mounted solar arrays, J. Wind Eng. Ind. Aerodyn. 174 (2018) 210–224. doi:https://doi.org/10.1016/j.jweia.2017.12.023.

[80] T. van Druenen, T. van Hooff, H. Montazeri, B. Blocken, CFD evaluation of building geometry modifications to reduce pedestrian-level wind speed, Build. Environ. 163 (2019) 106293. doi:10.1016/j.buildenv.2019.106293.

[81] H. Montazeri, F. Montazeri, CFD simulation of cross-ventilation in buildings using rooftop wind-catchers: Impact of outlet openings, Renew. Energy. 118 (2018) 502–520. doi:10.1016/j.renene.2017.11.032.

[82] J. Wang, Q. Yang, P. Van Phuc, Y. Tamura, Characteristics of conical vortices and their effects on wind pressures on flat-roof-mounted solar arrays by LES, J. Wind Eng. Ind.

Aerodyn. 200 (2020) 104146. doi:https://doi.org/10.1016/j.jweia.2020.104146.

[83] M. Alsailani, H. Montazeri, A. Rezaeiha, Towards optimal aerodynamic design of wind catchers: Impact of geometrical characteristics, Renew. Energy. 168 (2021) 1344–1363. doi:10.1016/j.renene.2020.12.053.

Chapter 4

Large-eddy simulation of pollutant dispersion in generic urban street canyons: Guidelines for domain size

This chapter has been published as a peer-reviewed journal paper:

Large-eddy simulation of pollutant dispersion in generic urban street canyons: Guidelines for domain size

X. Zheng, H. Montazeri, B. Blocken

Journal of Wind Engineering and Industrial Aerodynamics 211, 104527

Abstract: Pollutant dispersion in urban street canyons has been widely investigated by large-eddy simulation (LES). Many LES studies focused on generic street canyons under a wind direction perpendicular to the street axis. Accurate LES simulations require a sufficiently large domain size to minimize the effects of the artificial boundary conditions at the domain faces on the results. As opposed to RANS simulations, there is a lack of guidelines for an appropriate domain size for LES simulations of wind flow and pollutant dispersion in street canyons. The present study systematically investigates the effect of the domain width, domain height and upstream and downstream domain lengths on the wind flow and pollutant dispersion within a generic 2.5D street canyon with spanwise periodic boundary conditions. Following a validation study, 16 LES simulations are performed for different domain sizes. The results show that the minimum requirement for the domain width is 2.5H, where H is the roof height of the street canyon. For the domain height, upstream domain length and downstream domain length, 7.5H, 5H and 10H are recommended, respectively. These guidelines should help to reduce the computational costs of this type of simulation without significantly compromising the accuracy.

4.1 Introduction

Air pollution is a world-wide problem. The World Health Organization (WHO) reported in 2016 that more than 80% of people living in urban areas are exposed to levels of air pollution higher than the limits recommended for health reasons (World Health Organization, 2016). For a better prediction and understanding of the air quality and pollutant dispersion in the urban canopy, knowledge about the interactions between urban-canopy elements and the atmosphere is important (Kastner-Klein and Plate, 1999; Vervoort et al., 2019). Urban street canyons are basic urban-canopy elements where long narrow streets are bordered by building walls on both sides. They are known to be susceptible to high air pollution concentrations, certainly when the wind direction is perpendicular to the street axis (Kastner-Klein et al., 2004; Oke, 1988). Flow and dispersion fields inside and in the vicinity of urban street canyons are important aspects of urban air-quality studies (Antoniou et al., 2019; Ricci et al., 2019; Scungio et al., 2018). Apart from wind/water tunnel testing (Baratian-Ghorghi and Kaye, 2013; Gromke and Ruck, 2009, 2007; Kastner-Klein and Plate, 1999; Li et al., 2008a; Meroney et al., 1996; Nosek et al., 2017; Stabile et al., 2015), computational fluid dynamics (CFD) has been used to investigate pollutant dispersion in street canyons under the perpendicular wind. Many CFD studies have adopted the Reynolds-averaged Navier–Stokes (RANS) approach (Ding et al., 2019; He et al., 2017; Huang et al., 2016; Mei et al., 2016; Vranckx et al., 2015; Wen and Malki-Epshtein, 2018; Xie et al., 2020; Zhang et al., 2019). In the past decades, an increasing number of studies have been performed with large-eddy simulation (LES) (Antoniou et al., 2017; Blocken, 2018; Lateb et al., 2016; Salim et al., 2011a; Tominaga and Stathopoulos, 2011). LES resolves the large-scale unsteady motions and allows the reproduction of the highly transient nature of wind velocity and pollutant concentration in street canyons (Tominaga and Stathopoulos, 2013), which can lead to strongly improved accuracy (Tominaga and Stathopoulos, 2011).

Even though LES is intrinsically superior over RANS, LES results tend to be more sensitive to the many computational settings and parameters that have to be set by the user (Blocken, 2018), including the size of the computational domain, the computational grid topology, and the boundary conditions. A non-exhaustive overview of LES studies on generic street canyons under a perpendicular wind is provided in Table 1. These generic street canyons are categorized into type A (Fig. 1a), where the buildings are represented by protrusions above

the bottom of the domain, and type B, where the canyon cavity is represented by a recession in the bottom of the domain (Fig. 1b). Table 1 indicates that most studies focused on typical street canyons that have the aspect ratio (= building roof height H divided by street width W) equal to 1. Moreover, generic street canyons have been commonly simulated in full scale and treated as spanwise homogeneous 3D geometries, namely 2.5D (Geng et al., 2018) or quasi-2D (Chatzimichailidis et al., 2019) simulations. Periodic boundary conditions have generally been applied in the spanwise direction to reduce the size of the computational domain. From Table 1, it can be observed that a wide range of different values of domain width, ranging from H to 15H have been used for 2.5D street canyons. This is also the case for the domain height, which ranged from 5H to 8H for canyon type A and 1.5H to 6H for type B.

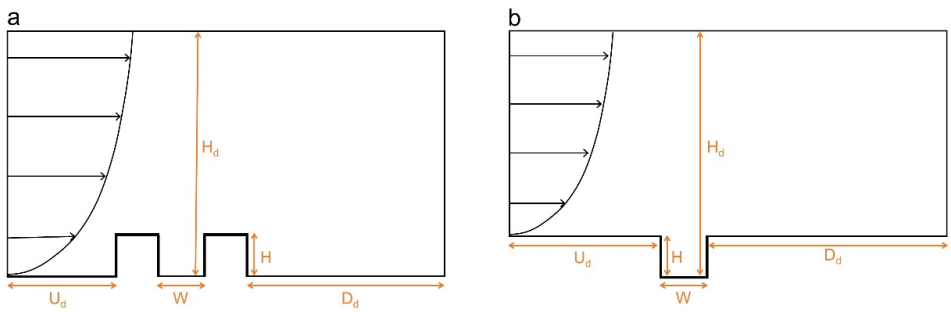

Fig. 1. (a) Configuration of street canyon type A and (b) same for type B.

Table 1. Overview of studies on wind flow and associated processes in generic street canyons using LES.

Ref.	Type	Aspect ratio (= H/W)	2.5D (if yes, domain width (W_d))	Spanwise boundary conditions	Domain height (H_d)	Scale
(Walton and Cheng, 2002)	B	1.2	Yes (1.25H)	Periodic	3.1H	Full
(Liu et al., 2004)	B	0.5, 1.0, 2.0	Yes (1H)[1]	Periodic	-	Reduced
(Baker et al., 2004)	B	1	Yes (2.2H)	Periodic	5.2H	Full
(Li et al., 2008b)	B	1.0, 2.0, 3.0, 5.0	Yes (-)	Periodic	2H[1]	Reduced
(Hu et al., 2009)	B	1	Yes (2.2H)	-	2.2H	Full
(Li et al., 2010)	B	1	Yes (-)	Periodic	2H	Reduced
(Salim et al., 2011a)	A	1	No	Symmetry	8H	Reduced
(Salim et al., 2011b)	A	1	No	Symmetry	8H	Reduced
(Moonen et al., 2011)	B	1	No	Periodic	9H	Full
(Zhang et al., 2011)	B	1	Yes (2H)	Periodic	2H	Full
(Cheng and Liu, 2011)	B	1	Yes (5H)	Periodic	6H	-
(Park et al., 2012)	B	1	Yes (2H)	Periodic	5.5H	Full
(Kikumoto and Ooka, 2012a)	A	1	Yes (3H)	Periodic	8H	Full
(Kikumoto and Ooka, 2012b)	A	1.0, 2.0	Yes (3H)[1]	Periodic	8H[1]	Full
(Moonen et al., 2013)	A	1	No	Symmetry	8.3H	Reduced
(Bright et al., 2013)	B	1	Yes (1.7H)	Periodic	5.2H	Full
(Lo and Ngan, 2015)	B	1	Yes (2H)	Periodic	3H	Full
(Zhong et al., 2015)	B	2	Yes (1.1H)	Periodic	3.1H	Full
(O'Neill et al., 2016)	B	1	Yes (2.2H)	Periodic	5.2H	Full
(Zhong et al., 2017) (2017)	B	2	Yes (1.1H)	Periodic	3.1H	Full
(Llaguno-Munitxa et al., 2017)	A	1	Yes (12H)	Wall	8H	Reduced

(Llaguno-Munitxa and Bou-Zeid, 2018)	A	1	Yes (12H)	Wall	8H	Reduced
(Merlier et al., 2018)	A	1	No	Wall	8.3H	Reduced
(Wang et al., 2018)	A	0.2, 1.0 , 0.5, 5.0	Yes (15H)[1]	Periodic	5H[1]	Full
(Han et al., 2018)	A	1	Yes (1.5H)	Periodic	5H	Full
(Duan and Ngan, 2018)	B	1	Yes (1.92H)	Periodic	3H	Full
(Chew et al., 2018)	B	1	Yes (1H)	Periodic	6H	Reduced
(Gallagher and Lago, 2019)	B	1	Yes (10H)	-	1.5H	Full
(Chatzimichailidis et al., 2019)	B	1	Yes (0.5H)	Periodic	3, 4, 5, 6H	Full

- = information has not been provided, Symmetry = zero normal gradients of all variables and zero normal velocity.

[1] For the studies considering more than one aspect ratio, H is the height of the case with an aspect ratio of 1.

In CFD simulation of 2.5D street canyons, a small domain height inevitably leads to a large blockage ratio, which can artificially accelerate the airflow and affect the simulation (Franke et al., 2007; Tominaga et al., 2008). A recent study (Chatzimichailidis et al., 2019) has examined the influence of domain height for a 2.5D street canyon of type B. The mean concentrations obtained with domain heights of 3H, 4H, 5H and 6H were compared. The results showed that the smaller the height of the domain, the lower the mean concentration at the windward side. The results with H_d = 6H were found to be marginally closer to the experimental data than the other domain heights (Chatzimichailidis et al., 2019). For 2.5D street canyons, although periodic boundary conditions are used in the spanwise direction, also a sufficient domain width is necessary to ensure the resolving of the largest coherent eddies occurring within the canyon. To the best of our knowledge, a sensitivity analysis on the minimum requirement for the domain width has not yet been performed.

Several documents providing best practice guidelines – albeit mainly for RANS simulations – have been provided in the past two decades. These include requirements for the size of the computational domain and the topology of the grid (Ai and Mak, 2017; Blocken, 2015; Franke et al., 2011, 2007; Meroney et al., 2016; Ramponi and Blocken, 2012; Tominaga et al., 2008). For example, guidelines (Franke et al., 2011) suggested that the inlet, lateral and top boundaries should be at least $5H_{max}$ (where H_{max} is the height of the tallest building) away from the building group. The full blockage ratio is defined as the ratio of the projected frontal (windward) area of the obstacles to the cross-sectional area of the computational domain, which should not be larger than 3%. The guidelines by Tominaga et al. (2008) also recommended a maximum full blockage ratio of 3%. They demanded the outflow boundary to be at least $10H_{max}$ away from the building group. Blocken (2015) proposed the concept of two directional blockage ratios, one in the horizontal and one in the vertical direction, which consists of the decomposition of the full blockage ratio, i.e. 17% (square root of 3%). This is to avoid unwanted artificial acceleration in some exceptional situations, e.g. for very wide buildings or for urban models with horizontal dimensions that are much larger than vertical dimensions. However, as mentioned earlier, the vast majority of these guidelines are directed to RANS simulations. Only a few best practice guidelines for building and urban aerodynamics simulations have been developed for LES (Ai and Mak, 2015; Gousseau et al., 2013; Iousef et al., 2017; Vasaturo et al., 2018). It has been argued that this is one of the reasons why LES is not applied more frequently for such applications

(Blocken, 2018). Another reason is that the establishment of guidelines has to be based on many LES simulations in extensive sensitivity studies (Blocken, 2018; Hanjalic, 2005). The present study aims to provide some guidelines on the domain size for LES. The focus will be on street canyons of type A (Fig. 1a), which is considered a more common and more realistic representation of a street canyon than type B.

The outline of the paper is as follows: Section 2 presents the CFD validation study. Section 3 introduces the reference case, the test matrix for the sensitivity study of the domain size, the boundary conditions, and the other computational settings for the LES simulations. The results of the sensitivity study on the domain width, domain height and domain lengths are presented in Sections 4, 5 and 6, respectively. Finally, discussion (Section 7) and conclusions and recommendations (Section 8) are provided.

4.2 Validation study

4.2.1 Description of the wind-tunnel experiment

In the wind-tunnel measurement by Gromke and Ruck (2009), the mean velocity field and the mean concentration of the tracer gas in a long street canyon model were measured in an open-circuit atmospheric boundary layer wind-tunnel at the Karlsruhe Institute of Technology. Note that in this experiment, different cases were considered with and without trees. In the present validation study, the results of the 1:1 aspect ratio street canyon without trees were used. The street canyon model, at the scale of 1:150, consisted of two parallel buildings of 0.12 m × 0.12 m × 1.2 m each (streamwise (x) × vertical (z) × spanwise (y) dimensions). The width of the street between the two parallel buildings was 0.12 m, yielding an aspect ratio equal to 1. The approach-flow wind was perpendicular to the street axis. The approach-flow profiles represented a turbulent boundary layer flow with power-law exponent $\alpha = 0.30$ for the mean velocity and $\alpha_I = 0.36$ for the turbulence intensity, with values of mean velocity (U_{ref}) and turbulence intensity at the roof height equal to 4.65 m/s and 16.20%, respectively (Gromke, 2008a). The streamwise pressure gradient was reduced by adjusting the wind-tunnel ceiling when the street canyon model was set up in the test section (Gromke and Ruck, 2009).

Sulfur hexafluoride (SF_6) was used as a tracer gas. The release of traffic exhausts was modeled by a tracer gas mixture that was emitted from four line sources mounted at the

bottom of the model. The line source strength was controlled and monitored by a flow controller of type 1259B from MKS instruments and flow meter of type 1258B, ensuring a constant tracer gas supply during the measurements (Gromke and Ruck, 2009). To sample the near-wall canyon air, each wall facing the street was equipped with concentration measurement taps protruding 5 mm out of the wall. An electron capture detector (model: Meltron LH 108) was used to analyze the mean concentration (Buccolieri et al., 2009; Gromke et al., 2008). The mean concentration of SF_6 was expressed in dimensionless as follows:

$$C^{+} = \frac{CU_{ref}H}{Q/l} \tag{1}$$

where C is the measured mean concentration, U_{ref} is the undisturbed approach-flow mean wind velocity at the building roof height H, and Q/l is the emission rate of the tracer gas per unit length. According to Gromke (2008b), the uncertainty of the measurement depended on the measured mean concentration. The smaller mean concentrations led to larger percentage errors that could go up to 14.0%, while the larger mean concentrations led to lower percentage errors that less than 2.5%.

Velocity measurements were performed using Laser-doppler Velocimetry (LDV). The LDV-system incorporated a 4 Watt argon-ion laser and an optical system. The mean vertical velocity component (W) was measured in a vertical plane perpendicular to the street axis near the center of the canyon (Gromke and Ruck, 2009).

4.2.2 Computational domain and grid

A computational domain is made of the street canyon in the wind-tunnel. The geometry is reproduced at the wind-tunnel scale. Fig. 2 illustrates the computational domain and grid. The width and height of the computational domain are equal to the width and height of the wind-tunnel, i.e. 2 m and 1 m, respectively. The upstream and downstream domain lengths are 1.2 m (10H) and 1.8 m (15H), respectively.

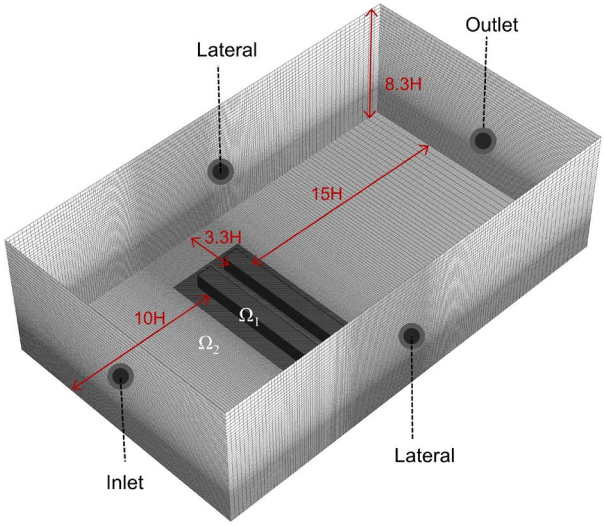

Fig. 2. Computational domain, grid, and boundary conditions of the basic grid (11.9 million cells).

A non-conformal grid is generated. The entire domain is divided into two subdomains, an inner domain Ω_1 and an outer domain Ω_2. Subdomain Ω_1 is extended up to a distance of 1H away from the model (see Fig. 2). Cubic cells with an edge length of 0.003 m (H/40) are applied in subdomain Ω_1. As recommended in Ref. (Iousef et al., 2017), a grid refinement ratio of 1:2 is applied between the adjacent subdomains. Subdomain Ω_2 is discretized with hexahedral cells with a stretching ratio of 1.05. The total number of cells is 11.9 million. The grid resolution is based on a grid-sensitivity analysis. Further information about the grid-sensitivity analysis will be provided in Subsection 2.4.

4.2.3 Boundary conditions and solver settings

No-slip walls are used for the top, bottom and lateral boundary conditions to reproduce the test section ceiling, ground and side walls in the experiment, respectively. No-slip walls are also applied on the surfaces of the canyon model. All walls are considered impermeable for species transport. For the inlet boundary conditions, the measured profiles of mean wind speed and turbulent kinetic energy (Gromke, 2008a) are used. The turbulence dissipation rate ε is calculated using Eq. (2) (Richards and Hoxey, 1993).

$$\varepsilon(z) = \frac{u_{ABL}^{*3}}{\kappa(z + z_0)} \quad (2)$$

where the friction velocity u^*_{ABL} = 0.59 m/s and the roughness length z_0 = 0.004 m (wind-tunnel scale, obtained from logarithmic law curve fitting of the mean velocity profile in the wind-tunnel (Gromke, 2008a)). The von Karman constant κ is 0.42. Time-dependent inlet conditions are generated by the vortex method (Mathey et al., 2006; Sergent, 2002). The number of vortices N_V takes 6700, which is estimated by N_V = N/4 (where N = number of inlet grid cells) (Gerasimov, 2016). Four line sources with 1.42 m × 0.003 m (reduced-scale values) are created on the domain bottom boundary (Fig. 3). According to the wind-tunnel experiment (Gromke, 2008a), the lines are located at about 0.23H, 0.35H, 0.65H and 0.77H from the leeward wall. The exhaust faces are velocity inlets injecting pure SF_6 in the domain with a constant velocity of 0.096 m/s. This results in an emission rate of Q = 10 g/s (Gromke et al., 2008).

The commercial CFD code ANSYS Fluent 18.0 is employed (ANSYS Inc., 2017). The LES simulation is started from the solution of a 3D steady RANS simulation. For the steady RANS simulation, the realizable k-ε turbulence model is used with turbulent Schmidt number of 0.7 (Tominaga and Stathopoulos, 2007). For pressure-velocity coupling, the SIMPLE algorithm is used. Pressure interpolation is second order and second-order discretization schemes are applied for both the convection and viscous terms of the governing equations.

LES simulations are conducted with the wall-adapting local eddy viscosity model (WALE) (Ducros et al., 1998) with the constant C_{wale} = 0.325. Pressure-velocity coupling is performed using the fractional step method in combination with the non-iterative time advancement (NITA) scheme. For pressure interpolation and time discretization, second-order schemes are applied. A second-order upwind scheme is used for the energy and SF_6 concentration equations. Werner-Wengle wall functions that assume either a linear or 1/7 power-law distribution of instantaneous velocity in the first cell, are applied (ANSYS Inc., 2017; Werner and Wengle, 1993). The time step (Δt) is 0.00019 s, and the resulting maximum and volume-averaged Courant-Friedrichs-Lewy (CFL) numbers are 0.98 and 0.11, respectively. Before the start of data averaging, the LES simulation runs during 7.3 s, corresponding to approximately 10 flow-through times ($T_{flow\text{-}through} = L_x/U_{ref}$, where L_x is the length of the computational

domain and U_{ref} = 4.65 m/s). After this LES initialization step, data are averaged over a period of 25 s (approximately 35 flow-through times) (Salim et al., 2011a, 2011b).

4.2.4 Grid sensitivity study

In order to assess the grid dependence, a fine, basic and coarse grid are made based on the same overall grid topology. Table 2 describes the characteristics of the three grids. The fine and coarse grid have 20.4 million and 5.5 million cells, respectively. For subdomain Ω_1, the edge lengths of the cubic cells are H/48 and H/30 for the fine and coarse grid, respectively (Fig. 3). The time steps of 0.00017 s and 0.00025 s are set for the fine and coarse grid, respectively, to ensure the maximum Courant-Friedrichs-Lewy number lower than 1.

Table 2. Characteristics of the grids for the grid-sensitivity analysis and the associated time steps.

	Grid size in Ω_1	Time step Δt	# cells (million)
Grid 1 (Coarse)	0.0040 m (H/30)	0.00025 s	5.5
Grid 2 (Basic)	0.0030 m (H/40)	0.00019 s	11.9
Grid 3 (Fine)	0.0025 m (H/48)	0.00017 s	20.4

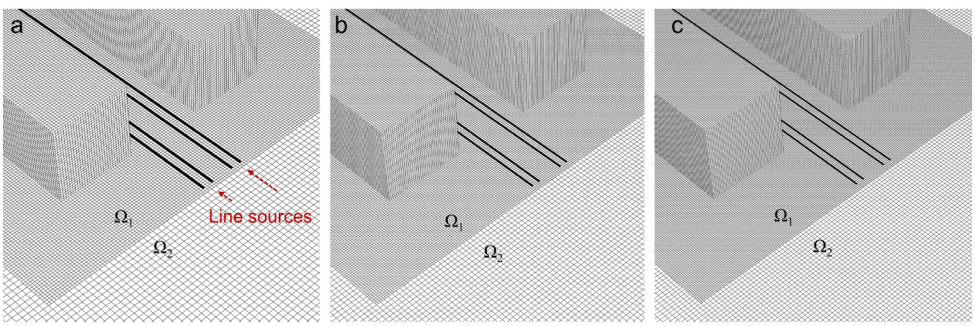

Fig. 3. LES computational grids near bottom of domain: (a) coarse grid (5.5 million cells); (b) basic grid (11.9 million cells) and (c) fine grid (20.4 million cells). The four black lines indicate the line sources.

Fig. 4a-d compares the profiles of C^+ obtained by the three grids along four vertical lines near the leeward wall: y/H = 4.92, 3.75, 1.25 and 0, respectively. The profiles along the four vertical lines near the windward wall: y/H = 4.92, 3.75, 1.25 and 0 are compared in Fig. 4e-h, respectively. Note that the lines are 5 mm away from the walls. Significant differences between the results obtained by the coarse grid and basic grid are observed. The average percentage differences between the results obtained by the coarse grid and basic grid are

16.40% and 16.01% for the lines near the leeward wall and windward wall, respectively. Less differences are found between the results obtained by the fine grid and the basic grid. In this case, the average percentage differences are 8.62% and 5.40%, for the lines near the leeward wall and windward wall, respectively. It is, therefore, concluded that the basic grid can be retained for the validation study.

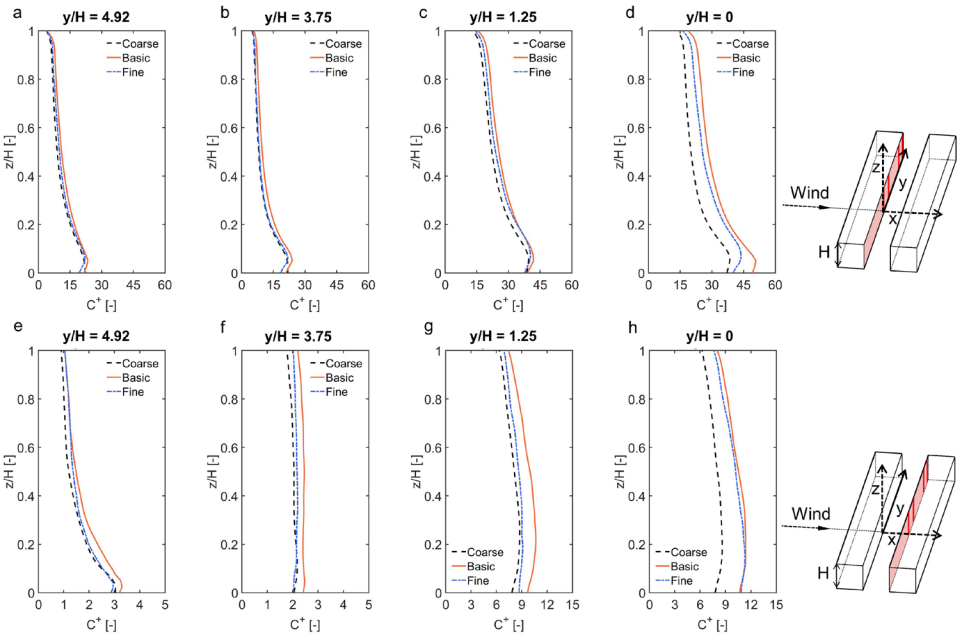

Fig. 4. Results of grid-sensitivity study along four vertical lines near (a-d) the leeward wall: (a) y/H = 4.92; (b) y/H = 3.75; (c) y/H = 1.25; (d) y/H = 0; (e-h) same near the windward wall.

4.2.5 Results

The CFD results are compared with the wind-tunnel data in terms of the dimensionless mean vertical velocity component (W/U_{ref}) and C^+ (Gromke and Ruck, 2009, 2007).

Fig. 5 shows a comparison between the simulated and measured W/U_{ref} along four vertical lines in the vertical plane near the canyon center (y/H = 0.5): x/H = 0.083, 0.250, 0.750 and 0.917. The agreement between CFD and measurements is good, especially for the points with relatively high wind speeds. The average absolute differences of W/U_{ref} along the four lines are 0.03, 0.03, 0.04 and 0.01, respectively.

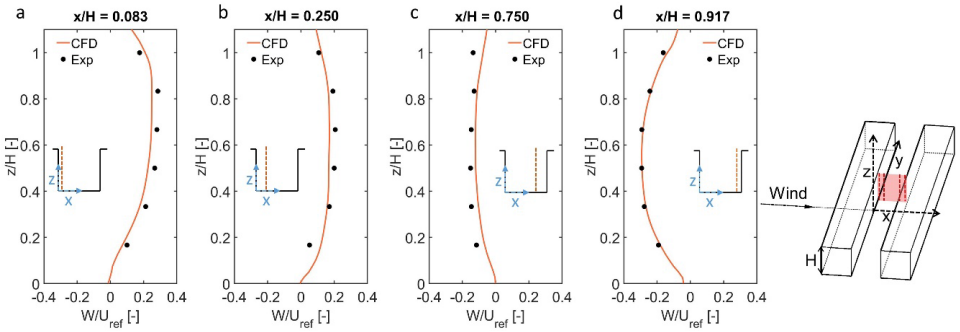

Fig. 5. Comparisons between the measured and simulated dimensionless mean vertical velocity component (W/U_{ref}) along four vertical lines in the vertical plane near the canyon center (y/H = 0.5): (a) x/H = 0.083; (b) x/H = 0.25; (c) x/H = 0.75; (d) x/H = 0.917.

Fig. 6 depicts the comparison between the simulated and measured C^+ along vertical lines: y/H = 4.92, 3.75, 1.25 and 0 near the leeward and windward walls. For the four lines near the leeward wall, the average absolute differences of C^+ are 1.38, 3.37, 1.50 and 1.46, respectively (Fig. 6a-d). For the windward wall, the average absolute differences along lines y/H = 4.92 and 3.75 are 1.07 and 1.01, respectively (Fig. 6e and f). The possible reason of these relatively large differences is the underestimation of wind speed near the corner of the canyon. For the other two lines closer to the center of the canyon, y/H = 1.25 and 0, good agreements are observed with average absolute differences of 0.14 and 0.53, respectively (Fig. 6g and h). This validation study shows that the LES simulation in combination with high-resolution grids, Werner-Wengle wall functions, and other solver settings can provide a satisfactory agreement of the mean wind velocity and mean concentration for a long street canyon, especially near the center of the canyon. Therefore, LES with the same grid resolution, sub-grid scale model, wall functions, and solver settings will be used for the sensitivity analysis with a focus on the center region of the canyon.

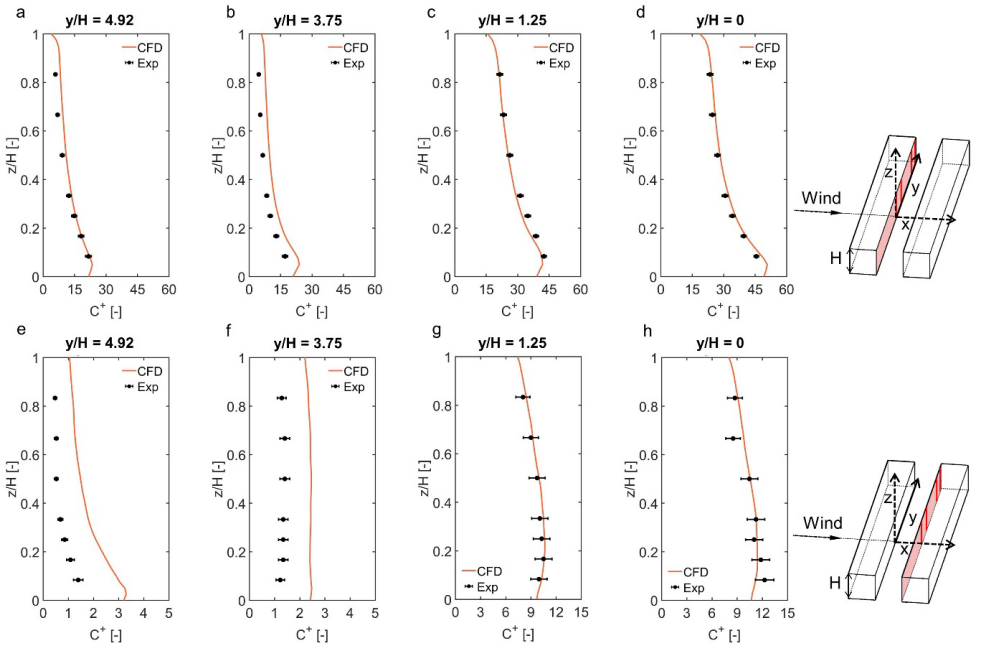

Fig. 6. Comparisons between the measured and simulated C^+ along four vertical lines near the leeward wall: (a) y/H = 4.92; (b) y/H = 3.75; (c) y/H = 1.25; (d) y/H = 0; (e-h) same for the windward wall. The error bar is added according to the measurement uncertainty reported by Gromke, (2008b).

4.3 Sensitivity analysis: reference case

4.3.1 Computational domain and grid

A reference case is defined as a starting point for the domain size sensitivity analysis. The simulations are performed at full scale. The 2.5D street canyon has a building height of 12 m and a street width of 12 m. A computational domain is made of the generic street canyon of type A (Fig. 7). It includes an initial domain width (W_d) of 5H, domain height (H_d) of 11H, upstream domain length (U_d) of 10H and downstream domain length (D_d) of 10H. Through a systematic variation of W_d, H_d, U_d and D_d, the effect of these four parameters on the simulation results is investigated. In total, 16 LES simulations are performed and the details are given in Table 3. Note that the values of W_d and H_d cover the ranges of those used in previous studies (as listed in Table 1), while those of U_d and D_d include extensions based on the validation study and guidelines (Tominaga et al., 2008). Non-conformal grids (Iousef et al., 2017) are generated. They consist of two subdomains and subgrids (Ω_1 and Ω_2), with

a grid refinement ratio of 1:2 between the adjacent subgrids. Subdomain Ω_1 is composed of cubic cells with edge length H/40, similar to the grid for the validation study in Subsection 2.2. Subdomain Ω_1 extends up to a distance of H away from the building surfaces. Subdomain Ω_2 uses hexahedral cells with a stretching ratio of less than 1.05.

Table 3. Test matrix for the sensitivity analysis. All sizes are given in the roof height of the street canyon (H). Note that for clarity the reference domain (marked as *) is listed four times (once for each parameter).

Parameter	W_d	H_d	Blockage ratio	U_d	D_d	# cells (million)
Domain width (W_d)	1.25	11.0	9.1%	10	10	0.97
	2.00					1.55
	2.50					1.94
	3.75					2.91
	5.00*					3.89
	7.50					5.82
Domain height (H_d)	5.00	3.0	33.3%			3.28
		5.0	20.0%			3.51
		6.0	16.7%			3.59
		7.5	13.3%			3.71
		11.0*	9.1%			3.89
		21.0	4.7%			4.16
Upstream domain length (U_d)	5.00	11.0	9.1%	10*	10	3.89
				7.5		3.77
				5		3.63
				2.5		3.61
Downstream domain length (D_d)	5.00	11.0	9.1%	10	10*	3.89
					6	3.63
					3	3.61

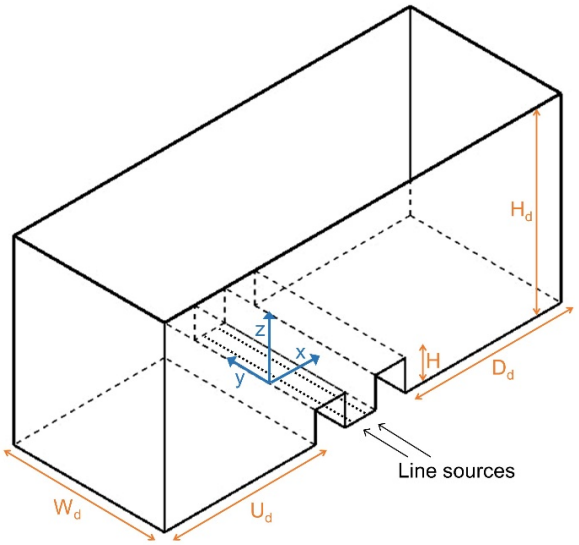

Fig. 7. Schematic of the computational domain: W_d, domain width; U_d, upstream domain length; D_d downstream domain length; and H_d, domain height.

4.3.2 Boundary conditions and solver settings

The inlet mean wind speed profile is the logarithmic law (Eq. (3)) with z_0 = 0.03 m and u^*_{ABL} = 0.3 m/s. The corresponding U_{ref} at the roof height is 4.28 m/s. Turbulent kinetic energy (k) and turbulence dissipation rate (ε) are given by Eq. (4) and (2), respectively (Richards and Hoxey, 1993). Periodic boundary conditions are applied at the lateral domain sides. At the outlet plane, zero static gauge pressure is applied. At the top of the domain, symmetry conditions are imposed, i.e. zero normal velocity and zero normal gradients of all variables. Tracer gas SF_6 representing the traffic exhaust is released from two continuous line sources that are parallel to the street axis and embedded at the street bottom surface. The width of each line source is 0.9 m and the center of each line is at a distance of 3.45 m to the nearest building wall (Fig. 7). The emission rate of tracer gas source per unit length is set as Q/l = 10 $g \cdot s^{-1} m^{-1}$.

$$U(z) = \frac{u^*_{ABL}}{\kappa} \ln\left(\frac{z + z_0}{z_0}\right) \quad (3)$$

$$k(z) = \frac{u^{*\,2}_{ABL}}{0.3} \quad (4)$$

For the LES simulations, the WALE model is used. The vortex method is adopted to impose a time-dependent velocity profile at the inlet of the domain. The number of vortices is estimated in the same way as in the validation study. The other computational settings are identical to those in the validation study in Subsection 2.3. The time step (Δt) is 0.024 s. For the reference case, the maximum and volume-averaged Courant-Friedrichs-Lewy (CFL) numbers are 0.84 and 0.10, respectively. For the other cases, the maximum CFL number is below 1. The LES simulations are initialized from the solution of RANS simulations. Before averaging, the simulations are run during 650 s (approximately 10 flow-through times) to remove the influence of the initial condition. Then, data are averaged over a period of 1920 s (80,000 time steps, approximately 30 flow-through times).

4.3.3 Monitoring of statistical convergence

Fig. 8 shows the evolution of the moving average of dimensionless SF_6 concentration and dimensionless velocity magnitude as a function of time at five monitoring points inside the street canyon. It should be noted that to evaluate the statistical convergence of the simulation, the results are provided for approximately 45 flow-through times. It appears that the variations of the mean concentration and velocity magnitude are relatively low after about 60,000 time steps. Small variations are observed in the second half of the averaging period, which could be due to the instability of the re-circulation vortex inside the street canyon induced by the shear layer shed from the upstream roof (Louka et al., 2000; Perret and Savory, 2013; Zhang et al., 2011). The convergence of the mean value is further quantified by e_{conv} (%) defined for a given range of time steps I as follows:

$$e_{conv}(I) = \frac{\left|Q_{max} - Q_{min}\right|}{\left|Q_{end}\right|} \times 100\% \quad (5)$$

where Q_{max} and Q_{min} are the maximum and minimum values, respectively, of a flow variable obtained within an interval I of time steps in the averaging period. Q_{end} is the value of a flow variable at the end of interval I. The 120,000 time steps of the averaging period are divided into twelve equal intervals for which the values of e_{conv} are calculated for both the dimensionless mean concentration (C^+) and dimensionless mean velocity magnitude (U_{3D}/U_{ref}). Table 4 shows the results for the five monitoring points. A strong influence of the instantaneous flow patterns on the mean concentration can be observed at the beginning

of the averaging period (I = 1). In this case, the value of e_{conv} goes up to 141.62%. The maximum e_{conv} reduces to 1.73% for the interval I =12 (after approximately 45 flow-through times). Note that for interval I = 8, e_{conv} is equal to or smaller than 5.54%, which indicates a good statistical convergence of the simulation.

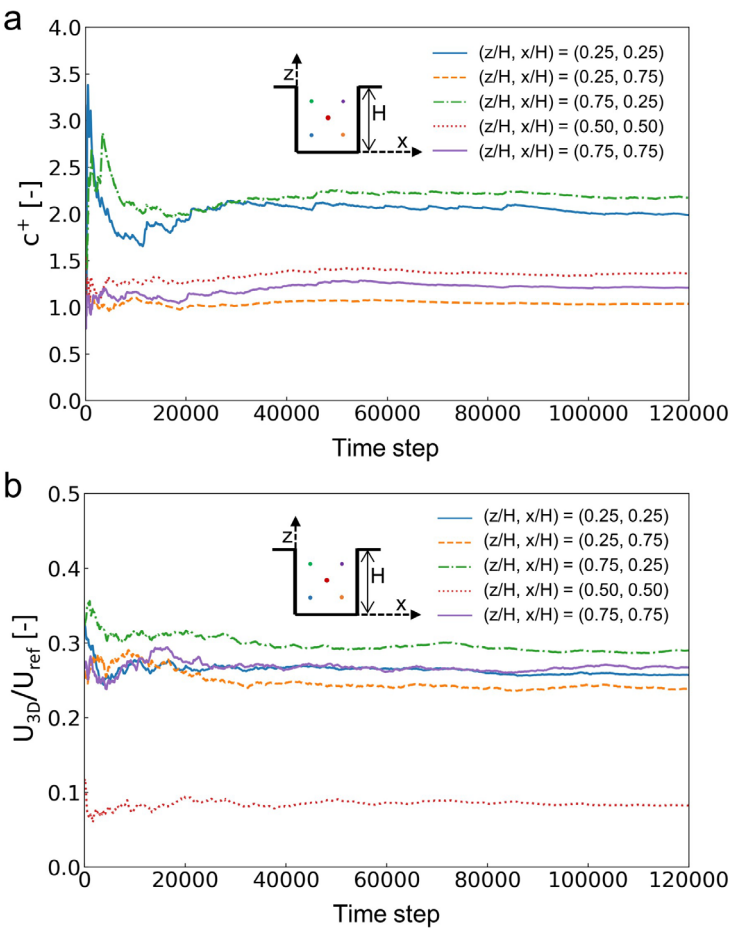

Fig. 8. Convergence monitoring for the reference case: (a) C^+ and (b) U_{3D}/U_{ref} at five points as a function of time step.

Table 4. Convergence monitoring: e_{conv} (%) of C^+ and U_{3D}/U_{ref} at the five points in the vertical centerplane (y/H = 0) for 12 equidistant intervals in the averaging period.

		(z/H, x/H) = (0.25, 0.25)		(z/H, x/H) = (0.25, 0.75)		(z/H, x/H) = (0.75, 0.25)		(z/H, x/H) = (0.5, 0.5)		(z/H, x/H) = (0.75, 0.75)	
I	Range of time step	e_{conv} (C^+)	e_{conv} (U_{3D}/U_{ref})	e_{conv} (C^+)	e_{conv} (U_{3D}/U_{ref})	e_{conv} (C^+)	e_{conv} (U_{3D}/U_{ref})	e_{conv} (C^+)	e_{conv} (U_{3D}/U_{ref})	e_{conv} (C^+)	e_{conv} (U_{3D}/U_{ref})
1	1-10000	141.62	29.57	23.92	15.93	79.46	17.50	36.80	74.36	36.86	16.49
2	10001-20000	15.18	6.63	12.62	9.31	6.42	3.83	6.24	22.56	11.33	11.25
3	20001-30000	9.77	3.68	3.44	6.42	7.01	3.90	4.99	8.65	7.69	6.00
4	30001-40000	2.39	2.26	4.52	3.13	2.88	3.80	5.08	9.24	6.80	3.38
5	40001-50000	3.84	1.69	1.49	2.80	4.18	1.89	2.48	10.16	4.12	3.05
6	50001-60000	2.36	1.34	1.89	1.11	2.29	1.43	1.66	8.61	2.20	3.64
7	60001-70000	2.01	1.16	2.07	2.33	1.48	1.84	2.93	5.32	2.48	2.81
8	70001-80000	1.44	2.57	1.33	2.05	0.95	2.59	1.16	5.54	1.89	1.84
9	80001-90000	2.61	1.55	0.71	1.97	1.39	1.39	1.61	4.06	1.30	1.41
10	90001-100000	3.20	1.34	1.15	2.71	1.88	1.04	1.03	3.08	1.53	2.46
11	100001-110000	0.95	0.97	0.60	1.88	0.79	0.92	1.81	2.05	1.28	1.93
12	110001-120000	1.17	0.43	0.41	1.27	1.14	1.38	0.84	1.73	0.97	1.37

4.4 Sensitivity analysis: impact of domain width

Fig. 9 compares the dimensionless mean vertical (W/U_{ref}) and streamwise (U/U_{ref}) velocity components along the three horizontal and three vertical lines. The domain with $W_d/H = 1.25$ clearly yields lower values than the others. The domain with $W_d/H = 2.0$ predicts slightly lower mean velocity components than the wider domains. Compared to the domain with $W_d/H = 7.5$ (the largest domain width), the average absolute differences of the dimensionless mean velocity magnitude (U_{3D}/U_{ref}) along the sampling lines are 0.091, 0.043, 0.020, 0.028 and 0.020 for domains with $W_d/H = 1.25$, 2.0, 2.5, 3.75 and 5, respectively.

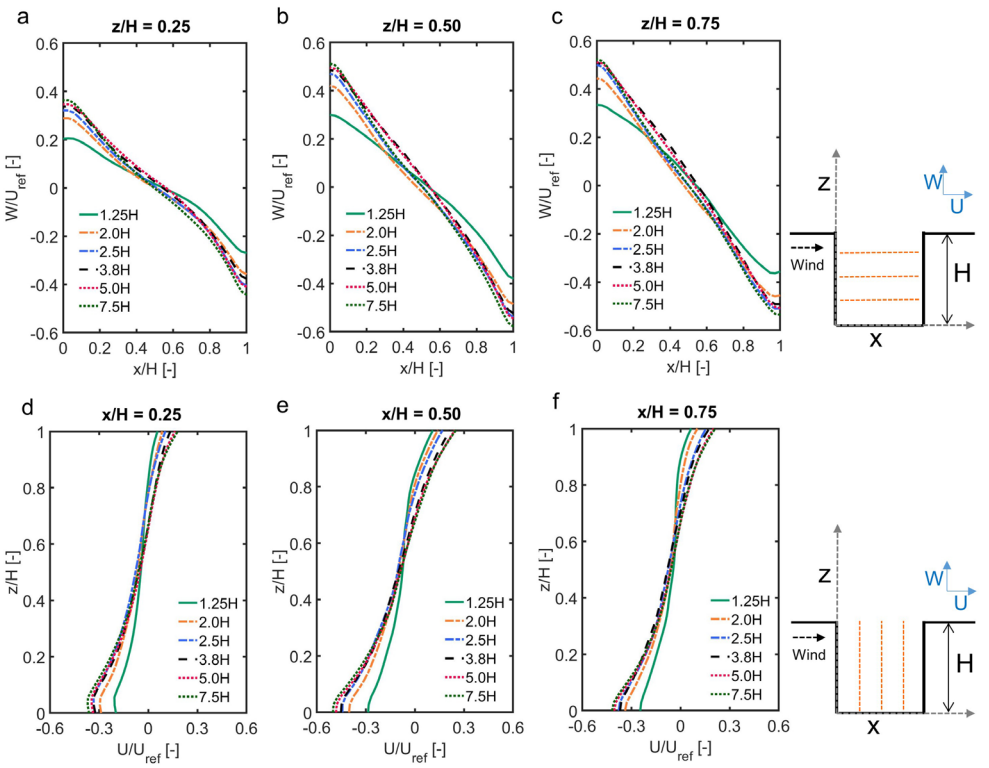

Fig. 9. Comparison of dimensionless mean velocity components obtained from six different domain widths: W/U_{ref} along three horizontal lines in the vertical centerplane: (a) z/H = 0.25; (b) z/H = 0.5; (c) z/H = 0.75, and U/U_{ref} along three vertical lines in the vertical centerplane: (d) x/H = 0.25; (e) x/H = 0.5; (f) x/H = 0.75.

Fig. 10 compares C^+ along the same vertical and horizontal lines, as obtained by the domains with different W_d. The domain with $W_d/H = 1.25$ predicts larger C^+ values than the other domains near the leeward wall (see Fig. 10d). For the C^+ along the horizontal lines, a

different trend is predicted by the domain with $W_d/H = 1.25$ compared to the other domains (Fig. 10a-c). The domains with $W_d/H = 2$, 2.5, 3.75, 5 and 7.5 generally predict similar values for C^+. Compared to the results from the domain with the largest W_d, i.e. $W_d/H = 7.5$, the average absolute differences of the C^+ along all the lines are 0.441, 0.197, 0.119, 0.122 and 0.130 for the domains with $W_d/H = 1.25$, 2.0, 2.5, 3.75 and 5, respectively.

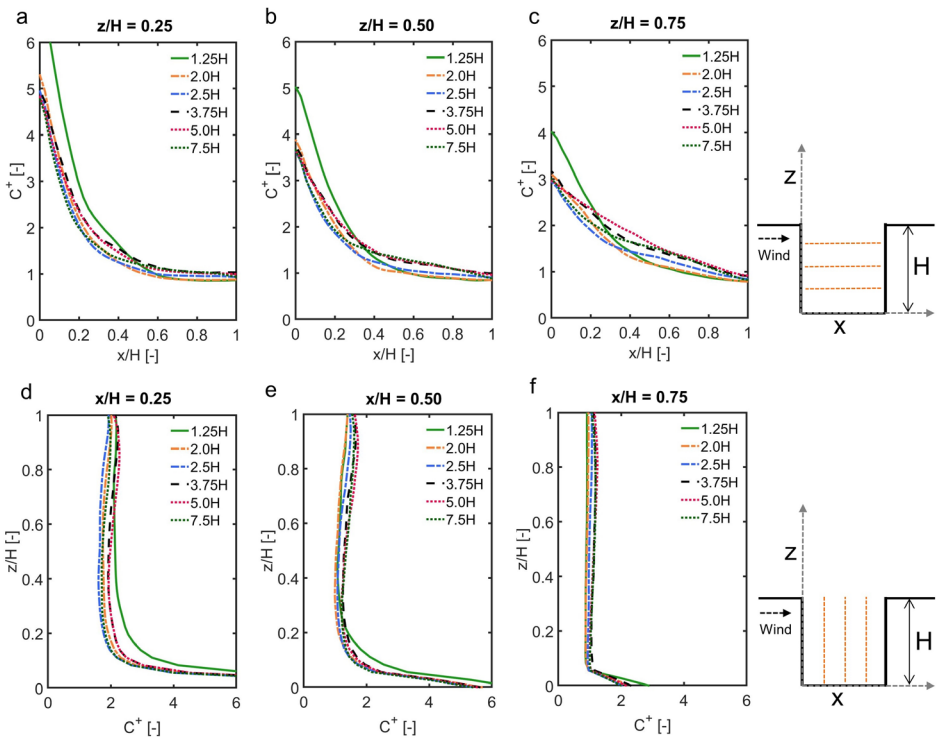

Fig. 10. Comparison of C^+ obtained from six different domain widths along three horizontal lines in the vertical centerplane: (a) z/H = 0.25; (b) z/H = 0.5; (c) z/H = 0.75; and three vertical lines in the vertical centerplane: (d) x/H = 0.25; (e) x/H = 0.5; (f) x/H = 0.75.

These results indicate that when the domain width is equal to or greater than 2.5H, the results in terms of mean velocity components and mean concentration within the street canyon become similar.

Fig. 11 displays the distribution of the dimensionless mean velocity magnitude (U_{3D}/U_{ref}) and the 2D velocity vector field, the mean concentration (C^+) and the dimensionless root mean square error concentration (c^+_{rms}) in the vertical centerplane by the domains with $W_d/H = 1.25$, 2.5 and 7.5. It is obvious that the domain with $W_d/H = 1.25$ predicts a lower

mean wind velocity and weaker vortex flow within the street canyon than the other two cases. This is because the domain width is too small to include the important coherent eddies occurring in the spanwise direction, which will be evaluated later. It leads to a higher C^+ near the leeward side than the other two domains. Small differences of the C^+ between the domains with W_d/H = 2.5 and 7.5 are found. In terms of c^+_{rms}, the domains with W_d/H = 2.5 and 7.5 also yield similar results, while W_d/H =1.25 predicts much higher c^+_{rms} near the leeward side.

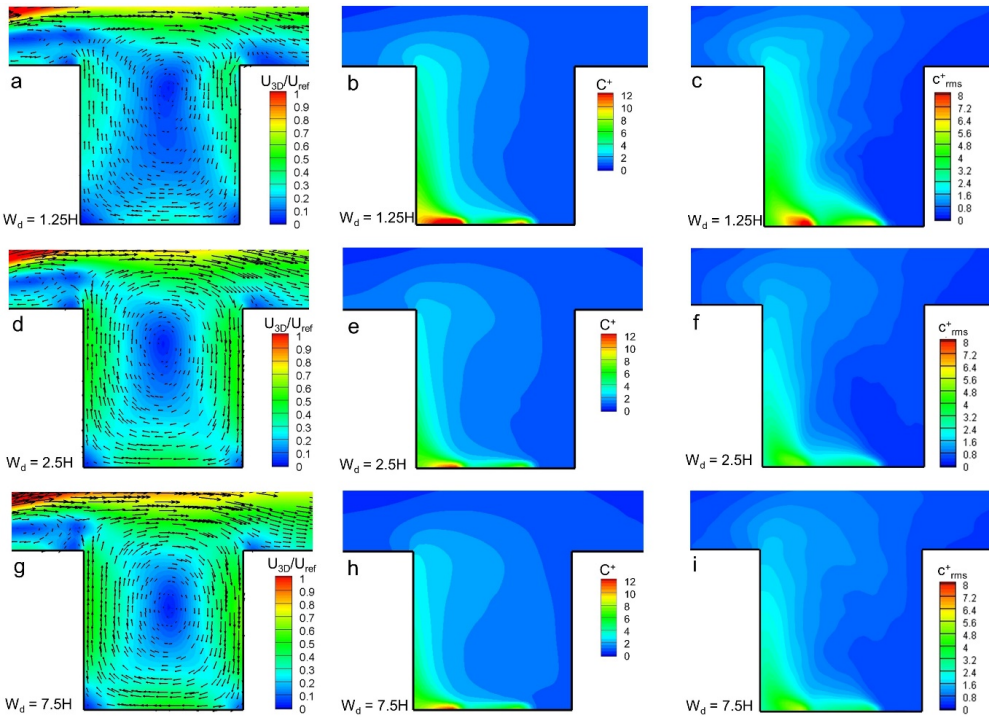

Fig. 11. (a) Distribution of U_{3D}/U_{ref} and 2D velocity vector field, (b) C^+, and (c) c^+_{rms} by the domains with W_d = 1.25, (d-f) W_d = 2.5H, and (g-i) W_d = 7.5H in the vertical centerplane.

Earlier studies have indicated that the domain width needs to be large enough to include the important and largest coherent eddies occurring in the spanwise direction (Moin and Kim, 1982; Walton and Cheng, 2002). We adopted the approach of computing the temporal correlations between two probe points on the same spanwise-oriented line to evaluate the adequacy of the domain width (Kitsios et al., 2011; Moin and Kim, 1982). Following the past study (Kitsios et al., 2011), the correlation coefficient of the fluctuation of the spanwise velocity component (y-direction), v', between the two points is:

$$r_{v'v'}(\Delta y) = \frac{\overline{v'(y,\,t)\;v'(y+\Delta y,\,t)}}{v'_{rms}(y)\;v'_{rms}(y+\Delta y)} \tag{6}$$

where the overbar denotes temporal averaging, Δy is the spanwise separation distance between the two points on the same line, and v'_{rms} is the root mean square error of the spanwise velocity component. The correlation coefficients $r_{v'v'}$ are averaged over the combinations of two points on the same line with the same value of Δy. If the velocity components in the periodic direction (v) become uncorrelated (e.g. the correlation coefficient decays to zero) within a separation distance of half the domain size in that direction, then the domain size can be considered to be sufficiently large (Fröhlich et al., 2005).

Based on the result from the reference domain ($W_d/H = 5$, $H_d/H = 11$, $U_d/H = 10$ and $D_d/H = 10$), the two-point correlation along the four lines in the spanwise direction (y) is shown in Fig. 12. The slow decay of $r_{v'v'}$ with Δy along the line of (z/H, x/H) = (0.75, 0.25) indicates that eddies close to the top and leeward region are highly elongated in the spanwise direction. The result along the line of (z/H, x/H) = (0.25, 0.75) shows that the spanwise extent of turbulence structures near the leeward wall close to the ground is much smaller than the others. All correlation coefficients decay to zero when $\Delta y/H$ reaches about 1.2, which means that W_d/H should be larger than 2.4. Considering that the domains with $W_d/H \geq 2.5$ yield similar mean concentration and mean velocity components, $W_d/H = 2.5$ can be considered as the minimum requirement of the domain width.

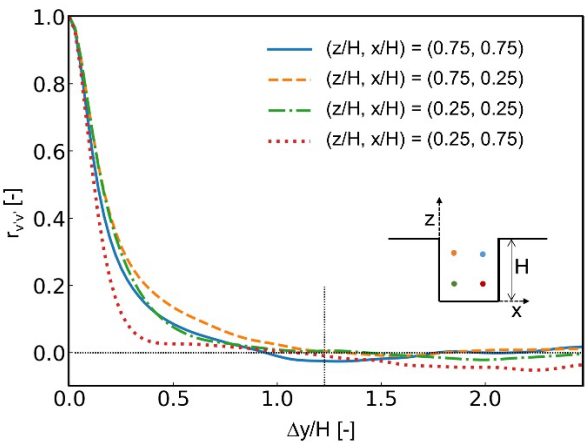

Fig. 12. Spanwise two-point correlation coefficient $r_{v'v'}$ along four lines.

4.5 Sensitivity analysis: impact of domain height

Fig. 13 displays W/U_{ref} and U/U_{ref} along the three horizontal lines and three vertical lines in the vertical centerplane obtained using six different domain heights. It shows that the blockage due to the presence of the building in the domain results in an artificial acceleration of the flow within the canyon. A monotonic and asymptotic increase of mean velocity components is found with a decrease of domain height. Compared to the domain with H_d/H = 21 (the largest domain height), the average absolute differences of the dimensionless mean velocity magnitude (U_{3D}/U_{ref}) along the sampling lines are 0.196, 0.052, 0.030, 0.014 and 0.007 for domains with H_d/H = 3, 5, 6, 7.5 and 11, respectively.

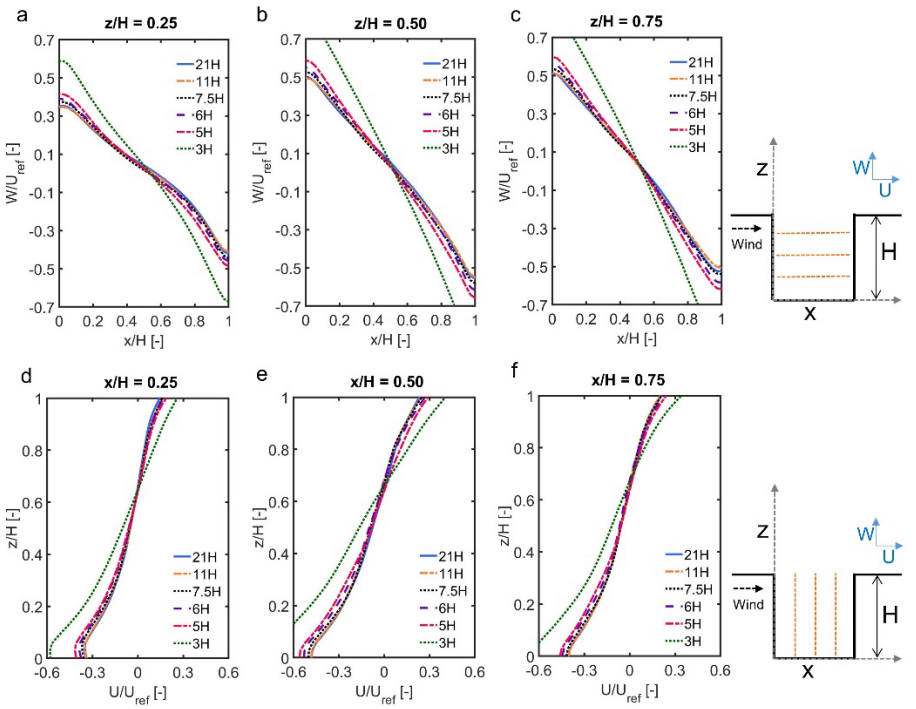

Fig. 13. Comparison of dimensionless mean velocity components obtained from six different domain heights: W/U_{ref} along three horizontal lines in the vertical centerplane (a) z/H = 0.25; (b) z/H = 0.5; and (c) z/H = 0.75, and U/U_{ref} along three vertical lines in the vertical centerplane (d) x/H = 0.25; (e) x/H = 0.5; and (f) x/H = 0.75.

Fig. 14 compares the profiles of C^+ along the same horizontal and vertical lines for the six domain heights. For the domains with H_d/H = 7.5, 11 and 21, negligible differences are

observed for the predicted C^+, while for the domains with H_d/H = 3, 5 and 6 C^+ is systematically underpredicted. Compared to the domain with H_d/H = 21 (the largest domain height), the average absolute differences of C^+ along all sampling lines for the domains with H_d/H = 3, 5, 6, 7.5 and 11 are 0.546, 0.218, 0.141, 0.047 and 0.042, respectively.

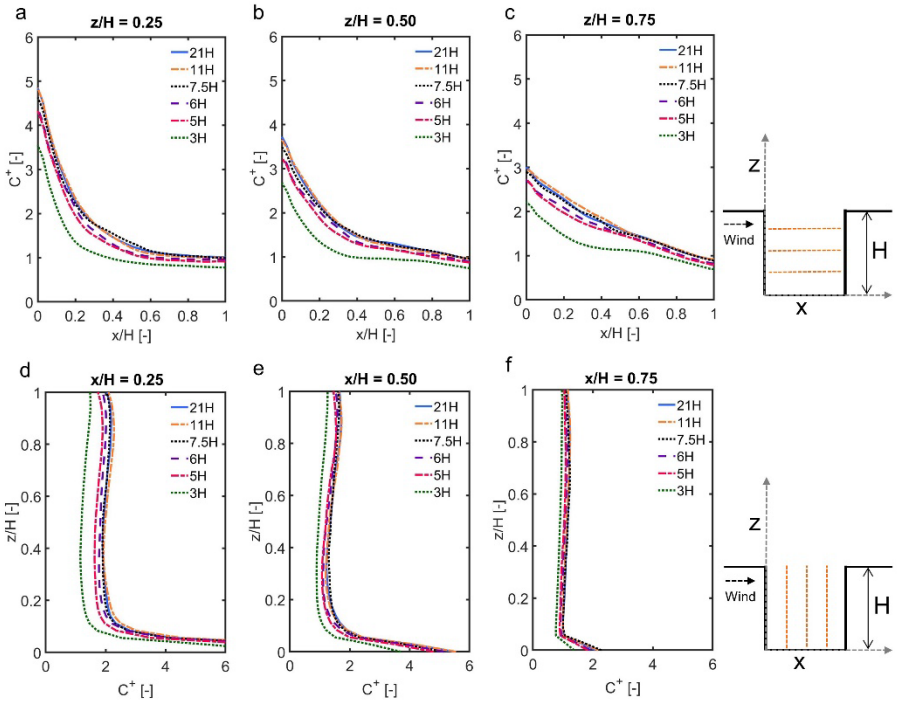

Fig. 14. Comparison of C^+ obtained from six different domain heights along three horizontal lines in the vertical centerplane: (a) z/H = 0.25; (b) z/H = 0.5; (c) z/H = 0.75; and three vertical lines in the vertical centerplane: (d) x/H = 0.25; (e) x/H = 0.5; (f) x/H = 0.75.

Fig. 15 shows the dimensionless mean velocity magnitude (U_{3D}/U_{ref}) and dimensionless mean concentration (C^+) along five vertical lines above the canyon in the vertical centerplane, as obtained from the six different domain heights. It is observed that the shear layer thickness increases when moving downstream. For the mean velocity within and below the shear layer, the largest value is achieved for the domain with H_d/H = 3 (Figs. 15a-e). For the mean wind velocity in the free stream flow, a monotonic increase is found with the decrease of the domain height. For C^+ within and below the shear layer, the domain with H_d/H = 3 predicts lower C^+ than the other five domains (see Fig. 15i and j).

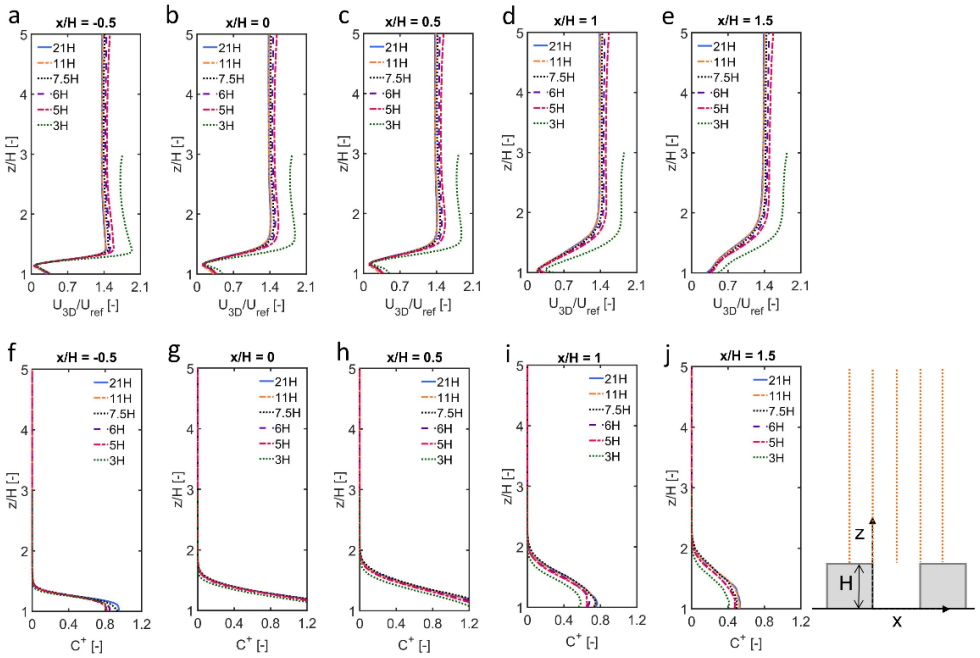

Fig. 15. Comparison of U_{3D}/U_{ref} obtained from six different domain heights along five vertical lines above the canyon in the vertical centerplane: (a) x/H = -0.5; (b) x/H = 0; (c) x/H = 0.5; (d) x/H = 1; and (e) x/H = 1.5; (f-j) same for C^+.

The effect of the domain height on the mean wind velocity inside and in the vicinity of the street canyon is negligible when H_d/H is equal to or greater than 7.5 (Figs. 13 and 15). The results of C^+ also indicate that the domain with H_d/H equal to or larger than 7.5 shows relatively similar results, and the smaller domain height (H_d) clearly yields larger C^+ (Figs. 14 and 15). These imply that a blockage ratio of 13.3% is sufficient to avoid the impact of flow acceleration on the results inside and around the street canyon.

4.6 Sensitivity analysis: impact of domain lengths

Fig. 16 shows W/U_{ref} and U/U_{ref} along the three horizontal lines and three vertical lines in the vertical centerplane obtained using four different upstream domain lengths. Fig. 17 displays C^+ along the same lines. It indicates that domain with $U_d/H = 2.5$ clearly yields lower values of W/U_{ref}, U/U_{ref}, and C^+ compared with the other domains, while $U_d/H = 5$, 7.5 and 10 show relatively similar results. Based on the large discrepancies, the use of U_d/H below 5

is not recommended. This is consistent with the guidelines (Franke et al., 2011) that the inlet boundary should be at least $5H_{max}$ to the building.

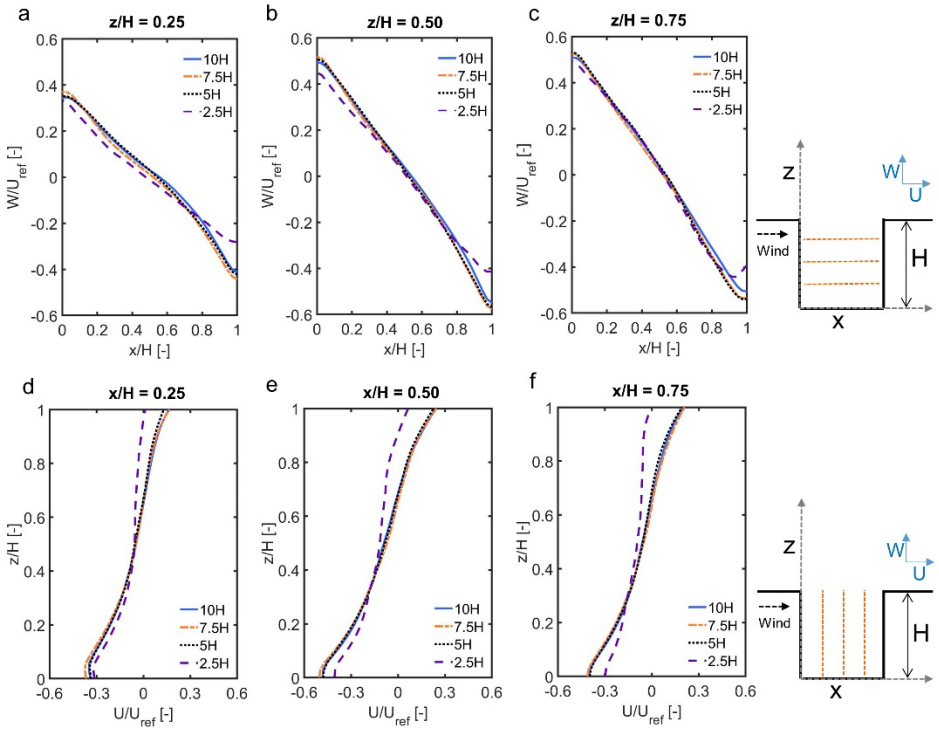

Fig. 16. Comparison of dimensionless mean velocity components obtained by four different upstream domain lengths: W/U_{ref} along three horizontal lines in the vertical centerplane (a) z/H = 0.25; (b) z/H = 0.5; (c) z/H = 0.75, and U/U_{ref} along three vertical lines in the vertical centerplane (d) x/H = 0.25; (e) x/H = 0.5; (f) x/H = 0.75.

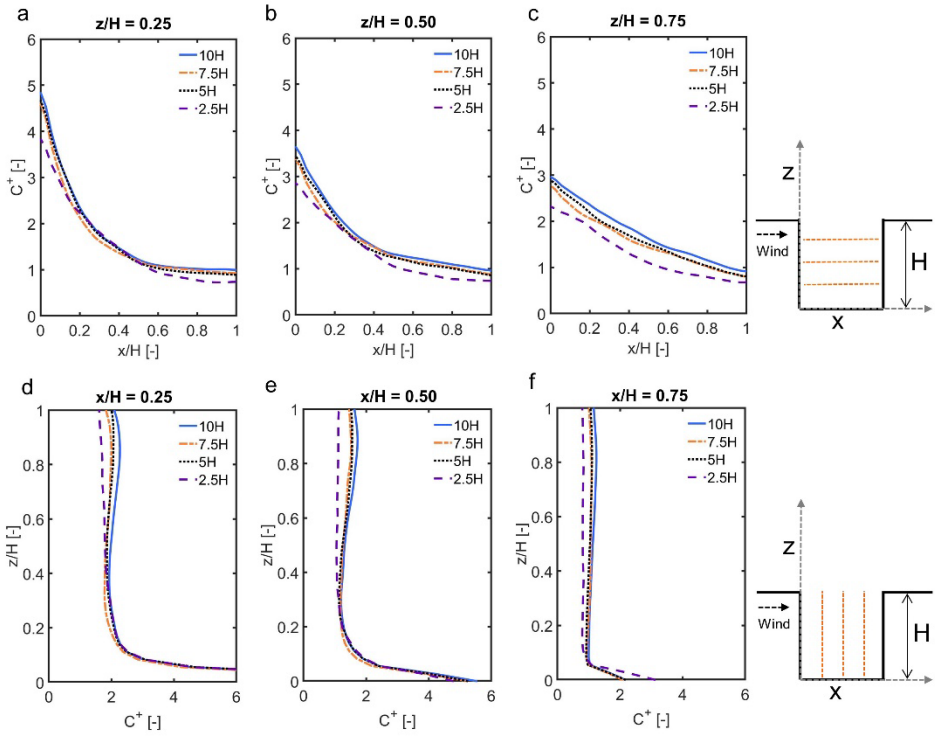

Fig. 17. Comparison of C^+ obtained from four different upstream domain lengths along three horizontal lines in the vertical centerplane: (a) z/H = 0.25; (b) z/H = 0.5; (c) z/H = 0.75; and three vertical lines in the vertical centerplane: (d) x/H = 0.25; (e) x/H = 0.5; (f) x/H = 0.75.

Fig. 18 displays W/U_{ref} and U/U_{ref} along the three horizontal lines and three vertical lines, as obtained using three different downstream domain lengths. The mean velocity components predicted by the domain with $U_d/H = 3$ are smaller than those by the other domains.

Fig. 19 displays C^+ along the same lines. Relatively large differences between the three domains are observed. During the simulation for domains with $D_d/H = 3$ and 6, reversed flow in large numbers of faces is reported in the outlet plane, which is not in line with recommendations by the best practice guidelines for CFD simulations of wind flow in urban areas (Franke et al., 2007). Guidelines for all applications of urban flow (Tominaga et al., 2008) indicated that the outflow boundary is recommended to be at least $10H_{max}$ away from the building group. Therefore, we also recommend 10H for this type of simulation.

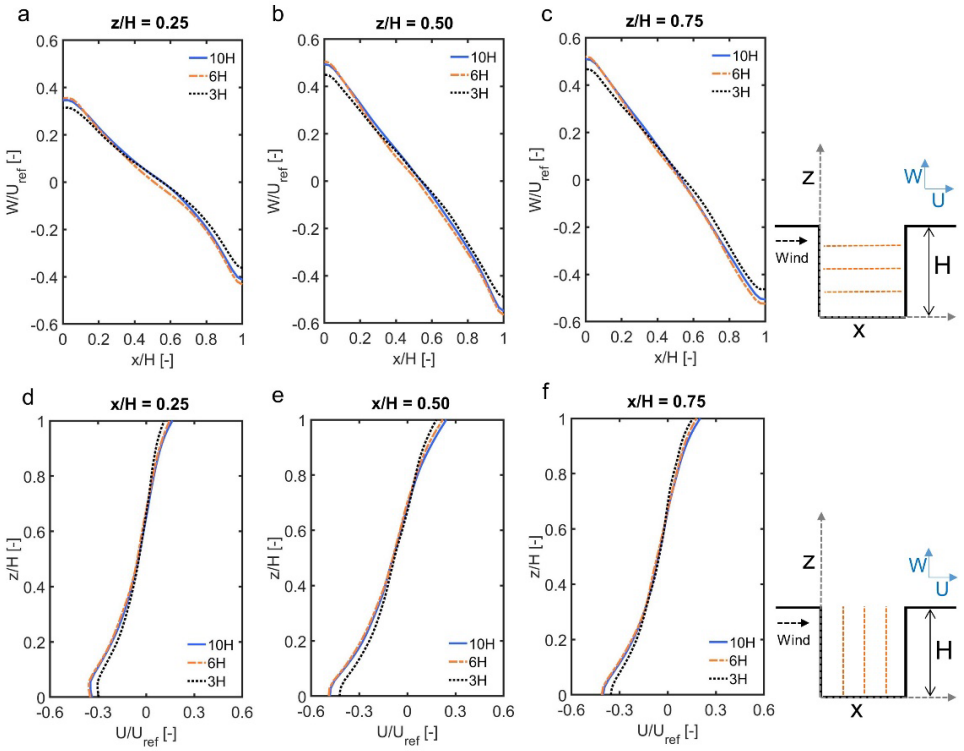

Fig. 18. Comparison of dimensionless mean velocity components obtained from three different downstream domain lengths: W/U_{ref} along three horizontal lines in the vertical centerplane (a) z/H = 0.25; (b) z/H = 0.5; (c) z/H = 0.75, and U/U_{ref} along three vertical lines in the vertical centerplane (d) x/H = 0.25; (e) x/H = 0.5; (f) x/H = 0.75.

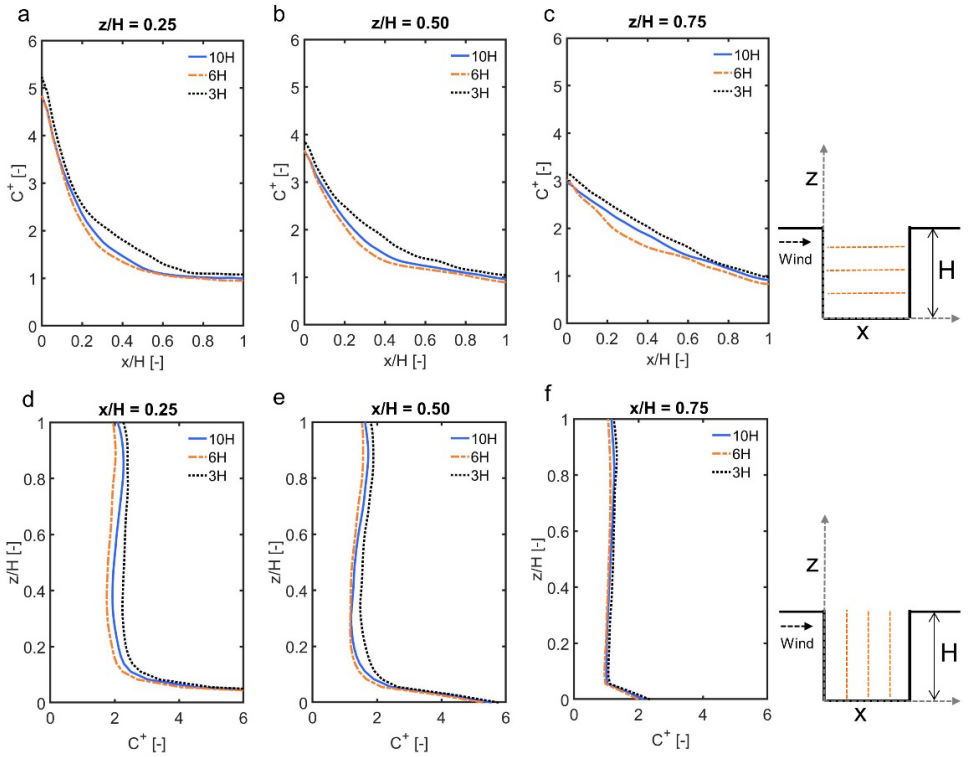

Fig. 19. Comparison of C^+ obtained from three different downstream domain lengths along three horizontal lines in the vertical centerplane: (a) z/H = 0.25; (b) z/H = 0.5; (c) z/H = 0.75; and three vertical lines in the vertical centerplane: (d) x/H = 0.25; (e) x/H = 0.5; (f) x/H = 0.75.

4.7 Discussion

The present finding of the blockage ratio is smaller than the recommended directional blockage ratio (Blocken, 2015) (i.e. about 17%). However, when compared with the full blockage ratio by best practice guidelines for urban flows (Blocken, 2015; Franke et al., 2011; Tominaga et al., 2008), i.e. maximum blockage ratio of 3%, the present finding of the blockage ratio is much larger. The possible reason for these differences is that best practice guidelines for urban flows were developed to avoid artificial accelerations occurring at both the top and sides of buildings. In the present study, the street canyon is simulated as 2.5D without considering the airflow near the sides of buildings but only focusing on the airflow and concentration inside the canyon.

The case evaluated in the present study is limited to a simple street canyon with the aspect ratio (= H/W) of 1, which is the common generic street canyon found in the literature (Table 1). As shown by the two-point correlation and the comparison of the mean velocity components and mean concentration in Section 4, the domain width needs to be large enough to include the important coherent eddies occurring in the spanwise direction. In this perspective, the spanwise extent of turbulence structures within street canyons is important. A recent experimental study investigated the effect of the upstream roughness and aspect ratio on the spanwise structure of the roof-level turbulence in long uniform street canyons (Jaroslawski et al., 2019a, 2019b). The results indicated that canyons with a large aspect ratio have large-scale vortex organization in the spanwise direction (Jaroslawski et al., 2019a). It also demonstrated that the upstream roughness and the aspect ratio have significant effects on the spanwise turbulence integral length at the roof-level (Jaroslawski et al., 2019b). The turbulence at the roof level may affect the spanwise turbulence within the canyon. Therefore, it is important to highlight that the aforementioned minimum domain size in Section 4 is recommended for 1:1 single street canyon cases exposed to an atmospheric boundary layer, which may not be valid for other cases.

As shown by past studies (Montazeri and Blocken, 2013; Montazeri et al., 2013; Stathopoulos and Zhu, 1988; Zheng et al., 2020), the presence of building façade geometrical details such as balconies may introduce a high level of complexity in the airflow. Therefore, the domain width obtained in the present study may not be valid for cases with façade geometrical details. Further studies should focus on cases with upstream obstacles, with multiple street canyons in sequence, with other aspect ratios, and with façade geometrical details.

4.8 Conclusions

The current study evaluated the influence of the domain width, domain height, and upstream and downstream domain lengths on the prediction of the wind field and pollutant dispersion in generic single street canyons. The study has led to a set of conclusions and recommendations towards the application of LES simulation for a 2.5D street canyon with spanwise periodic boundary conditions. The following conclusions aim at reducing the size of the computational domain without significantly compromising the accuracy:

Compared to the domain with W_d/H = 7.5 (the largest domain width), the average absolute differences between the dimensionless mean velocity magnitude (U_{3D}/U_{ref}) along the sampling lines by domains with W_d/H = 1.25, 2.0, 2.5, 3.75 and 5 are 0.091, 0.043, 0.020, 0.028 and 0.020, respectively. The differences for the C^+ are 0.441, 0.197, 0.119, 0.122 and 0.130, respectively. It indicates that when the domain width is equal to or greater than 2.5H, a similarity of results in terms of mean velocity and mean concentration within the street canyon is obtained. The two-point correlation analysis indicates that the domain width should be larger than 2.4H. As a result, this study recommends the minimum safe value of W_d = 2.5H.

Compared to the domain with H_d/H = 21 (the largest domain height), the average absolute differences of the dimensionless mean velocity magnitude along the sampling lines for domains with H_d/H = 3, 5, 6, 7.5 and 11 are 0.196, 0.052, 0.030, 0.014 and 0.007, respectively. These differences for the C^+ are 0.546, 0.218, 0.141, 0.047 and 0.042, respectively. The domain height of 7.5H is recommended to minimize the effect of the blockage effect. This is equivalent to a blockage ratio of 13.3%. Smaller domain height can result in the overprediction of mean velocity and underprediction of mean concentration.

For the upstream domain length (U_d) and downstream domain length (D_d), the present findings are consistent with the existing guidelines for RANS simulations, with minimum values for U_d and D_d equal to 5H and 10H, respectively.

Acknowledgments

This work has been sponsored by NWO Exacte en Natuurwetenschappen (Physical Sciences) for the use of supercomputer facilities, with financial support from the Nederlandse Organisatie voor Wetenschappelijk Onderzoek (Netherlands Organization for Scientific Research, NWO). The authors would like to express sincere thanks to Dr. Christof Bernhard Gromke for his comments and advice. The authors also gratefully acknowledge the partnership with ANSYS CFD.

References

Ai, Z.T., Mak, C.M., 2017. CFD simulation of flow in a long street canyon under a

perpendicular wind direction: Evaluation of three computational settings. Build. Environ. 114, 293–306. https://doi.org/10.1016/j.buildenv.2016.12.032

Ai, Z.T., Mak, C.M., 2015. Large-eddy Simulation of flow and dispersion around an isolated building: Analysis of influencing factors. Comput. Fluids 118, 89–100. https://doi.org/10.1016/j.compfluid.2015.06.006

ANSYS Inc., 2017. Release 18.0, Theory Guide. ANSYS Inc, Canonsburg, PA 15317, USA.

Antoniou, N., Montazeri, H., Neophytou, M., Blocken, B., 2019. CFD simulation of urban microclimate: Validation using high-resolution field measurements. Sci. Total Environ. 695, 133743. https://doi.org/https://doi.org/10.1016/j.scitotenv.2019.133743

Antoniou, N., Montazeri, H., Wigo, H., Neophytou, M.K.-A., Blocken, B., Sandberg, M., 2017. CFD and wind-tunnel analysis of outdoor ventilation in a real compact heterogeneous urban area: Evaluation using "air delay." Build. Environ. 126, 355–372. https://doi.org/10.1016/j.buildenv.2017.10.013

Baker, J., Walker, H.L., Cai, X., 2004. A study of the dispersion and transport of reactive pollutants in and above street canyons—a large eddy simulation. Atmos. Environ. 38, 6883–6892. https://doi.org/10.1016/j.atmosenv.2004.08.051

Baratian-Ghorghi, Z., Kaye, N.B., 2013. The effect of canyon aspect ratio on flushing of dense pollutants from an isolated street canyon. Sci. Total Environ. 443, 112–122. https://doi.org/https://doi.org/10.1016/j.scitotenv.2012.10.064

Blocken, B., 2018. LES over RANS in building simulation for outdoor and indoor applications: A foregone conclusion? Build. Simul. https://doi.org/10.1007/s12273-018-0459-3

Blocken, B., 2015. Computational Fluid Dynamics for urban physics: Importance, scales, possibilities, limitations and ten tips and tricks towards accurate and reliable simulations. Build. Environ. 91, 219–245. https://doi.org/10.1016/j.buildenv.2015.02.015

Bright, V.B., Bloss, W.J., Cai, X., 2013. Urban street canyons: Coupling dynamics, chemistry and within-canyon chemical processing of emissions. Atmos. Environ. 68, 127–142. https://doi.org/10.1016/j.atmosenv.2012.10.056

Buccolieri, R., Gromke, C., Di Sabatino, S., Ruck, B., 2009. Aerodynamic effects of trees on pollutant concentration in street canyons. Sci. Total Environ. 407, 5247–5256. https://doi.org/https://doi.org/10.1016/j.scitotenv.2009.06.016

Chatzimichailidis, A.E., Argyropoulos, C.D., Assael, M.J., Kakosimos, K.E., 2019. Qualitative and quantitative investigation of multiple large eddy simulation aspects for pollutant dispersion in street canyons using OpenFOAM. Atmosphere (Basel). 10.

https://doi.org/10.3390/atmos10010017

Cheng, W.C., Liu, C.-H., 2011. Large-eddy simulation of turbulent transports in urban street canyons in different thermal stabilities. J. Wind Eng. Ind. Aerodyn. 99, 434–442. https://doi.org/10.1016/j.jweia.2010.12.009

Chew, L.W., Glicksman, L.R., Norford, L.K., 2018. Buoyant flows in street canyons: Comparison of RANS and LES at reduced and full scales. Build. Environ. 146, 77–87. https://doi.org/10.1016/j.buildenv.2018.09.026

Ding, S., Huang, Y., Cui, P., Wu, J., Li, M., Liu, D., 2019. Impact of viaduct on flow reversion and pollutant dispersion in 2D urban street canyon with different roof shapes - Numerical simulation and wind tunnel experiment. Sci. Total Environ. 671, 976–991. https://doi.org/https://doi.org/10.1016/j.scitotenv.2019.03.391

Duan, G., Ngan, K., 2018. Effects of time-dependent inflow perturbations on turbulent flow in a street canyon. Boundary-Layer Meteorol. 167, 257–284. https://doi.org/10.1007/s10546-017-0327-1

Ducros, F., Nicoud, F., Poinsot, T., 1998. Wall-adapting local eddy-viscosity models for simulations in complex geometries, in: Oxford University Computing Laboratory. 16th Conference on Numerical Methods in Fluid Dynamics, Arcachon, France, pp. 293–299.

Franke, J., Hellsten, A., Schlunzen, H., Carissimo, B., 2011. The COST 732 Best practice guideline for CFD simulation of flows in the urban environment: a summary. Int. J. Environ. Pollut. 44, 419. https://doi.org/10.1504/ijep.2011.038443

Franke, J., Hellsten, A., Schlünzen, H., Carissimo, B., 2007. Best practice guideline for the CFD simulation of flows in the urban environment. Meteorological Inst., COST, Hamburg, Germany.

Fröhlich, J., Mellen, C.P., Rodi, W., Temmerman, L., Leschziner, M.A., 2005. Highly resolved large-eddy simulation of separated flow in a channel with streamwise periodic constrictions. J. Fluid Mech. 526, 19–66. https://doi.org/10.1017/S0022112004002812

Gallagher, J., Lago, C., 2019. How parked cars affect pollutant dispersion at street level in an urban street canyon? A CFD modelling exercise assessing geometrical detailing and pollutant decay rates. Sci. Total Environ. 651, 2410–2418. https://doi.org/10.1016/j.scitotenv.2018.10.135

Geng, F., Kalkman, I., Suiker, A.S.J., Blocken, B., 2018. Sensitivity analysis of airfoil aerodynamics during pitching motion at a Reynolds number of 1.35×105. J. Wind Eng. Ind. Aerodyn. 183, 315–332. https://doi.org/10.1016/j.jweia.2018.11.009

Gerasimov, A., 2016. Quick guide to setting up LES-type simulations, version 1.4. European Technology Group, ANSYS Sweden AB.

Gousseau, P., Blocken, B., Van Heijst, G.J.F., 2013. Quality assessment of Large-Eddy Simulation of wind flow around a high-rise building: Validation and solution verification. Comput. Fluids 79, 120–133. https://doi.org/10.1016/j.compfluid.2013.03.006

Gromke, C., 2008a. Database, 2008. Concentration data of street canyon. Internet database. [WWW Document]. URL http://www.codasc.de

Gromke, C., 2008b. Einfluss von Bäumen auf die Durchlüftung von innerstädtischen Straßenschluchten. KIT Scientific Publishing.

Gromke, C., Buccolieri, R., Di Sabatino, S., Ruck, B., 2008. Dispersion study in a street canyon with tree planting by means of wind tunnel and numerical investigations – Evaluation of CFD data with experimental data. Atmos. Environ. 42, 8640–8650. https://doi.org/10.1016/j.atmosenv.2008.08.019

Gromke, C., Ruck, B., 2009. On the impact of trees on dispersion processes of traffic emissions in street canyons. Boundary-Layer Meteorol. 131, 19–34. https://doi.org/10.1007/s10546-008-9301-2

Gromke, C., Ruck, B., 2007. Influence of trees on the dispersion of pollutants in an urban street canyon—Experimental investigation of the flow and concentration field. Atmos. Environ. 41, 3287–3302. https://doi.org/10.1016/j.atmosenv.2006.12.043

Han, B.-S., Baik, J.-J., Kwak, K.-H., Park, S.-B., 2018. Large-eddy simulation of reactive pollutant exchange at the top of a street canyon. Atmos. Environ. 187, 381–389. https://doi.org/10.1016/j.atmosenv.2018.06.012

Hanjalic, K., 2005. Will RANS survive LES? A view of perspectives. J. Fluids Eng. 127, 831. https://doi.org/10.1115/1.2037084

He, L., Hang, J., Wang, X., Lin, B., Li, X., Lan, G., 2017. Numerical investigations of flow and passive pollutant exposure in high-rise deep street canyons with various street aspect ratios and viaduct settings. Sci. Total Environ. 584-585, 189–206. https://doi.org/10.1016/j.scitotenv.2017.01.138

Hu, L.H., Huo, R., Yang, D., 2009. Large eddy simulation of fire-induced buoyancy driven plume dispersion in an urban street canyon under perpendicular wind flow. J. Hazard. Mater. 166, 394–406. https://doi.org/10.1016/j.jhazmat.2008.11.105

Huang, Y.-D., Xu, X., Liu, Z.-Y., Deng, J.-T., Kim, C.-N., 2016. Impacts of shape and height of building roof on airflow and pollutant dispersion inside an isolated street canyon.

Environ. Forensics 17, 361–379. https://doi.org/10.1080/15275922.2016.1230912

Iousef, S., Montazeri, H., Blocken, B., van Wesemael, P.J.V., 2017. On the use of non-conformal grids for economic LES of wind flow and convective heat transfer for a wall-mounted cube. Build. Environ. 119, 44–61. https://doi.org/10.1016/j.buildenv.2017.04.004

Jaroslawski, T., Perret, L., Blackman, K., Savory, E., 2019a. The Spanwise Variation of Roof-Level Turbulence in a Street-Canyon Flow. Boundary-Layer Meteorol. 170, 373–394. https://doi.org/10.1007/s10546-018-0405-z

Jaroslawski, T., Savory, E., Perret, L., 2019b. The characterization of the spanwise roof-level turbulence in a street canyon flow. University of Western Ontario.

Kastner-Klein, P., Berkowicz, R., Britter, R., 2004. The influence of street architecture on flow and dispersion in street canyons. Meteorol. Atmos. Phys. 87, 121–131. https://doi.org/10.1007/s00703-003-0065-4

Kastner-Klein, P., Plate, E.J., 1999. Wind-tunnel study of concentration fields in street canyons. Atmos. Environ. 33, 3973–3979. https://doi.org/10.1016/S1352-2310(99)00139-9

Kikumoto, H., Ooka, R., 2012a. A numerical study of air pollutant dispersion with bimolecular chemical reactions in an urban street canyon using large-eddy simulation. Atmos. Environ. 54, 456–464. https://doi.org/10.1016/j.atmosenv.2012.02.039

Kikumoto, H., Ooka, R., 2012b. A study on air pollutant dispersion with bimolecular reactions in urban street canyons using large-eddy simulations. J. Wind Eng. Ind. Aerodyn. 104-106, 516–522. https://doi.org/10.1016/j.jweia.2012.03.001

Kitsios, V., Cordier, L., Bonnet, J.-P., Ooi, A., Soria, J., 2011. On the coherent structures and stability properties of a leading-edge separated aerofoil with turbulent recirculation. J. Fluid Mech. 683, 395–416. https://doi.org/10.1017/jfm.2011.285

Lateb, M., Meroney, R.N., Yataghene, M., Fellouah, H., Saleh, F., Boufadel, M.C., 2016. On the use of numerical modelling for near-field pollutant dispersion in urban environments − A review. Environ. Pollut. 208, 271–283. https://doi.org/10.1016/j.envpol.2015.07.039

Li, X.-X., Britter, R.E., Yong Koh, T., Norford, L.K., Liu, C.-H., Entekhabi, D., C Leung, D.Y., 2010. Large-eddy simulation of flow and pollutant transport in urban street canyons with ground heating. Boundary-Layer Meteorol. 137, 187–204. https://doi.org/10.1007/s10546-010-9534-8

Li, X.-X., Leung, D.Y.C., Liu, C.-H., Lam, K.M., 2008a. Physical modeling of flow field inside

urban street canyons. J. Appl. Meteorol. Climatol. 47, 2058–2067. https://doi.org/10.1175/2007JAMC1815.1

Li, X.-X., Liu, C.-H., Leung, D.Y.C., 2008b. Large-eddy simulation of flow and pollutant dispersion in high-aspect-ratio urban street canyons with wall model. Boundary-Layer Meteorol. 129, 249–268. https://doi.org/10.1007/s10546-008-9313-y

Liu, C.-H., Barth, M.C., Leung, D.Y.C., 2004. Large-eddy simulation of flow and pollutant transport in street canyons of different building-height-to-street-width ratios. J. Appl. Meteorol. 43, 1410–1424. https://doi.org/10.1175/JAM2143.1

Llaguno-Munitxa, M., Bou-Zeid, E., 2018. Shaping buildings to promote street ventilation: A large-eddy simulation study. Urban Clim. 26, 76–94. https://doi.org/10.1016/j.uclim.2018.08.006

Llaguno-Munitxa, M., Bou-Zeid, E., Hultmark, M., 2017. The influence of building geometry on street canyon air flow: Validation of large eddy simulations against wind tunnel experiments. J. Wind Eng. Ind. Aerodyn. 165, 115–130. https://doi.org/10.1016/j.jweia.2017.03.007

Lo, K.W., Ngan, K., 2015. Characterising the pollutant ventilation characteristics of street canyons using the tracer age and age spectrum. Atmos. Environ. 122, 611–621. https://doi.org/10.1016/j.atmosenv.2015.10.023

Louka, P., Belcher, S.E., Harrison, R.G., 2000. Coupling between air flow in streets and the well-developed boundary layer aloft. Atmos. Environ. 34, 2613–2621.

Mathey, F., Cokljat, D., Bertoglio, J.P., Sergent, E., 2006. Assessment of the vortex method for Large Eddy Simulation inlet conditions. Prog. Comput. Fluid Dyn. An Int. J. 6, 58. https://doi.org/10.1504/PCFD.2006.009483

Mei, S.-J., Liu, C.-W., Liu, D., Zhao, F.-Y., Wang, H.-Q., Li, X.-H., 2016. Fluid mechanical dispersion of airborne pollutants inside urban street canyons subjecting to multi-component ventilation and unstable thermal stratifications. Sci. Total Environ. 565, 1102–1115. https://doi.org/https://doi.org/10.1016/j.scitotenv.2016.05.150

Merlier, L., Jacob, J., Sagaut, P., 2018. Lattice-boltzmann large-eddy simulation of pollutant dispersion in street canyons including tree planting effects. Atmos. Environ. 195, 89–103. https://doi.org/10.1016/j.atmosenv.2018.09.040

Meroney, R., Ohba, R., Leitl, B., Kondo, H., Grawe, D., Tominaga, Y., 2016. Review of CFD guidelines for dispersion modeling. Fluids 1, 14. https://doi.org/10.3390/fluids1020014

Meroney, R.N., Pavageau, M., Rafailidis, S., Schatzmann, M., 1996. Study of line source

characteristics for 2-D physical modelling of pollutant dispersion in street canyons. J. Wind Eng. Ind. Aerodyn. 62, 37–56. https://doi.org/10.1016/S0167-6105(96)00057-8

Moin, P., Kim, J., 1982. Numerical investigation of turbulent channel flow. J. Fluid Mech. 118, 341. https://doi.org/10.1017/S0022112082001116

Montazeri, H., Blocken, B., 2013. CFD simulation of wind-induced pressure coefficients on buildings with and without balconies: Validation and sensitivity analysis. Build. Environ. 60, 137–149. https://doi.org/10.1016/j.buildenv.2012.11.012

Montazeri, H., Blocken, B., Janssen, W.D., van Hooff, T., 2013. CFD evaluation of new second-skin facade concept for wind comfort on building balconies: Case study for the Park Tower in Antwerp. Build. Environ. 68, 179–192. https://doi.org/10.1016/j.buildenv.2013.07.004

Moonen, P., Dorer, V., Carmeliet, J., 2011. Evaluation of the ventilation potential of courtyards and urban street canyons using RANS and LES. Jnl. Wind Eng. Ind. Aerodyn. 99, 414–423. https://doi.org/10.1016/j.jweia.2010.12.012

Moonen, P., Gromke, C., Dorer, V., 2013. Performance assessment of Large Eddy Simulation (LES) for modeling dispersion in an urban street canyon with tree planting. Atmos. Environ. 75, 66–76. https://doi.org/10.1016/j.atmosenv.2013.04.016

Nosek, Š., Kukačka, L., Jurčáková, K., Kellnerová, R., Jaňour, Z., 2017. Impact of roof height non-uniformity on pollutant transport between a street canyon and intersections. Environ. Pollut. 227, 125–138. https://doi.org/10.1016/j.envpol.2017.03.073

O'Neill, J.J., Cai, X.-M., Kinnersley, R., 2016. Stochastic backscatter modelling for the prediction of pollutant removal from an urban street canyon: A large-eddy simulation. Atmos. Environ. 142, 9–18. https://doi.org/10.1016/j.atmosenv.2016.07.024

Oke, T.R., 1988. Street design and urban canopy layer climate. Energy Build. 11, 103–113. https://doi.org/10.1016/0378-7788(88)90026-6

Park, S.-B., Baik, J.-J., Raasch, S., Letzel, M.O., 2012. A large-eddy simulation study of thermal effects on turbulent flow and dispersion in and above a street canyon. J. Appl. Meteorol. Climatol. 51, 829–841. https://doi.org/10.1175/JAMC-D-11-0180.1

Perret, L., Savory, E., 2013. Large-Scale Structures over a Single Street Canyon Immersed in an Urban-Type Boundary Layer. Boundary-Layer Meteorol. 148, 111–131. https://doi.org/10.1007/s10546-013-9808-z

Ramponi, R., Blocken, B., 2012. CFD simulation of cross-ventilation for a generic isolated building: Impact of computational parameters. Build. Environ. 53, 34–48. https://doi.org/10.1016/j.buildenv.2012.01.004

Ricci, A., Burlando, M., Repetto, M.P., Blocken, B., 2019. Simulation of urban boundary and canopy layer flows in port areas induced by different marine boundary layer inflow conditions. Sci. Total Environ. 670, 876–892. https://doi.org/https://doi.org/10.1016/j.scitotenv.2019.03.230

Richards, P.J., Hoxey, R.P., 1993. Appropriate boundary conditions for computational wind engineering models using the k-ε turbulence model. J. Wind Eng. Ind. Aerodyn. 145–153. https://doi.org/10.1016/B978-0-444-81688-7.50018-8

Salim, S.M., Buccolieri, R., Chan, A., Sabatino, S. Di, 2011a. Numerical simulation of atmospheric pollutant dispersion in an urban street canyon: Comparison between RANS and LES. Jnl. Wind Eng. Ind. Aerodyn. 99, 103–113. https://doi.org/10.1016/j.jweia.2010.12.002

Salim, S.M., Cheah, S.C., Chan, A., 2011b. Numerical simulation of dispersion in urban street canyons with avenue-like tree plantings: Comparison between RANS and LES. Build. Environ. 46, 1735–1746. https://doi.org/10.1016/j.buildenv.2011.01.032032

Scungio, M., Stabile, L., Rizza, V., Pacitto, A., Russi, A., Buonanno, G., 2018. Lung cancer risk assessment due to traffic-generated particles exposure in urban street canyons: A numerical modelling approach. Sci. Total Environ. 631-632, 1109–1116. https://doi.org/https://doi.org/10.1016/j.scitotenv.2018.03.093

Sergent, E., 2002. Vers une méthodologie de couplage entre la simulation des grandes échelles et les modèles statistiques. Ecully, Ecole centrale de Lyon.

Stabile, L., Arpino, F., Buonanno, G., Russi, A., Frattolillo, A., 2015. A simplified benchmark of ultrafine particle dispersion in idealized urban street canyons: A wind tunnel study. Build. Environ. 93, 186–198. https://doi.org/10.1016/j.buildenv.2015.05.045

Stathopoulos, T., Zhu, X., 1988. Wind pressures on building with appurtenances. J. Wind Eng. Ind. Aerodyn. 31, 265–281. https://doi.org/10.1016/0167-6105(88)90008-6

Tominaga, Y., Mochida, A., Yoshie, R., Kataoka, H., Nozu, T., Yoshikawa, M., Shirasawa, T., 2008. AIJ guidelines for practical applications of CFD to pedestrian wind environment around buildings. J. Wind Eng. Ind. Aerodyn. 96, 1749–1761. https://doi.org/10.1016/j.jweia.2008.02.058

Tominaga, Y., Stathopoulos, T., 2013. CFD simulation of near-field pollutant dispersion in the urban environment: A review of current modeling techniques. Atmos. Environ. 79, 716–730. https://doi.org/10.1016/j.atmosenv.2013.07.028

Tominaga, Y., Stathopoulos, T., 2011. CFD modeling of pollution dispersion in a street canyon: Comparison between LES and RANS. J. Wind Eng. Ind. Aerodyn. 99, 340–348. https://doi.org/10.1016/j.jweia.2010.12.005

Tominaga, Y., Stathopoulos, T., 2007. Turbulent Schmidt numbers for CFD analysis with various types of flowfield. Atmos. Environ. 41, 8091–8099. https://doi.org/10.1016/j.atmosenv.2007.06.054

Vasaturo, R., Kalkman, I., Blocken, B., Wesemael, P.J.V. Van, 2018. Large eddy simulation of the neutral atmospheric boundary layer: performance evaluation of three inflow methods for terrains with different roughness. J. Wind Eng. Ind. Aerodyn. 173, 241–261. https://doi.org/10.1016/j.jweia.2017.11.025

Vervoort, R., Blocken, B., van Hooff, T., 2019. Reduction of particulate matter concentrations by local removal in a building courtyard: Case study for the Delhi American Embassy School. Sci. Total Environ. 686, 657–680. https://doi.org/10.1016/j.scitotenv.2019.05.154

Vranckx, S., Vos, P., Maiheu, B., Janssen, S., 2015. Impact of trees on pollutant dispersion in street canyons: A numerical study of the annual average effects in Antwerp, Belgium. Sci. Total Environ. 532, 474–483. https://doi.org/https://doi.org/10.1016/j.scitotenv.2015.06.032

Walton, A., Cheng, A.Y.S., 2002. Large-eddy simulation of pollution dispersion in an urban street canyon—Part II: idealised canyon simulation. Atmos. Environ. 36, 3615–3627. https://doi.org/10.1016/S1352-2310(02)00260-1

Wang, C., Li, Q., Wang, Z.-H., 2018. Quantifying the impact of urban trees on passive pollutant dispersion using a coupled large-eddy simulation – lagrangian stochastic model. Build. Environ. 145, 33–49. https://doi.org/10.1016/j.buildenv.2018.09.014

Wen, H., Malki-Epshtein, L., 2018. A parametric study of the effect of roof height and morphology on air pollution dispersion in street canyons. J. Wind Eng. Ind. Aerodyn. 175, 328–341. https://doi.org/10.1016/j.jweia.2018.02.006

Werner, H., Wengle, H., 1993. Large-eddy simulation of turbulent flow over and around a cube in a plate channel, in: Turbulent Shear Flows 8. Springer Berlin Heidelberg, Berlin, Heidelberg, pp. 155–168. https://doi.org/10.1007/978-3-642-77674-8_12

World Health Organization, 2016. WHO Global Urban Ambient Air Pollution Database (update 2016). Geneva, Switzerland.

Xie, X., Hao, C., Huang, Y., Huang, Z., 2020. Influence of TiO2-based photocatalytic coating road on traffic-related NOx pollutants in urban street canyon by CFD modeling. Sci. Total Environ. 724, 138059. https://doi.org/https://doi.org/10.1016/j.scitotenv.2020.138059

Zhang, K., Chen, G., Wang, X., Liu, S., Mak, C.M., Fan, Y., Hang, J., 2019. Numerical evaluations of urban design technique to reduce vehicular personal intake fraction in

deep street canyons. Sci. Total Environ. 653, 968–994. https://doi.org/https://doi.org/10.1016/j.scitotenv.2018.10.333

Zhang, Y.-W., Gu, Z.-L., Cheng, Y., Lee, S.-C., 2011. Effect of real-time boundary wind conditions on the air flow and pollutant dispersion in an urban street canyon—Large eddy simulations. Atmos. Environ. 45, 3352–3359. https://doi.org/10.1016/j.atmosenv.2011.03.055

Zheng, X., Montazeri, H., Blocken, B., 2020. CFD simulations of wind flow and mean surface pressure for buildings with balconies: Comparison of RANS and LES. Build. Environ. 173, 106747. https://doi.org/10.1016/j.buildenv.2020.106747

Zhong, J., Cai, X.-M., Bloss, W.J., 2017. Large eddy simulation of reactive pollutants in a deep urban street canyon: Coupling dynamics with O3-NOx-VOC chemistry. Environ. Pollut. 224, 171–184. https://doi.org/10.1016/j.envpol.2017.01.076

Zhong, J., Cai, X.-M., Bloss, W.J., 2015. Modelling the dispersion and transport of reactive pollutants in a deep urban street canyon: Using large-eddy simulation. Environ. Pollut. 200, 42–52. https://doi.org/10.1016/j.envpol.2015.02.009

Chapter 5

Impact of façade geometrical details on pollutant dispersion in street canyons

This chapter has been submitted to a peer-reviewed journal:

Impact of façade geometrical details on pollutant dispersion in street canyons

X. Zheng, H. Montazeri, B. Blocken

(Submitted)

Abstract: The present study investigates the impact of building façade geometrical details on the pollutant transport mechanism in long street canyons. Large-eddy simulations (LES), extensively validated with experiments, are performed for four cases: (i) street canyon without façade balconies, (ii) street canyon with balconies at both windward and leeward façades, (ii) street canyon with balconies only at the windward façade and (iv) street canyon with balconies only at the leeward façade. The results show that the building balconies can strongly affect the wind flow field and pollutant dispersion in street canyons. The most significant impact is observed for the two street canyon cases with balconies at the windward façade, which strongly obstruct the airflow from penetrating deep into the bottom of the canyon. The presence of balconies only at the windward façade and at both façades can increase the area-weighted mean pollutant concentration in the vertical center plane inside the canyon by 80% and 106%, respectively, and reduce the mean pollutant exchange velocity (U_e) by 46% and 54%, respectively. The analysis of the vertical mean convective and turbulent mass fluxes indicates that the presence of balconies mainly decreases the convective contribution to U_e, while the impact on the turbulent contribution is smaller.

5.1 Introduction

Air quality in urban areas is an important environmental issue worldwide as it contributes to human morbidity and mortality [1–3]. Street canyons are typical elements in urban environments that can represent highly polluted spaces near buildings, due to the low wind speed and accumulation of vehicular pollution inside the canyon. Air pollutants in street canyons can enter the indoor space via window and door openings, ventilation openings and infiltration, this way contributing to indoor air pollution [4,5]. In addition, high localized pollutant concentrations might cause continuous damage to historic buildings [6,7].

Computational fluid dynamics (CFD) can be used to predict the wind flow and pollutant dispersion in urban street canyons. Previous studies have shown that CFD simulations using the steady Reynolds-Averaged Navier–Stokes (RANS) approach are deficient in modeling the complexities of the wind flow and near-field pollutant dispersion, which motivates the use of large-eddy simulations (LES) [8–12]. Pollutants emitted in urban areas are transported by the interaction between the incoming atmospheric boundary layer and the turbulent flow around buildings, both of which are highly unsteady. The pollutant dispersion process can be seen as the combination of convection, molecular diffusion and turbulent diffusion. In turbulent flows, the molecular mass fluxes are generally negligibly small compared with the turbulent mass fluxes. The accurate reproduction of pollutant dispersion using steady RANS is generally not only limited by the inaccuracies of wind flow prediction, but also by the inaccuracies in modeling turbulent mass transport. With RANS, the turbulent mass transfer is generally computed based on the gradient of the mean concentration, i.e. the gradient-diffusion hypothesis. However, previous studies [13–15] showed that counter-gradient (CG) diffusion can occur, i.e. a turbulent mass flux from low to high concentration areas, contradicting the gradient-diffusion hypothesis. LES on the other hand can predict the turbulent mass transport process more accurately as it captures the large turbulent structures associated with the inherently unsteady wind flow [16,17]. Previous studies on pollutant dispersion around buildings have indicated that LES can reproduce the above-mentioned CG turbulent transport, while steady RANS with the gradient-diffusion hypothesis evidently fails to do so [14,18].

Earlier studies on pollution dispersion in urban street canyons have investigated the impact of canyon aspect ratios [19,20], building packing densities [21], building morphology

[22] and roof shape [23–26]. However, the vast majority of these studies focused on street canyons with smooth façades without protrusions or recessions. The presence of building façade roughness details like balconies can strongly change the near-building wind flow pattern [27,28], surface pressure [29–33], and indoor and outdoor air quality [34,35], as shown by previous studies on isolated buildings. On the other hand, studies on street canyons with façade geometrical details are scarce [36–39] and focused on street canyons exposed to wind perpendicular to the canyon axis ($\theta = 0°$). In these studies that considered pollutant dispersion, the 3D steady RANS approach [37,38,40] or scale-adaptive simulations [39] were adopted. To the best knowledge of the authors, a systematical investigation of the impact of balconies at the windward façade, leeward façade or both facades on the pollutant dispersion process in street canyons using LES has not yet been performed.

This study aims to provide more insight into the impact of façade geometrical details on the transport process of pollutants in street canyons based on LES simulations. The effective pollutant removal capacity has been evaluated and the contributions of the two main pollutant removal mechanisms, i.e., convection and turbulent diffusion, on the pollutant removal have been quantified. The focus is on street canyons with balconies.

Section 2 describes the CFD validation study. The computational settings are presented in Section 3. Section 4 provides the results of the simulations. Finally, discussion and conclusions are given in Section 5 and Section 6, respectively.

5.2 CFD validation study

Two sets of CFD validations are conducted in the present study.

5.2.1 Validation I: Mean pressure coefficients on a building with balconies

For the first part of the CFD validation, atmospheric boundary-layer (ABL) wind-tunnel (WT) measurements of mean surface pressure coefficients on a building with balconies [31,41] are used. As this validation study has been published as a separate paper [42], the outline is only briefly mentioned here.

The building dimensions were $0.152 \times 0.152 \times 0.3$ m^3 (width × depth × height, at 1:400 scale). Balconies were present on one of the façades and extended along the entire width of the façade. The reduced-scale balcony depth was 0.01 m and the height of the balcony

parapet walls was 0.0025 m. For the façade with balconies, pressure taps were placed along vertical lines to measure the wind-induced surface pressure. The mean pressure coefficients (C_p) were calculated as:

$$C_p = \frac{P - P_o}{0.5\rho U_g^2} \quad (1)$$

where P is the mean surface pressure, P_0 is the reference static pressure (= 3.5 Pa) and ρ is the air density (1.225 kg/m^3). U_g is the reference mean wind speed taken at gradient height (14 m/s at the reduced-scale height of 0.625 m). Three approach-flow wind directions were considered: θ = 0° (wind direction perpendicular to the façade with balconies), 90°, and 180°. The overall uncertainty of the C_p measurements was below 5% [41].

In this validation study, the wind directions θ = 0° and 180° are examined. The quality of the grid is measured by the LES index of quality. The result shows that the volume-averaged amount of total kinetic energy resolved is 92.9%, which is larger than the threshold of 80%, indicating a well-resolved computation [42]. LES simulations are performed using the commercial CFD code ANSYS Fluent 18.0 [43]. The wall-adapting local eddy viscosity (WALE) subgrid-scale (SGS) model [44] with the constant C_{wale} = 0.325 is used. The fractional step method is used for non-iterative time advancement. Time discretization and pressure interpolation are second-order. The Werner-Wengle wall functions are employed [45]. More detailed information about the computational grids, boundary conditions, and the numerical procedure can be found in Ref. [42].

Fig. 1 shows the measured and simulated mean surface pressure coefficients along two lines located at reduced-scale distances of 0.061 m and 0.0015 m from the edge of the façade with balconies. For θ = 0°, the agreement between the WT and CFD results along the center line is fair, with an average absolute deviation of 0.027. This deviation is 0.133 for the edge line. For θ = 180°, a good agreement between the WT and CFD results is observed for both lines. In this case, the average absolute deviations are about 0.041 and 0.036 for the center line and edge line, respectively. Possible reasons for the small deviations are discussed in detail in Ref. [42].

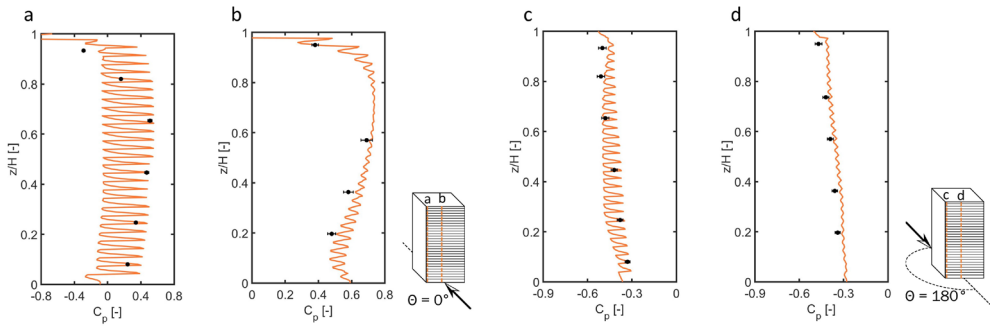

Fig. 1. Validation I: Comparisons between measured and simulated C_p on (a) edge line and (b) center line on the windward façade. (c-d) Same on the leeward façade. Error bars represent the measurement uncertainty reported in Ref. [41].

5.2.2 Validation II: Mean velocities and pollutant concentrations in a street canyon

For the second part of the CFD validation, ABL wind-tunnel measurements of mean velocity and mean tracer gas concentrations for generic street canyons [46,47] are used. As this validation study has been published as a separate paper [48], the outline is only briefly mentioned here.

The street canyon model was composed of two parallel buildings with width × depth × height = 1.2 × 0.12 × 0.12 m^3 each (at scale 1:150). The reduced-scale distance between the two buildings was 0.12 m. The approach-flow was perpendicular to the canyon axis. The tracer gas, i.e., sulfur hexafluoride (SF_6), was emitted constantly from four line-like sources embedded in the street at ground level [46]. Concentration measurement taps were placed along vertical lines at a reduced-scale distance of 5 mm from each of the canyon building façades to sample the local concentration of tracer gas [49]. The dimensionless mean SF_6 concentration was calculated using Eq. (2):

$$C^+ = \frac{CU_{ref}H}{Q/l} \tag{2}$$

where C is the mean SF_6 concentration, U_{ref} (= 4.65 m/s) is the mean wind speed of the approaching flow at the roof height H (= 0.12 m), and Q/l is the SF_6 emission rate per unit length of the line source. The mean vertical velocity components (W) were measured along four vertical lines (reduced scale: x/H = 0.083, 0.25, 0.75 and 0.917) in the xz-plane that perpendicular to the canyon axis (y/H = 0.5) using laser-Doppler velocimetry [46] (Fig. 2).

In the CFD simulations, four line-like sources are embedded at the street ground according to their locations in the experiment. The emission rate is assumed to be Q = 10 g/s, as recommended in Ref. [50]. The grid resolution is adopted based on a grid-sensitivity analysis reported in Ref. [48]. The resulting LES index of quality indicates that the volume-averaged amount of total kinetic energy resolved is 92.8% for the whole volume. LES simulations are performed using the commercial CFD code ANSYS Fluent 18.0 [43] and the WALE SGS model [44] is employed. Second-order discretization schemes are selected for the energy and SF_6 concentration equations. The other computational settings are the same as in the first validation study (see Section 2.1). More details about the computational grids, settings and parameters can be found in Ref. [48].

Fig. 2 compares the WT and CFD results of the dimensionless mean vertical velocity component (W/U_{ref}) along the four vertical lines. The agreement between the WT and CFD is considered to be good. The average absolute differences between measurements and CFD along lines x/H = 0.083, 0.25, 0.75 and 0.917 are 0.03, 0.03, 0.04 and 0.01, respectively.

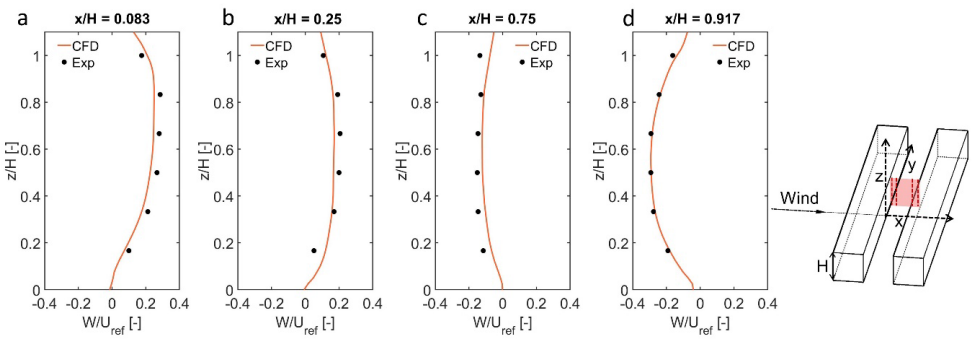

Fig. 2. Validation II: Comparisons between measured and simulated W/U_{ref} along 4 vertical lines in a vertical plane at y/H = 0.5 : (a) x/H = 0.083, (b) x/H = 0.25, (c) x/H = 0.75 and (d) x/H = 0.917.

Fig. 3 compares the WT results and CFD results of C^+ along four vertical lines at y/H = 0 and 1.25 near the windward and leeward façades, indicating a close agreement. The average absolute deviations of C^+ along the lines at y/H = 0 and 1.25 near the leeward façade are 1.46 and 1.50, respectively. These deviations are 0.53 and 0.14 for these two lines near the windward façade.

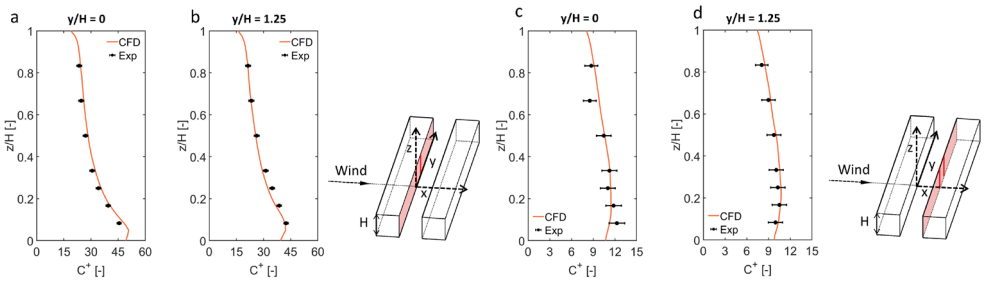

Fig. 3. Validation II: Comparisons between measured and simulated C^+ along two vertical lines near the leeward façade: (a) y/H = 0 and (b) y/H = 1.25. (c-d) Same for two vertical lines near the windward façade. Error bars represent the measurement uncertainty reported in Ref. [47].

5.3 CFD simulations

5.3.1 List of cases

Four cases are considered (Fig. 4):

1) Case NB: street canyon without balconies (smooth walls);

2) Case BWL: street canyon with balconies positioned at both windward and leeward façades;

3) Case BW: street canyon with balconies positioned only at the windward façade;

4) Case BL: street canyon with balconies positioned only at the leeward façade;

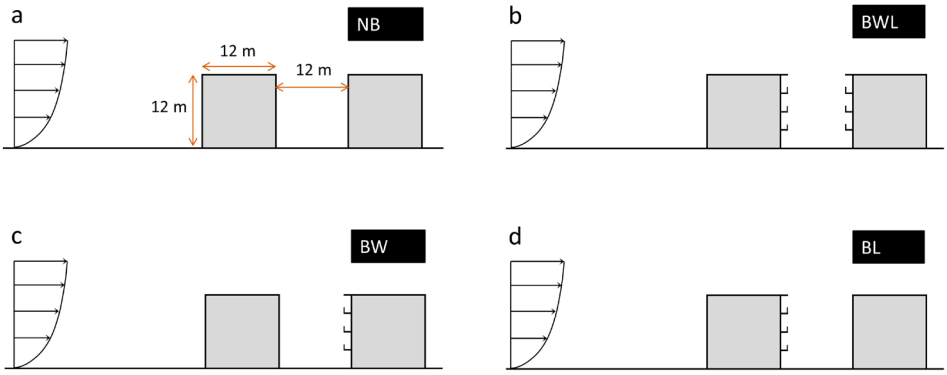

Fig. 4. Schematic of four cases (vertical center plane): (a) street canyon without balconies, (b) street canyon with balconies on both windward and leeward façades, (c) street canyon with balconies only on windward façade, and (d) street canyon with balconies only on leeward façade.

5.3.2 Computational domain and grid

For all balconies, the depth is 1 m and the parapet wall height is 1 m. In all cases, the street canyons are formed by two 4-story buildings, with a floor height of 3 m. The height and depth of the buildings are 12 m and the distance in between is 12 m (aspect ratio W/H = 1). Two continuous line-like sources of tracer gas are embedded in the street at ground level parallel to the canyon axis. The width of each source is 1 m and the distance between the center of the source and the building façade is 3.5 m (see Fig 5b and Fig. 6b).

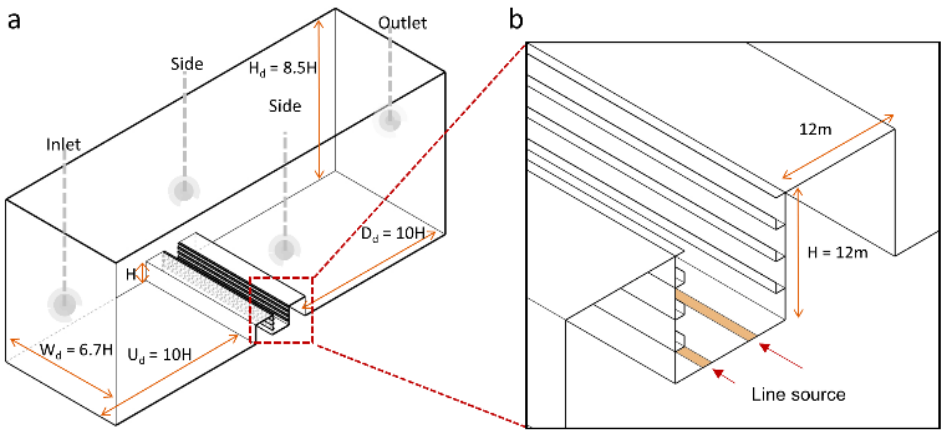

Fig. 5. Computational domain for the case with balconies at both windward and leeward façades (case BWL): (a) computational domain and (b) detail near the street canyon.

The upwind domain distance (U_d), the downwind domain distance (D_d), the domain height (H_d) and domain width (W_d) are 10H, 10H, 8.5H and 6.7H (Fig. 5a), respectively, where H is the building height. These dimensions are in line with the recommendations for LES simulations of generic street canyons [48]. Block-structured grids are generated for the four cases using the surface-grid extrusion technique [51,52]. Fig. 6 shows the computational grid for case BWL. The grid consists of three blocks (Ω_1, Ω_2 and Ω_3). The grid refinement ratio between each adjacent block is 1:2, following the recommendations provided in Ref. [53]. Block Ω_1 uses cubic cells ($\Delta x = \Delta y = \Delta z = H/96$, i.e., 8 cells are applied along the depth of the balcony). Block Ω_1 refers to the domain inside the street canyon, extending from the ground to the roof height. Block Ω_2 consists of cubic cells ($\Delta x = \Delta y = \Delta z = H/48$), extended up to a distance of H out of the building surfaces. Block Ω_3 consists of hexahedral cells with

stretching ratios below 1.05. The grid resolution is determined based on a grid-sensitivity study (detailed in Section 3.6).

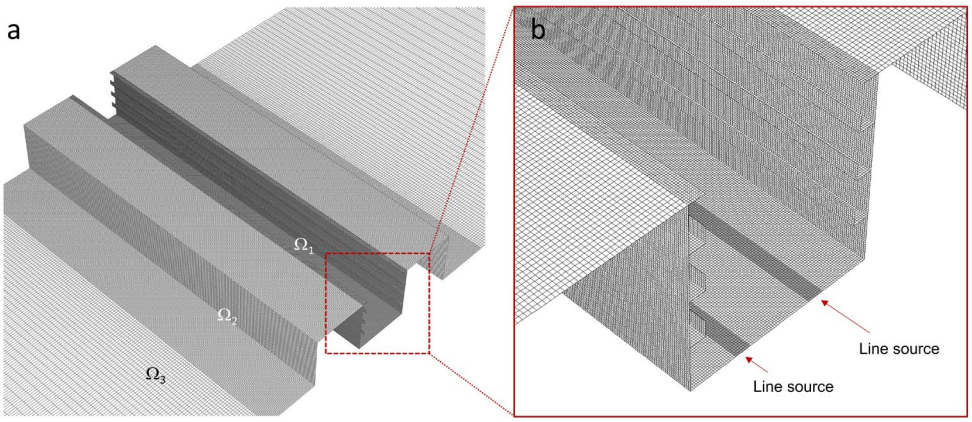

Fig. 6. Computational grid for the case with balconies at both windward and leeward façades (case BWL): (a) Grid at street canyon ground surfaces and (b) detail of grid at building balconies and ground surface.

5.3.3 Boundary condition

The street canyons are simulated as spanwise homogeneous 3D geometries. At the inlet plane, neutral ABL approach-flow profiles of mean wind speed (U, Eq. (3)), turbulent kinetic energy (k, Eq. (4)) and turbulence dissipation rate (ε, Eq. (5)) are imposed [54], where z_0 = 0.03 m is the aerodynamic roughness length, u^*_{ABL} = 0.3 m/s is the ABL friction velocity, κ = 0.41 is the von Karman constant, C_μ = 0.09 is the empirical constant, and U_{ref} = 4.28 m/s is the wind speed at the roof height.

$$U(z) = \frac{u^*_{ABL}}{\kappa} ln(\frac{z+z_0}{z_0}) \quad (3)$$

$$k(z) = \frac{\left(u^*_{ABL}\right)^2}{\sqrt{C_\mu}} \quad (4)$$

$$\varepsilon(z) = \frac{u^{*3}_{ABL}}{\kappa\left(z+z_0\right)} \quad (5)$$

The vortex method [55] is used to generate the fluctuations of the inflow profile. The number of vortices N_{vor} is 3720, obtained from $N_{vor} = N_{in}/4$ where N_{in} is the number of cells at the inlet plane [56]. Periodic boundary conditions are used at the lateral domain sides (Fig. 5a). A constant static gauge pressure of 0 Pa is used at the outlet plane. The upper boundary of the domain is set as a slip wall, which implies that the normal velocity component and the normal gradients of all variables at this boundary are zero. Tracer gas SF_6 that represents the vehicular exhausts is discharged from the two continuous line-like sources with the total emission rate per unit length (Q/l) of 10 $g \cdot s^{-1} m^{-1}$.

5.3.4 Turbulence and dispersion modeling

The isothermal LES simulations are conducted with the WALE SGS model with constant C_w = 0.325 [43]. The instantaneous pollutant concentration is treated as a scalar whose transport is described by an Eulerian advection-diffusion equation. The time-averaged (mean) convective mass flux Q_c is defined as follows:

$$Q_{c,i} = \left\langle \overline{u}_i \right\rangle \left\langle \overline{c} \right\rangle \tag{6}$$

where i indicates the coordinate (u_x, u_y, u_z = u, v, w), the angle brackets denote the time averaging operator and the overbar denotes the filtering operation. The total mean turbulent mass flux $Q_{t,i}$ in LES is defined as follows:

$$Q_{t,i} = \left\langle \overline{u_i' c'} \right\rangle + \left\langle q_{SGS,i} \right\rangle \tag{7}$$

where u_i' and c' are the fluctuating components of velocity and concentration and q_{SGS} is the modeled SGS mass flux representing the effect of the unresolved small-scale eddies on the larger-scale dispersion. The instantaneous SGS mass flux is assumed proportional to the gradient of resolved concentration:

$$q_{SGS,i} = \overline{u_i c} - \overline{u}_i \overline{c} = -D_{SGS} \frac{\partial \overline{c}}{\partial x_i} \tag{8}$$

where c is the instantaneous SF_6 concentration, u_i represents the instantaneous velocity components and D_{SGS} is the SGS mass diffusivity that links the SGS Schmidt number (Sc_{SGS}) and the SGS viscosity (ν_{SGS}):

$$Sc_{SGS} = \frac{\nu_{SGS}}{D_{SGS}} \tag{9}$$

5.3.5 Numerical procedure

The solver settings are similar to those used in the validation studies. The LES simulations are initialized with solutions from 3D steady RANS simulations. For the RANS simulations, the realizable k-ε turbulence model [57] is used. For the LES simulations of the four cases, the time step Δt is set to be 0.0095 s. The maximum Courant-Friedrichs-Lewy (CFL) number ranges from 0.91 to 1.04, which occurs in a small area above the canyon. Ahead of the data sampling, the LES simulation run for an initialization period of 640 s, i.e. about 10 flow-through times ($T_{ft} = L/U_{ref}$, where L is the total streamwise domain length). This period allows removing the dependence on the non-physical initial state. After this initialization period, the data are sampled and averaged for 2560 s (about 40 T_{ft}).

5.3.6 Grid-sensitivity study

A detailed grid-sensitivity study is conducted for case BWL. A coarse, basic and fine grid (shown in Fig. 7) are generated in which 6, 8 and 10 cells are applied along the depth of the balcony, respectively. Time steps of 0.018, 0.012 and 0.0095 are set for these grids of case BWL, ensuring the maximum CFL number to be lower than 1.

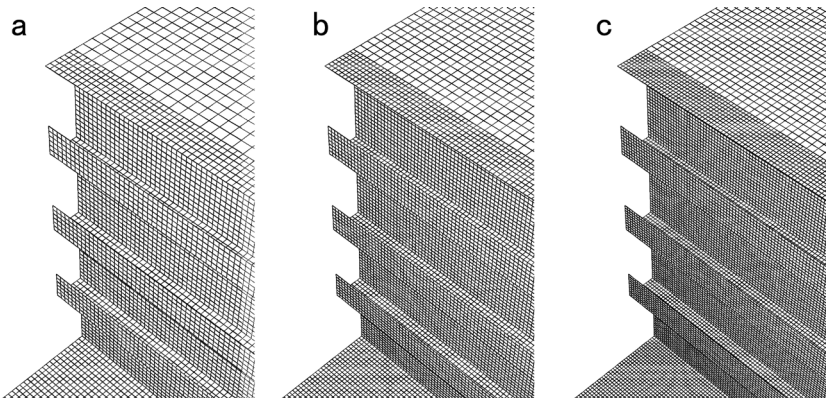

Fig. 7. Detail of the computational grids near the windward façade for the grid-sensitivity analysis: (a) coarse, (b) basic and (c) fine grids.

Fig. 8 displays the profiles of the dimensionless mean concentration (C^+) from the three grids along 5 vertical lines in the street canyon: x/H = 0.04, 0.25, 0.50, 0.75 and 0.96. Note that in LES with implicit filtering, as used here, the local filter width equals the computational cell size. Therefore, strictly, a grid-independent solution cannot be achieved [58]. It appears that the C^+ obtained by the coarse grid is significantly lower than that by the basic and fine grids (Fig. 8). Compared to the basic grid, the average absolute differences of the coarse grid and fine grid are 0.96 and 0.40, respectively. The relatively small differences between the basic and fine grids do not appear to justify the large increase in the computational time by the fine grid. Therefore, the resolution of the basic grid is retained for all the simulations.

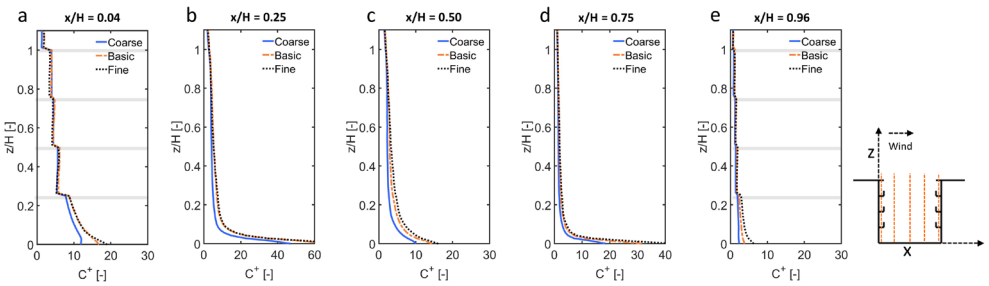

Fig. 8. Grid-sensitivity study: C^+ for three grids along vertical lines in vertical center plane: (a) x/H = 0.04; (b) x/H = 0.25; (c) x/H = 0.5; (d) x/H = 0.75; and (e) x/H = 0.96 (Grey lines in parts a and e indicate the location of each balcony floor and the roof).

5.4 Results

The following target parameters are evaluated:

- Mean wind velocity and mean concentration field:

  The dimensionless mean velocity magnitude (U/U_{ref}) is defined as the local mean wind velocity magnitude divided by the "undisturbed" mean approach-flow wind speed at building roof height U_{ref} (= 4.28 m/s). The mean concentrations are expressed in the dimensionless form (C^+) using Eq. (2), where H is the building roof height (12 m) and Q/l (= 10 $g \cdot s^{-1} m^{-1}$) is the SF_6 emission rate per unit length.

- Mean mass flux:

  Since the street canyons are simulated as 2.5D geometry, all the pollutants are released at the bottom and dispersed through the top horizontal surface of the canyon. Therefore, the vertical dimensionless mean convective mass flux ($Q_{c,z}/Q_0$)

and turbulent mass flux ($Q_{t,z}/Q_0$) of the tracer gas are systematically investigated. Note that Q_0 is the reference mass flux ($g \cdot m^{-2} \cdot s^{-1}$) given by:

$$Q_0 = (Q/l)/H \tag{10}$$

- Mean pollutant exchange velocity:

  The dimensionless mean pollutant exchange velocity (U_e/U_{ref}) is a direct indicator for the actual exchange rate of the pollutants between the street canyon and the overlying atmosphere. The definition of U_e (m/s) follows Refs. [59,60] and is composed of the convective part (the first term on the right-hand side of Eq. (11)) and the turbulent part (second term on the right-hand side of Eq. (11)):

$$U_e = U_{e,c} + U_{e,t} = \frac{\int_A Q_{c,z} dA}{A[C]} + \frac{\int_A Q_{t,z} dA}{A[C]} \tag{11}$$

  where the numerators denote the pollutant fluxes across the exchange surface A (m^2), i.e., the mean vertical convective ($Q_{c,z}$) and turbulent mass fluxes ($Q_{t,z}$) through the top horizontal surface of the canyon. [C] is the spatially-averaged pollutant concentration (g/m^3) over the control volume, i.e., the volume of the entire street canyon extending up to the roof height.

5.4.1 Mean wind velocity and mean concentration field

Fig. 9 shows the distributions of the mean velocity vector field and contours of U/U_{ref} in the vertical center plane and C^+ distributions in the same plane for the four cases.

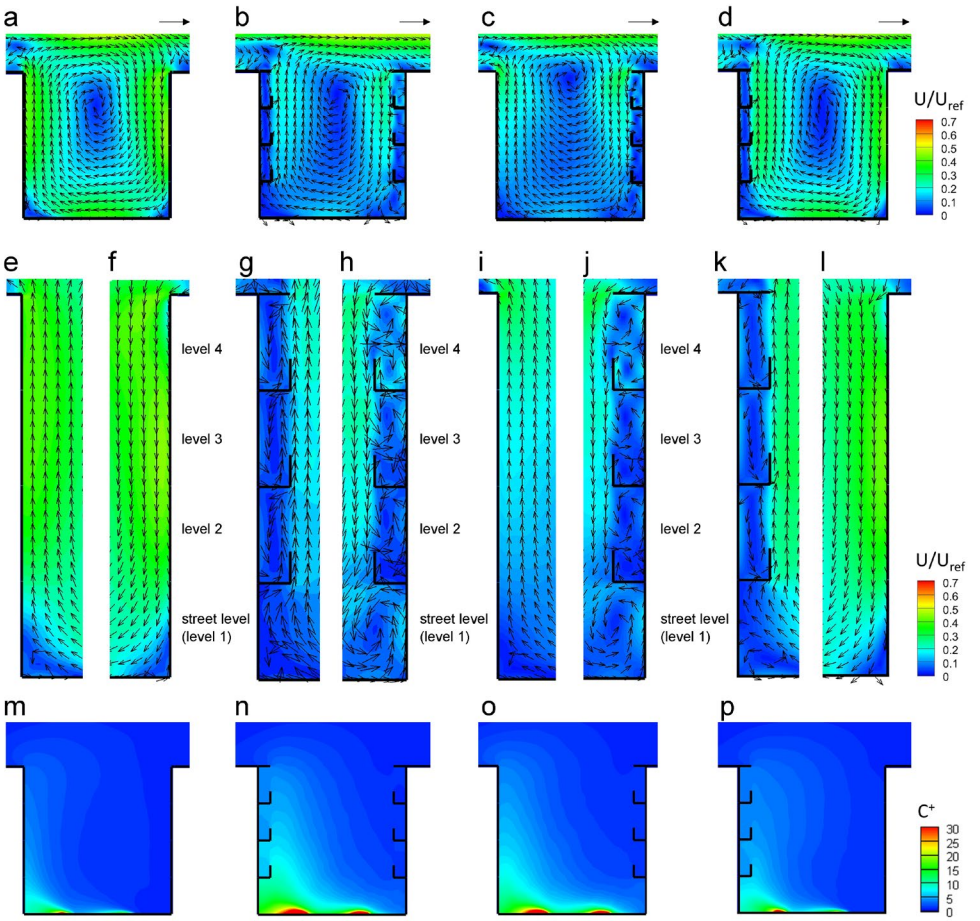

Fig. 9. Distributions of U/U_{ref} and 2D velocity vector field in vertical center plane (a) inside the canyon (e) near leeward façade, (f) near windward façade of case NB; (m) distributions of C^+ in vertical center plane inside the canyon of case NB. (b, g, h and n): same for case BWL; (c, i, j and o): same for case BW; (d, k, l and p): same for case BL.

For the case without balconies (NB), the wind flow is directed downwards along the windward facade and is slightly decelerated towards the street surface (Fig. 9f). A primary recirculation vortex is formed between the two buildings, with the core at a height of about 0.78H (Fig. 9a). Relatively high pollutant concentrations are observed near street level at the leeward side and near the pollutant sources. This is in line with previous studies on pollutant dispersion in 1:1 long street canyons [61,62].

For the case with balconies at both windward and leeward façades (case BWL), the incoming wind flow separates at the roof above the windward balcony at level 4 and is

directed downwards, leading to two small counter-rotating vortices on each balcony space at the windward façade: a counter-clockwise vortex at the higher half and a clockwise vortex at the lower half (Fig. 9h). The flow also separates at the lower edge of the lowest balcony, i.e. the one at level 2. Consequently, a secondary vortex forms at the street level (level 1) close to the windward corner due to the presence of this balcony. The core of the primary recirculation is located at the height of 0.83H, which is higher than case NB (Fig. 9b). For the leeward side, the upward flow induces a counterclockwise vortex on each balcony space (Fig. 9g). The area-weighted average mean velocity within the canyon (below the roof height) in the vertical center plane is 54% lower than case NB. Fig. 9n indicates that higher C^+ values appear especially in regions near the leeward side of the canyon. The balconies not only obstruct the canyon flow but also act as compartments that yield nearly constant concentration within the balcony spaces. The area-weighted average dimensionless mean concentration (C^+_{avg}) within the canyon in the vertical center plane is 106% higher than case NB.

For the case with balconies only at the windward façade (case BW), the incoming airflow also separates at the roof at level 4 (Fig. 9j). The vortices on the balcony spaces and in the windward corner near the street level are similar to those in case BWL. The core of the primary recirculation is located at a height of about 0.92H (Fig. 9c). The area-weighted average mean velocity within the canyon in the vertical center plane of case BW is 51% lower than case NB. Similar to case BWL, pollutants accumulate near the leeward side and the ground (Fig. 9o). The C^+_{avg} within case BW in the vertical center plane is 80% higher than case NB. The results of the aforementioned cases indicate that every street canyon with balconies at the windward façade has a much lower mean velocity and higher C^+ than case NB. It can be concluded that the presence of windward balconies strongly resists the airflow from penetrating strongly and deeply into the canyon, resulting in a much lower wind speed at the street level and higher pollutant concentrations.

For the case with balconies only at the leeward façade (case BL), the flow field in the downstream half of the canyon is similar to case NB. The core of the primary recirculation vortex is located at a height of about 0.65H (Fig. 9d). The interaction between the upward flow and balconies at the leeward façade leads to a counter-clockwise vortex with low wind speed on these balcony spaces (Fig. 9k), which is similar to case BWL. However, for the region outside the balcony spaces near the leeward façade, the wind velocity is much higher

than case BWL. The area-weighted average mean velocity within the canyon in the vertical center plane is only 21% lower than case NB. Fig. 9p indicates that pollutants accumulate in the leeward corner near the ground, with a concentration slightly higher than case NB. The C^{+}_{avg} within the canyon in the vertical center plane is only 28% higher than case NB.

To investigate the pollutant concentration in the area where residents and pedestrians may be present, eight zones in the vertical center plane inside the canyon are considered, i.e. four at the windward side and four at the leeward side (see Fig. 10): (i) street sidewalk space (S1); (ii) balcony space on level 2 (B2); (iii) balcony space on level 3 (B3), and (iv) balcony space on level 4 (B4). Note that the width of the street sidewalk space is considered to be 2.5 m, which is in line with a typical sidewalk that allows four adults to walk comfortably next to each other [63]. Fig. 10a and b displays the C^{+}_{avg} for these zones in the leeward side and windward side, respectively. Note that the results of the zones where no balcony is present are also displayed in the figure. It can be seen that for all cases, the concertation decreases with increasing elevation. In addition, higher concentrations are observed for zones at the leeward side than at the windward side. The following observations are made for the zones at the leeward side (Fig. 10a):

- For zone S1, the highest C^{+}_{avg} is observed for case BWL, which is 94% higher than that for case NB. It is followed by case BW and case BL with about 61% and 21% higher C^{+}_{avg} than case NB.
- For zones B2, B3 and B4, the highest C^{+}_{avg} is observed for case BW, although balconies are not present in these leeward zones. This is followed by case BWL, case BL and case NB.

For the zones at the windward side (Fig. 10b), the following observations are made:

- For zone S1, the C^{+}_{avg} of cases BW, BWL and BL is 211%, 202% and 21% higher than that for case NB, respectively. These rather high pollutant concentrations in zone S1 of cases BW and BWL can be attributed to the counter-clockwise vortex inside this zone, which exacerbates the accumulation of pollutants (see Fig. 9j and f).
- For zones B2, B3 and B4, case BWL has the highest C^{+}_{avg}, followed by case BW, case BL and case NB.

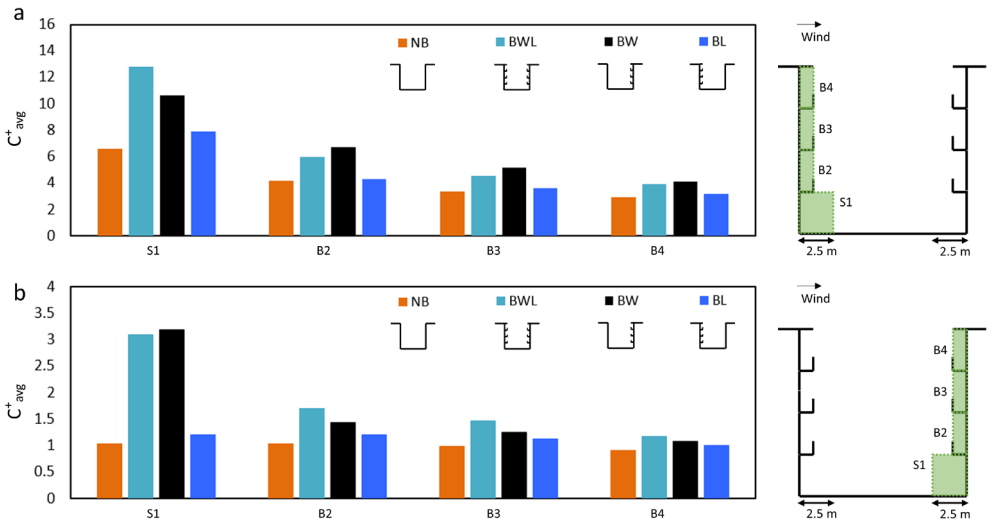

Fig. 10. Area-weighted average dimensionless mean concentration (C^+_{avg}) of street sidewalk space (zone S1) and balcony spaces on levels 2-4 (zones B2-4) in the vertical center plane of the four cases: (a) zones near leeward facade and (b) near windward side.

5.4.2 Mean mass fluxes and mean pollutant exchange velocity

In LES simulations of the highly turbulent pollutant dispersion in the built environment, the proportion of the turbulent mass fluxes modeled by the SGS model to the total turbulent mass fluxes is usually negligible [64]. Fig. 11 shows the ratio of the mean vertical SGS mass flux to the total mean vertical turbulent mass flux ($|Q_{SGS,z}/Q_{t,z}|$) in the vertical center plane of the case with balconies at both windward and leeward façades (case BWL). The analysis is performed only for case BWL because the grid resolutions of the four cases are identical. This ratio is smaller than 0.01 in a large part of the canyon. An exception is the area near ground level near the leeward façade, where the ratio is mostly smaller than 0.1.

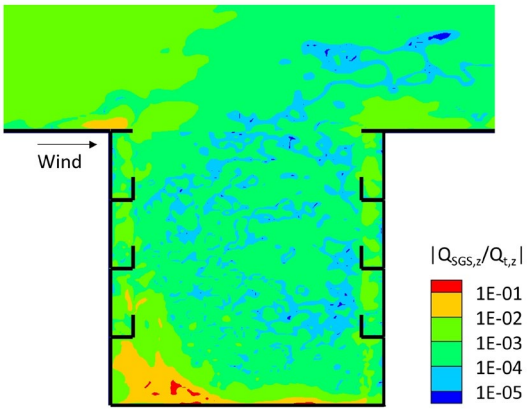

Fig. 11. The relative contribution of the mean vertical SGS mass flux to the total mean vertical turbulent mass flux ($|Q_{SGS,z}/Q_{t,z}|$) for case BWL in the vertical center plane.

Fig. 12 displays the distribution of the dimensionless mean vertical convective ($Q_{c,z}/Q_0$) and vertical turbulent ($Q_{t,z}/Q_0$) mass fluxes in the vertical center plane for the four cases. Overall, the convective fluxes are much larger than the turbulent fluxes, up to a factor 8, while the former occur mainly near the windward and leeward facades while the latter occur throughout most of the canyon volume with two clear maxima near the top of the leeward façade and near the windward pollutant source. The following observations can be made for the four cases:

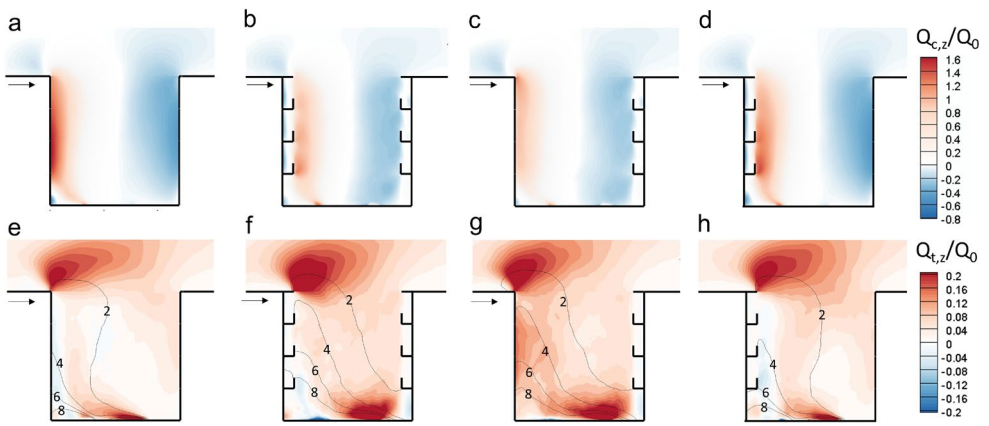

Fig. 12. Contours of dimensionless mean vertical convective mass flux ($Q_{c,z}/Q_0$) in vertical center plane for (a) case NB, (b) case BWL, (c) case BW and (d) case BL. (e-h) Same for dimensionless mean vertical turbulent mass flux ($Q_{t,z}/Q_0$). Isolines of C^+ are also shown.

- Case NB (Fig. 12a and e): $Q_{c,z}$ dominates the vertical pollutant exchanges within the largest part of the canyon. A high positive $Q_{c,z}/Q_0$ with value up to 1.56 is observed near the leeward facade and a negative $Q_{c,z}/Q_0$ with value down to -0.60 is observed near the windward facade. This implies that fresh air with low pollutant concentration is convected into the street canyon along the windward side, while the highly polluted air is convected upwards and partly out of the canyon along the leeward side. Concerning the turbulent mass fluxes, high positive values of $Q_{t,z}/Q_0$ occur close to the windward pollutant source and also above the roof level of the leeward façade (see Fig. 12e). This is in line with an observation of a long street canyon in Ref. [62]. Negative $Q_{t,z}/Q_0$ values occur in a small area near the leeward façade. Note that the isolines of C^+ in Fig. 12e indicate negative vertical gradients of concentration in this region. This implies that the vertical turbulent mass fluxes are directed from a low-concentration region to a high-concentration region, i.e., the so-called CG mechanism. [65]. The region with CG mechanism observed here is in line with a previous study on a cubic enclosure ventilated by a wall jet, in which the CG area is observed at the bottom leeward corner [14].
- Case BWL (Fig. 12b and f): Compared to case NB, the absolute values of $Q_{c,z}/Q_0$ of case BWL are substantially smaller (Fig. 12b). The maximum and minimum $Q_{c,z}/Q_0$ near the leeward and windward façade of the canyon are 1.24 and -0.56, respectively, the absolute value of which is 21% and 7% lower than in case NB, respectively. This is attributed to the obstruction of the flow within the canyon due to the presence of the balconies (see Fig. 9). The CG mechanism is observed in a small area near the leeward façade and in the windward street sidewalk space (Fig. 12f).
- Case BW (Fig. 12c and g): Also here the absolute values of $Q_{c,z}/Q_0$ of case BW are substantially smaller than case NB (Fig. 12c). The maximum and minimum value of $Q_{c,z}/Q_0$ are 1.31 and -0.51, respectively, the absolute value of which is 16% and 15% lower than in case NB. Compared to other cases, higher positive values of $Q_{t,z}/Q_0$ are observed in a large part of the canyon, including the area close to the leeward façade.
- Case BL (Fig. 12d and h): A relatively large positive $Q_{c,z}/Q_0$ is found near the leeward façade, and large negative values near the windward façade, which contribute

considerably to the pollutant removal. The maximum and minimum values of $Q_{c,z}/Q_0$ are 1.41 and -0.54, respectively, the absolute value of which is 10% and 10% lower compared to case NB. Fig. 12h shows a pattern resembling that of case NB, apart from the details near the balconies. Negative $Q_{t,z}/Q_0$ with the CG mechanism is observed close to the balconies at the leeward façade.

Fig. 13a and b show the area-weighted average dimensionless mean vertical outflow and inflow mass fluxes at the top horizontal surface (z/H =1) of the four canyon cases. It can be observed that case NB has the largest mean inflow and outflow mass fluxes, followed by cases BL, BW and BWL. The largest component in the outflow mass flux is the convective component, while the inflow mean turbulent mass fluxes are always zero for all the cases.

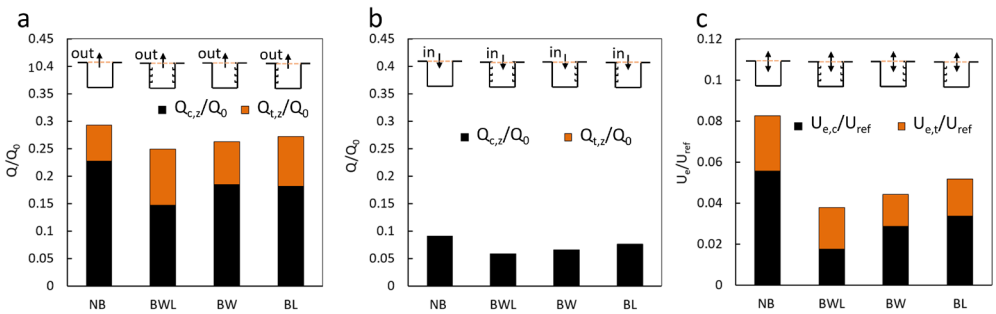

Fig. 13. Area-weighted average (a) outflow and (b) inflow dimensionless mean vertical convective mass flux ($Q_{c,z}/Q_0$) and mean turbulent mass flux ($Q_{t,z}/Q_0$) and (c) dimensionless mean pollutant-exchange velocity (U_e/U_{ref}) at the top boundary surface of the canyon for four cases, displaying in convective ($U_{e,c}/U_{ref}$) and turbulent parts ($U_{e,t}/U_{ref}$).

Fig. 13c presents the mean pollutant exchange velocity (U_e/U_{ref}). The highest total U_e/U_{ref} of 0.083 is observed for case NB, while this number is 0.052, 0.044 and 0.037 for case BL, BW and BWL, respectively, i.e. 37%, 46% and 54% smaller than that for case NB. The U_e/U_{ref} is displayed in two parts: the convective part ($U_{e,c}/U_{ref}$, obtained from the first term on the right-hand side of Eq. (11)) and the turbulent part ($U_{e,t}/U_{ref}$, obtained from the second term on the right-hand side of Eq. (11)). The relative importance of mean convective and turbulent mass fluxes as pollutant removal mechanism depends on the presence and location of balconies. The ratio of convective contribution to the total pollutant exchange velocity is 68% for case NB. This ratio reduces to 65%, 65% and 47% for case BW, case BL and case BWL, respectively. It can be concluded that the presence of balconies at both

façades can strongly reduce the U_e, mainly by decreasing the inflow and outflow convective mass fluxes.

5.5 Discussion

The focus of the present study is on long street canyons with an aspect ratio (canyon width/height) of 1. As a change in aspect ratio will impact the wind flow pattern in the canyon [66], future work can extend this study towards other aspect ratios. It is expected that large differences in conclusions compared to the present study will only emerge when the aspect ratio becomes so larger that the skimming flow regime is abandoned and the interaction flow regime sets in [67].

Balconies with 1 m depth and 1 m parapet wall are evaluated in this study. Previous studies have demonstrated that the balcony dimensions can affect the wind flow around isolated buildings [68,69]. Thus, the impacts of balcony dimensions for street canyons are therefore identified as a topic for further research. Recent studies have shown that façade and roof roughness details can strongly modify the near-building flow structures [70–74]. This study focuses on balconies as one of the most common façade details. Other forms of building surface and roof roughness details can be evaluated in the future.

This study focuses on the perpendicular wind direction. Previous studies have shown that street-level pollutant concentrations significantly depend on the wind direction [75-77]. The impact of balconies on street canyons under other wind directions can be evaluated in the future.

5.6 Conclusions

This paper presents a systematic evaluation of the impact of balconies on the wind flow and pollutant dispersion in long street canyons with an aspect ratio of 1. The large-eddy simulation (LES) approach, validated with wind-tunnel measurements, is employed. The main conclusions of this study are:

The presence of building balconies can strongly modify the wind flow pattern within street canyons, especially for balconies at the windward façade. The presence of windward balconies prevents the airflow from penetrating deep into the canyon, resulting in low wind

speed inside the canyon and therefore also at the street level. Compared to the case without balconies (case NB), the area-weighted average mean velocity in the vertical center plane within the canyons with balconies at both windward and leeward façades (case BWL), balconies at the windward façade (case BW), and balconies at the leeward façade (case BL) are reduced by 54%, 51% and 21%, respectively. The area-weighted average dimensionless mean concentration (C^+_{avg}) in the same plane for cases BWL, BW, and BL are 106%, 80% and 28% higher than case NB, respectively. The presence of windward balconies (case BWL and case BW) can strongly increase the pollution exposure for pedestrians and residents on balcony spaces. For example, compared to case NB, the C^+_{avg} in the windward and leeward street sidewalk spaces of case BWL is 94% and 211% higher, respectively. These are 61% and 202% for case BWL, respectively. While the presence of balconies only at the leeward façade (case BL) has less impact on the pollutant concentration.

The rate of pollutant removal from street canyons, expressed by the dimensionless mean pollutant exchange velocity (U_e/U_{ref}), is strongly reduced by the presence of balconies. The U_e/U_{ref} of case BL, case BW and case BWL is 54%, 46% and 37% smaller than that for case NB, respectively. The relative importance of mean convective and turbulent mass fluxes as pollutant removal mechanism depends on the presence and location of balconies. The results indicate that the presence of balconies has a crucial influence on the pollutant transport mechanism. The ratio of convective contribution to the total pollutant exchange velocity is 68% for case NB. This ratio decreases to 65%, 65% and 47% for case BW, case BL and case BWL, respectively.

The results above also suggest that in studies of urban ventilation and outdoor air quality, the presence of façade geometrical details need to be taken into account to avoid the overestimation of wind velocity and underestimation of pollutant concentrations within urban street canyons.

Acknowledgments

The authors would like to express sincere thanks to Dr. Christof Bernhard Gromke and Dr. Twan van Hooff for their contributing advice and comments. The authors also gratefully acknowledge the partnership with ANSYS CFD. This work has been sponsored by NWO Exacte en Natuurwetenschappen (Physical Sciences) for the use of supercomputer facilities, with financial support from the Nederlandse Organisatie voor Wetenschappelijk Onderzoek

(Netherlands Organization for Scientific Research, NWO). This work was carried out on the Dutch national e-infrastructure with the support of SURF Cooperative.

Reference

[1] B.Y. Yang, Y. Guo, Z. Zou, Z. Gui, W.W. Bao, L.W. Hu, G. Chen, J. Jing, J. Ma, S. Li, Y. Ma, Y.J. Chen, G.H. Dong, Exposure to ambient air pollution and visual impairment in children: A nationwide cross-sectional study in China, J. Hazard. Mater. 407 (2021) 124750. doi:10.1016/j.jhazmat.2020.124750.

[2] J. Cao, C. Yang, J. Li, R. Chen, B. Chen, D. Gu, H. Kan, Association between long-term exposure to outdoor air pollution and mortality in China: A cohort study, J. Hazard. Mater. 186 (2011) 1594–1600. doi:10.1016/j.jhazmat.2010.12.036.

[3] M.N. Anwar, M. Shabbir, E. Tahir, M. Iftikhar, H. Saif, A. Tahir, M.A. Murtaza, M.F. Khokhar, M. Rehan, M. Aghbashlo, M. Tabatabaei, A.S. Nizami, Emerging challenges of air pollution and particulate matter in China, India, and Pakistan and mitigating solutions, J. Hazard. Mater. 416 (2021) 125851. doi:10.1016/j.jhazmat.2021.125851.

[4] C. Chen, B. Zhao, W. Zhou, X. Jiang, Z. Tan, A methodology for predicting particle penetration factor through cracks of windows and doors for actual engineering application, Build. Environ. 47 (2012) 339–348. doi:10.1016/j.buildenv.2011.07.004.

[5] X. Yang, Y. Zhang, J. Hang, Y. Lin, M. Mattsson, M. Sandberg, M. Zhang, K. Wang, Integrated assessment of indoor and outdoor ventilation in street canyons with naturally-ventilated buildings by various ventilation indexes, Build. Environ. 169 (2020) 106528. doi:10.1016/j.buildenv.2019.106528.

[6] C.M. Grossi, P. Brimblecombe, Effect of long-term changes in air pollution and climate on the decay and blackening of European stone buildings, Geol. Soc. London, Spec. Publ. 271 (2007) 117–130. doi:10.1144/gsl.sp.2007.271.01.13.

[7] P. Spezzano, Mapping the susceptibility of UNESCO World Cultural Heritage sites in Europe to ambient (outdoor) air pollution, Sci. Total Environ. 754 (2021) 142345. doi:10.1016/j.scitotenv.2020.142345.

[8] Y. Tominaga, T. Stathopoulos, CFD modeling of pollution dispersion in a street canyon: Comparison between LES and RANS, J. Wind Eng. Ind. Aerodyn. 99 (2011) 340–348. doi:10.1016/j.jweia.2010.12.005.

[9] Y. Tominaga, T. Stathopoulos, CFD simulation of near-field pollutant dispersion in the urban environment: A review of current modeling techniques, Atmos. Environ. 79 (2013) 716–730. doi:10.1016/j.atmosenv.2013.07.028.

[10] B. Blocken, 50 years of Computational Wind Engineering: Past, present and future, J. Wind Eng. Ind. Aerodyn. 129 (2014) 69–102. doi:https://doi.org/10.1016/j.jweia.2014.03.008.

[11] B. Blocken, LES over RANS in building simulation for outdoor and indoor applications: A foregone conclusion?, Build. Simul. 11 (2018) 821–870. doi:10.1007/s12273-018-0459-3.

[12] M. Lateb, R.N. Meroney, M. Yataghene, H. Fellouah, F. Saleh, M.C. Boufadel, On the use of numerical modelling for near-field pollutant dispersion in urban environments − A review, Environ. Pollut. 208 (2016) 271–283. doi:10.1016/j.envpol.2015.07.039.

[13] R. Rossi, D.A. Philips, G. Iaccarino, A numerical study of scalar dispersion downstream of a wall-mounted cube using direct simulations and algebraic flux models, Int. J. Heat Fluid Flow. 31 (2010) 805–819. doi:10.1016/j.ijheatfluidflow.2010.05.006.

[14] T. van Hooff, B. Blocken, P. Gousseau, G.J.F. van Heijst, Counter-gradient diffusion in a slot-ventilated enclosure assessed by LES and RANS, Comput. Fluids. 96 (2014) 63–75. doi:10.1016/j.compfluid.2014.02.020.

[15] P. Gousseau, B. Blocken, G.J.F. van Heijst, CFD simulation of pollutant dispersion around isolated buildings: On the role of convective and turbulent mass fluxes in the prediction accuracy, J. Hazard. Mater. 194 (2011) 422–434. doi:10.1016/j.jhazmat.2011.08.008.

[16] W. Rodi, Comparison of LES and RANS calculations of the flow around bluff bodies, J. Wind Eng. Ind. Aerodyn. 69-71 (1997) 55–75. doi:10.1016/S0167-6105(97)00147-5.

[17] S. Murakami, A. Mochida, K. Hibi, Three-dimensional numerical simulation of air flow around a cubic model by means of large eddy simulation, J. Wind Eng. Ind. Aerodyn. 25 (1987) 291–305. doi:10.1016/0167-6105(87)90023-7.

[18] P. Gousseau, B. Blocken, T. Stathopoulos, G.J.F. van Heijst, CFD simulation of near-field pollutant dispersion on a high-resolution grid: A case study by LES and RANS for

a building group in downtown Montreal, Atmos. Environ. 45 (2011) 428–438. doi:10.1016/j.atmosenv.2010.09.065.

[19] C.-H. Liu, M.C. Barth, D.Y.C. Leung, Large-eddy simulation of flow and pollutant transport in street canyons of different building-height-to-street-width ratios, J. Appl. Meteorol. 43 (2004) 1410–1424. doi:10.1175/jam2143.1.

[20] D.M.S. Madalozzo, A.L. Braun, A.M. Awruch, I.B. Morsch, Numerical simulation of pollutant dispersion in street canyons: Geometric and thermal effects, Appl. Math. Model. 38 (2014) 5883–5909. doi:10.1016/j.apm.2014.04.041.

[21] J. Hang, Y. Li, Age of air and air exchange efficiency in high-rise urban areas and its link to pollutant dilution, Atmos. Environ. 45 (2011) 5572–5585. doi:10.1016/j.atmosenv.2011.04.051.

[22] C. Sha, X. Wang, Y. Lin, Y. Fan, X. Chen, J. Hang, The impact of urban open space and “lift-up” building design on building intake fraction and daily pollutant exposure in idealized urban models, Sci. Total Environ. 633 (2018) 1314–1328. doi:10.1016/j.scitotenv.2018.03.194.

[23] P. Kastner-Klein, R. Berkowicz, R. Britter, The influence of street architecture on flow and dispersion in street canyons, Meteorol. Atmos. Phys. 87 (2004) 121–131. doi:10.1007/s00703-003-0065-4.

[24] Y. Huang, X. Xu, Z. Liu, J. Deng, C. Kim, Impacts of shape and height of building roof on airflow and pollutant dispersion inside an isolated street canyon, Environ. Forensics. 17 (2016) 361–379. doi:10.1080/15275922.2016.1230912.

[25] Y. Huang, W. He, C. Kim, Impacts of shape and height of upstream roof on airflow and pollutant dispersion inside an urban street canyon, Environ. Sci. Pollut. Res. 22 (2015) 2117–2137. doi:10.1007/s11356-014-3422-6.

[26] Y. Takano, P. Moonen, On the influence of roof shape on flow and dispersion in an urban street canyon, Jnl. Wind Eng. Ind. Aerodyn. 123 (2013) 107–120. doi:10.1016/j.jweia.2013.10.006.

[27] H. Montazeri, B. Blocken, CFD simulation of wind-induced pressure coefficients on buildings with and without balconies: Validation and sensitivity analysis, Build. Environ. 60 (2013) 137–149. doi:10.1016/j.buildenv.2012.11.012.

[28] H. Montazeri, B. Blocken, W.D. Janssen, T. van Hooff, CFD evaluation of new second-skin facade concept for wind comfort on building balconies: Case study for the Park

Tower in Antwerp, Build. Environ. 68 (2013) 179–192. doi:10.1016/j.buildenv.2013.07.004.

[29] I. Chand, P.K. Bhargava, N.L.V. Krishak, Effect of balconies on ventilation inducing aeromotive force on low-rise buildings, Build. Environ. 33 (1998) 385–396. doi:10.1016/S0360-1323(97)00054-1.

[30] K. Yuan, Y. Hui, Z. Chen, Effects of facade appurtenances on the local pressure of high-rise building, J. Wind Eng. Ind. Aerodyn. 178 (2018) 26–37. doi:10.1016/j.jweia.2018.05.004.

[31] T. Stathopoulos, X. Zhu, Wind pressures on building with appurtenances, J. Wind Eng. Ind. Aerodyn. 31 (1988) 265–281. doi:10.1016/0167-6105(88)90008-6.

[32] T. Stathopoulos, X. Zhu, Wind pressures on buildings with mullions, J. Struct. Eng. 116 (1990) 2272–2291.

[33] Y. Hui, K. Yuan, Z. Chen, Q. Yang, Characteristics of aerodynamic forces on high-rise buildings with various façade appurtenances, J. Wind Eng. Ind. Aerodyn. 191 (2019) 76–90. doi:10.1016/j.jweia.2019.06.002.

[34] Z. Ai, C.M. Mak, Large eddy simulation of wind-induced interunit dispersion around multistory buildings, Indoor Air. 26 (2016) 259–273. doi:10.1111/ina.12200.

[35] Z. Ai, C. Mak, J. Niu, Numerical investigation of wind-induced airflow and interunit dispersion characteristics in multistory residential buildings, Indoor Air. 23 (2013) 417–429. doi:10.1111/ina.12041.

[36] M. Llaguno-Munitxa, E. Bou-Zeid, M. Hultmark, The influence of building geometry on street canyon air flow: Validation of large eddy simulations against wind tunnel experiments, J. Wind Eng. Ind. Aerodyn. 165 (2017) 115–130. doi:10.1016/j.jweia.2017.03.007.

[37] D. Cui, X. Li, Y. Du, C.M. Mak, K. Kwok, Effects of envelope features on wind flow and pollutant exposure in street canyons, Build. Environ. (2020) 106862. doi:10.1016/j.buildenv.2020.106862.

[38] V.A. Karkoulias, P.E. Marazioti, D.P. Georgiou, E.A. Maraziotis, Computational Fluid Dynamics modeling of the trace elements dispersion and comparison with measurements in a street canyon with balconies in the city of Patras, Greece, Atmos. Environ. (2019) 117210. doi:10.1016/j.atmosenv.2019.117210.

[39] F. Murena, B. Mele, Effect of balconies on air quality in deep street canyons, Atmos. Pollut. Res. 7 (2016) 1004–1012. doi:10.1016/j.apr.2016.06.005.

[40] D. Cui, X. Li, J. Liu, L. Yuan, C.M. Mak, Y. Fan, K. Kwok, Effects of building layouts and envelope features on wind flow and pollutant exposure in height-asymmetric street canyons, Build. Environ. (2021) 108177. doi:10.1016/j.buildenv.2021.108177.

[41] X. Zhu, Wind pressures on buildings with appurtenances, MSc thesis, Concordia University, 1987.

[42] X. Zheng, H. Montazeri, B. Blocken, CFD simulations of wind flow and mean surface pressure for buildings with balconies: Comparison of RANS and LES, Build. Environ. 173 (2020) 106747. doi:10.1016/j.buildenv.2020.106747.

[43] ANSYS Inc., Release 18.0, Theory Guide, ANSYS Inc, Canonsburg, PA 15317, USA, 2017.

[44] F. Ducros, F. Nicoud, T. Poinsot, Wall-adapting local eddy-viscosity models for simulations in complex geometries, in: Oxford Univ. Comput. Lab., 16th Conference on Numerical Methods in Fluid Dynamics, Arcachon, France, 1998: pp. 293–299.

[45] H. Werner, H. Wengle, Large-eddy simulation of turbulent flow over and around a cube in a plate channel, in: Turbul. Shear Flows 8, Springer Berlin Heidelberg, Berlin, Heidelberg, 1993: pp. 155–168. doi:10.1007/978-3-642-77674-8_12.

[46] C. Gromke, B. Ruck, On the impact of trees on dispersion processes of traffic emissions in street canyons, Boundary-Layer Meteorol. 131 (2009) 19–34. doi:10.1007/s10546-008-9301-2.

[47] C. Gromke, Einfluss von Bäumen auf die Durchlüftung von innerstädtischen Straßenschluchten, Ph.D. Thesis, Karlsruhe Institute of Technology, 2008.

[48] X. Zheng, M. Montazeri, B. Blocken, Large-eddy simulation of pollutant dispersion in generic urban street canyons: guidelines for domain size, J. Wind Eng. Ind. Aerodyn. 211 (2021) 104527.

[49] R. Buccolieri, C. Gromke, S. Di Sabatino, B. Ruck, Aerodynamic effects of trees on pollutant concentration in street canyons, Sci. Total Environ. 407 (2009) 5247–5256. doi:https://doi.org/10.1016/j.scitotenv.2009.06.016.

[50] C. Gromke, R. Buccolieri, S. Di Sabatino, B. Ruck, Dispersion study in a street canyon with tree planting by means of wind tunnel and numerical investigations –

Evaluation of CFD data with experimental data, Atmos. Environ. 42 (2008) 8640–8650. doi:10.1016/j.atmosenv.2008.08.019.

[51] T. van Hooff, B. Blocken, Coupled urban wind flow and indoor natural ventilation modelling on a high-resolution grid: A case study for the Amsterdam ArenA stadium, Environ. Model. Softw. 25 (2010) 51–65. doi:10.1016/j.envsoft.2009.07.008.

[52] B. Blocken, Computational Fluid Dynamics for urban physics: Importance, scales, possibilities, limitations and ten tips and tricks towards accurate and reliable simulations, Build. Environ. 91 (2015) 219–245. doi:10.1016/j.buildenv.2015.02.015.

[53] S. Iousef, H. Montazeri, B. Blocken, P.J.V. van Wesemael, On the use of non-conformal grids for economic LES of wind flow and convective heat transfer for a wall-mounted cube, Build. Environ. 119 (2017) 44–61. doi:10.1016/j.buildenv.2017.04.004.

[54] P.J. Richards, R.P. Hoxey, Appropriate boundary conditions for computational wind engineering models using the k-ε turbulence model, J. Wind Eng. Ind. Aerodyn. (1993) 145–153. doi:10.1016/B978-0-444-81688-7.50018-8.

[55] E. Sergent, Vers une méthodologie de couplage entre la simulation des grandes échelles et les modèles statistiques, Ph.D. thesis, Ecole centrale de Lyon, 2002.

[56] A. Gerasimov, Quick guide to setting up LES-type simulations, version 1.4., European Technology Group, ANSYS Sweden AB, 2016.

[57] T. Shih, W. Liou, A. Shabbir, Z. Yang, J. Zhu, A new k-ϵ eddy viscosity model for high reynolds number turbulent flows, Comput. Fluids. 24 (1995) 227–238. doi:10.1016/0045-7930(94)00032-T.

[58] M. Klein, An attempt to assess the quality of large eddy simulations in the context of implicit filtering, Flow, Turbul. Combust. 75 (2005) 131–147. doi:10.1007/s10494-005-8581-6.

[59] R. Buccolieri, P. Salizzoni, L. Soulhac, V. Garbero, S. Di Sabatino, The breathability of compact cities, Urban Clim. 13 (2015) 73–93. doi:10.1016/j.uclim.2015.06.002.

[60] A. Kubilay, M.K.-A. Neophytou, S. Matsentides, M. Loizou, J. Carmeliet, The pollutant removal capacity of urban street canyons as quantified by the pollutant exchange velocity, Urban Clim. 21 (2017) 136–153. doi:https://doi.org/10.1016/j.uclim.2017.06.003.

[61] S.M. Salim, R. Buccolieri, A. Chan, S. Di Sabatino, Numerical simulation of atmospheric pollutant dispersion in an urban street canyon: Comparison between RANS and LES, Jnl. Wind Eng. Ind. Aerodyn. 99 (2011) 103–113. doi:10.1016/j.jweia.2010.12.002.

[62] D. Marucci, M. Carpentieri, Effect of local and upwind stratification on flow and dispersion inside and above a bi-dimensional street canyon, Build. Environ. 156 (2019) 74–88. doi:10.1016/j.buildenv.2019.04.013.

[63] G.D.C. Initiative, N.A. of City Transportation Officials, Global street design guide, Island Press, 2016.

[64] P. Gousseau, B. Blocken, T. Stathopoulos, G.J.F. van Heijst, Near-field pollutant dispersion in an actual urban area: Analysis of the mass transport mechanism by high-resolution Large Eddy Simulations, Comput. Fluids. 114 (2015) 151–162. doi:10.1016/j.compfluid.2015.02.018.

[65] P. Gousseau, B. Blocken, G.J.F. van Heijst, Large-Eddy Simulation of pollutant dispersion around a cubical building: Analysis of the turbulent mass transport mechanism by unsteady concentration and velocity statistics, Environ. Pollut. 167 (2012) 47–57. doi:10.1016/j.envpol.2012.03.021.

[66] T. Jaroslawski, L. Perret, K. Blackman, E. Savory, The Spanwise Variation of Roof-Level Turbulence in a Street-Canyon Flow, Boundary-Layer Meteorol. 170 (2019) 373–394. doi:10.1007/s10546-018-0405-z.

[67] T.R. Oke, Street design and urban canopy layer climate, Energy Build. 11 (1988) 103–113. doi:10.1016/0378-7788(88)90026-6.

[68] S. Omrani, V. Garcia-Hansen, B.R. Capra, R. Drogemuller, On the effect of provision of balconies on natural ventilation and thermal comfort in high-rise residential buildings, Build. Environ. 123 (2017) 504–516. doi:10.1016/j.buildenv.2017.07.016.

[69] X. Zheng, M. Montazeri, B. Blocken, CFD analysis of the impact of geometrical characteristics of building balconies on near-façade wind flow and surface pressure, Build. Environ. (2021) 107904. doi:10.1016/j.buildenv.2021.107904.

[70] L. Chew, N. Nazarian, L. Norford, Pedestrian-Level Urban Wind Flow Enhancement with Wind Catchers, Atmosphere (Basel). 8 (2017) 159. doi:10.3390/atmos8090159.

[71] M. Alsailani, H. Montazeri, A. Rezaeiha, Towards optimal aerodynamic design of wind catchers: Impact of geometrical characteristics, Renew. Energy. 168 (2021) 1344–1363. doi:10.1016/j.renene.2020.12.053.

[72] Z. Li, T. Ming, T. Shi, H. Zhang, C.-Y. Wen, X. Lu, X. Dong, Y. Wu, R. de Richter, W. Li, C. Peng, Review on the dispersion of traffic-related air pollutants in urban areas: Local mitigation strategies, optimization framework, and evaluation theory, Build. Environ. (2021) 107890. doi:10.1016/j.buildenv.2021.107890.

[73] J. Wang, Q. Yang, P. Van Phuc, Y. Tamura, Characteristics of conical vortices and their effects on wind pressures on flat-roof-mounted solar arrays by LES, J. Wind Eng. Ind. Aerodyn. 200 (2020) 104146. doi:10.1016/j.jweia.2020.104146.

[74] J. Wang, P. Van Phuc, Q. Yang, Y. Tamura, LES study of wind pressure and flow characteristics of flat-roof-mounted solar arrays, J. Wind Eng. Ind. Aerodyn. 198 (2020) 104096. doi:10.1016/j.jweia.2020.104096.

[75] A. McNabola, B.M. Broderick, L.W. Gill, A numerical investigation of the impact of low boundary walls on pedestrian exposure to air pollutants in urban street canyons, Sci. Total Environ. 407 (2009) 760–769. doi:10.1016/j.scitotenv.2008.09.036.

[76] R. Buccolieri, S.M. Salim, L.S. Leo, S. Di Sabatino, A. Chan, P. Ielpo, G. de Gennaro, C. Gromke, Analysis of local scale tree–atmosphere interaction on pollutant concentration in idealized street canyons and application to a real urban junction, Atmos. Environ. 45 (2011) 1702–1713. doi:10.1016/j.atmosenv.2010.12.058.

[77] C. Gromke, B. Ruck, Pollutant Concentrations in Street Canyons of Different Aspect Ratio with Avenues of Trees for Various Wind Directions, Boundary-Layer Meteorol. 144 (2012) 41–64. doi:10.1007/s10546-012-9703-z.

Chapter 6
Limitations, future work and discussion

The main limitations of the thesis and, accordingly, recommendations for future research are provided in this Chapter. A discussion on the main contributions of this thesis concludes this Chapter.

6.1 Limitations and future work

The CFD validation for a building with balconies, presented in Chapter 2, is performed based on mean surface pressure coefficients. Future research can explore the possibility of performing Particle Image Velocimetry wind tunnel tests to capture the wind velocity field on balcony spaces, and compare the wind tunnel data with CFD results. Moreover, given the importance of peak pressures for wind loads (Etheridge, 2000; Le Roux et al., 2012; Wang et al., 2020), further analysis can focus on the performance of LES in predicting peak surface pressure for buildings with balconies. Note that the existing experimental data pertaining to peak surface pressure for buildings with façade geometrical details were obtained at scales of 1:400 (Yuan et al., 2018) or 1:300 (Liu et al., 2021). A recent study showed that the peak loads of buildings with surface protrusions such as solar panels measured in wind tunnels are sensitive to geometric scaling. (Alrawashdeh and Stathopoulos, 2020). Also wind tunnel testing of peak pressures for buildings with façade geometrical details such as balconies could be sensitive to the geometric scaling. In this case, CFD simulation with the LES approach is an option since the simulation can be conducted in full scale.

The parametric investigation presented in Chapter 3 focused on the mean wind speed on balcony spaces and the mean surface pressure for generic high-rise buildings. In addition to the mean wind speed, wind gusts also contribute to pedestrian wind discomfort and especially wind danger. Besides, peak pressure is important for wind loads, as stated earlier. Future studies can focus on the impact of geometrical characteristics of balconies on the

peak surface pressure and peak wind speed on balcony spaces. The study in Chapter 3 considered buildings with balconies for two perpendicular wind directions (θ = 0° and θ = 180°). This work can also be extended to buildings with other dimensions, with other types of surface geometrical details and buildings under oblique wind directions. All the studies in Chapter 2 and Chapter 3 only considered isolated buildings with balconies. The presence of surrounding buildings is expected to increase the complexity of wind flow such as additional flow recirculation and reattachment, and to modify the mean surface pressure and wind speed on balcony spaces (Blocken and Carmeliet, 2008; Chang and Meroney, 2003; Nozu et al., 2015). Further studies can include the impact of façade geometrical details considering building surroundings.

The two-point correlation and the comparison of the mean velocity components and mean concentration in Chapter 4 indicated that the domain width needs to be large enough to include the important coherent eddies occurring in the spanwise direction. In this Chapter, the sensitivity studies of domain size for LES simulations were conducted for a generic single street canyon with an aspect ratio (H/W) of 1, which has been widely investigated in the past. Note that recent experimental studies have shown that the aspect ratio and upstream roughness have significant effects on the spanwise turbulence integral length scale at the roof level of street canyons (Jaroslawski et al., 2019a, 2019b). Therefore, the minimum domain width of 2.5H is recommended for single street canyon cases with an aspect ratio of 1. This work can be extended to cases with upstream obstacles, multiple street canyons in sequence, and other aspect ratios. Two-point correlation measurements are suggested to explore the spanwise extent of turbulence structures inside street canyons.

In Chapter 5, the focus was on a long street canyon. The results represent the flow and pollutant dispersion in the region where the canyon vortex is dominating the flow pattern. In real cities, street canyons can be short. In such a scenario, the flow field near the lateral ends of the canyon is the result of the superposition of the corner eddy and the canyon vortex, which render the flow pattern much more 3-dimensional and complex. Future studies can evaluate the impact of the vertical and horizontal façade geometrical details on the wind flow and pollutant dispersion in short street canyons. This Chapter focused on street canyons with an aspect ratio (H/W) of 1 and balconies with 1 m depth and 1 m parapet walls. This study can be extended to façade geometrical details with other dimensions and other types of building façade geometrical details. Street canyons with other aspect ratios

can be considered in the future. Given that modeling façade geometrical details requires additional efforts and would increase the number of cells, CFD studies for wind flow and air quality at the urban microscale usually do not take these façade geometrical details into account. However, the work in this thesis in Chapters 3 and 5 showed that the large-scale façade geometrical details can considerably change the near-building wind flow pattern and pollutant concentration. Neglecting these large-scale façade geometrical details can result in an overestimation of the ventilation rate and an underestimation of the pollutant concentration in street canyons. Future studies can explore the size and relative scale of building façade geometrical details that are needed to be considered in CFD simulations of urban microclimate. Regarding the non-negligible façade geometrical details, it would be very interesting to see more research being conducted to develop a feasible correction methodology without exactly modeling the details. The simulations in the present study were isothermal. The solar-radiation induced thermal effects on façades and ground surfaces can alter the airflow pattern and pollutant dispersion in street canyons, especially when low wind velocities are present (Allegrini et al., 2013). Future studies can focus on the combined effects of wind and buoyancy for street canyons considering heated façade geometrical details and surfaces. Note that there is still a lack of experimental data on street canyons with façade geometrical details for flows with thermally induced buoyancy. Therefore, high-quality wind-tunnel or full-scale measurements for such configurations and conditions should also be performed in the future.

6.2 Discussion

First, previous CFD validation studies for buildings with façade geometrical details have revealed that the good performance of RANS approach in predicting mean surface pressure was only observed on the windward side (Montazeri and Blocken, 2013). The validation study for a high-rise building with balconies (Chapter 2) provided a quantitative comparison between the RANS and LES approaches for three wind directions: $\theta = 0°$, 90°, and 180°. Recommendations were given with respect to the performance of the two approaches for the reproduction of mean surface pressure and mean wind speed. These recommendations can be relevant, for instance, in practical applications for the prediction of building ventilation flow rates and wind nuisance levels on balcony spaces.

Second, the majority of previous CFD studies on buildings with balconies were case-specific and the focus was on either the surface pressure or the wind speed. The parametric investigation with LES simulations (Chapter 3) provided an insight into the impact of five geometrical characteristics of building balconies on the near-façade wind flow and surface pressures. The balcony geometry were shown to have significant impacts on the mean wind speed on balcony spaces and the local and façade-averaged mean pressure coefficient. It is recommended that the design of balconies should consider aerodynamic optimization. The findings in Chapter 3 can help architects choose the optimal strategy in the earlier stages of architecture design. For instance, to reduce the wind speed on balcony spaces, using partition walls is the most effective strategy. For civil engineers and building services engineers, the findings provide quantitative information for developing, designing and constructing buildings with façade geometrical details aimed at improving ventilation and wind comfort.

Third, in previous LES simulations of wind flow and pollutant dispersion in long street canyons, a wide range of different values of domain width or domain height were used because there is a clear lack of guidelines for domain size. The sensitivity study of domain size performed in Chapter 4 revealed that special attention needs to be paid to select the appropriate computational domain size for 2.5D LES simulations for long street canyons. Too small domain sizes lead to inaccurate results, while too large domain sizes would increase the computational cost. Based on the sensitivity study, guidelines for domain size of LES simulations for wind flow and pollutant dispersion in 1:1 generic long street canyons were provided. A comparison was given between the existing best practice guidelines for all applications of urban flow (Franke et al., 2011; Tominaga et al., 2008) and the present guidelines for generic street canyons. The presented guidelines can help to reduce the size of the computational domain of LES simulations for generic street canyons, therefore, reduce the computational cost without significantly compromising the accuracy.

Finally, a literature study suggested that studies on pollutant dispersion in long street canyons with façade geometrical details are scarce and mostly performed with the RANS approach. The analysis based on LES simulations in Chapter 5 provides insight into the impact of building balconies on the mechanism of pollutant removal from generic long street canyons. The results demonstrated that the façade geometrical details can significantly influence the ventilation and air quality in street canyons. Researchers and professionals

focusing on microclimate simulations are advised to take into account the influence of large-scale façade geometrical details. On the practical side, in certain areas, the construction of buildings with façade geometrical details might have a negative impact on air quality in surrounding areas. Such negative consequences can be analyzed by CFD simulations, thus, relevant measures can be taken in the early phases of the design process. In regions expected to have high air pollution, it is recommended that project developers request wind tunnel tests or CFD simulations from relevant professionals to demonstrate that the façade design will not deteriorate urban ventilation and air quality. CFD setups such as those in Chapter 5 can be used as a predictive tool to identify the potential impact of building façade geometrical details and thus provide guidelines to policymakers and designers for developing and designing buildings in urban street canyons with the aim of improving air quality for residents and pedestrians.

References

Allegrini, J., Dorer, V., Carmeliet, J., 2013. Wind tunnel measurements of buoyant flows in street canyons. Build. Environ. 59, 315–326. https://doi.org/10.1016/j.buildenv.2012.08.029

Alrawashdeh, H., Stathopoulos, T., 2020. Wind loads on solar panels mounted on flat roofs: Effect of geometric scale. J. Wind Eng. Ind. Aerodyn. 206, 104339. https://doi.org/10.1016/j.jweia.2020.104339

Blocken, B., Carmeliet, J., 2008. Pedestrian wind conditions at outdoor platforms in a high-rise apartment building: generic sub-configuration validation, wind comfort assessment and uncertainty issues. Wind Struct. 11, 51–70. https://doi.org/10.12989/was.2008.11.1.051

Chang, C.-H., Meroney, R.N., 2003. The effect of surroundings with different separation distances on surface pressures on low-rise buildings. J. Wind Eng. Ind. Aerodyn. 91, 1039–1050. https://doi.org/10.1016/S0167-6105(03)00051-5

Etheridge, D.W., 2000. Unsteady flow effects due to fluctuating wind pressures in natural ventilation design—instantaneous flow rates. Build. Environ. 35, 321–337. https://doi.org/https://doi.org/10.1016/S0360-1323(99)00021-9

Franke, J., Hellsten, A., Schlunzen, H., Carissimo, B., 2011. The COST 732 Best practice guideline for CFD simulation of flows in the urban environment: a summary. Int. J. Environ. Pollut. 44, 419. https://doi.org/10.1504/ijep.2011.038443

Jaroslawski, T., Perret, L., Blackman, K., Savory, E., 2019a. The Spanwise Variation of Roof-Level Turbulence in a Street-Canyon Flow. Boundary-Layer Meteorol. 170, 373–394. https://doi.org/10.1007/s10546-018-0405-z

Jaroslawski, T., Savory, E., Perret, L., 2019b. The characterization of the spanwise roof-level turbulence in a street canyon flow. University of Western Ontario.

Le Roux, N., Faure, X., Inard, C., Soares, S., Ricciardi, L., 2012. Reduced-scale study of wind influence on mean airflows inside buildings equipped with ventilation systems. Build. Environ. 58, 231–244. https://doi.org/https://doi.org/10.1016/j.buildenv.2012.07.007

Liu, J., Hui, Y., Yang, Q., Tamura, Y., 2021. Flow field investigation for aerodynamic effects of surface mounted ribs on square-sectioned high-rise buildings. J. Wind Eng. Ind. Aerodyn. 211, 104551. https://doi.org/10.1016/j.jweia.2021.104551

Montazeri, H., Blocken, B., 2013. CFD simulation of wind-induced pressure coefficients on buildings with and without balconies: Validation and sensitivity analysis. Build. Environ. 60, 137–149. https://doi.org/10.1016/j.buildenv.2012.11.012

Nozu, T., Tamura, T., Takeshi, K., Akira, K., 2015. Mesh-adaptive LES for wind load estimation of a high-rise building in a city. J. Wind Eng. Ind. Aerodyn. 144, 62–69. https://doi.org/10.1016/j.jweia.2015.05.007

Tominaga, Y., Mochida, A., Yoshie, R., Kataoka, H., Nozu, T., Yoshikawa, M., Shirasawa, T., 2008. AIJ guidelines for practical applications of CFD to pedestrian wind environment around buildings. J. Wind Eng. Ind. Aerodyn. 96, 1749–1761. https://doi.org/10.1016/j.jweia.2008.02.058

Wang, J., Van Phuc, P., Yang, Q., Tamura, Y., 2020. LES study of wind pressure and flow characteristics of flat-roof-mounted solar arrays. J. Wind Eng. Ind. Aerodyn. 198, 104096. https://doi.org/https://doi.org/10.1016/j.jweia.2020.104096

Yuan, K., Hui, Y., Chen, Z., 2018. Effects of facade appurtenances on the local pressure of high-rise building. J. Wind Eng. Ind. Aerodyn. 178, 26–37. https://doi.org/10.1016/j.jweia.2018.05.004

Chapter 7
Conclusions

This thesis aimed to analyze the impact of façade geometrical details on the wind flow and pollutant dispersion around buildings and adjacent streets using high-fidelity numerical simulations with computational fluid dynamics (CFD).

Chapter 2 evaluated the performance of steady RANS and LES in predicting the near-façade mean airflow patterns and mean surface pressure coefficient (C_p) for a building with balconies. Three wind directions were considered: $\theta = 0°$, 90°, and 180°. The evaluation was based on validation with wind tunnel measurements of C_p on the façade with balconies. The results showed that LES can predict C_p more accurately compared to RANS. For $\theta = 0°$, both RANS and LES can accurately predict C_p on the windward façade with average absolute deviations of 0.113 and 0.091 from the measured data, respectively. For the other two wind directions, LES is clearly superior. For $\theta = 90°$, the average absolute deviations for RANS and LES are 0.302 and 0.096, while these are 0.161 and 0.038 for $\theta = 180°$, respectively. A further detailed analysis was performed based on the comparison between RANS and LES. It was concluded that in studies of natural ventilation of buildings and wind comfort on building balconies, for which distributions of building façade C_p are required, using RANS instead of LES can result in underestimated computed ventilation airflow rates and in underestimated computed wind speed ratios. Building design based on RANS might result in too high actual ventilation flow rates and in too high actual wind speed, resulting in too high wind nuisance levels.

In Chapter 3, the focus was on the impact of various geometrical characteristics of building balconies on the near-façade mean wind flow field, the mean wind speed on balcony spaces and the wind-induced C_p for a high-rise building. LES simulations were performed to investigate the impact of (i) balconies present or not, (ii) balcony depth, (iii) balcony parapet walls, (iv) balcony partition walls and (v) density of balconies. The results

showed that the presence of balconies increases the façade-averaged C_p on both the windward façade and the leeward façade by 5.2% and 8.9%, respectively. These numbers rose to 23.5% and 23.3% when two partition walls were added at the lateral edges of the façades. Adding five partition walls can reduce the overall area-averaged wind speed on balcony spaces by 68.0% compared to the case without partition walls. Increasing the depth of balconies led to larger recirculation zones with higher mean wind speed on windward balcony spaces. For example, by increasing the depth of balconies from 1 m to 4 m, the overall area-averaged wind speed increased by 75.6%. Increasing the height of the parapet walls from 1 m to 2 m can substantially reduce the maximum mean wind speed at pedestrian height on windward balconies. By decreasing the balcony density, the mean wind speed on windward balconies below the stagnation area substantially reduce.

Chapter 4 evaluated the effect of the domain width, domain height and upstream and downstream domain lengths on the prediction of the wind field and pollutant dispersion in long street canyons. The sensitivity analysis led to a set of recommendations towards the application of 2.5D LES simulation for long street canyons with spanwise periodic boundary conditions. The minimum requirement for the domain width of 2.5H was recommended. For the domain height, 7.5H was recommended, which was equivalent to a blockage ratio of 13.3%. Concerning the upstream domain length and downstream domain length, the findings were consistent with best practice guidelines for CFD simulations of wind flow in urban areas (Franke et al., 2011; Tominaga et al., 2008), which should be at least 5H and 10H, respectively.

Chapter 5 presented an evaluation of the impact of balconies on the wind flow and pollutant dispersion in long street canyons. Four street canyon cases: (i) the street canyon without balcony, (ii) the street canyon with balconies positioned on both windward and leeward façades, (iii) the street canyon with balconies positioned only on the windward façade, and (iv) the street canyon with balconies positioned only on the leeward façade have been evaluated with LES simulations. The results showed that the wind flow field and pollutant dispersion in street canyons can be strongly affected by the location of building façade geometrical details. Significant impact was observed in the two canyon cases with balconies at the windward façade, which strongly resisted the airflow from penetrating deep into the bottom of the canyon. The presence of balconies at both façades and only at the windward façade can reduce the area-weighted mean wind velocity by 54% and 51% and

increase the area-weighted mean pollutant concentration by 106% and 80%, respectively, in the vertical center plane of the street canyon. The pollutant removal efficiency was significantly reduced by the balconies, as quantified by the pollutant exchange velocity (U_e). The presence of balconies at both façades reduced U_e by 54%. The analysis of the vertical convective and turbulent mass fluxes indicated that the presence of balconies increased the contribution of turbulence to U_e.

References

Franke, J., Hellsten, A., Schlunzen, H., Carissimo, B., 2011. The COST 732 Best practice guideline for CFD simulation of flows in the urban environment: a summary. Int. J. Environ. Pollut. 44, 419. https://doi.org/10.1504/ijep.2011.038443

Tominaga, Y., Mochida, A., Yoshie, R., Kataoka, H., Nozu, T., Yoshikawa, M., Shirasawa, T., 2008. AIJ guidelines for practical applications of CFD to pedestrian wind environment around buildings. J. Wind Eng. Ind. Aerodyn. 96, 1749–1761. https://doi.org/10.1016/j.jweia.2008.02.058

Curriculum vitae

Xing Zheng was born in 1990 in Chongqing (P.R. China).

He graduated with honors as a Bachelor of Architecture from Chongqing University in China in 2014. In 2016, he received a Master's degree in Architecture from Southeast University in China. In the same year, his wish to bridge Architecture and Building physics brought him to the Eindhoven University of Technology where he enrolled as a PhD student in the Department of the Built Environment in 2016. His PhD research work was conducted in the Unit of Building Physics and Services of Eindhoven University of Technology (TU/e) under the supervision of prof.dr.ir. B. Blocken. During his PhD studies, he was also an active member of E.S.D.A. Chronos (Debate association in Eindhoven). He has published 3 peer-reviewed ISI journal publications based on his PhD project, submitted/prepared for submission an additional peer-reviewed ISI journal paper, and has published several papers in international conference proceedings. He is reviewer of 7 international ISI journals including Building and Environment, Journal of Wind Engineering & Industrial Aerodynamics, Atmospheric Environment, Sustainable Cities and Society, Urban climate, Geoscientific model development and Building Simulation.

List of publications

ISI journal papers (published)

Zheng, X., Montazeri, H. & Blocken, B. (2021). CFD analysis of the impact of geometrical characteristics of building balconies on near-façade airflow and pressure. Building and Environment 200: 107904.

Zheng, X., Montazeri, H. & Blocken, B. (2021). Large-eddy simulation of pollutant dispersion in generic urban street canyons: Guidelines for domain size. Journal of Wind Engineering and Industrial Aerodynamics 211: 104527.

Zheng, X., Montazeri, H. & Blocken, B. (2020). CFD simulations of wind flow and mean surface pressure for buildings with balconies: Comparison of RANS and LES. Building and Environment 173: 106747.

ISI journal papers (submitted)

Zheng, X., Montazeri, H. & Blocken, B. (2021). Impact of façade geometrical details on pollutant dispersion in street canyons. Submitted.

Conference proceedings

Zheng, X., Montazeri, H. & Blocken, B. (2019). Numerical analysis of pollutant dispersion in street canyons with façade appurtenances. The 15th International Conference on Wind Engineering, 1-6 September 2019, Beijing, China.

Zheng, X., Montazeri, H. & Blocken, B. (2018). A numerical study of pressure coefficients distribution on high-rise buildings with balconies. The 15th Conference of the Italian association for wind engineering, 9-12 September 2018, Napoli, Italy.

Zheng, X., Montazeri, H. & Blocken, B. (2017). A numerical study of pressure coefficients distribution on high-rise buildings with balconies. International Conference on Urban Comfort and Environmental Quality, 28-29 September 2017, Genova, Italy.

Bouwstenen is een publicatiereeks
van de Faculteit Bouwkunde,
Technische Universiteit Eindhoven.
Zij presenteert resultaten van
onderzoek en andere activiteiten op
het vakgebied der Bouwkunde,
uitgevoerd in het kader van deze
Faculteit.

Bouwstenen en andere proefschriften van de
TU/e zijn online beschikbaar via:
https://research.tue.nl/

Reeds verschenen in de serie
Bouwstenen

nr 1
Elan: A Computer Model for Building Energy Design: Theory and Validation
Martin H. de Wit
H.H. Driessen
R.M.M. van der Velden

nr 2
Kwaliteit, Keuzevrijheid en Kosten: Evaluatie van Experiment Klarendal, Arnhem
J. Smeets
C. le Nobel
M. Broos
J. Frenken
A. v.d. Sanden

nr 3
Crooswijk: Van 'Bijzonder' naar 'Gewoon'
Vincent Smit
Kees Noort

nr 4
Staal in de Woningbouw
Edwin J.F. Delsing

nr 5
Mathematical Theory of Stressed Skin Action in Profiled Sheeting with Various Edge Conditions
Andre W.A.M.J. van den Bogaard

nr 6
Hoe Berekenbaar en Betrouwbaar is de Coëfficiënt k in x-ksigma en x-ks?
K.B. Lub
A.J. Bosch

nr 7
Het Typologisch Gereedschap: Een Verkennende Studie Omtrent Typologie en Omtrent de Aanpak van Typologisch Onderzoek
J.H. Luiten

nr 8
Informatievoorziening en Beheerprocessen
A. Nauta
Jos Smeets (red.)
Helga Fassbinder (projectleider)
Adrie Proveniers
J. v.d. Moosdijk

nr 9
Strukturering en Verwerking van Tijdgegevens voor de Uitvoering van Bouwwerken
ir. W.F. Schaefer
P.A. Erkelens

nr 10
Stedebouw en de Vorming van een Speciale Wetenschap
K. Doevendans

nr 11
Informatica en Ondersteuning van Ruimtelijke Besluitvorming
G.G. van der Meulen

nr 12
Staal in de Woningbouw, Korrosie-Bescherming van de Begane Grondvloer
Edwin J.F. Delsing

nr 13
Een Thermisch Model voor de Berekening van Staalplaatbetonvloeren onder Brandomstandigheden
A.F. Hamerlinck

nr 14
De Wijkgedachte in Nederland: Gemeenschapsstreven in een Stedebouwkundige Context
K. Doevendans
R. Stolzenburg

nr 15
Diaphragm Effect of Trapezoidally Profiled Steel Sheets: Experimental Research into the Influence of Force Application
Andre W.A.M.J. van den Bogaard

nr 16
Versterken met Spuit-Ferrocement: Het Mechanische Gedrag van met Spuit-Ferrocement Versterkte Gewapend Betonbalken
K.B. Lubir
M.C.G. van Wanroy

nr 17
De Tractaten van Jean Nicolas Louis Durand
G. van Zeyl

nr 18
Wonen onder een Plat Dak: Drie Opstellen over Enkele Vooronderstellingen van de Stedebouw
K. Doevendans

nr 19
Supporting Decision Making Processes: A Graphical and Interactive Analysis of Multivariate Data
W. Adams

nr 20
Self-Help Building Productivity: A Method for Improving House Building by Low-Income Groups Applied to Kenya 1990-2000
P. A. Erkelens

nr 21
De Verdeling van Woningen: Een Kwestie van Onderhandelen
Vincent Smit

nr 22
Flexibiliteit en Kosten in het Ontwerpproces: Een Besluitvormingondersteunend Model
M. Prins

nr 23
Spontane Nederzettingen Begeleid: Voorwaarden en Criteria in Sri Lanka
Po Hin Thung

nr 24
Fundamentals of the Design of Bamboo Structures
Oscar Arce-Villalobos

nr 25
Concepten van de Bouwkunde
M.F.Th. Bax (red.)
H.M.G.J. Trum (red.)

nr 26
Meaning of the Site
Xiaodong Li

nr 27
Het Woonmilieu op Begrip Gebracht: Een Speurtocht naar de Betekenis van het Begrip 'Woonmilieu'
Jaap Ketelaar

nr 28
Urban Environment in Developing Countries
editors: Peter A. Erkelens
George G. van der Meulen (red.)

nr 29
Stategische Plannen voor de Stad: Onderzoek en Planning in Drie Steden
prof.dr. H. Fassbinder (red.)
H. Rikhof (red.)

nr 30
Stedebouwkunde en Stadsbestuur
Piet Beekman

nr 31
De Architectuur van Djenné: Een Onderzoek naar de Historische Stad
P.C.M. Maas

nr 32
Conjoint Experiments and Retail Planning
Harmen Oppewal

nr 33
Strukturformen Indonesischer Bautechnik: Entwicklung Methodischer Grundlagen für eine 'Konstruktive Pattern Language' in Indonesien
Heinz Frick arch. SIA

nr 34
Styles of Architectural Designing: Empirical Research on Working Styles and Personality Dispositions
Anton P.M. van Bakel

nr 35
Conjoint Choice Models for Urban Tourism Planning and Marketing
Benedict Dellaert

nr 36
Stedelijke Planvorming als Co-Produktie
Helga Fassbinder (red.)

nr 37
Design Research in the Netherlands
editors: R.M. Oxman
M.F.Th. Bax
H.H. Achten

nr 38
Communication in the Building Industry
Bauke de Vries

nr 39
Optimaal Dimensioneren van Gelaste Plaatliggers
J.B.W. Stark
F. van Pelt
L.F.M. van Gorp
B.W.E.M. van Hove

nr 40
Huisvesting en Overwinning van Armoede
P.H. Thung
P. Beekman (red.)

nr 41
Urban Habitat: The Environment of Tomorrow
George G. van der Meulen
Peter A. Erkelens

nr 42
A Typology of Joints
John C.M. Olie

nr 43
Modeling Constraints-Based Choices for Leisure Mobility Planning
Marcus P. Stemerding

nr 44
Activity-Based Travel Demand Modeling
Dick Ettema

nr 45
Wind-Induced Pressure Fluctuations on Building Facades
Chris Geurts

nr 46
Generic Representations
Henri Achten

nr 47
Johann Santini Aichel: Architectuur en Ambiguiteit
Dirk De Meyer

nr 48
Concrete Behaviour in Multiaxial Compression
Erik van Geel

nr 49
Modelling Site Selection
Frank Witlox

nr 50
Ecolemma Model
Ferdinand Beetstra

nr 51
Conjoint Approaches to Developing Activity-Based Models
Donggen Wang

nr 52
On the Effectiveness of Ventilation
Ad Roos

nr 53
Conjoint Modeling Approaches for Residential Group preferences
Eric Molin

nr 54
Modelling Architectural Design Information by Features
Jos van Leeuwen

nr 55
A Spatial Decision Support System for the Planning of Retail and Service Facilities
Theo Arentze

nr 56
Integrated Lighting System Assistant
Ellie de Groot

nr 57
Ontwerpend Leren, Leren Ontwerpen
J.T. Boekholt

nr 58
Temporal Aspects of Theme Park Choice Behavior
Astrid Kemperman

nr 59
Ontwerp van een Geïndustrialiseerde Funderingswijze
Faas Moonen

nr 60
Merlin: A Decision Support System for Outdoor Leisure Planning
Manon van Middelkoop

nr 61
The Aura of Modernity
Jos Bosman

nr 62
Urban Form and Activity-Travel Patterns
Daniëlle Snellen

nr 63
Design Research in the Netherlands 2000
Henri Achten

nr 64
Computer Aided Dimensional Control in Building Construction
Rui Wu

nr 65
Beyond Sustainable Building
editors: Peter A. Erkelens
Sander de Jonge
August A.M. van Vliet
co-editor: Ruth J.G. Verhagen

nr 66
Das Globalrecyclingfähige Haus
Hans Löfflad

nr 67
Cool Schools for Hot Suburbs
René J. Dierkx

nr 68
A Bamboo Building Design Decision Support Tool
Fitri Mardjono

nr 69
Driving Rain on Building Envelopes
Fabien van Mook

nr 70
Heating Monumental Churches
Henk Schellen

nr 71
Van Woningverhuurder naar Aanbieder van Woongenot
Patrick Dogge

nr 72
Moisture Transfer Properties of Coated Gypsum
Emile Goossens

nr 73
Plybamboo Wall-Panels for Housing
Guillermo E. González-Beltrán

nr 74
The Future Site-Proceedings
Ger Maas
Frans van Gassel

nr 75
Radon transport in Autoclaved Aerated Concrete
Michel van der Pal

nr 76
The Reliability and Validity of Interactive Virtual Reality Computer Experiments
Amy Tan

nr 77
Measuring Housing Preferences Using Virtual Reality and Belief Networks
Maciej A. Orzechowski

nr 78
Computational Representations of Words and Associations in Architectural Design
Nicole Segers

nr 79
Measuring and Predicting Adaptation in Multidimensional Activity-Travel Patterns
Chang-Hyeon Joh

nr 80
Strategic Briefing
Fayez Al Hassan

nr 81
Well Being in Hospitals
Simona Di Cicco

nr 82
Solares Bauen: Implementierungs- und Umsetzungs-Aspekte in der Hochschulausbildung in Österreich
Gerhard Schuster

nr 83
Supporting Strategic Design of Workplace Environments with Case-Based Reasoning
Shauna Mallory-Hill

nr 84
ACCEL: A Tool for Supporting Concept Generation in the Early Design Phase
Maxim Ivashkov

nr 85
Brick-Mortar Interaction in Masonry under Compression
Ad Vermeltfoort

nr 86
Zelfredzaam Wonen
Guus van Vliet

nr 87
Een Ensemble met Grootstedelijke Allure
Jos Bosman
Hans Schippers

nr 88
On the Computation of Well-Structured Graphic Representations in Architectural Design
Henri Achten

nr 89
De Evolutie van een West-Afrikaanse Vernaculaire Architectuur
Wolf Schijns

nr 90
ROMBO Tactiek
Christoph Maria Ravesloot

nr 91
External Coupling between Building Energy Simulation and Computational Fluid Dynamics
Ery Djunaedy

nr 92
Design Research in the Netherlands 2005
editors: Henri Achten
Kees Dorst
Pieter Jan Stappers
Bauke de Vries

nr 93
Ein Modell zur Baulichen Transformation
Jalil H. Saber Zaimian

nr 94
Human Lighting Demands: Healthy Lighting in an Office Environment
Myriam Aries

nr 95
A Spatial Decision Support System for the Provision and Monitoring of Urban Greenspace
Claudia Pelizaro

nr 96
Leren Creëren
Adri Proveniers

nr 97
Simlandscape
Rob de Waard

nr 98
Design Team Communication
Ad den Otter

nr 99
Humaan-Ecologisch Georiënteerde Woningbouw
Juri Czabanowski

nr 100
Hambase
Martin de Wit

nr 101
Sound Transmission through Pipe Systems and into Building Structures
Susanne Bron-van der Jagt

nr 102
Het Bouwkundig Contrapunt
Jan Francis Boelen

nr 103
A Framework for a Multi-Agent Planning Support System
Dick Saarloos

nr 104
Bracing Steel Frames with Calcium Silicate Element Walls
Bright Mweene Ng'andu

nr 105
Naar een Nieuwe Houtskeletbouw
F.N.G. De Medts

nr 106 and 107
Niet gepubliceerd

nr 108
Geborgenheid
T.E.L. van Pinxteren

nr 109
Modelling Strategic Behaviour in Anticipation of Congestion
Qi Han

nr 110
Reflecties op het Woondomein
Fred Sanders

nr 111
On Assessment of Wind Comfort by Sand Erosion
Gábor Dezsö

nr 112
Bench Heating in Monumental Churches
Dionne Limpens-Neilen

nr 113
RE. Architecture
Ana Pereira Roders

nr 114
Toward Applicable Green Architecture
Usama El Fiky

nr 115
Knowledge Representation under Inherent Uncertainty in a Multi-Agent System for Land Use Planning
Liying Ma

nr 116
Integrated Heat Air and Moisture Modeling and Simulation
Jos van Schijndel

nr 117
Concrete Behaviour in Multiaxial Compression
J.P.W. Bongers

nr 118
The Image of the Urban Landscape
Ana Moya Pellitero

nr 119
The Self-Organizing City in Vietnam
Stephanie Geertman

nr 120
A Multi-Agent Planning Support System for Assessing Externalities of Urban Form Scenarios
Rachel Katoshevski-Cavari

nr 121
Den Schulbau Neu Denken, Fühlen und Wollen
Urs Christian Maurer-Dietrich

nr 122
Peter Eisenman Theories and Practices
Bernhard Kormoss

nr 123
User Simulation of Space Utilisation
Vincent Tabak

nr 125
In Search of a Complex System Model
Oswald Devisch

nr 126
Lighting at Work: Environmental Study of Direct Effects of Lighting Level and Spectrum on Psycho-Physiological Variables
Grazyna Górnicka

nr 127
Flanking Sound Transmission through Lightweight Framed Double Leaf Walls
Stefan Schoenwald

nr 128
Bounded Rationality and Spatio-Temporal Pedestrian Shopping Behavior
Wei Zhu

nr 129
Travel Information: Impact on Activity Travel Pattern
Zhongwei Sun

nr 130
Co-Simulation for Performance Prediction of Innovative Integrated Mechanical Energy Systems in Buildings
Marija Trčka

nr 131
Niet gepubliceerd

nr 132
Architectural Cue Model in Evacuation Simulation for Underground Space Design
Chengyu Sun

nr 133
Uncertainty and Sensitivity Analysis in Building Performance Simulation for Decision Support and Design Optimization
Christina Hopfe

nr 134
Facilitating Distributed Collaboration in the AEC/FM Sector Using Semantic Web Technologies
Jacob Beetz

nr 135
Circumferentially Adhesive Bonded Glass Panes for Bracing Steel Frame in Façades
Edwin Huveners

nr 136
Influence of Temperature on Concrete Beams Strengthened in Flexure with CFRP
Ernst-Lucas Klamer

nr 137
Sturen op Klantwaarde
Jos Smeets

nr 139
Lateral Behavior of Steel Frames with Discretely Connected Precast Concrete Infill Panels
Paul Teewen

nr 140
Integral Design Method in the Context of Sustainable Building Design
Perica Savanović

nr 141
Household Activity-Travel Behavior: Implementation of Within-Household Interactions
Renni Anggraini

nr 142
Design Research in the Netherlands 2010
Henri Achten

nr 143
Modelling Life Trajectories and Transport Mode Choice Using Bayesian Belief Networks
Marloes Verhoeven

nr 144
Assessing Construction Project Performance in Ghana
William Gyadu-Asiedu

nr 145
Empowering Seniors through Domotic Homes
Masi Mohammadi

nr 146
An Integral Design Concept for Ecological Self-Compacting Concrete
Martin Hunger

nr 147
Governing Multi-Actor Decision Processes in Dutch Industrial Area Redevelopment
Erik Blokhuis

nr 148
A Multifunctional Design Approach for Sustainable Concrete
Götz Hüsken

nr 149
Quality Monitoring in Infrastructural Design-Build Projects
Ruben Favié

nr 150
Assessment Matrix for Conservation of Valuable Timber Structures
Michael Abels

nr 151
Co-simulation of Building Energy Simulation and Computational Fluid Dynamics for Whole-Building Heat, Air and Moisture Engineering
Mohammad Mirsadeghi

nr 152
External Coupling of Building Energy Simulation and Building Element Heat, Air and Moisture Simulation
Daniel Cóstola

nr 153
Adaptive Decision Making In Multi-Stakeholder Retail Planning
Ingrid Janssen

nr 154
Landscape Generator
Kymo Slager

nr 155
Constraint Specification in Architecture
Remco Niemeijer

nr 156
A Need-Based Approach to Dynamic Activity Generation
Linda Nijland

nr 157
Modeling Office Firm Dynamics in an Agent-Based Micro Simulation Framework
Gustavo Garcia Manzato

nr 158
Lightweight Floor System for Vibration Comfort
Sander Zegers

nr 159
Aanpasbaarheid van de Draagstructuur
Roel Gijsbers

nr 160
'Village in the City' in Guangzhou, China
Yanliu Lin

nr 161
Climate Risk Assessment in Museums
Marco Martens

nr 162
Social Activity-Travel Patterns
Pauline van den Berg

nr 163
Sound Concentration Caused by Curved Surfaces
Martijn Vercammen

nr 164
Design of Environmentally Friendly Calcium Sulfate-Based Building Materials: Towards an Improved Indoor Air Quality
Qingliang Yu

nr 165
Beyond Uniform Thermal Comfort on the Effects of Non-Uniformity and Individual Physiology
Lisje Schellen

nr 166
Sustainable Residential Districts
Gaby Abdalla

nr 167
Towards a Performance Assessment Methodology using Computational Simulation for Air Distribution System Designs in Operating Rooms
Mônica do Amaral Melhado

nr 168
Strategic Decision Modeling in Brownfield Redevelopment
Brano Glumac

nr 169
Pamela: A Parking Analysis Model for Predicting Effects in Local Areas
Peter van der Waerden

nr 170
A Vision Driven Wayfinding Simulation-System Based on the Architectural Features Perceived in the Office Environment
Qunli Chen

nr 171
Measuring Mental Representations Underlying Activity-Travel Choices
Oliver Horeni

nr 172
Modelling the Effects of Social Networks on Activity and Travel Behaviour
Nicole Ronald

nr 173
Uncertainty Propagation and Sensitivity Analysis Techniques in Building Performance Simulation to Support Conceptual Building and System Design
Christian Struck

nr 174
Numerical Modeling of Micro-Scale Wind-Induced Pollutant Dispersion in the Built Environment
Pierre Gousseau

nr 175
Modeling Recreation Choices over the Family Lifecycle
Anna Beatriz Grigolon

nr 176
Experimental and Numerical Analysis of Mixing Ventilation at Laminar, Transitional and Turbulent Slot Reynolds Numbers
Twan van Hooff

nr 177
Collaborative Design Support: Workshops to Stimulate Interaction and Knowledge Exchange Between Practitioners
Emile M.C.J. Quanjel

nr 178
Future-Proof Platforms for Aging-in-Place
Michiel Brink

nr 179
Motivate: A Context-Aware Mobile Application for Physical Activity Promotion
Yuzhong Lin

nr 180
Experience the City: Analysis of Space-Time Behaviour and Spatial Learning
Anastasia Moiseeva

nr 181
Unbonded Post-Tensioned Shear Walls of Calcium Silicate Element Masonry
Lex van der Meer

nr 182
Construction and Demolition Waste Recycling into Innovative Building Materials for Sustainable Construction in Tanzania
Mwita M. Sabai

nr 183
Durability of Concrete with Emphasis on Chloride Migration
Przemysław Spiesz

nr 184
Computational Modeling of Urban Wind Flow and Natural Ventilation Potential of Buildings
Rubina Ramponi

nr 185
A Distributed Dynamic Simulation Mechanism for Buildings Automation and Control Systems
Azzedine Yahiaoui

nr 186
Modeling Cognitive Learning of Urban Networks in Daily Activity-Travel Behavior
Şehnaz Cenani Durmazoğlu

nr 187
Functionality and Adaptability of Design Solutions for Public Apartment Buildings in Ghana
Stephen Agyefi-Mensah

nr 188
A Construction Waste Generation Model for Developing Countries
Lilliana Abarca-Guerrero

nr 189
Synchronizing Networks: The Modeling of Supernetworks for Activity-Travel Behavior
Feixiong Liao

nr 190
Time and Money Allocation Decisions in Out-of-Home Leisure Activity Choices
Gamze Zeynep Dane

nr 191
How to Measure Added Value of CRE and Building Design
Rianne Appel-Meulenbroek

nr 192
Secondary Materials in Cement-Based Products: Treatment, Modeling and Environmental Interaction
Miruna Florea

nr 193
Concepts for the Robustness Improvement of Self-Compacting Concrete: Effects of Admixtures and Mixture Components on the Rheology and Early Hydration at Varying Temperatures
Wolfram Schmidt

nr 194
Modelling and Simulation of Virtual Natural Lighting Solutions in Buildings
Rizki A. Mangkuto

nr 195
Nano-Silica Production at Low Temperatures from the Dissolution of Olivine - Synthesis, Tailoring and Modelling
Alberto Lazaro Garcia

nr 196
Building Energy Simulation Based Assessment of Industrial Halls for Design Support
Bruno Lee

nr 197
Computational Performance Prediction of the Potential of Hybrid Adaptable Thermal Storage Concepts for Lightweight Low-Energy Houses
Pieter-Jan Hoes

nr 198
Application of Nano-Silica in Concrete
George Quercia Bianchi

nr 199
Dynamics of Social Networks and Activity Travel Behaviour
Fariya Sharmeen

nr 200
Building Structural Design Generation and Optimisation including Spatial Modification
Juan Manuel Davila Delgado

nr 201
Hydration and Thermal Decomposition of Cement/Calcium-Sulphate Based Materials
Ariën de Korte

nr 202
Republiek van Beelden:
De Politieke Werkingen van het Ontwerp in Regionale Planvorming
Bart de Zwart

nr 203
Effects of Energy Price Increases on Individual Activity-Travel Repertoires and Energy Consumption
Dujuan Yang

nr 204
Geometry and Ventilation:
Evaluation of the Leeward Sawtooth Roof Potential in the Natural Ventilation of Buildings
Jorge Isaac Perén Montero

nr 205
Computational Modelling of Evaporative Cooling as a Climate Change Adaptation Measure at the Spatial Scale of Buildings and Streets
Hamid Montazeri

nr 206
Local Buckling of Aluminium Beams in Fire Conditions
Ronald van der Meulen

nr 207
Historic Urban Landscapes:
Framing the Integration of Urban and Heritage Planning in Multilevel Governance
Loes Veldpaus

nr 208
Sustainable Transformation of the Cities:
Urban Design Pragmatics to Achieve a Sustainable City
Ernesto Antonio Zumelzu Scheel

nr 209
Development of Sustainable Protective Ultra-High Performance Fibre Reinforced Concrete (UHPFRC):
Design, Assessment and Modeling
Rui Yu

nr 210
Uncertainty in Modeling Activity-Travel Demand in Complex Uban Systems
Soora Rasouli

nr 211
Simulation-based Performance Assessment of Climate Adaptive Greenhouse Shells
Chul-sung Lee

nr 212
Green Cities:
Modelling the Spatial Transformation of the Urban Environment using Renewable Energy Technologies
Saleh Mohammadi

nr 213
A Bounded Rationality Model of Short and Long-Term Dynamics of Activity-Travel Behavior
Ifigeneia Psarra

nr 214
Effects of Pricing Strategies on Dynamic Repertoires of Activity-Travel Behaviour
Elaheh Khademi

nr 215
Handstorm Principles for Creative and Collaborative Working
Frans van Gassel

nr 216
Light Conditions in Nursing Homes: Visual Comfort and Visual Functioning of Residents
Marianne M. Sinoo

nr 217
Woonsporen: De Sociale en Ruimtelijke Biografie van een Stedelijk Bouwblok in de Amsterdamse Transvaalbuurt
Hüseyin Hüsnü Yegenoglu

nr 218
Studies on User Control in Ambient Intelligent Systems
Berent Willem Meerbeek

nr 219
Daily Livings in a Smart Home: Users' Living Preference Modeling of Smart Homes
Erfaneh Allameh

nr 220
Smart Home Design: Spatial Preference Modeling of Smart Homes
Mohammadali Heidari Jozam

nr 221
Wonen: Discoursen, Praktijken, Perspectieven
Jos Smeets

nr 222
Personal Control over Indoor Climate in Offices: Impact on Comfort, Health and Productivity
Atze Christiaan Boerstra

nr 223
Personalized Route Finding in Multimodal Transportation Networks
Jianwe Zhang

nr 224
The Design of an Adaptive Healing Room for Stroke Patients
Elke Daemen

nr 225
Experimental and Numerical Analysis of Climate Change Induced Risks to Historic Buildings and Collections
Zara Huijbregts

nr 226
Wind Flow Modeling in Urban Areas Through Experimental and Numerical Techniques
Alessio Ricci

nr 227
Clever Climate Control for Culture: Energy Efficient Indoor Climate Control Strategies for Museums Respecting Collection Preservation and Thermal Comfort of Visitors
Rick Kramer

nr 228
Fatigue Life Estimation of Metal Structures Based on Damage Modeling
Sarmediran Silitonga

nr 229
A multi-agents and occupancy based strategy for energy management and process control on the room-level
Timilehin Moses Labeodan

nr 230
Environmental assessment of Building Integrated Photovoltaics: Numerical and Experimental Carrying Capacity Based Approach
Michiel Ritzen

nr 231
Performance of Admixture and Secondary Minerals in Alkali Activated Concrete: Sustaining a Concrete Future
Arno Keulen

nr 232
World Heritage Cities and Sustainable Urban Development: Bridging Global and Local Levels in Monitoring the Sustainable Urban Development of World Heritage Cities
Paloma C. Guzman Molina

nr 233
Stage Acoustics and Sound Exposure in Performance and Rehearsal Spaces for Orchestras: Methods for Physical Measurements
Remy Wenmaekers

nr 234
Municipal Solid Waste Incineration (MSWI) Bottom Ash: From Waste to Value Characterization, Treatments and Application
Pei Tang

nr 235
Large Eddy Simulations Applied to Wind Loading and Pollutant Dispersion
Mattia Ricci

nr 236
Alkali Activated Slag-Fly Ash Binders: Design, Modeling and Application
Xu Gao

nr 237
Sodium Carbonate Activated Slag: Reaction Analysis, Microstructural Modification & Engineering Application
Bo Yuan

nr 238
Shopping Behavior in Malls
Widiyani

nr 239
Smart Grid-Building Energy Interactions: Demand Side Power Flexibility in Office Buildings
Kennedy Otieno Aduda

nr 240
Modeling Taxis Dynamic Behavior in Uncertain Urban Environments
Zheng Zhong

nr 241
Gap-Theoretical Analyses of Residential Satisfaction and Intention to Move
Wen Jiang

nr 242
Travel Satisfaction and Subjective Well-Being: A Behavioral Modeling Perspective
Yanan Gao

nr 243
Building Energy Modelling to Support the Commissioning of Holistic Data Centre Operation
Vojtech Zavrel

nr 244
Regret-Based Travel Behavior Modeling: An Extended Framework
Sunghoon Jang

nr 245
Towards Robust Low-Energy Houses: A Computational Approach for Performance Robustness Assessment using Scenario Analysis
Rajesh Reddy Kotireddy

nr 246
Development of sustainable and functionalized inorganic binder-biofiber composites
Guillaume Doudart de la Grée

nr 247
A Multiscale Analysis of the Urban Heat Island Effect: From City Averaged Temperatures to the Energy Demand of Individual Buildings
Yasin Toparlar

nr 248
Design Method for Adaptive Daylight Systems for buildings covered by large (span) roofs
Florian Heinzelmann

nr 249
Hardening, high-temperature resistance and acid resistance of one-part geopolymers
Patrick Sturm

nr 250
Effects of the built environment on dynamic repertoires of activity-travel behaviour
Aida Pontes de Aquino

nr 251
Modeling for auralization of urban environments: Incorporation of directivity in sound propagation and analysis of a framework for auralizing a car pass-by
Fotis Georgiou

nr 252
Wind Loads on Heliostats and Photovoltaic Trackers
Andreas Pfahl

nr 253
Approaches for computational performance optimization of innovative adaptive façade concepts
Roel Loonen

nr 254
Multi-scale FEM-DEM Model for Granular Materials: Micro-scale boundary conditions, Statics, and Dynamics
Jiadun Liu

nr 255
Bending Moment - Shear Force Interaction of Rolled I-Shaped Steel Sections
Rianne Willie Adriana Dekker

nr 256
Paralympic tandem cycling and handcycling: Computational and wind tunnel analysis of aerodynamic performance
Paul Fionn Mannion

nr 257
Experimental characterization and numerical modelling of 3D printed concrete: Controlling structural behaviour in the fresh and hardened state
Robert Johannes Maria Wolfs

nr 258
Requirement checking in the building industry: Enabling modularized and extensible requirement checking systems based on semantic web technologies
Chi Zhang

nr 259
A Sustainable Industrial Site Redevelopment Planning Support System
Tong Wang

nr 260
Efficient storage and retrieval of detailed building models: Multi-disciplinary and long-term use of geometric and semantic construction information
Thomas Ferdinand Krijnen

nr 261
The users' value of business center concepts for knowledge sharing and networking behavior within and between organizations
Minou Weijs-Perrée

nr 262
Characterization and improvement of aerodynamic performance of vertical axis wind turbines using computational fluid dynamics (CFD)
Abdolrahim Rezaeiha

nr 263
In-situ characterization of the acoustic impedance of vegetated roofs
Chang Liu

nr 264
Occupancy-based lighting control: Developing an energy saving strategy that ensures office workers' comfort
Christel de Bakker

nr 265
Stakeholders-Oriented Spatial Decision Support System
Cahyono Susetyo

nr 266
Climate-induced damage in oak museum objects
Rianne Aleida Luimes

nr 267
Towards individual thermal comfort: Model predictive personalized control of heating systems
Katarina Katic

nr 268
Modelling and Measuring Quality of Urban Life: Housing, Neighborhood, Transport and Job
Lida Aminian

nr 269
Optimization of an aquifer thermal energy storage system through integrated modelling of aquifer, HVAC systems and building
Basar Bozkaya

nr 270
Numerical modeling for urban sound propagation: developments in wave-based and energy-based methods
Raúl Pagán Muñoz

nr 271
Lighting in multi-user office environments: improving employee wellbeing through personal control
Sanae van der Vleuten-Chraibi

nr 272
A strategy for fit-for-purpose occupant behavior modelling in building energy and comfort performance simulation
Isabella I. Gaetani dell'Aquila d'Aragona

nr 273
Een architectuurhistorische waardestelling van naoorlogse woonwijken in Nederland: Het voorbeeld van de Westelijke Tuinsteden in Amsterdam
Eleonore Henriette Marie Mens

nr 274
Job-Housing Co-Dependent Mobility Decisions in Life Trajectories
Jia Guo

nr 275
A user-oriented focus to create healthcare facilities: decision making on strategic values
Emilia Rosalia Catharina Maria Huisman

nr 276
Dynamics of plane impinging jets at moderate Reynolds numbers – with applications to air curtains
Adelya Khayrullina

nr 277
Valorization of Municipal Solid Waste Incineration Bottom Ash - Chemical Nature, Leachability and Treatments of Hazardous Elements
Qadeer Alam

nr 278
Treatments and valorization of MSWI bottom ash - application in cement-based materials
Veronica Caprai

nr 279
Personal lighting conditions of office workers - input for intelligent systems to optimize subjective alertness
Juliëtte van Duijnhoven

nr 280
Social influence effects in tourism travel: air trip itinerary and destination choices
Xiaofeng Pan

nr 281
Advancing Post-War Housing: Integrating Heritage Impact, Environmental Impact, Hygrothermal Risk and Costs in Renovation Design Decisions
Lisanne Claartje Havinga

nr 282
Impact resistant ultra-high performance fibre reinforced concrete: materials, components and properties
Peipeng Li

nr 283
Demand-driven Science Parks: The Perceived Benefits and Trade-offs of Tenant Firms with regard to Science Park Attributes
Wei Keat Benny Ng

nr 284
Raise the lantern; how light can help to maintain a healthy and safe hospital environment focusing on nurses
Maria Petronella Johanna Aarts

nr 285
Modelling Learning and Dynamic Route and Parking Choice Behaviour under Uncertainty
Elaine Cristina Schneider de Carvalho

nr 286
Identifying indoor local microclimates for safekeeping of cultural heritage
Karin Kompatscher

nr 287
Probabilistic modeling of fatigue resistance for welded and riveted bridge details. Resistance models and estimation of uncertainty.
Davide Leonetti

nr 288
Performance of Layered UHPFRC under Static and Dynamic Loads: Effects of steel fibers, coarse aggregates and layered structures
Yangyueye Cao

nr 289
Photocatalytic abatement of the nitrogen oxide pollution: synthesis, application and long-term evaluation of titania-silica composites
Yuri Hendrix

nr 290
Assessing knowledge adoption in post-disaster reconstruction: Understanding the impact of hazard-resistant construction knowledge on reconstruction processes of self-recovering communities in Nepal and the Philippines
Eefje Hendriks

nr 291
Locating electric vehicle charging stations: A multi-agent based dynamic simulation
Seheon Kim

nr 292
De invloed van Lean Management op de beheersing van het bouwproces
Wim van den Bouwhuijsen

nr 293
Neighborhood Environment and Physical Activity of Older Adults
Zhengying Liu

nr 294
Practical and continuous luminance distribution measurements for lighting quality
Thijs Willem Kruisselbrink

nr 295
Auditory Distraction in Open-Plan Study Environments in Higher Education
Pieternella Elizabeth Braat-Eggen

nr 296
Exploring the effect of the sound environment on nurses' task performance: an applied approach focusing on prospective memory
Jikke Reinten

nr 297
Design and performance of water resistant cementitious materials– Mechanisms, evaluation and applications
Zhengyao Qu

nr 298
Design Optimization of Seasonal Thermal Energy Storage Integrated District Heating and Cooling System: A Modeling and Simulation Approach
Luyi Xu

nr 299
Land use and transport: Integrated approaches for planning and management
Zhongqi Wang

nr 300
Multi-disciplinary optimization of building spatial designs: co-evolutionary design process simulations, evolutionary algorithms, hybrid approaches
Sjonnie Boonstra

nr 301
Modeling the spatial and temporal relation between urban land use, temperature, and energy demand
Hung-Chu Chen

nr 302
Seismic retrofitting of masonry walls with flexible deep mounted CFRP strips
Ömer Serhat Türkmen

nr 303
Coupled Aerostructural Shape and Topology Optimization of Horizontal-Axis Wind Turbine Rotor Blades
Zhijun Wang

nr 304
Valorization of Recycled Waste Glass and Converter Steel Slag as Ingredients for Building Materials: Hydration and Carbonation Studies
Gang Liu

nr 305
Low-Carbon City Development based on Land Use Planning
Gengzhe Wang

nr 306
Sustainable energy transition scenario analysis for buildings and neighborhoods - Data driven optimization
Shalika Saubhagya Wickramarachchi Walker

nr 307
In-between living and manufactured: an exploratory study on biobuilding components for building design
Berrak Kirbas Akyurek

nr 308
Development of alternative cementitious binders and functionalized materials: design, performance and durability
Anna Monika Kaja

nr 309
Development a morphological approach for interactive kinetic façade design: Improving multiple occupants' visual comfort
Seyed Morteza Hosseini

nr 310
PV in urban context: modeling and simulation strategies for analyzing the performance of shaded PV systems
Ádám Bognár

nr 311
Life Trajectory, Household Car Ownership Dynamics and Home Renewable Energy Equipment Adoption
Gaofeng Gu

nr 312
Impact of Street-Scale Built Environment on Walking/Cycling around Metro Stations
Yanan Liu

nr 313
Advances in Urban Traffic Network Equilibrium Models and Algorithms
Dong Wang

nr 314
Development of an uncertainty analysis framework for model-based consequential life cycle assessment: application to activity-based modelling and life cycle assessment of multimodal mobility
Paul Martin Baustert

nr 315
Variable stiffness and damping structural joints for semi-active vibration control
Qinyu Wang

nr 316
Understanding Carsharing-Facilitating Neighborhood Preferences
Juan Wang

nr 317
Dynamic alignment of Corporate Real Estate to business strategies: An empirical analysis using historical data and in-depth modelling of decision making
Howard Cooke

nr 318
Local People Matter: Towards participatory governance of cultural heritage in China
Ji Li

nr 319
Walkability and Walkable Healthy Neighborhoods
Bojing Liao

nr 320
On the role of light directionality in design of healthy offices
Parisa Khademagha

nr 321
Room acoustic modeling with the time-domain discontinuous Galerkin method
Huiqing Wang

nr 322
Sustainable insulating lightweight materials for enhancing indoor building performance: miscanthus, aerogel and nano-silica
Yuxuan Chen